

From the Boiling Point to the Glass Transition: Reorientational Dynamics as Revealed by Dynamic Light Scattering

Von der Universität Bayreuth genehmigte
Abhandlung zur Erlangung des Grades eines
Doktors der Naturwissenschaften (Dr. rer. nat.)

von
Bernd Schmidtke
geboren am 25.10.1982 in Weiden i.d.OPf.

1. Gutachter: Prof. Dr. Ernst Rößler
2. Gutachter: Prof. Dr. Werner Köhler

Contents

1 Abstract.....	1
2 Kurzdarstellung	3
3 Extended Abstract	5
3.1 Introduction	5
3.1.1 What is a Liquid, what a Glass?	5
3.1.2 Experimental Setup.....	8
3.1.3 Dynamic Light Scattering – Theoretical Approach	17
3.1.4 Dynamics in Liquids	19
3.2 Results	23
3.2.1 Susceptibility Spectrum of Glass Formers	23
3.2.2 Time Constants of the α -process	36
3.3.3 Theories of the Glass Transition	43
3.3 Summaries of the Publications	55
3.3.1 From boiling point to glass transition temperature: Transport coefficients in molecular liquids follow three-parameter scaling	55
3.3.2 Reorientational dynamics in molecular liquids as revealed by dynamic light scattering: From boiling point to glass transition temperature	57
3.3.3 From Boiling Point down to the Glass Transition - Dynamics of Molecular Liquids Described by a Generalized Angell Plot	59
3.3.4 Relaxation Stretching, Fast Dynamics and Activation Energy: a Comparison of Molecular and Ionic Liquids as Revealed by Depolarized Light Scattering	61
3.3.5 Depolarized light scattering spectra of molecular liquids: Described in terms of mode coupling theory	62
4 Publications	63
Bibliography	133

1 Abstract

In this thesis depolarized dynamic light scattering (DLS) is applied to measure the rotational dynamics of molecular and ionic liquids in a temperature range from around the glass transition temperature T_g up to the boiling point T_b . We investigate depolarized light scattering spectra measured with a tandem Fabry-Pérot interferometer (TFPI) and a double monochromator (DM) of a series of sixteen molecular and six room temperature ionic liquids. As most susceptibility spectra of glass forming liquids reported so far do not cover high temperatures, they usually do not detect the crossover from “glassy dynamics” to “simple liquid” spectra, where the α -relaxation and the contribution of the microscopic (vibrational) dynamics have essentially merged. The aim of this work was to complement several available spectra, measured during some preceding thesis, up to highest frequencies and temperatures as well as to investigate and evaluate new samples. We focused on low- T_g liquids for which the high-temperature limit $\tau \cong 10^{-12}$ s is easily accessed by standard spectroscopic equipment (up to 440 K).

The susceptibility spectra and likewise the corresponding reorientational correlation functions are characterized by the stretching parameter β_{CD} , the time constant τ for the long-time decay (α -process), the strength of fast dynamics $1 - f$, and the time scale at shortest times expressed by $k_B T / I^*$ with the apparent inertial quantity I^* . In addition, an intermediate power-law regime (or excess wing in the frequency domain) between fast dynamics and α -process has to be taken into account. For a given system the spectral parameters are virtually temperature independent up to the boiling point, in particular, frequency-temperature-superposition applies for the α -process. Among the liquids, the quantity I^* correlates with molecular mass and anticorrelates with $1 - f$. No correlation among $1 - f$ and β_{CD} is revealed. Testing for correlation of β_{CD} or $1 - f$ with parameters describing the temperature dependence of the correlation time τ , which are the high-temperature activation energy E_∞ , the fragility m or the glass transition temperature T_g , no significant correlation is found. Regarding molecular vs. ionic liquids, no relevant differences in the evolution of their DLS spectra are observed.

Analyzing the DLS spectra, we developed a procedure to determine the reorientational correlation time τ of these liquids from the susceptibility spectra and complemented them

with data from literature. Correlation times in the range 10^{-12} s – 100 s are compiled, i.e., the full temperature interval between the boiling point and the glass transition temperature T_g was covered. Regarding the temperature dependence, we developed a new interpolation formula, decomposing the apparent activation energy $E_A(T)$ in a constant high temperature value E_∞ and a "cooperative part" $E_{\text{coop}}(T)$ depending exponentially on temperature, and quantitatively compared it with two other approaches, which are the widely used Vogel-Fulcher-Tammann function and a newer expression developed by Mauro *et al.* [J. C. Mauro, Y. Yue, A. J. Ellison, P. K. Gupta, D. C. Allen, Proc. Natl. Acad. Sci. USA 103, 19780 (2009).] Introducing E_∞ instead of T_g as a reference energy, it allows the discussion of the temperature dependence of the liquid's dynamics in terms of the "generalized Angell plot" $E_{\text{coop}}(T)/E_\infty$ vs. T/E_∞ and suggests that E_∞ controls the energy scale of the glass transition phenomenon.

The susceptibility spectra are also analyzed in the frame work of the mode coupling theory (MCT). They are fitted to numerical solutions of the schematic F_{12} model, which allows to go beyond the asymptotic laws and to discuss their applicability. The model is able to quantitatively describe the spectra up to the boiling point. The changes of the spectra with temperature are mapped to only two control parameters, which show a smooth variation with temperature. The numerical solutions are extrapolated down to T_c , where the asymptotic scaling laws can be applied. Although the spectra apparently follow scaling relations, the application of the asymptotic laws usually overestimates T_c . In all the cases the experimental spectra are outside the applicability regime of the asymptotic laws. This is explained by more or less strong vibrational contributions. Within a phenomenological approach which extends the spectral analysis down to T_g and which allows for separating fast and slow dynamics, the strength of the fast dynamics $1 - f_{\text{rel}}$ is revealed. It shows the cusp-like anomaly predicted by MCT; yet, the corresponding critical temperature is significantly higher than that derived from the F_{12} model. In addition, we demonstrate that close to T_g , the susceptibility minimum is controlled by the interplay of the excess wing, alias intermediate power-law and the fast dynamics contribution.

2 Kurzdarstellung

Im Laufe dieser Arbeit wurde mit Hilfe der depolarisierten dynamischen Lichtstreuung (DLS) die Rotationsdynamik von molekularen und ionischen Flüssigkeiten im Temperaturintervall zwischen der Glasübergangstemperatur T_g und dem Siedepunkt T_b gemessen. Es werden depolarisierte Lichtstreuungsspektren von sechzehn molekularen und sechs ionischen Flüssigkeiten untersucht. Diese wurden mit einem Doppelmonochromator (DM) und einem Tandem Fabry-Pérot Interferometer (TFPI) gemessen. Da die meisten bisher veröffentlichten Suszeptibilitätsspektren von Glasbildnern keine hohen Temperaturen einschließen, erfassen sie nicht den Übergang von „glasartiger Dynamik“ zur Dynamik einfacher Flüssigkeiten, bei denen die Beiträge der α -Relaxation und der mikroskopischen (vibrations-) Dynamik praktisch verschmolzen sind. Das Ziel dieser Arbeit war die Ergänzung einiger existierender Spektren, welche im Rahmen vorangegangener Arbeiten gemessen wurden, sowie die Untersuchung und Auswertung neuer Proben. Wir legten den Schwerpunkt auf nieder- T_g Flüssigkeiten, bei welchen der Hochtemperatur-Grenzwert von $\tau \cong 10^{-12}$ s leicht mit spektroskopischer Standardausrüstung (Temperaturen bis etwa 440K) erreicht werden kann.

Die Suszeptibilitätsspektren und ebenso die entsprechenden Reorientierungskorrelationsfunktionen werden durch einen Streckungsparameter des Langzeiterfalls (α -Prozess) β_{CD} , der Relaxationsstärke der schnellen Dynamik $1 - f$ und der Zeitskala zu kürzesten Zeiten $k_B T / I^*$, mit dem effektiven Trägheitsmoment I^* charakterisiert. Ein zusätzliches (intermediäres) Potenzgesetz, welches dem „Excess wing“ in der Frequenzdomäne entspricht, muss zwischen der schnellen Dynamik und dem α -Prozess berücksichtigt werden. Die spektralen Parameter einer jeden Molekülsorte sind praktisch temperaturunabhängig bis hinauf zum Siedepunkt, also gilt das Frequenz-Temperatur-Superpositionsprinzip für den α -Prozess. Bei der Betrachtung aller Flüssigkeiten findet man eine Korrelation der Größe I^* mit dem Molekulargewicht und eine Antikorrelation mit $1 - f$. Es zeigt sich keine Korrelation zwischen $1 - f$ und β_{CD} . Weiterhin wurden keine signifikanten Korrelationen zwischen β_{CD} oder $1 - f$ und Parametern, welche die Temperaturabhängigkeit der Korrelationszeiten beschreiben, also der Hochtemperaturaktivierungsenergie E_∞ , der Fragilität m oder der Glasübergangstemperatur T_g gefunden. Auch zeigen sich keine relevanten Unterschiede in den Spektren von molekularen und ionischen Flüssigkeiten.

Wir entwickelten ein Verfahren um die Reorientierungskorrelationszeiten τ von Flüssigkeiten aus den Suszeptibilitätsspektren zu bestimmen und vervollständigten diese mit Literaturwerten. Korrelationszeiten im Bereich von 10^{-12} s – 100 s wurden zusammengetragen, was dem kompletten Temperaturbereich zwischen dem Siedepunkt und der Glasübergangstemperatur entspricht. Wir entwickelten eine neue Interpolationsfunktion für die Temperaturabhängigkeit der Korrelationszeiten, welche die apparente Aktivierungsenergie $E_A(T)$ in einen konstanten Hochtemperaturwert E_∞ und einen „kooperativen Anteil“ $E_{\text{coop}}(T)$, der exponentiell von der Temperatur abhängt, aufteilt. Diese wurde mit zwei weiteren, bereits bestehenden Ansätzen quantitativ verglichen. Die Einführung von E_∞ an Stelle der Glasübergangstemperatur T_g als Referenzenergie erlaubt die Diskussion der Temperaturabhängigkeit der Dynamik von Flüssigkeiten im Rahmen eines „generalized Angell plot“, also von $E_{\text{coop}}(T)/E_\infty$ in Abhängigkeit von T/E_∞ . Diese Darstellung legt nahe, dass E_∞ die Energieskala des Glasüberganges bestimmt.

Die Suszeptibilitätsspektren werden auch im Rahmen der Modenkopplungstheorie (MCT) untersucht. Numerische Lösungen des schematischen F_{12} Modells werden an sie angepasst, was eine Auswertung jenseits der asymptotischen Skalengesetze und die Diskussion deren Anwendbarkeit ermöglicht. Das Modell kann die Spektren quantitativ bis hinauf zum Siedepunkt beschreiben. Die Temperaturabhängigkeit der Spektren wird dabei auf nur zwei Kontrollparameter abgebildet, die glatte Funktionen der Temperatur sind. Die numerischen Lösungen werden bis hinab zur kritischen Temperatur T_c extrapoliert, wo die asymptotischen Skalengesetze sicher angewendet werden können. Obwohl die Spektren augenscheinlich den Skalierungsregeln genügen, überschätzen die asymptotischen Skalengesetze üblicherweise T_c . Dies lässt sich durch mehr oder weniger starke Vibrationsbeiträge erklären. Mit einem phänomenologischen Ansatz, der die Analyse der Spektren bis hinab zur Glasübergangstemperatur T_g erweitert und der die Trennung der schnellen Dynamik von langsamen Beiträgen erlaubt, wird die Stärke der schnellen Dynamik $1 - f_{\text{rel}}$ bestimmt. Sie zeigt die von der MCT vorhergesagte Anomalie, jedoch ist die zugehörige kritische Temperatur deutlich höher als diejenige welche aus dem F_{12} Modell bestimmt wurde. Zusätzlich zeigen wir, dass das Suszeptibilitätsminimum in der Nähe der Glasübergangstemperatur vom Zusammenspiel des „Excess wings“ mit der schnellen Dynamik bestimmt wird.

3 Extended Abstract

3.1 Introduction

3.1.1 What is a Liquid, what a Glass?

Already in ancient times, men used the volcanic glass obsidian to manufacture tools like knives and arrow tips.[1] The first glass vessels were built in Egypt about 1500 BC and the discovery of glassblowing was probably made in Phoenicia in the 1st century BC. Today glasses are materials of technological importance, not only in the classical fields, for example architecture or packaging, but also in more recent applications, like communication techniques (optical fibers) or medicine (bioactive implants). This is especially true considering the modern definition of glass as a non-crystalline solid, i.e., a state of matter, rather than the silica-based transparent material associated by everyday language to the term glass.[2]

A liquid could be defined as a form of condensed matter, i.e., an ensemble of particles (e.g. atoms, molecules, monomeric units of polymer chains, particles of colloidal suspensions) with inter-particle distances of the order of the particle size.[3] This discriminates liquids very well from gases, which show much larger inter-particle distances, but it is also valid for crystals. Therefore one needs to add that liquids show a short range order in their structure, but, in contrast to crystals, they do not have a long range order. As an example, Figure 1.1 shows the radial distribution function $g(r)$ of liquid argon (taken from [4]). On short distances $g(r)$ has sharp peaks defining the first coordination spheres, at longer distances $g(r)$ flattens out to unity, indicating vanishing structural correlations.

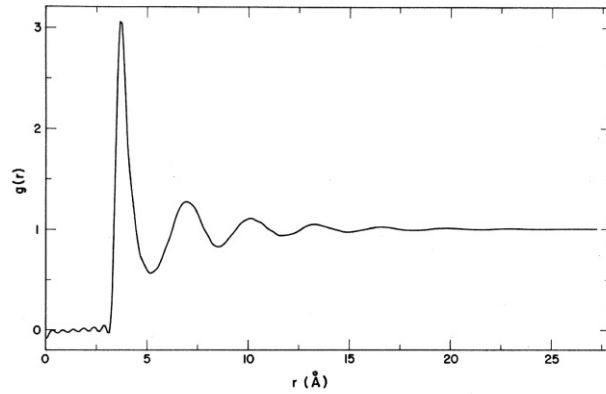


Figure 1.1 Radial distribution function $g(r)$ of liquid Argon at $T = 86$ K. Figure taken from [4]

There is still another group of condensed matter, glasses, for which all this is true. Also properties like density or compressibility are not suited to discriminate liquids from glasses. But in contrast to glasses, liquids show a finite viscosity. One could define a liquid as a dense ensemble of particles which will flow, if an infinitesimal small (effective) force is applied for an infinite time. This is equal to a vanishing shear modulus $G'(\omega)$ at zero frequency

$$\lim_{\omega \rightarrow 0} G'(\omega) = 0 \quad (1.1)$$

In a liquid the particles are able to rearrange, as they are dense but still mobile. The Stokes-Einstein equation

$$D = \frac{k_B T}{6\pi\eta R} \quad (1.2)$$

connects the self-diffusion coefficient D (a microscopic quantity, expressing the mobility of the particles) with the viscosity η (a macroscopic quantity, expressing the ability of the particle ensemble to flow). On long time scales, the mean square displacement $\langle r^2 \rangle$ of one particle in the liquid is given by [3][5]

$$\langle r^2 \rangle = 6Dt. \quad (1.3)$$

The only relevant differences between liquids and glasses are found in variables describing the dynamics of the system, whereas those describing the structure are practically indistinguishable. On cooling down, variables like the thermodynamic potentials, heat

capacity or specific volume undergo only small changes, while the viscosity η and thus the corresponding structural relaxation time, reflecting the translational and rotational dynamics of the molecules, increases over 14 decades.[6] As soon as this relaxation time exceeds the experimental time scales, the sample falls out of equilibrium and behaves as a solid. This means that glasses are nothing else than liquids in a non-ergodic state. The ratio of the characteristic response time of a material to the time of observation is called Deborah number, named after the Biblical prophetess Deborah, who said that the mountains flow before the Lord.[7]

The glass transition temperature T_g is usually defined by the convention that

$$\tau(T_g) = 100 \text{ s} \quad (1.4)$$

which is a convenient time scale for human beings. It is approximately equal to the onset of the “glass-step” in a DSC (differential scanning calorimetry) experiment performed at a heating rate of ten Kelvin per minute. The experimental time scale dependence leads to a heating rate dependence of T_g . Of course, the structural relaxation rate, which is closely related to the correlation time τ of molecular reorientation, can be accessed by many experimental methods, including dynamic light scattering.[5][8][9]

3.1.2 Experimental Setup

An overview of different methods suited for the measurement of particle dynamics is shown in Figure 1.2 with the frequency domain depolarized light scattering methods used for this work, double monochromator spectroscopy and tandem Fabry-Pérot interferometry marked in green. The method of choice concerning molecular reorientations at high frequencies is depolarized light scattering (DM / FPI), as it is not limited at the high-frequency side and provides superior resolution compared to dielectric spectroscopy (DS). Photon correlation spectroscopy (PCS) is a time-domain light scattering method which is fully comparable to DM / FPI and has a time window comparable to DS. Other important short time methods are neutron scattering (NS) [10]-[13] and optical Kerr effect spectroscopy (OKE) [14]-[16], which also probes molecular reorientations.

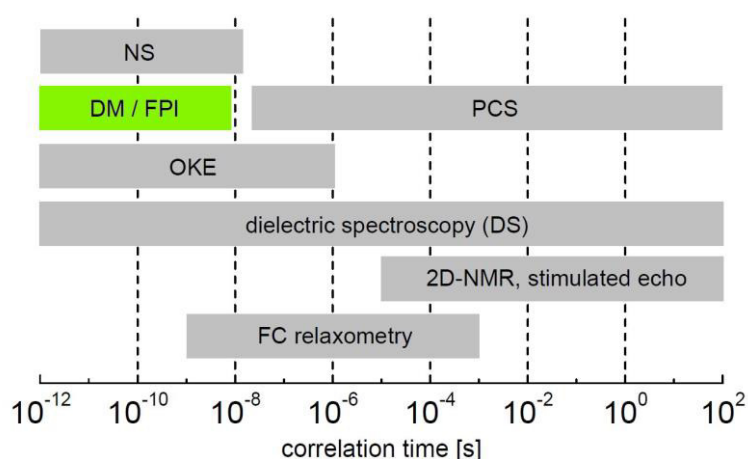


Figure 1.2 Time windows of the most important methods probing dynamics in dense molecular liquids: neutron scattering (NS), Field cycling (FC) relaxometry, two-dimensional NMR (2D NMR), double monochromator / Fabry-Pérot interferometry (DM/FPI), photon correlation spectroscopy (PCS), and optical Kerr effect (OKE) (Figure taken from [17]).

The experimental setup used for this work mainly consisted of a Nd:YVO₄-Laser, a furnace or cryostat, a double monochromator, a Fabry-Pérot interferometer and further optical components for beam guidance.

We measured two frequency ranges with the monochromator with wave number steps of 0.2 cm^{-1} and 2.0 cm^{-1} at frequency intervals of 50 GHz to 1.5 THz and 1.2 THz to 45 THz, respectively. The tandem Fabry-Pérot interferometer was used with three different mirror distances (1mm, 5mm, 20mm), which result in three overlapping frequency intervals of 4.5 GHz to 145 GHz, 0.9 GHz to 29 GHz and 0.35 GHz to 7.2 GHz, respectively. These five sub-spectra are then joined to a single intensity spectrum by adjusting the relative intensity of each sub-spectrum in order to match the overlapping parts. The spectra measured at different temperatures are normalized to each other by assuming temperature independence of the high frequency Raman modes.

General Aspects of the Optical Setup

As can be seen in Figure 1.3, the light created by the laser is sent via two mirrors to a small prism. On its way, it runs through a polarizer to enhance the polarization of the already polarized laser beam. After deflection by the prism, the beam is focused on the sample.

The detection of the scattered light takes place via two separate optical paths. On the one hand, the scattered light is collected by the focusing lens itself in quasi-backscattering geometry (about 175 degree). By the use of a mirror, it is focused on the pinhole of the tandem Fabry-Pérot interferometer after passing through an analyzer. On the other hand, the scattered light is simultaneously collected by a collimating lens at an angle of about 90 degree and then focused on the entry slit of the monochromator after passing a shutter. The whole setup is placed in an air conditioned lab to prevent loss of alignment caused by thermal expansion.

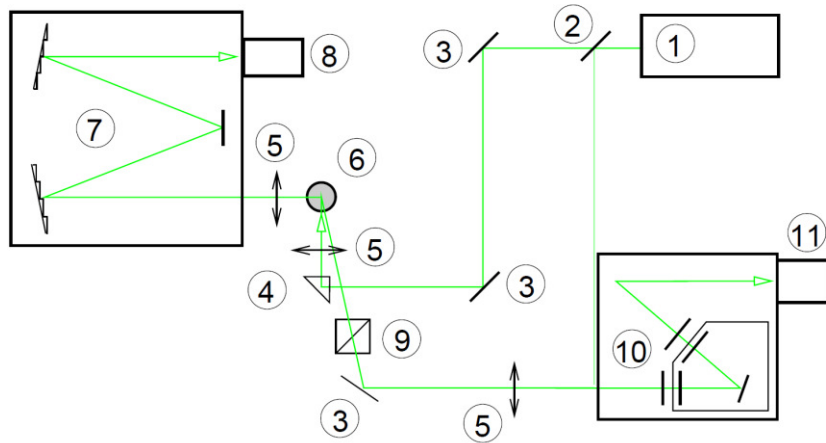


Figure 1.3 Schematic experimental setup; containing laser (1), beam splitter (2), mirrors (3), prism (4), lens (5), sample holder (6), monochromator (7), photo multiplier (8), polarizer (9), tandem Fabry-Pérot interferometer (10), and avalanche photodiode (11). Figure taken from [18].

The Light Source

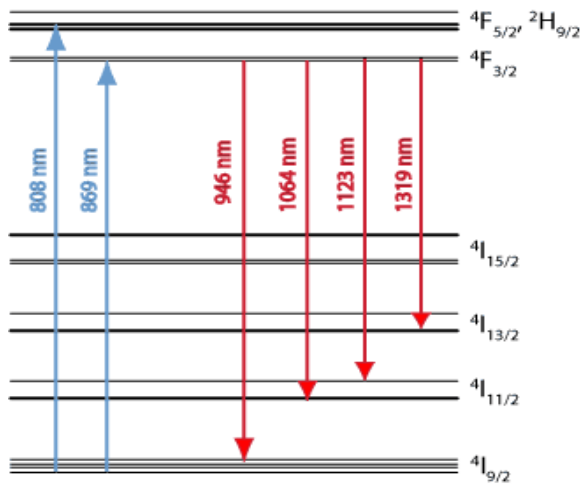


Figure 1.4 Energy level structure of the trivalent neodymium ion. For pumping, the transition from $4I_{9/2}$ to $4F_{5/2}$ is used. Inversion between $4F_{3/2}$ and $4I_{15/2}$ is used for emission. Figure adapted from [19].

The laser used was a *Verdi V2* from the manufacturer *Coherent*. It is a diode pumped, frequency doubled solid state laser. The resonator is designed as a ring resonator with the active medium, the optical active crystal and an etalon being integrated. The whole laser head is aligned and encapsulated by the manufacturer, no maintenance by the user is necessary. The active medium consists of a neodymium doped yttrium orthovanadate crystal ($ND:YVO_4$), emitting at a wavelength of 1064nm (infrared). In order to limit the width of the

emission, a temperature stabilized etalon is integrated in the ring resonator. The light used for the experiments with a wavelength of 532nm is created as the second harmonic in a nonlinear optical crystal, a lithium-tri-borate crystal.

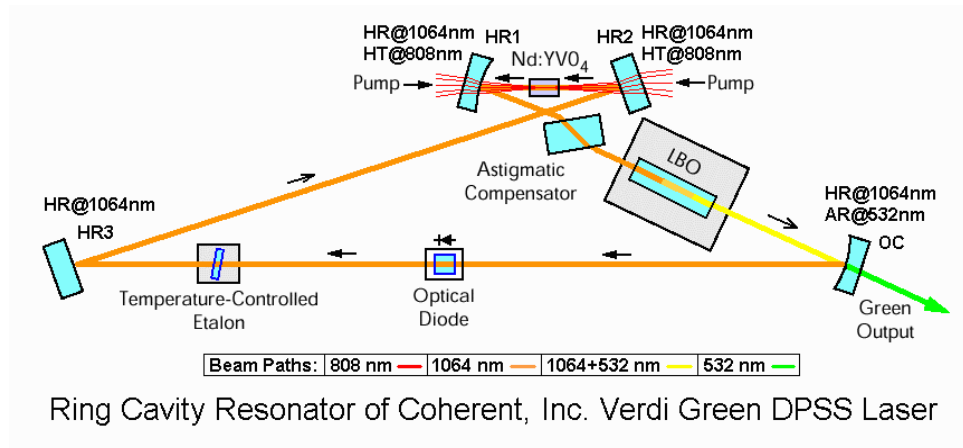


Figure 1.5 Sketch of the beam path and the relevant optical elements of the Verdi V2; adapted from [20].

The laser reaches an extraordinary stability concerning emission power (optical noise < 0.02% RMS) and a line width narrower than 5 MHz. As this is about two orders of magnitude smaller than the resolution of the Fabry-Pérot interferometer of about 300 MHz, the influence of the laser line width on the measured spectra can be neglected. Inside the ring resonator, where no stationary waves can show up, an optical diode is integrated. By the design of this setup, no mode jump can occur. The pump light of the two titan sapphire laser diodes is guided via optical fibers to the laser head and then focused on the active medium along the optical axes. Only the transversal TEM₀₀-mode is supported.

The active frequency stabilization is implemented by the temperature stabilization of the etalon. The stability of the TEM₀₀-mode is provided by the active temperature control of the active medium. To keep the emitted power constant over a long time, on the one hand the temperature of the pump diodes is controlled to keep their emission resonant with the absorption of the neodymium ions, on the other hand the nonlinear optical crystal is kept at a temperature of 148 °C, because only then it has the same refractive index at both wave

lengths 1064 nm and 532 nm. Small deviations of this temperature may lead to mayor deviations of the emission power. The active control of the emission power is implemented via a photodiode in the laser head and an adjustment of the pump power. A long term power stability of about 1% is reached.[21]

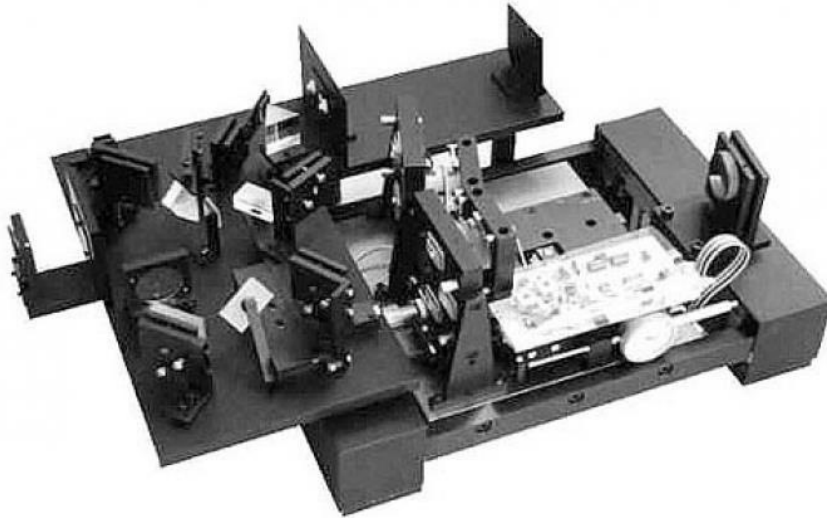
The *Verdi V2* is designed for a maximum power emission of 2 W, but for the light scattering experiments only output powers of about 200 mW were used to prevent heating of the sample in the focus of the beam.

Sample Temperature Control

For measurements higher than ambient temperatures, a small, self-built furnace was used. It uses resistive heating and contains a temperature sensor. Combined with a *Lakeshore 330* temperature controller, a given temperature can be approached and kept constant. The relative temperature stability is, after some built up effects, less than the resolution of the temperature controller of 0.1 K. The oven is covered by a metal cylinder with a cap, to reduce cooling by air flow and establish a more homogeneous temperature distribution. For gauging the absolute temperature, the voltage-temperature line was calibrated with boiling water and ice water. The upper temperature limit of the oven is 440 K, which is not limited by the power of the thermal heating, but by the stability of the used materials.

For measurements below ambient temperatures, a *Cryovac Spectro 3* cryostat was used. It is equipped with an open heat exchanger, which means that the temperature controlled gaseous nitrogen flows into the sample chamber around the sample itself. The gas is sucked in by a defined pressure from the exhaust flange. The nitrogen flow is manually adjusted to a value where the *Lakeshore 330* temperature controller works centered in its control range. To avoid condensation and nitrogen consumption, an isolation vacuum of about 10^{-3} mbar is created.

The Tandem Fabry-Pérot Interferometer



Centerpiece of the experimental setup is the *JRS Scientific Instruments* tandem Fabry-Pérot interferometer *TFP-1*. It consists of two plane mirrors mounted accurately parallel to one another, with an optical spacing L between them.

The beam path inside the interferometer can be described, according to Figure 1.6 as follows. The scattered light, entering the interferometer via the input pinhole P1, is transformed by the lens L1 into a parallel beam. This is led orthogonally onto the first etalon FP1. The transmitted light is reflected by mirror M3 onto the second etalon FP2. After passing both etalons, the light is directed twice through both etalons again, before it is focused by lens L2 on the output pinhole P2. Thereby, higher order contributions are eliminated by the prism PR2 and an upgraded interference filter F. An avalanche photodiode is used as detector.

The Double Monochromator

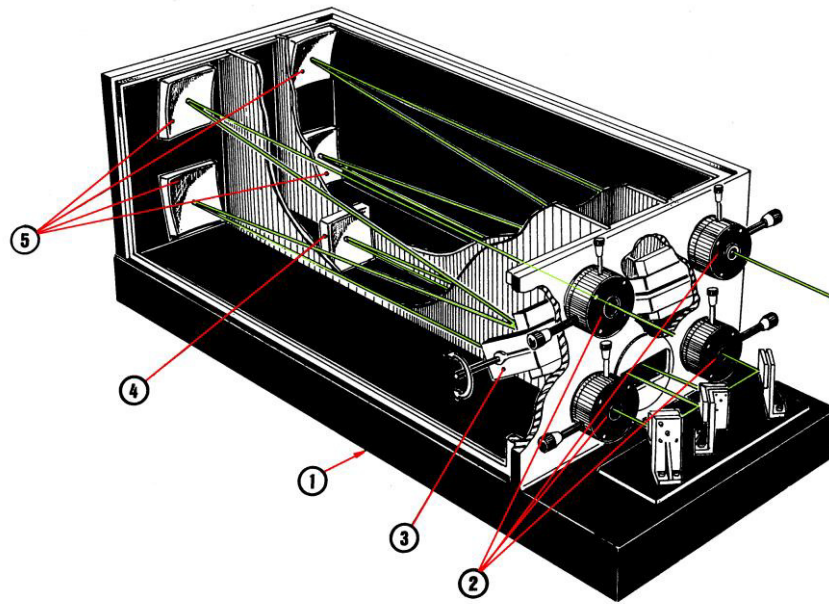


Figure 1.7 Sketch of the monochromator, consisting of a base plate (1), input and output pinholes (2), optical gratings (3), a coupling mirror (4) and collimation mirrors (5). Figure adapted from [24]

For measuring frequencies above about 100 GHz, the *Yobin-Yvon U1000* double monochromator is used. It is built from two identical monochromators with plane gratings and concave mirrors. These reshape the spherical wave emerging behind the entrance slit into a plane wave, illuminating the grating as homogeneously as possible. The first order diffracted light hits a second mirror, focusing it on the current exit slit. Via a coupling mirror, the light leaving the first monochromator is sent to the second one. The two diffraction gratings are fixed on a common axis, which is rotated for varying the transmission frequency. A sketch of the monochromator and its components is shown in Figure 1.7.

As the axis is aligned horizontally, the lines of the diffraction grating and the slits are aligned horizontally, too. The focal length of each monochromator is 1000 mm, giving the whole device some remarkable extent. A long focal length is quite desirable, as it allows detection of small angular changes of the diffracted light. The collimator mirrors have a size of about 100 x 100 mm; an optimal illumination is achieved with an aperture of $f/8$.

The angular dependence of the intensity of a diffracted wave is given by [25]

$$I(\theta) = \left(\frac{\sin N\alpha}{\sin \alpha} \right)^2, \text{ with } \alpha = \frac{\pi a}{\lambda} \sin \theta \quad (1.6)$$

where N denotes the number of illuminated lines, a the line distance, and λ the wavelength. The grating used for the experiments shown in this work has a line density of 2400 lines per millimeter and a size of 110 mm.

The calculated resolution $\lambda/\Delta\lambda$ is about 2.4×10^5 , equivalent to 2.2 pm at a wavelength of 532 nm. This more or less theoretical value is not reached in practical use, as the slits have finite sizes.

3.1.3 Dynamic Light Scattering – Theoretical

Approach

Light scattering is, as any interaction between matter and radiation, a quantum electrodynamic effect. In the present context, the electrodynamics picture should provide a sufficient explanation.[26]-[28] This chapter is mainly based on ref. [29]

In 1910, A. Einstein already stated, that local fluctuations of the medium's dielectric constant cause scattering of light.[30] A shift in frequency of the scattered light only occurs in the case that the spatial Fourier transform of the dielectric fluctuations $\delta\epsilon(\vec{q}, t)$ changes with time. The spectral density for light scattering, which will be treated in the following sections in detail, is given by [29]

$$I(\vec{q}, \omega_f, R) = \frac{I_0 k_f^4}{16\pi^2 R^2 \epsilon_0^2} \frac{1}{2\pi} \int_{-\infty}^{\infty} e^{-i(\omega_f - \omega_i)t} \langle \delta\epsilon_{if}^*(\vec{q}, t), \delta\epsilon_{if}(\vec{q}, 0) \rangle dt \quad (1.7)$$

where $\delta\epsilon_{if}(\vec{q}, t)$ is the component of the fluctuation tensor of the dielectric constant, which is aligned along the polarization of initial and the final wave respectively; \vec{q} denotes the wave vector of the scattering process; R is the distance between the detector and the scattering region; ω_i and ω_f are the frequency of the initial and the final light wave, respectively. In comparison with equation 1.14, it is obvious that light scattering detects the Fourier transform of an autocorrelation function.

From this equation, some general statements on light scattering can be derived:

- The spectral density is proportional to k_f^4 or λ_f^{-4} . This is the reason for blue skies and makes shorter wavelength better suited for light scattering experiments.
- The scattered intensity decays as that of a spherical wave proportional to R^{-2}
- The shape of the spectral density does not depend on the absolute frequency ω_i , but only on the relative frequency $\omega_i - \omega_f$, therefore results obtained by the use of different light sources can be compared to each other.

- In media not showing temporal fluctuations of the dielectric constant $\delta\epsilon_{if}(\vec{q}, t)$, one only gets an elastic signal at $\omega_i - \omega_f = 0$.

The dielectric fluctuations $\delta\epsilon(\vec{q}, t)$ can be mapped on fluctuations of the molecular polarizability $\delta\alpha(t)$. In the case of molecules with cylindrical symmetry and an anisotropic part $\beta = \alpha_{\parallel} - \alpha_{\perp}$, one gets after some calculation the time-domain expression:[29]

$$I_{if}^{\alpha}(\vec{q}, t) = \langle N \rangle \left(\frac{2\pi}{15} \right) \beta^2 \left(F_{1,1}^{(2)}(t) + F_{1,-1}^{(2)}(t) + F_{-1,1}^{(2)}(t) + F_{-1,-1}^{(2)}(t) \right) \cdot \langle \exp \{ i\vec{q} \cdot (\vec{r}(t) - \vec{r}(0)) \} \rangle \quad (1.8)$$

Where $F_{m,m'}^{(l)}(t) = \langle Y_{l,m}^*(\theta(0), \varphi(0)) Y_{l,m'}(\theta(t), \varphi(t)) \rangle$ denote the orientation correlation functions, which reflect the temporal development of the molecular angles θ and φ .

On inspecting equation 1.8, one recognizes that the light scattering signal is proportional to β^2 , therefore molecules with small anisotropy are inappropriate for the measurement of rotational dynamics.

As the orientation correlation functions $F_{m,m'}^{(l)}(t)$ only depend on the second order spherical harmonics $Y_{2,m}(t)$, light scattering spectroscopy is sensitive to variation of second order Legendre polynomials $P_2(\cos \theta)$ only. This is a common feature with nuclear magnetic resonance spectroscopy (NMR) and optical Kerr effect spectroscopy (OKE), hence the results, e.g. time constants, are comparable without assuming models of motion. In contrast, dielectric spectroscopy (DS) detects the variation of the first order Legendre polynomial $P_1(\cos \theta)$, what may lead to differences depending on the nature of motion.

Basically, via a variation of \vec{q} (usually done via a variation of the scattering angle) information on the spatial correlation of fluctuations can be obtained. As \vec{q} in the case of light scattering is small, more precisely $|\vec{q}|\xi \ll 1$, with ξ being the correlation length of the studied process, it is sufficient to consider the limit $|\vec{q}| \rightarrow 0$, where the exponential factor in equation 1.8 can be omitted, what leads to a \vec{q} -independent spectral density $I(\omega_f, R)$. [31]

3.1.4 Dynamics in a Liquid

The molecular movement (rotation as well as translation) of particles is erratic, therefore any detected signal is erratic, too. One could speak of noise. It is obvious that the theory of noise and fluctuations is relevant for light scattering, as well as for any other measurement of liquid dynamics. The most important result of *linear response theory* is:[32] If two systems are coupled only weakly, information on the uncoupled systems suffice to describe how one system reacts to the other one. Thus, the response of the system is completely described by the time correlation function of a dynamic variable, which characterizes the “noise” in the unperturbed system. In the case of light scattering, the incident light is supposed to be weak enough, that one can assume the equilibrated system’s reaction to be linear.

Correlation Functions

Time dependent correlation functions have a long tradition in being used in the theory of stochastic processes.[33] They provide an expression on how much two dynamic variables are correlated in a given period of time.

Let the variable A depend on positions and velocities of all particles in a given ensemble of particles. Even though every single particle moves obeying Newton’s laws, the variable A shows only noise caused by the huge number of particles in the systems. This concept is used by molecular dynamics simulations.[34] By limiting the number of particles and the calculated time steps, the equations of motion can be solved stepwise for each particle.

Let the quantity A be a noise signal with the following properties: The value $A(t)$ at the time t and the one at the time t' , $A(t')$, differ. If the difference between t and t' is small compared to the typical time scale of the fluctuations, it is probable that the value $A(t')$ is close to the $A(t)$. Therefore one can claim that $A(t)$ and $A(t')$ are correlated, and that this correlation decays at long times $\Delta t = t' - t$. A measure for such a correlation is the autocorrelation function of A , which is defined by

$$\langle A(0)A(\Delta t) \rangle = \lim_{T \rightarrow \infty} \frac{1}{T} \int_0^T A(t)A(t + \Delta t) dt \quad (1.9)$$

It is obvious that the correlation reaches its highest value at shortest times

$$\langle A(0)A(0) \rangle \geq \langle A(0)A(\Delta t) \rangle \quad (1.10)$$

At times Δt , which are considerably longer than the typical time scale of the fluctuations of $A(t)$, one expects that the correlation among $A(0)$ and $A(\Delta t)$ exists no longer:

$$\lim_{\Delta t \rightarrow \infty} \langle A(0)A(\Delta t) \rangle = \langle A(0) \rangle \langle A(\Delta t) \rangle = \langle A(0) \rangle^2 \quad (1.11)$$

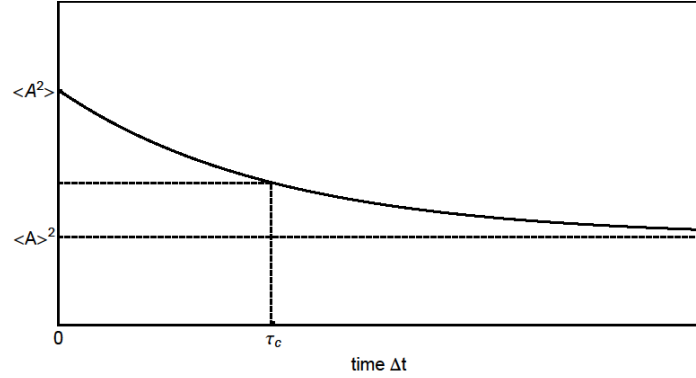


Figure 1.8 Sketch of the autocorrelation function of $A(t)$, decaying from $\langle A^2 \rangle$ down to $\langle A \rangle^2$ at a time scale of Δt .

By the definition of the quantity $\delta A(t) = A(t) - \langle A(t) \rangle$, which is the deviation of $A(t)$ from its average value, the autocorrelation function of $\delta A(t)$ has a more simple structure, as the constant part vanishes.

$$\lim_{\Delta t \rightarrow \infty} \langle \delta A(0) \delta A(\Delta t) \rangle = 0 \quad (1.12)$$

One can define a model independent time scale τ_c of the fluctuations of $A(t)$ by the integral over the normalized autocorrelation function:

$$\tau_c = \int_0^\infty \frac{\langle \delta A(0) \delta A(\Delta t) \rangle}{\langle \delta A^2 \rangle} d(\Delta t) \quad (1.13)$$

Spectral Density

The spectral density (or power spectrum) $I_A(\omega)$ of a stochastic process described by the autocorrelation function $\langle A(0)A(t) \rangle$ is, following the Wiener-Chintschin-theorem,[35] given by:

$$I_A(\omega) = \frac{1}{2\pi} \int_{-\infty}^\infty e^{-i\omega t} \langle A(0)A(t) \rangle dt \quad (1.14)$$

This quantity plays an important role in the following, as the spectral is directly measured by the light scattering setup used for this work. The correlation function can be calculated from the spectral density.

$$\langle A(0)A(t) \rangle = \int_{-\infty}^{\infty} e^{i\omega t} I_A(\omega) d\omega \quad (1.15)$$

The autocorrelation function and the spectral density are their mutual Fourier transforms. The quantity $I_A(\omega)d\omega$ can be interpreted as the amount of $\langle A^2 \rangle$ in the frequency interval between ω and $\omega+d\omega$.

Considering the short-time limit of equation (1.15), one gets the mean square value of the quantity A in equilibrium.

$$\langle A(0)A(0) \rangle = \langle |A(0)|^2 \rangle = \int_{-\infty}^{\infty} I_A(\omega) d\omega \quad (1.16)$$

Considering instead the low-frequency limit of equation (1.14) together with equation (1.13), one gets

$$I_A(0) = \frac{1}{2\pi} \int_{-\infty}^{\infty} \langle A(0)A(t) \rangle dt = \tau_c \frac{\langle A^2 \rangle}{2\pi} \quad (1.17)$$

This means that for normalized correlation functions decaying from 1 for $t=0$ down to 0 at long times, the spectral density at $t=0$ gives the time constant $\tau_c/2\pi$.

Susceptibility

The imaginary part of the susceptibility χ'' of a given system is connected to the spectral density via the fluctuation-dissipation-theorem:[36]-[38]

$$\chi'' = \frac{1}{2\hbar} \left(1 - e^{-\frac{\hbar\omega}{k_B T}} \right) I_A(\omega) = \frac{1}{2\hbar} \frac{I_A(\omega)}{n(\omega) + 1} \quad (1.18)$$

with the Bose factor

$$n(\omega) = \frac{1}{e^{\frac{\hbar\omega}{k_B T}} - 1} \quad (1.19)$$

where k_B denotes the Boltzmann constant and T the absolute temperature. The left side of equation (1.18) describes a system relaxing to the equilibrium state, while the right side describes fluctuations of a system around its equilibrium state. The imaginary part of the susceptibility χ'' is proportional to the power dissipated by the system from a perturbation with frequency ω .

Dielectric spectroscopy is one of most powerful and most applied methods for the investigation of super-cooled liquids' dynamics. Usually, the dielectric loss ε'' , which is equivalent to the dielectric susceptibility χ'' is plotted versus frequency. Therefore light scattering spectra may also be analyzed in the susceptibility representation for comparability reasons.

The factor $1 - \exp\left(-\frac{\hbar\omega}{k_B T}\right)$ in equation (1.19) is in literature sometimes replaced by $\frac{\hbar\omega}{k_B T}$,

what is a approximation for $\hbar\omega \ll k_B T$. For example at a frequency of 1THz and a temperature of 300K, this approximation deviates about 8% from the correct value. Therefore this approximation was not used in this work.

Pulse Response

The autocorrelation function of a dynamic variable A can be understood as describing the reaction of a system on a jump from one state to another one, the step response. The system approaches the new equilibrium at a time scale τ_c .

The pulse response describes the reaction of a dynamic variable A of the system on a Kronecker-Delta shaped pulse. Still assuming linear response theory, it is proportional to the negative time derivative of the step response function:

$$F_p(t) \propto -\frac{\partial \langle A(0)A(t) \rangle}{\partial t} \quad (1.20)$$

Analogously to the connection of correlation function to the spectral density, the pulse response is connected to the susceptibility via Fourier transformation.

This relation is becoming relevant as some methods, for example the optical Kerr effect (OKE), directly measure the pulse response function. OKE detects the reaction of a system to a first strong laser pulse with a second delayed laser pulse. The results of the method may directly be compared to the results of dynamic light scattering, as the same correlation function is probed.[39]-[41]

3.2 Results

3.2.1 Spectrum of Glass Formers

Glass formers show dynamics on virtually all observable time scales. While at the glass transition temperature T_g , the α -relaxation is found at about 0.01 Hz, the microscopic dynamics are found at about 1 THz. In order to fully capture the dynamics, a very broad frequency interval has to be measured. This is usually done by the combination of different methods (see Fig. 1.2).

Figure 2.1 schematically shows the typical development of the susceptibility spectrum $\chi''(\omega)$ of a liquid when cooling down from the boiling point (a) down to temperatures below the glass transition temperature T_g (d). At high temperatures, the α -peak merges with the microscopic (vibrational) dynamics to a broad single peak and the temperature dependence of this simple liquid spectrum is weak. The microscopic dynamics, including the boson peak can be thought of highly damped acoustic modes in the phonon spectrum of a crystal. At even higher frequencies, say above 5 THz, only Raman lines occur. These are independent of glassy dynamics as they are caused by intramolecular vibrations. The situation displayed in Figure 2.1 (a) and (b) is the one which is comparable to most experimental spectra used in this thesis. A minimum has shown up between the α -process at the low frequency side and the microscopic / fast dynamics at the high frequency side. On further cooling down the system, secondary processes emerge between the α -peak and the fast dynamics. Finally, at lowest temperatures, below T_g , the time scale of the α -process exceeds all experimental time scales and shifts out of the frequency window.

As most susceptibility spectra of glass forming liquids reported so far do not cover high temperatures (near the boiling point), and therefore do not detect the crossover from two well separated contributions to a single broadened peak. The aim of this work was to complement several available spectra, measured during some preceding thesis, up to highest frequencies and temperatures as well as to investigate and evaluate new samples. We focused on low- T_g liquids for which the high-temperature limit $\tau \cong 10^{-12}$ s is easily accessed by standard spectroscopic equipment (up to 440 K).

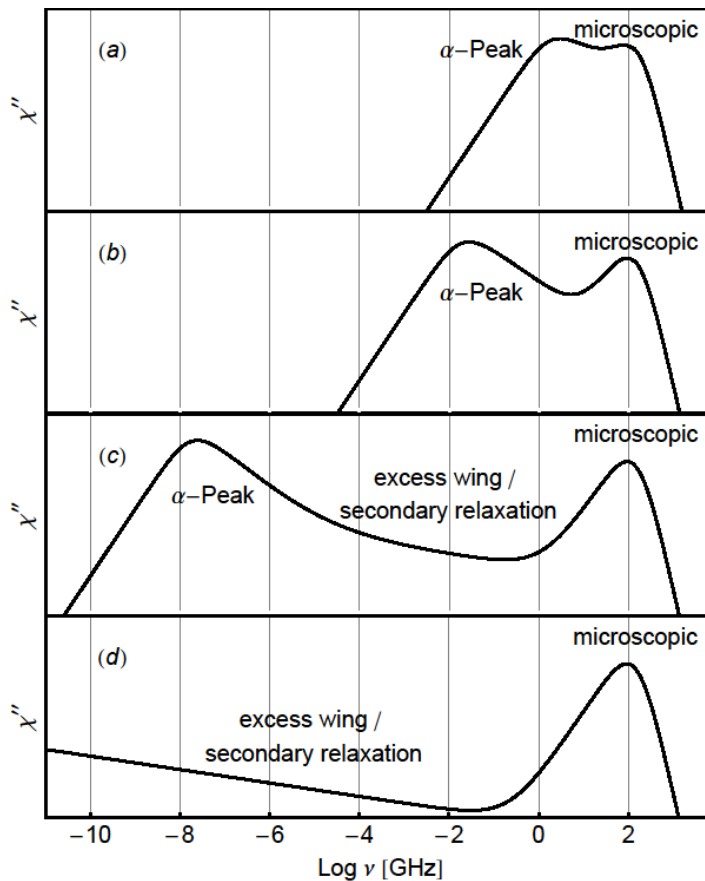


Figure 2.1 Double logarithmic sketch of the susceptibility spectrum of a typical glass former from high temperatures (a) down to low temperatures (d) as expected for a DS or DLS measurement. The α -process shifts through the frequency window, while the microscopic dynamics remain essentially unchanged.

Dynamics of liquids and glasses are usually and most conveniently studied by dielectric spectroscopy, as it comprises about thirteen decades in frequency. But at frequencies typical for a liquid, above 10^{10} Hz, experiments become complicated and resolution suffers. An example of an up to date dielectric spectrum of the glass former xylitol from the Lunkenheimer group is shown in Figure 2.2. [42] The different regimes discussed above show up, but this liquid shows a beta process instead of the excess wing, or in addition to it. Clearly, the situation sketched in Figure 2.1 (a), the merging of the α -process with the microscopic dynamics is not reached.

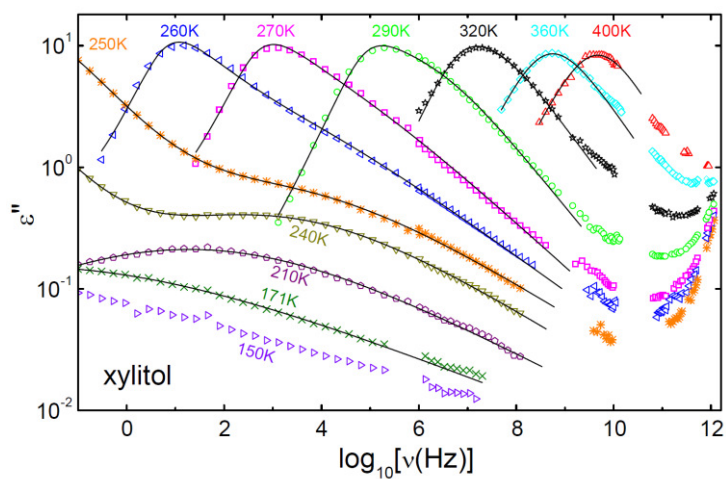


Figure 2.2 Dielectric loss spectra of xylitol at selected temperatures. Figure taken from [42].

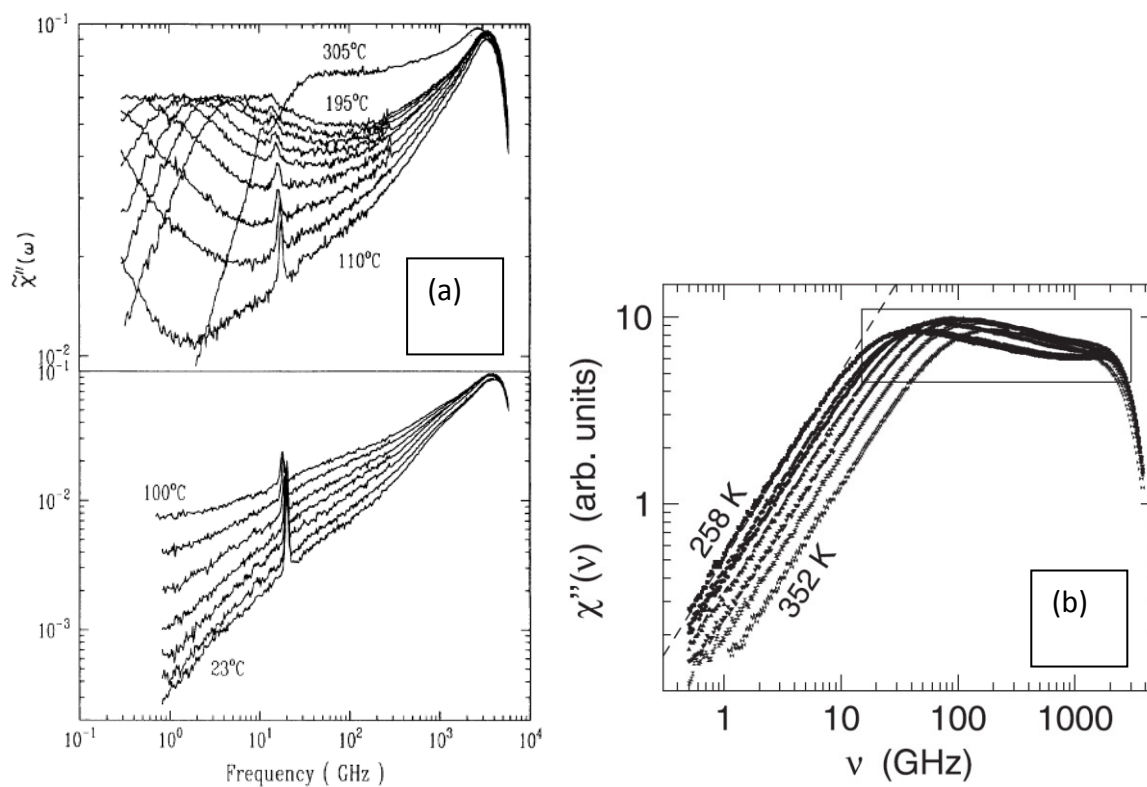


Figure 2.3 Susceptibilities measured by TFPI / DM:

(a) spectra of CKN. Figure taken from [43].

(b) spectra of benzene. Figure taken from [44].

A typical light scattering spectrum from the Cummins group, pioneering TFPI, is shown in Figure 2.3 (a).[43] Compared to dielectric spectroscopy, it comprises a much narrower spectral interval, which, yet, reaches up to highest frequencies. The merging of the α -process with the microscopic dynamics is also not reached in this case, as high enough temperatures have not been reached. In Figure 2.3 (b), the susceptibility spectrum of the highly fluid liquid benzene is shown.[44] They reached the merging, but could not follow the spectral development on super-cooling, as benzene crystallizes.

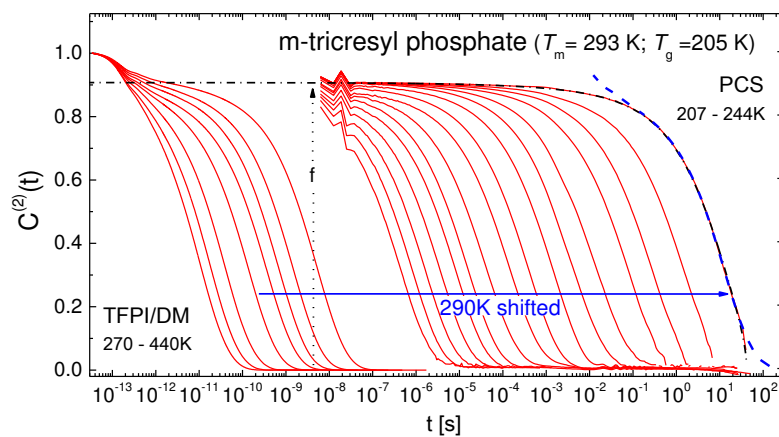


Figure 2.4 The correlation function, $C_2(t)$, obtained from photon correlation spectroscopy (PCS) as well as from tandem-Fabry-Pérot interferometry (DM/TFPI) data after Fourier transformation; dash-dotted line: fit by a Kohlrausch law including excess wing contribution, solid blue line: correlation function at $T = 290$ K shifted to coincide with that at $T = 207$ K; dotted line: amplitude f of α -process. DM/TFPI data obtained as a part of this thesis, PCS data measured by N. Petzold. Figure taken from [50].

The same behavior as sketched above in the frequency domain in Figure 2.1 can be discussed in the time domain in terms of correlation functions. As an example, Figure 2.4 shows the correlation function of m-tricresyl phosphate (m-TCP), which was obtained by PCS and DM/TFPI [50]. Covering 15 decades in time, it shows very similar relaxation features as were reported previously for o-terphenyl.[58] This representation of the data allows to explain the main relaxation features of glassy dynamics which establish when the liquid is cooled from high temperatures ($T > T_m$) down to T_g .

- At high temperatures an essentially single-step function is recognized which transforms into a two-step correlation function at low temperatures.
- Its long-time decay, determined by the α -relaxation, is invariably stretched. In most liquids the non-exponential correlation function can be well reproduced by a stretched exponential (Kohlrausch) function or by the corresponding time domain representation of the Cole-Davidson function with a temperature independent parameter β_{CD} . [59],[60]
- As the α -relaxation does not change stretching, one can write the (normalized) correlation function or the corresponding normalized susceptibility, respectively, in form of scaling laws $C(t) = C\left(\frac{t}{\tau}\right)$ and $\chi''(\omega) = \chi''(\omega\tau)$. [3],[61],[62] This property constitutes what is called the time-temperature superposition (TTS) and the frequency-temperature superposition (FTS), respectively, and it is an important property of cooperative dynamics and it persists up to the boiling point. In susceptibility representation, this is directly shown in Figure 2.5 (b).
- The relaxation strength f of the α -process is constant for all temperatures, at least the variations, which were proven to exist in the frequency domain (see Figure 3.2), are too small to be perceived in this plot.
- Interpolating the long-time tail of the correlation function with some appropriate function yields the time constants $\tau(T)$ which exhibit a super-Arrhenius temperature dependence setting in already above the melting point T_m . The temperature dependence of these time constants will be treated in detail in the next section.

Figure 2.5 (a) shows the susceptibility spectrum of 2-methyl tetrahydrofuran (MTHF), a glass former with a particularly low T_g of 92K, which was measured during this work. Due to its rather low electronic polarizability, a lot of accumulations were necessary to obtain data quality comparable to other liquids. The different regimes sketched in Figure 2.1 can be well resolved as temperatures well above the boiling point were reached. We analyzed several spectra like these and extracted parameters like high frequency slope β_{CD} and the time constants of the α -process. We developed a reproducible, quasi model independent way for their extraction. At lower temperatures, where $\tau(T) \geq 10^{-10}$ s, this is done straight forward by fitting a Cole-Davidson function at the data, which gives about the same result as reading off

the maximum frequency, often referred to as “peak picking”. But at higher temperatures, the contribution of the α -relaxation and the microscopic dynamics merge to become a broadened single peak.

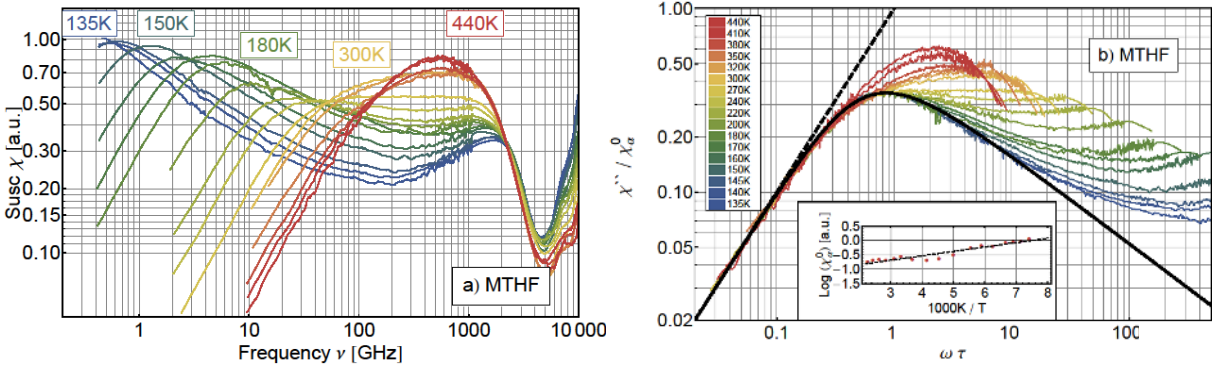


Figure 2.5 (a) Susceptibility spectra of 2-methyl tetrahydrofuran (MTHF; $T_g = 92$ K, $T_m = 137$ K and $T_b = 352$ K) obtained by applying DM/TFPI for different temperatures. (b) Susceptibility master curve obtained by rescaling the spectra shown in (a); solid line: Cole-Davidson (CD) function with $\beta_{CD} = 0.48$; dashed line: low-frequency limiting behavior $\chi''/\chi_\alpha^0 = \omega\tau$; insert: amplitude χ_α^0 of α -relaxation as revealed by constructing the master curve showing a smooth change with temperature. Figure adapted from [Pub. 2].

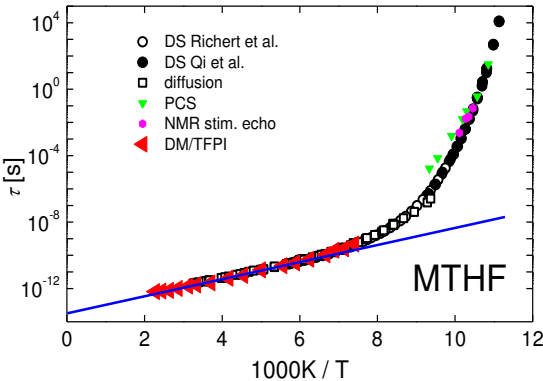


Figure 2.6 Time constants of 2-methyl tetrahydrofuran (MTHF, $T_g = 92$ K, $T_m = 137$ K and $T_b = 352$ K) obtained from different techniques (as indicated) showing a crossover to Arrhenius law at high temperatures (solid line). Figure taken from [Pub. 2].

Here, we extracted time constants by scaling the spectra to a common low-frequency envelope, explicitly $\chi''/\chi_\alpha^0 = \omega\tau$. This way of building a master curve is unique, as long as the α -process contributes to the spectrum in form of an additional shoulder. As a crosscheck, the amplitude χ_α^0 follows the temperature dependence established at low temperatures up to highest temperatures in a regular smooth way, cf. insert Fig. 2.5 (b). The time constants extracted this way are shown in Figure 2.6 and match very well with those from other methods. [Pub. 1],[45],[46]. A very large temperature interval of about 350 K is covered in the case of the low- T_g liquid MTHF and time constants down to about $5 \cdot 10^{-13}$ s are shown in this Figure, and the crossover to an Arrhenius law is clearly visible. The description of these time constants was a substantial part of this thesis and is treated in the next sections.

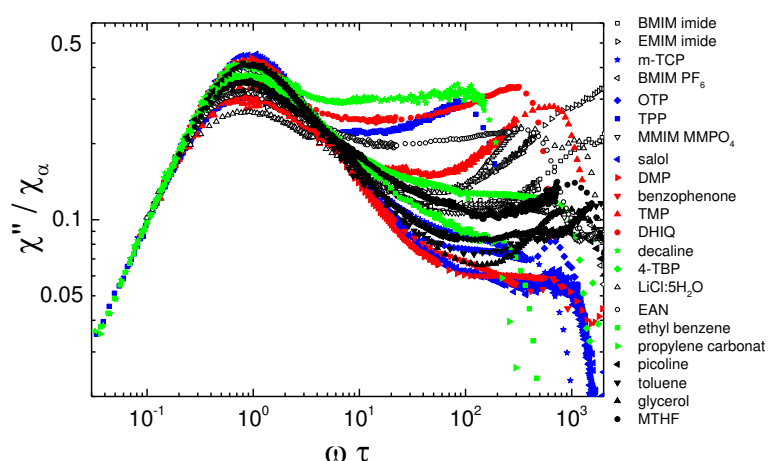


Figure 2.7 Susceptibility spectra of 22 molecular and ionic liquids (cf. Table 1 in [Pub. 4]) normalized by the intensity of the α -process and plotted versus the rescaled frequency $\omega\tau$. Pronounced differences are recognized regarding the width of the α -relaxation and the relative amplitude of the microscopic peak. Figure taken from [Pub. 4].

The spectra of all liquids are quite similar, yet there are differences. These are best recognized in Figure 2.7, where the normalized spectra of all liquids taken at comparatively low temperature, yet still displaying a full α -peak in the present frequency window, are plotted as a function of reduced frequency $\omega\tau$. For all liquids a common low-frequency envelope, explicitly $\chi''/\chi_\alpha = \omega\tau$ is found, and the different widths of the α -relaxations are

directly reflected in the heights of its peaks. In addition, one clearly recognizes a strong variation in the height of the microscopic peak.

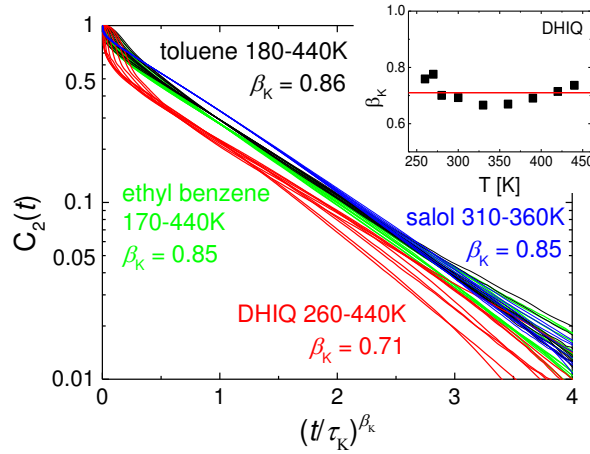


Figure 2.8 Logarithmic plot of $C_2(t)$ versus $(t/\tau_K)^{\beta_K}$ yielding linear long-time behavior. For each system, the stretching parameter β_K of the α -process is kept temperature independent. The inset shows variation of β_K around its mean value, if it was allowed to vary. Figure taken from [Pub. 4].

As stated above, the correlation function $C_2(t)$ can be approximated by a stretched exponential (Kohlrausch) function at long times at which the α -process dominates. The amplitude f describes the strength of the α -process also known as non-ergodicity parameter. The Kohlrausch parameter τ_K is related to the (mean) correlation time τ via $\tau = \tau_K \Gamma(1/\beta_K)/\beta_K$, where Γ denotes the Gamma function. The Kohlrausch function can be linearized by plotting $C_2(t)$ on logarithmic scales versus $(t/\tau_K)^{\beta_K}$ as it is shown in Figure 2.8 for TFPI/DM data obtained in this thesis. The values of β_K are system specific but not temperature dependent, and parallel straight lines are found at long times for the different systems. This plot demonstrates directly two features already partly obvious from the correlation function shown in Figure 2.4 itself. First, the relaxation stretching does not change with temperature, as the decays fall on straight lines by applying a unique β_K for each molecule, thus FTS applies. Even up to highest temperatures close to the boiling point, unchanged relaxation stretching is observed. No crossover to an exponential relaxation is recognized. Glassy dynamics, like relaxation stretching, has nothing to do with super-cooling,

even liquids which cannot be super-cooled, e. g. benzene,[44] show such glassy dynamics. Second, the amplitude f is practically temperature independent, too, yet as β_k it varies among the different systems. Below we investigate their correlation with other quantities characterizing the glass transition.

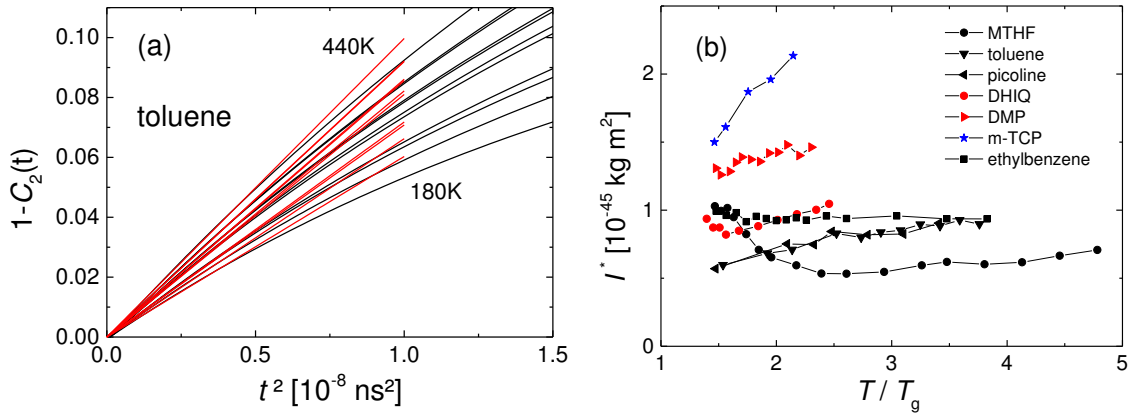


Figure 2.9 (a) $1-C_2(t)$ plotted versus squared time t^2 . The initial slope M_2 (red lines) is related to some effective moment of inertia I^* . (b) Temperature dependence of I^* for some selected liquids. Figures taken from [Pub. 4].

For short times, for the reorientational correlation function, one has $C_2(t) = 1 - M_2 t^2 + O(t^4)$, as it is an even function in time. Figure 2.5 (a) shows that correlation function can in deed be expanded in such a way, as the choice of the axis linearizes the short time behavior. In the case of linear molecules, the coefficient M_2 is related to the moment of inertia I^* via $I^* = 3k_B T / M_2$. [63],[64] Figure 2.5 (b) shows the calculated I^* for some molecules versus relative temperature. At high temperatures, this quantity is found to be temperature independent and thus being an attribute characterizing the molecule. In [Pub 4] and Figure 2.10, these inertial quantities I^* are compared with other parameters describing a given liquid.

Having measured depolarized light scattering spectra, we compared the spectra and checked for peculiarities and correlations among the parameters describing the spectra. Therefore

we characterized every liquid by a set of three parameters, which are the stretching parameter β_{CD} of the α -process, the strength of the fast dynamics $1 - f$, and the time scale at shortest times expressed by $k_B T / I^*$ with the apparent quantity I^* reflecting essentially inertia effects. All these turned out to be temperature independent and we correlated them among each other and with parameters describing the temperature dependence of the correlation time τ , namely high-temperature activation energy E_∞ , fragility m or glass transition temperature T_g .

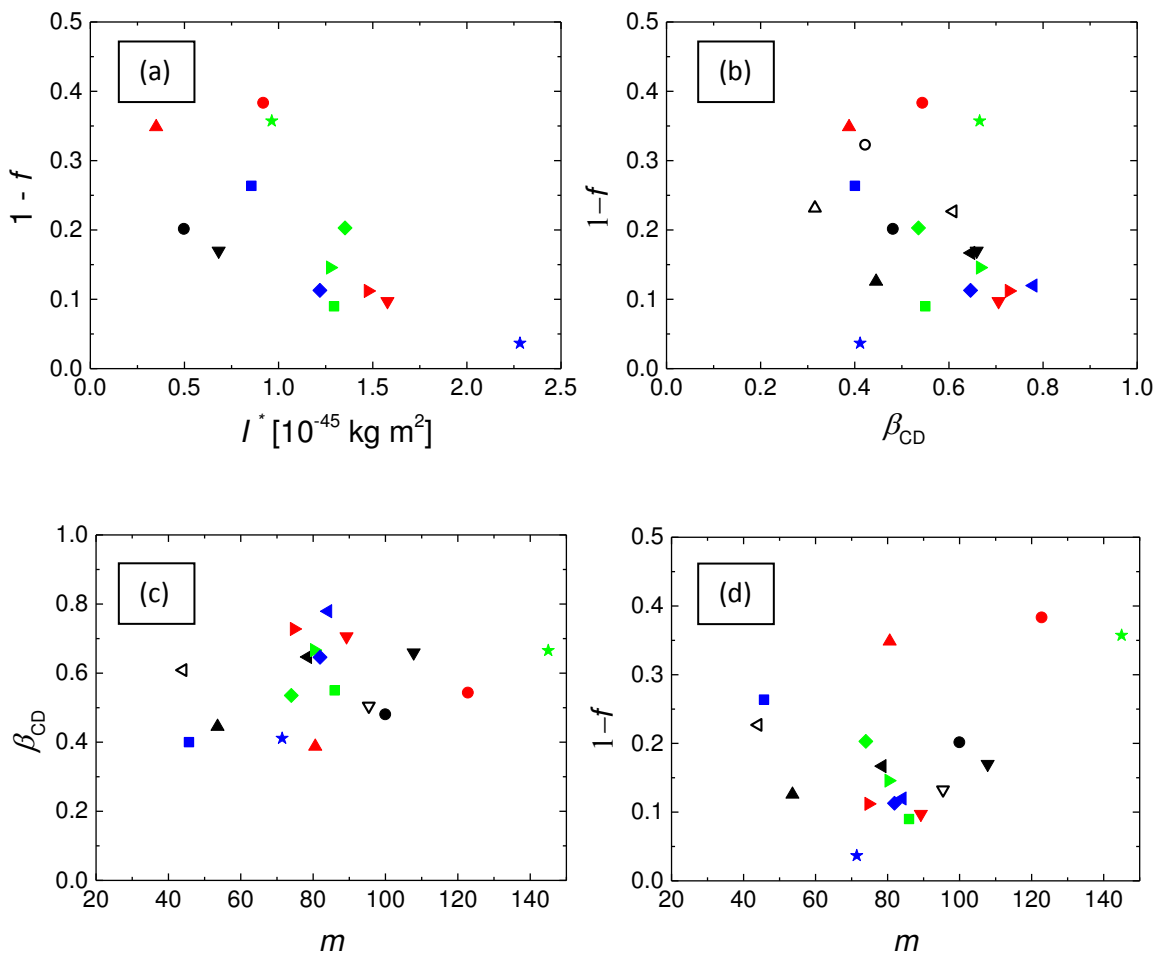


Figure 2.10 (a) Correlation between the strength of the microscopic dynamics $1 - f$ and the effective moment of inertia I^* indicating some correlations. (b) No correlation is found between the intensity of the fast dynamics $1 - f$ and the stretching parameter β_{CD} . (c) High-temperature activation energy E_∞ versus β_{CD} . (d) Correlating relaxation strength of the fast dynamics $1 - f$ and fragility index m . Taken from [Pub. 4]

One finds a trend that molecules with high molar mass M have a high quantity I^* . Of course, different molecular geometries and sizes disturb a clear cut relation between I^* and M . In Figure 2.10 (a) the quantity $1 - f$ (relaxation strength of the fast dynamics) is plotted versus I^* . With a correlation coefficient of -0.64 we find a negative correlation: The higher $1 - f$ the lower is the inertial quantity I^* . Finally, in Figure 2.10 (b) we consider the correlation among $1 - f$ and the stretching parameter β_{CD} . No, correlation is observed. The width parameter lies in the range 0.32 – 0.80; no indication for a preferential value of $\beta_{CD} = 0.5$ is found as suggested by Nielsen *et al.*[55]

We also discuss the connection between the spectral parameters and those characterizing the temperature dependence of the time scale of the α -process $\tau_\alpha(T)$, namely the high-temperature activation energy E_∞ , fragility index m , and the glass transition temperature T_g itself. In Figure 2.10 (c) the stretching parameter β_{CD} versus fragility index m is considered. Again, we do not find any correlation; relaxation stretching is independent of fragility. This is at variance with the conclusion of Böhmer *et al.*[56] which has been drawn when analyzing relaxation data close to T_g . A weak trend between $1 - f$ and fragility m may be observed in Figure 2.10 (d): the more fragile, the higher is $1 - f$. Comprising also inorganic network glasses, an opposite trend was reported by Sokolov *et al.*[57]

In all cases and all representations of the spectra, the ionic liquids do not show any particular behavior.

We are further interested in the differences between the spectra measured by different methods on the same liquid. This was mainly investigated in [Pub. 3], where dielectric spectra and those obtained from NMR have been included. Figure 2.11 (a) shows the α -peak master curves of the liquid m-tricresyl phosphate (m-TCP) as measured by Field Cycling (FC) ^1H NMR, photon correlation spectroscopy (PCS) and from dielectric spectroscopy (DS). DS probes rank-one correlation function $C_1(t)$ while LS and NMR probe a rank-two correlation function $C_2(t)$. At highest frequencies, the amplitude of the excess wing differs by a factor of about three, as would be expected when assuming that the reorientation is highly hindered and proceeds via small angle steps,[47]-[49] while the exponent of the excess wing appears to be about the same.

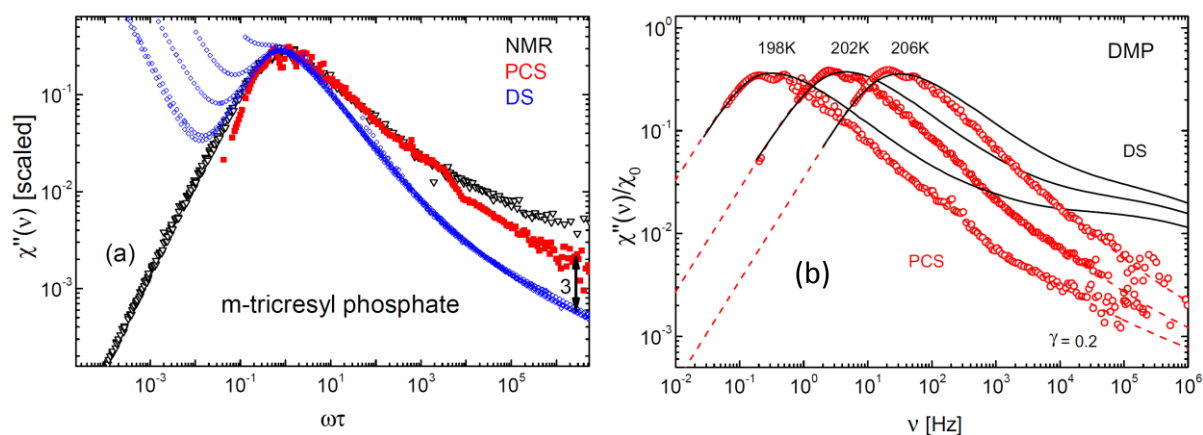


Figure 2.11 (a) Comparing susceptibilities of m-tricresyl phosphate as obtained from PCS (red squares, measured by N. Petzold), from Field Cycling (FC) ^1H NMR (black triangles, measured by M. Hofmann) and dielectric spectroscopy (blue diamonds, measured by R. Kahlau); (b) Comparison of the susceptibility of dimethyl phthalate (DMP) from photon correlation spectroscopy (PCS, measured by N. Petzold) and from dielectric spectroscopy (DS, measured by R. Kahlau); the slow β -process is not probed by PCS, instead an excess wing is observed; adapted with permission from ref. [50]. Figures taken from [Pub. 3].

Many glass formers show in addition or instead of an excess wing a β -process, which is a secondary relaxation caused by small angle motion, for example seen in the dielectric spectrum in Figure 2.11 (b). There, the dielectric spectra are compared with the PCS results for DMP after transforming the time domain data into the frequency domain at quite the same temperatures. The β -process is not recognized in DLS, although a well resolved excess wing is found. Therefore one may draw the conclusion that the excess wing is a different phenomenon than the β -process and it shows quite universal features whereas relaxation strength and spectral width of the β -relaxation vary and depend on the probing technique.

The identification of different power-laws dominating the correlation loss is done most conveniently in the pulse-response representation of the DLS data. This is shown for the molecular liquids m-TCP, toluene, salol, DMP and the room temperature ionic liquids (RTIL) EAN on a reduced time scale t/τ in Figure 2.12 (a).[Pub. 4] Indeed, in the case of salol, two power-laws are well discernible. On the one hand, the intermediate power-law at short times with an exponent $1 - \gamma = 0.8$ and on the other hand a second one at longer times with

exponent $1 - \beta_{CD} = 0.21$. The latter is the short-time decay or high-frequency contribution of the α -process and is called the von Schweidler law. It is somehow surprising that the intermediate power-law can be identified in this representation, although no traces of it are recognized in the susceptibility representation (*cf.* Figure 2.17). Even in the case of the ionic liquid EAN, the intermediate power-law is found, despite the stretching exponent $1 - \beta_{CD} = 0.61$ of EAN is quite close to that of the intermediate power-law. As has been discussed by Brodin and coworkers [51]-[53], the intermediate power-law [16] is nothing else than the excess wing usually identified in dielectric spectroscopy (*cf.* Figure 2.11 (b)). As molecular liquids (full symbols) as well as (RTIL, open symbols) are included in this Figure (and in Figure 2.7), we can draw the obvious conclusion that RTIL do not show any striking differences in their DLS spectra compared with molecular liquids. This is somewhat surprising, as RTIL show peculiarities in DS spectra.[54]

By plotting the position of the minimum vs. position of the α -peak, as is done in Figure 2.12 (b), a kink in the power-law behavior is found. We attribute this to the emergence of the excess wing, which influences the minimum position, but not that of the maximum. This kink is found for all liquids around $\tau \cong 10^{-9}$ s.

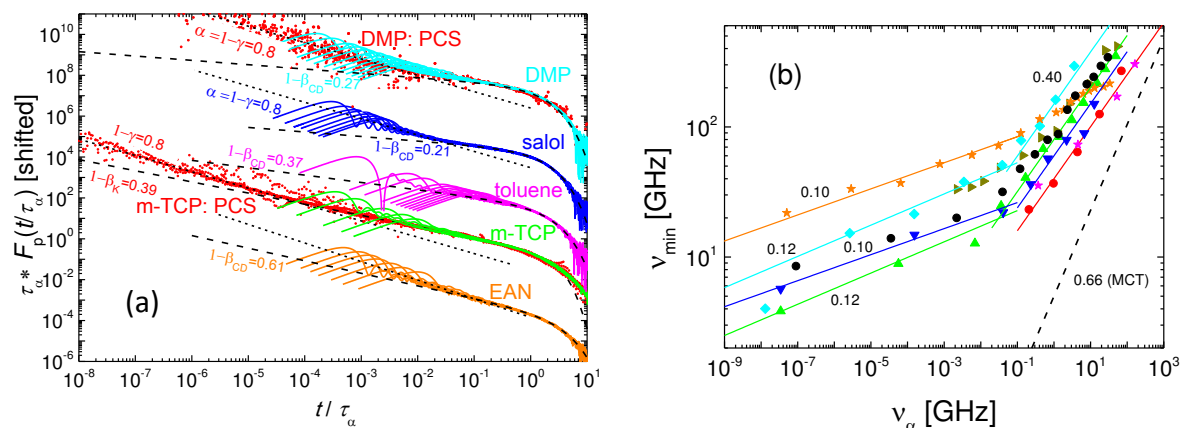


Figure 2.12 (a) Pulse-response representation of the DLS data for the four molecular liquids m-TCP, toluene, salol, DMP and the ionic liquid EAN obtained by PCS (points) and TFPI/DM (lines). The excess wings are indicated by dotted lines, whereas the dashed lines mark the α -process. (b) ν_{min} plotted vs. ν_α , solids lines reflect high and low temperature power-laws with slopes indicated; dashed lines: MCT prediction. Figures adapted from [Pub. 4] and [Pub. 5].

3.2.2 Time Constants of the α -process

Concerning time constants τ of the α -process, the well established interpolation function by Vogel, Fulcher and Tammann [65] is widely used, although it is known that it does not work when a large temperature range is taken into account. Sometimes two VFT-interpolations are given to one dataset, one for high and one for low temperatures.[66] There are also some theoretical issues on the *free volume theory*, on which the VFT equation is based, as the divergence at a finite temperature.[67] Recently, Mauro *et al.*[68] discussed an interpolation formula which we and others [69] found not to work that much better than VFT, compare Figure 2.13 (a). Usually those interpolation formulae work rather well on the description of the data around T_g and do not set much focus on highest temperatures ($T > T_m$). Having measured high temperature time constants, we decided to go the opposite way and start the description from this side.

The analysis of Stickel *et al.*[66] has shown that for molecular glass formers the Arrhenius regime is reached by dielectric experiments in some cases. However, the analysis included only time scales below 10^{10} Hz, which is not always sufficient to reach the high-temperature range. There are also some theoretical considerations on the behavior of time constants in liquids.[70]-[75]

Mode-Coupling theory also provides a prediction on the temperature dependence of the time constants, but only for temperatures above a critical temperature T_c which is located between T_g and T_m . [76]

There are also approaches for a parabolic interpolation of the time constants by Elmatad *et al.* [77] (Figure 2.13 (b)). This form could be interpreted in terms of a random energy model, where activation barriers are assumed to be distributed as Gaussian variables. From the Boltzmann distribution, they predict an activation energy that grows as $1/T$, so that $\log \tau$ grows as $1/T^2$. But this interpolation does of course not cover high temperature behavior as well.

Publications 1 & 2 deal with the description of time constants, as a new interpolation formula was developed and tested.

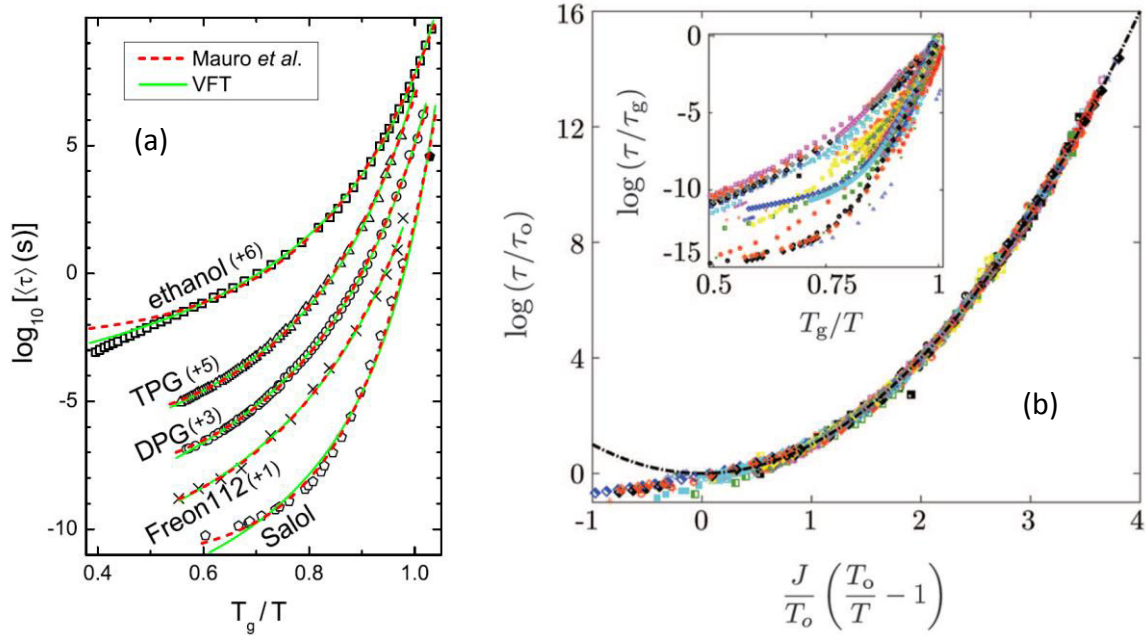


Figure 2.13 (a) Scaled Arrhenius plots ($\log \tau$ vs. reduced inverse temperature T_g/T) of the average relaxation times with fits using VFT and the expression by Mauro *et al.*[68] Figure taken from [69]. (b) Collapse to a parabolic form of the structural relaxation times, τ , and viscosities, η , as functions of temperature T for fragile glass forming liquids. Parameters τ_0 (sets time scale), T_0 (sets temperature scale), and J (sets energy scale) are determined by scaling. The inset shows the same data when graphed in Angell-type plot. Figure taken from [77].

As we measured $\chi''(\omega)$ up to high temperatures (around the boiling point), we combined $\tau(T)$ for a series of glass formers collected from dielectric spectroscopy and dynamic light scattering covering a range $10^{-12} \text{ s} < \tau(T) < 10^2 \text{ s}$. Some examples are shown in Figure 2.13 with interpolations by the VFT-equation, the interpolation formula by Mauro *et al.*[68] and our own approach (which will be explained below), which all have three parameters. A more comprehensive plot of the time constants is shown in Figure 2.14(a). In the case of the high- T_g system o-terphenyl the approaches by VFT and by Mauro *et al.* fail to interpolate the data in particular at high temperatures. Yet, VFT works rather well for the low- T_g liquid MTHF for which again the Mauro *et al.* approach fails. In contrast our current approach interpolates the data rather well in all cases. The high-temperature behavior is well reproduced by an Arrhenius law, in the case of MTHF, it is observed over more than 250 K. This is also proven

by Figure 2.17, where the activation energy is plotted versus temperature. Constant activation energy corresponds to Arrhenius behavior. Consequently, in such well studied systems the high-temperature activation energy E_∞ can be assessed model independently.

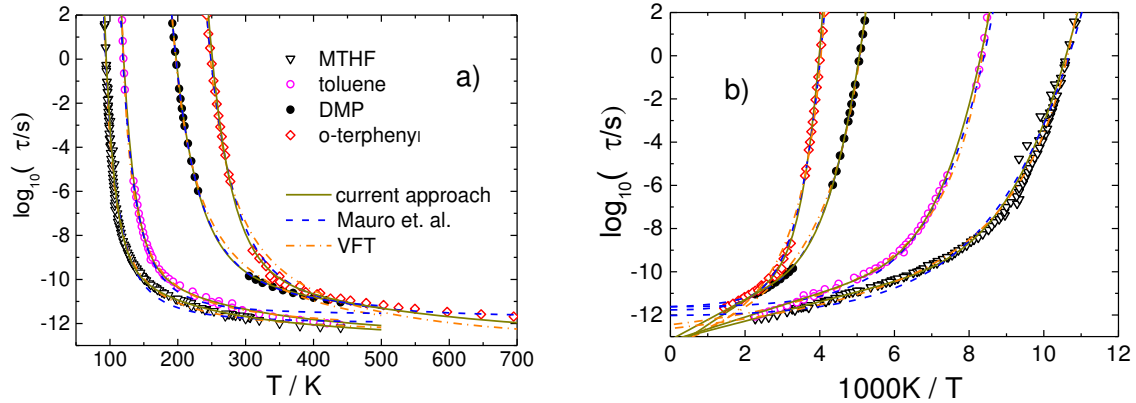


Figure 2.14 Reorientational correlation time of 2-methyl tetrahydrofuran (MTHF), toluene, dimethyl phthalate (DMP) and o-terphenyl (OTP) plotted versus temperature (a) and versus inverse temperature (b); Interpolation by VFT-equation, interpolation by Mauro *et al.* and current approach (eq. 3.1). Figure taken from [Pub. 2]

Tarjus *et al.* [71] already discussed the time constants in terms of temperature dependent activation energies $E(T)$

$$\tau = \tau_\infty \exp\left(\frac{E(T)}{k_B T}\right) \quad (2.1)$$

and interpreted its increase at low temperatures with increasing cooperativity. They gave a power-law dependence of $E(T)$ on temperature:

$$E(T) = \begin{cases} E_\infty & \text{for } T > T^* \\ E_\infty + B(T^*) \left(1 - \frac{T}{T^*}\right)^{8/3} & \text{for } T < T^* \end{cases} \quad (2.2)$$

This corresponds to a decomposition in a low temperature non-Arrhenius regime ($T < T^*$) and a high temperature ($T > T^*$) regime with constant activation energy. But these approaches are not fully accepted yet.

Analogously, describing the dynamics in terms of an activation energy $E(T)$, we distinguish a high-temperature regime characterized by an Arrhenius law and a low-temperature regime. The Arrhenius regime has been observed since quite long ago in non-glass forming systems,[78],[79] although it's activation energy is not connected to a single particle barrier. In deed, we found an Arrhenius behavior for all liquids investigated and, inspired by the approach by Tarjus *et al.* (eq. 2.1), mapped $\tau(T)$ on an temperature dependent activation energy $E_{coop}(T)$ via

$$\tau(T) = \tau_{\infty} \exp\left[\frac{E_{\infty} + E_{coop}(T)}{T}\right], \quad (2.3)$$

where E_{∞} is the constant high-temperature activation energy and τ_{∞} a pre-exponential time on the order of 10^{-13} s. The quantity $E_{coop}(T)$ reflects the cooperative dynamics becoming dominant at low temperature, and its properties have been discussed by several authors. [72],[75],[80],[81]

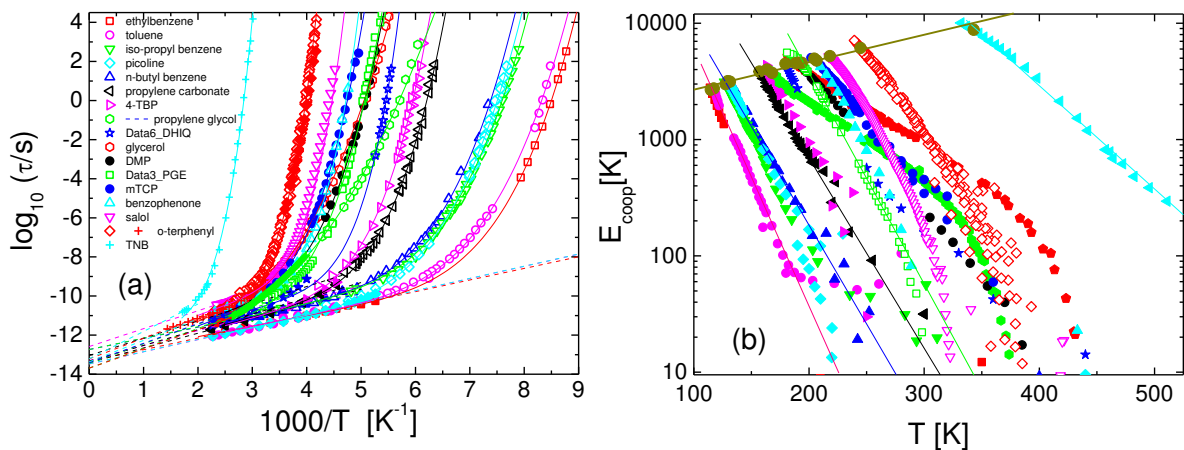


Figure 2.15 (a) Reorientational correlation times of molecular liquids obtained by dielectric spectroscopy (open symbols) and dynamic light scattering (full symbols). Viscosity data for o-terphenyl, trisnaphthyl benzene (TNB) and propylene glycol (crosses); for toluene, ^2H NMR data have been included; straight dashed lines: high-temperature Arrhenius behavior; solid lines: full fit by eq. (3.1). (b) $E_{coop}(T)$ in a semi logarithmic plot; straight lines signal exponential dependence in particular for low- T_g liquids. Marked points indicate $E_{coop}(T_g)$.

Figure taken from [Pub 1].

Inspecting $E_{coop}(T)$, we found it can best be described by an exponential function decaying with temperature, as it is shown in Figure 2.15 (b), like

$$E_{coop}(T) \propto \exp[-cT] \quad (2.4)$$

with a slope parameter c . We attribute deviations from this exponential behavior (especially seen in the cases of the non-fragile glass formers glycerol and propylene carbonate) to a slight overestimation of the high temperature activation energy E_∞ . Taking a closer look to $E_{coop}(T)$, there was another peculiarity: $E_{coop}(T_g)$ seemed to be proportional to T_g itself. This is illustrated by the marked points in Figure 2.15 (b), which form a straight line. But why should the “man-defined” glass transition temperature T_g be extraordinary? We updated equation (2.4) by introducing an energy scale, E_∞ , and a reference temperature T_A , which is defining an isoenergetic point by $E_{coop}(T_A) = E_\infty$:

$$E_{coop}(T) = E_\infty \exp\left[-\lambda\left(\frac{T}{T_A} - 1\right)\right]. \quad (2.5)$$

Herein λ is introduced as a “generalized fragility parameter” [Pub. 1] which controls the “steepness” of $E_{coop}(T)$. Four fit parameters, namely τ_∞ , E_∞ , λ and T_A are needed to describe the full temperature dependence of $\tau(T)$ in the present state of analysis. This four-parameter description of $\tau(T)$ provides very satisfying interpolations.

In Figure 2.16 (a) the apparent activation energy $E_A(T)$ as given by the derivative of $\tau(T)$ with respect to the reciprocal temperature $1/T$ is shown with interpolations included. In this representation, strong evidence is found that the apparent activation energy finally becomes constant at highest temperatures. The present approach captures all features of $\tau(T)$; in particular, the crossover to E_∞ at highest temperatures is well reproduced. Of course this is not unexpected, as our approach was constructed that way.

In Figure 2.16 (a), it appears that the lower E_∞ , the more the onset of cooperative dynamics shifts to lower temperatures. In other words, this is a model independent hint that T_A and E_∞ are likely to be correlated. Thus, we plotted the reduced activation energy $E_A(T)/E_\infty$ vs. T/E_∞ in Figure 2.16 (b). Within the scatter of the data a universal dependence is observed. MTHF

and OTP, for example, systems with rather different T_g as well as E_∞ display very similar behavior. Not surprising, fragility parameters m are quite alike in these systems.

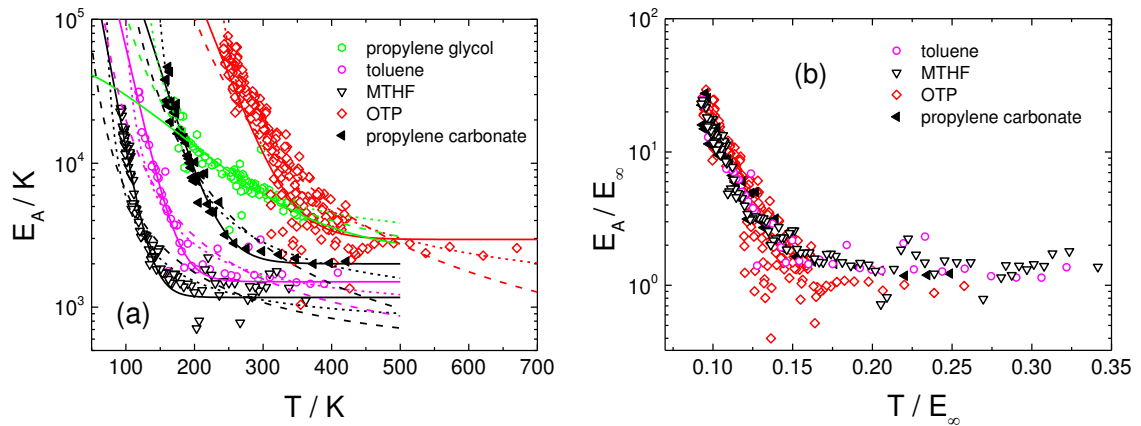


Figure 2.16 Apparent activation energy $E_A(T)$ for selected molecular liquids as function of (a) temperature; dotted lines: VFT equation [65], dashed lines: interpolation by Mauro *et al.*[68], and solid lines: our current model (eq. (3.1)). (b) Reduced activation energy $E_A(T)/E_\infty$ vs. T/E_∞ . Figure adapted from [Pub. 2].

We found a strong correlation between E_∞ and T_A , which can best be expressed by $T_A = bE_\infty$, with $b \cong 0.104$, as displayed in Figure 2.17. This numerical value is, of course, obtained by an optimization and may change slightly if different liquids are considered. The resulting values of T_A are between 1.1 and 1.2 T_g , and thus possibly close to T_c of mode coupling theory. This correlation leads to a three parameter interpolation (equation (3.1)) of the time constants $\tau(T)$ of the α -process. All the fits shown in Figures 2.14, 2.15 and 2.17 (a) are done with three parameters and lead to very satisfying interpolations. Mirigan and Schweizer recently discussed our approach as a “phenomenological 2-barrier model” in terms of the “Elastically Cooperative Nonlinear Langevin Equation (ECNLE)” theory and found similar values of T_A/T_g and $E_{coop}(T_g)/E_\infty$. Therefore they found our model to be consistent with the ECNLE theory. [82]

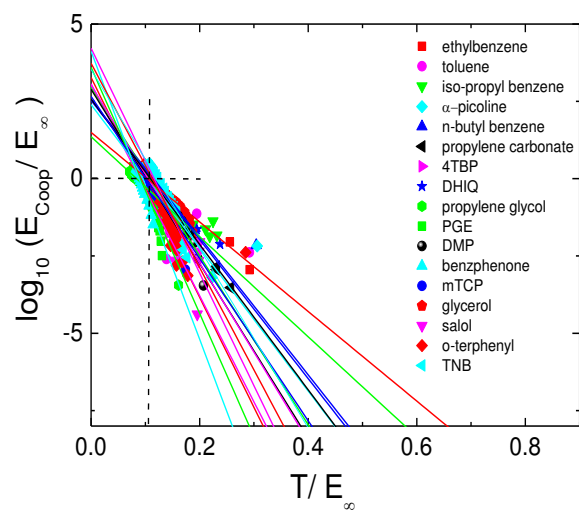


Figure 2.17 “generalized Angel plot”: Reduced energy $E_{\text{coop}}(T)/E_{\infty}$ versus reduced temperature T/E_{∞} , dashed lines mark optimal intersection. Figure taken from [Pub. 1]

3.2.3 Theories of the Glass Transition

Overview

Mode-coupling theory (MCT) is a microscopic theory of liquids which takes an N -particle-problem as a starting point. It was first introduced by Kawasaki, who was interested in the description of a liquid approaching its critical point.[83] In 1984 the theory was extended to dense liquids by Bengtzelius, Götze and Sjölander,[84] and Leutheusser.[85] Therefore the theory begins with the description of the onset of glassy dynamics beginning from high temperatures, which means from the liquid state. Later the approach was extended to molecular liquids with rotational degrees of freedom.[86]-[89] As Review Articles, the publications of Schilling, Götze, Das and Cummins have to be mentioned.[90]-[94]

The relevant time scale is the GHz-Regime, where the glassy dynamic separates from the microscopic (vibrational) dynamics, the latter is located in the THz-Regime. Hence the predictions of mode-coupling theory can be compared to results obtained by dynamic light scattering, optical Kerr effect spectroscopy, neutron scattering and in some cases also dielectric spectroscopy.[14],[69] Mode-coupling theory can also be used in analyzing molecular dynamic simulations data, as it was shown by Barrat, Kob and Sciortino.[34],[95]-[97] Even experiments on colloidal systems can be described. [92],[98],[99]

It has to be mentioned that there is another microscopic theory of the glass transition, the *replica theory*.[100][101] It is based on the *spin glass theory* developed by Kirkpatrick and Thirumalai,[102] but no details on the shape of the susceptibility spectrum have been worked out yet. Another explanation of the glass transition was given by the theory of *frustration limited domains*.[81][103] Caused by the dominance of locally favored structures, which are incompatible to long range ordering, frustration phenomena show up. (cf. equation 2.2)

Another view on the glass transition is known as *potential energy landscape*.[104]-[108] In this model, the state vector, containing all the particles coordinates moves on a potential energy landscape. This view is particularly useful for low temperatures, as the time development of the system can be described as the sum of vibrations in the local minima

and erratic jumps between these minima. The shape of the potential energy landscape is, according to Angell,[104],[105] depending on the fragility of the liquids. In fragile liquids, the minima of the potential energy landscape can be divided in so-called *metabassins*. Molecular dynamic simulations have shown that transitions between these *metabassins* are involved in the α -process.

MCT in Detail

Here we sketch mode coupling theory (MCT) and especially the schematic F₁₂ model in more detail, as it was used to describe the DLS spectra of the present work. Starting point of the mode coupling theory is a generalized Langevin equation for the correlation function connected to the wave vector q with a memory kernel $M_q(t)$:

$$0 = \Omega_q^{-2} \ddot{\phi}_q(t) + \phi_q(t) + \int_0^t M_q(t-t') \dot{\phi}_q(t') \quad (2.6)$$

The memory kernel $M_q(t)$ is split in a fast part, which can be approximated by a delta function giving a damping term and a slow part $m_q(t)$. In mode coupling theory, this $m_q(t)$ is expanded in a series of polynoms of density fluctuations. Then all terms are expressed as products of correlation functions. In first order, one gets

$$m\{\phi(t)\} = \sum_{p+k=q} V_{qpk} \phi_p(t) \phi_k(t) \quad (2.7)$$

With the coefficients V_{qpk} depending only on the static structure factors $S(q)$, $S(p)$ and $S(k)$. The dynamics of the system is completely determined by equation (2.7). The correlation functions decay, depending on the values of V_{qpk} and the temperature to zero or to a finite value $f_q(T)$, which can be interpreted as a Debye-Waller factor.

$$\phi_q(t \rightarrow \infty) = \begin{cases} 0, & T > T_c \\ f_q, & T < T_c \end{cases} \quad (2.8)$$

For temperatures higher than the critical temperature T_c , $\phi_q(t)$ first decays down to a plateau value of $f_q(T)$ then, for longer times, it finally decays down to zero. This relaxation models the α -process.

Mode coupling theory predicts a divergence of the relaxation times of the α -process on approaching T_c . The experimentally found critical temperatures are well above the glass transition temperature T_g , the predicted divergence is not observed. This is explained with the approach that the relaxation via density-density coupling (described by equation (2.7)) freezes out, but other transport mechanisms, which are not included in the theory (as *phonon assisted hopping*), survive or take over. They keep ergodicity of the system between T_c and T_g .

The Asymptotic Scaling Laws

There is no analytical solution for equation (2.7) and the exact values of all the coefficients V_{qpk} are unknown. But numerical solution for some reasonable assumptions on the V_{qpk} can be obtained. These solutions were expanded around the plateau at $\phi_q(t = t_\sigma) \cong f_q$, which describes the transition between the fast microscopic dynamics and the final α -relaxation. A scaling law with an amplitude h_q and a scaling function $g_\lambda(t/t_\sigma)$ is found

$$\phi(t) = f_q + h_q g_\lambda(t/t_\sigma) \quad (2.9)$$

As asymptotic cases, one has

$$g_\lambda(t) \propto \begin{cases} t^{-a}, & t < t_\sigma \\ -t^b, & t > t_\sigma \end{cases} \quad (2.10)$$

Where the exponents a and b are defined by the exponent parameter λ :

$$\lambda = \frac{\Gamma^2(1-a)}{\Gamma(1-2a)} = \frac{\Gamma^2(1+b)}{\Gamma(1+2b)} \quad (2.11)$$

Herein Γ denotes the gamma function. Equation (2.10) predicts a scaling rule around the plateau and this defines the shape of the minimum between the fast dynamics and the α -process in the susceptibility spectrum. This is shown for the case of salol in Figure 2.18. Here, the MCT prediction for the minimum (equation (2.12)) indeed interpolated the minima. These are scaled to a common master curve, what proves the temperature independence of the exponents a and b .

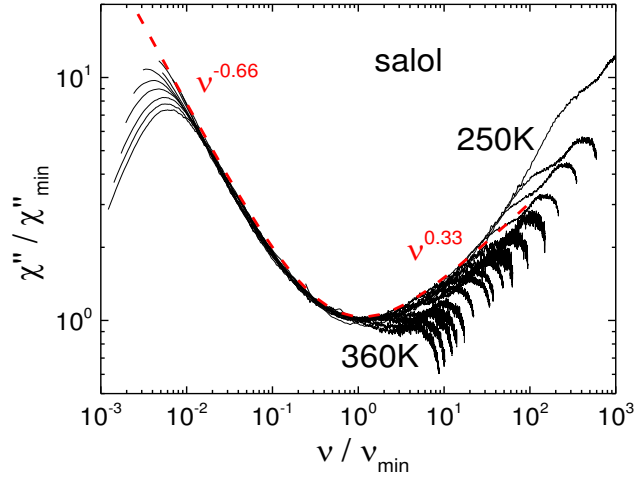


Figure 2.18 Master curve (“minimum scaling”) for the susceptibility minimum for salol (250 – 360 K) with interpolation according to the asymptotic laws of MCT (dashed red line, equation 2.12). The exponents a and b are not independent, as they are linked by equation (2.11). Figure taken from [Pub. 5].

Equation 2.10 implies that mode coupling theory gives the interpolation function for the susceptibility minimum

$$\chi(\nu) = \chi_{\min} \left(b \left(\frac{\nu}{\nu_{\min}} \right)^a + a \left(\frac{\nu}{\nu_{\min}} \right)^{-b} \right) / (a + b), \quad (2.12)$$

where χ_{\min} and ν_{\min} are the frequency and amplitude of the minimum. For their temperature dependence, one expects

$$\begin{aligned} \chi_{\min} &\propto (T - T_c)^{1/2} \\ \nu_{\min} &\cong 1/t_\sigma \propto (T - T_c)^{1/2a} \end{aligned} \quad (2.13)$$

Using this proportionality, T_c can be obtained by extrapolating experimental data by plotting rectified amplitudes and positions of the minimum versus temperature. Mode coupling theory also predicts a scaling of the α -process, this means that normalized correlation function follows a temperature independent shape.

$$\phi(t) = F\left(\frac{t}{\tau_\alpha} \right) \quad (2.14)$$

This statement is equivalent to the time-temperature superposition discussed above. Further, for the relaxation times of the α -process a power-law is found

$$\tau \propto |\sigma|^{-\gamma_{MCT}} = |\sigma|^{-\frac{1}{2a} - \frac{1}{2b}} \quad \text{for } T > T_c \quad (2.15)$$

with the reduced temperature $\sigma = \frac{T - T_c}{T_c}$.

As the temperature dependence of relaxation times is treated in detail in this work, a check of this relation is done (in [Pub. 5]). One may be tempted to state that relation (2.15) contradicts our new interpolation formula (equation (3.2)) for time constants. Figure 2.19 shows our current interpolation function (equation (3.2)) with typical values ($\tau_\infty = 5 \cdot 10^{-14}$ s, $E_\infty = 2500$ K, $\mu = 60$) scaled in a way that linearizes equation (2.15). The spectral parameter were assumed to be $a = 0.33$ and $b = 0.66$, what corresponds to $\gamma_{MCT} = 2.27$. One finds that in deed, for high temperatures, a linear behavior is found as equation 2.12 predicts and a value for T_c can be extracted. This of course is not a mathematical proof, but it shows that different approaches may indeed lead to similar asymptotic behavior. The dependence of these T_c from the values τ_∞ , E_∞ and μ was not investigated in this work.

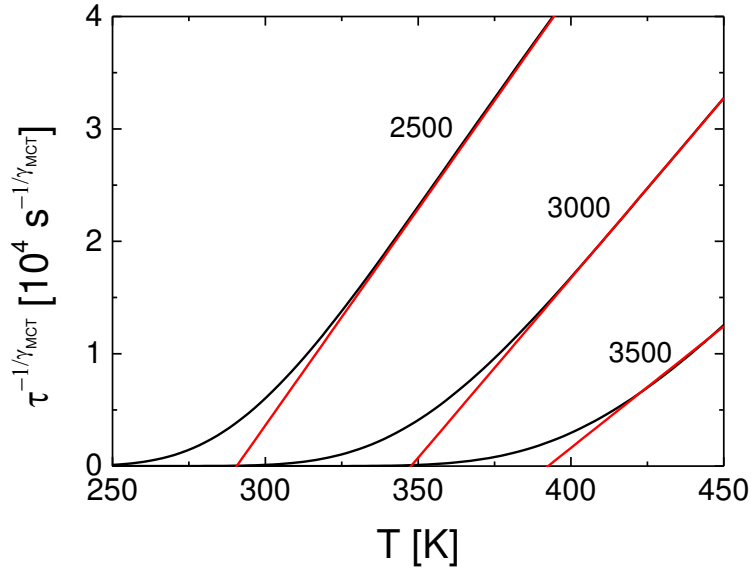


Figure 2.19 Calculated time constants by our new approach (equation (3.2)) with typical values ($\tau_\infty = 5 \cdot 10^{-14} \text{ s}$, $\mu = 60$, E_∞ [K] indicated in the Figure) scaled to linearize the prediction by MCT (equation (2.15)).

One expects the asymptotic scaling laws of MCT (equations (2.13) and (2.15)) to be valid as one approaches the critical temperature from the liquid regime. Close to T_c , yet above the glass transition temperature T_g , other relaxation processes, are believed to become more and more important and lead to a breakdown of MCT scaling laws. Therefore there is no well-defined temperature interval in which the scaling laws are expected to hold.

An alternative way to these scaling laws is the analysis of the full spectra by an approach called schematic model. In this model, one gets the complete correlation function including α -process and microscopic dynamics as the solution to a simplified set of differential equations still containing the essential nonlinear feedbacks, therefore it allows the analysis and discussion of the spectra beyond the regime of applicability of the scaling laws.[76]

The F_{12} Model

One weakness of the above presented scaling laws (equations (2.13) and (2.15)) is that it is not clear from the beginning in which temperature interval they are valid. As they are an expansion around T_c , one expects deviations at higher temperatures. Near T_c , however, MCT predicts a divergence of time constants not found in experimental data. The relaxation process described by MCT gets more and more inefficient and other processes gain dominance. Therefore one expects a collapse of the scaling laws also near T_c .

The approach of the F_{12} model is to solve equation (2.6) numerically with some reasonable assumptions made. For this schematic model, equation (2.7) is reduced to only two correlators, which are not derived from interaction potentials, but instead have to be taken as parameter showing smooth temperature dependence.

The origins of this model go back to the description of the so-called *tagged-particle* movement in atomic liquids, where also a memory kernel (compare equation (2.21)) for the coupling of $\phi_s(t)$ to $\phi(t)$ was used, while $\phi(t)$ was modeled by an exponential relaxation only.[109]-[113] A model describing $\phi_s(t)$ as well as $\phi(t)$ self consistently with memory kernels was first introduced for the description of the glass transition.[84]

This model was already applied to several glass formers.[116]-[119] The capability of the F_{12} model to even describe distinctly non-glassy dynamics at high temperatures was already demonstrated for the non-glass forming liquid benzene by Wiebel and Wuttke.[44] It's applicability on OKE results have been shown for instance in the case of benzene and recently for water.[120],[121] The theoretical background was extensively treated by Götze and Voigtmann,[122] and the numerical stability of the fits was confirmed by a numerical analysis.[123]

One reduces equation (2.3) to one component $\phi(t)$, with a damping constant γ and takes a polynomial of $\phi(t)$ to describe the slow memory kernel $m(t)$.

$$0 = \Omega^{-2} \ddot{\phi}(t) + \gamma \dot{\phi}(t) + \phi(t) + \int_0^t m(t-t') \dot{\phi}(t') \quad (2.16)$$

$$m(t) = \sum_{n=1}^N v_n (\phi(t))^n \quad (2.17)$$

This is called the F_N -model. For being able to calculate a numerical solution, only a finite number of summands can be considered. The most simple case of $N=1$ is only able to describe exponential decay of $\phi(t)$ and is therefore inadequate for the description of real liquids. One faces the same problem for all other F_N -models with only one term of arbitrary power. The simplest non-trivial model is the F_{12} model, where the memory kernel is given by

$$m(t) = v_1 \phi(t) + v_2 (\phi(t))^2, \quad (2.18)$$

but it already provides nearly all relevant details found in experimental spectra.[114]

In the v_1/v_2 parameter space, one may discriminate areas describing ergodic (liquid) from those describing nonergodic (glassy) states. The critical crossover can be parameterized by the exponent parameter λ , already used in the asymptotic laws.

$$\begin{aligned} v_1^c &= \frac{2\lambda - 1}{\lambda^2} \\ v_2^c &= \frac{1}{\lambda^2} \end{aligned} \quad (2.19)$$

Therein λ is limited to values between 0.5 and 1. The shape of the crossover in the v_1/v_2 parameter space is displayed in Figure 2.20, together with some sets of parameters v_1 and v_2 that model experimental spectra.

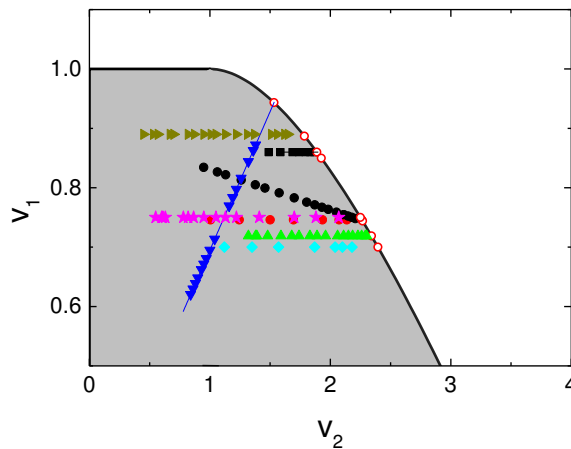


Figure 2.20 v_1/v_2 parameter space with the transition between liquid and glassy state parameterized by the exponent parameter λ . Open red circles show extrapolated critical parameters. Figure from [Pub. 5]

In order to be able to calculate experiment-like spectra, one needs to introduce another correlator $\phi_s(t)$, which describes the coupling of the experimental observable to the correlator $\phi(t)$. It obeys the same equation as $\phi(t)$ itself does

$$0 = \Omega_s^{-2} \ddot{\phi}_s(t) + \gamma_s \dot{\phi}_s(t) + \phi_s(t) + \int_0^t m_s(t-t') \dot{\phi}_s(t') \quad (2.20)$$

with slightly different values for the frequency Ω_s and the damping ν_s and the memory kernel [115]

$$m_s(t) = \nu_s \phi(t)_s \phi(t), \quad (2.21)$$

wherein $\phi(t)$ resembles a solution to equation (2.17). By this construction, it is ensured that $\phi_s(t)$ is coupled to $\phi(t)$, but there is no feedback from $\phi_s(t)$ to $\phi(t)$ itself. As one describes spectra obtained by different measurement techniques, it is expected that the values of Ω , γ , ν_1 and ν_2 are equal as they describe the dynamics of the system itself, whereas the values of Ω_s , γ_s and ν_s are expected to vary as they describe the method dependent coupling to the dynamics of the system. So in total, there are seven parameters and one amplitude to be determined by fitting the experimental susceptibility spectrum. The values of Ω , γ , Ω_s and γ_s are mainly responsible for the microscopic dynamics and the boson peak and can be kept constant for all temperatures. In contrast, the values of ν_1 and ν_2 are approaching the critical crossover line in the ν_1/ν_2 parameter space on cooling down a liquid (see Figure 2.20 and 2.22 (a)). The parameter ν_s describes the relative amplitude of the α -process and is in most cases constantly increasing on decreasing temperature.

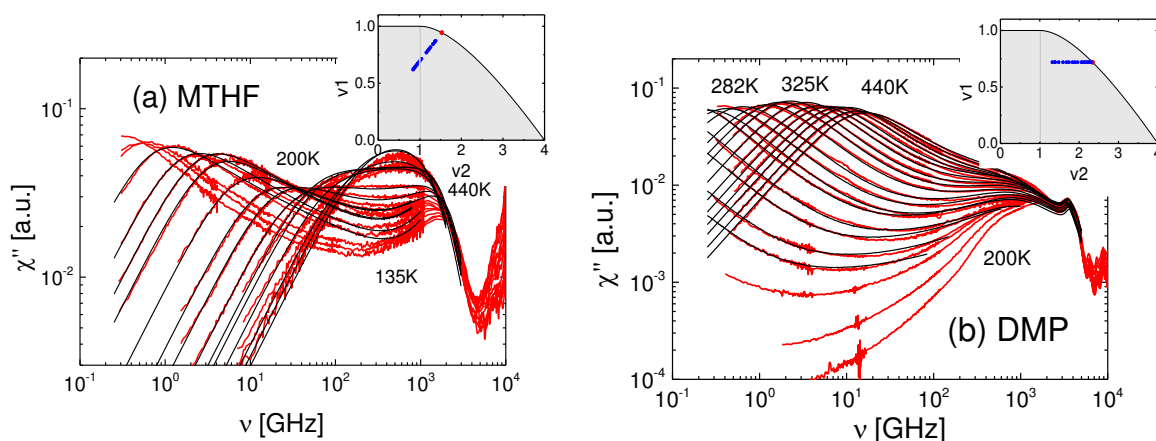


Figure 2.21 DLS susceptibility spectra of (a) MTHF and (b) dimethyl phthalate (DMP) fitted to the F_{12} model of MCT (black line). The v_1/v_2 parameter space is shown in the inset.

Figure taken from [Pub. 5].

As glassy as well as simple liquid dynamics are covered by the present work, we tested the F_{12} model whether it allows describing this crossover. Therefore, eight DLS spectra have been fitted by the F_{12} model and as an example the results are given as solid black lines in Figure 2.21. In most cases, a quite satisfying description is provided up to highest temperatures, in the case of toluene, ethyl benzene and MTHF even up to the boiling for which contributions of α -process and fast dynamics have merged. Some deviations occur at low temperatures for which the fits not fully reproduce the susceptibility minimum. They become the larger the closer T_g is approached and we refrained to fit the spectra at the lowest temperatures. This is expected as according to MCT the F_{12} model does not contain contributions from thermally activated hopping processes, which are expected to become important near and below T_c .

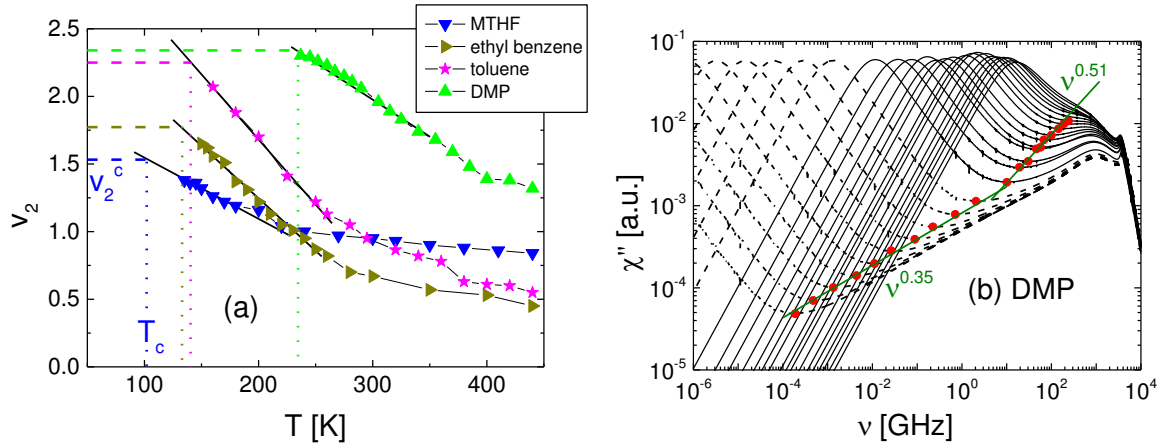


Figure 2.22 (a) Temperature dependence of the control parameter v_2 , approaching its critical value (dashed lines) at T_c ; Solid lines show a linear extrapolation towards T_c (dotted lines).

(b) Extrapolation of the F_{12} model fits to temperatures very close to T_c . Dashed lines represent spectra for extrapolated, full ones for experimental temperatures. Red dots mark the position of each minimum. The minimum positions follow two power laws indicated as green lines. Figure taken from [Pub. 5]

The changes of the spectra with temperature are mapped to only two control parameters (v_2 and v_s) showing a smooth variation with temperature shown in Figure 2.22 (a), which allows to determine T_c and to extrapolate the fits to some lower temperatures around T_c . Such an extrapolation is shown in Figure 2.22 (b). According to the asymptotic scaling laws (equation (2.13)) one expects a power-law behavior of the minimum coordinates with a slope around 0.35. Instead, in all our experimental spectra we found a value of around 0.50. Similar values were already found some time ago.[124] This can be seen as an indication that the experimental spectra are not in the regime where the asymptotic scaling laws can be applied. This is our explanation for the systematic deviation we found in the critical temperatures estimated by F_{12} model and the asymptotic laws. We used a third way to extract the critical temperature T_c , which uses a phenomenological model only, therefore we determined the strength of the fast dynamics $1 - f_{rel}$ by subtracting the α -process and excess wing from the spectrum and integrating up to an upper cutoff frequency of 100 GHz. As it is seen in Figure 2.23, it shows a cusp-like behavior as MCT predicts. The critical temperature extracted this way is about 30 K above T_c from the F_{12} model.

All in all, we can state that most results from earlier MCT analyses, regarding the applicability and the quantitative aspects of mode coupling theory have been confirmed. For the first time, a variety of systems is considered in this work, which allows drawing quantitative statements on the typical deviations and limitation of the asymptotic laws and the F_{12} model as well. The discrepancy between T_c from the F_{12} model and from the phenomenological approach revealing clearly the cusp-like behavior of $1 - f_{\text{rel}}$ deserves an explanation.

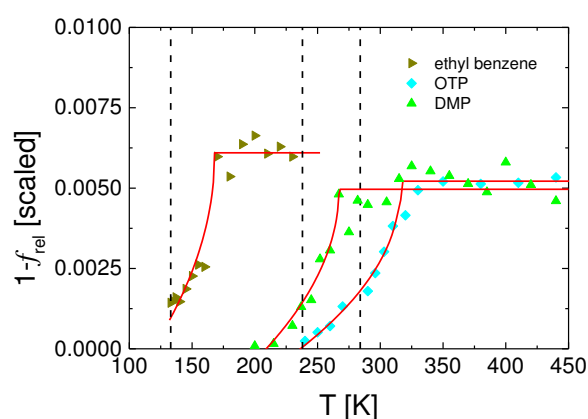


Figure 2.23 Square root singularity observed for the temperature dependence of the amplitude of the fast dynamics $1 - f_{\text{rel}}$ in the case of ethyl benzene and DMP as well as o-terphenyl (OTP).[58] Red lines are guide-for-the-eyes. Straight dashed lines represent the T_c values obtained by the F_{12} model. Figure taken from [Pub. 5].

3.3 Summaries of the publications

3.2.1 From boiling point to glass transition temperature: Transport coefficients in molecular liquids follow three-parameter scaling [Pub. 1]

This publication describes one of the most prominent features of the glass transition: The super-Arrhenius temperature dependence of the transport coefficients. For a series of molecular glass formers, we combined the time constants $\tau(T)$ collected from dielectric spectroscopy, photon correlation spectroscopy and dynamic light scattering covering a range $10^{-12} \text{ s} < \tau(T) < 10^2 \text{ s}$, covering the dynamics between the glass transition temperature T_g up to high temperatures around the boiling point T_b . The focus was set on low- T_g systems, where the boiling point T_b could be reached. Describing the dynamics in terms of an activation energy $E(T)$, we distinguish two regimes: A high-temperature regime characterized by an Arrhenius law with a constant activation energy E_∞ and a low-temperature regime, where $E_{\text{coop}}(T) \equiv E(T) - E_\infty$ increases while cooling. It is demonstrated that this increase can be described by an exponential function, specifically $E_{\text{coop}}(T)/E_\infty \propto \exp(-\lambda(T/T_A-1))$, where λ is a fragility parameter, and T_A a reference temperature which showed to be proportional to E_∞ .

The new three-parameter interpolation formula

$$\tau(T) = \tau_\infty \exp \left[\frac{E_\infty}{T} \left(1 + \exp \left[-\lambda \left(\frac{T}{bE_\infty} - 1 \right) \right] \right) \right], \text{ with } b \cong 0.104 \quad (3.1)$$

provides interpolations better than the well-established VFT expression. This comparison was done explicitly in Publication 2.

The further results of this publication are:

- E_∞ could be determined, as high temperature data were used, especially well at low- T_g liquids.

- A variety of 17 systems with a quite broad range in T_g and fragility was investigated, to allow systematic comparisons.
- $E_{\text{coop}}(T)$ shows an exponential dependence on temperature.
- A common intersection point was found in a $E_{\text{coop}}(T)/E_\infty$ vs. T/E_∞ plot, which allows to replace T_A by bE_∞ .

3.2.2 Reorientational dynamics in molecular liquids as revealed by dynamic light scattering: From boiling point to glass transition temperature [Pub. 2]

As time constants $\tau(T)$ are discussed in Publication 1, the first part of this publication gives a detailed description of how time constants can be extracted quite model independently from the measured high-temperature DLS spectra. At lower temperatures, where $\tau(T) \geq 10^{-10}$ s, this is done straight forward by fitting a Cole-Davidson function at the data, which gives about the same result as reading off the maximum frequency, often referred to as “peak picking”. But at higher temperatures, the contribution of the α -relaxation and the microscopic dynamics merge to a broadened single peak. Here, we extracted time constants by scaling the spectra to a common low-frequency envelope, explicitly $\chi''/\chi_{\alpha}^{\circ} = \omega\tau$. This way of building a master curve is unique, as long as the α -process contributes to the spectrum in form of an additional curvature. As a crosscheck, the amplitude χ_{α}° follows the temperature dependence established at low temperatures up to highest temperatures in a regular smooth way. The time constants extracted this way match very well with those from other methods.

In the frame of this publication, we decided to rewrite our interpolation formula for the time constants:

$$\tau(T) = \tau_{\infty} \exp \left[\frac{E_{\infty}}{T} \left(1 + \exp \left[-\mu \left(\frac{T}{E_{\infty}} - b \right) \right] \right) \right] \quad (3.2)$$

With the only difference being the newly introduced parameter μ , which is linked to the original λ via $\mu = \lambda/b$. This leads to values comparable with the fragility m .

The other main results of this Publication can be summarized as:

- DM/TFPI as well as PCS data of the low- T_g liquid MTHF has been included, together with some literature DS, diffusion coefficient and NMR data. This allows precise estimation of E_{∞} as the Arrhenius regime is observed for about 250K.

- The three-parameter description of $\tau(T)$ gives good interpolations, better than those following the VFT equation or the equation presented by Mauro *et al.*[68]. As the deviations are quite small (but systematic), also the derivatives of the models were compared with the derivatives of $\tau(T)$.
- The crossover of $\tau(T)$ to an Arrhenius behavior was identified model-independently by the use of the apparent activation energy. It was calculated using the derivative of $\ln(\tau(T))$ with respect to $(1/T)$.
- The parameter E_∞ has a physical meaning; its values match the high temperature activation energy, which can be determined model-independent if enough high-temperature data are available.
- The newly introduced “generalized fragility parameter” μ shows a strong correlation

with the conventionally defined fragility $m = \left. \frac{d \lg(\tau)}{d \left(\frac{T_g}{T} \right)} \right|_{T=T_g}$ and may provide an absolute measure of fragility.

3.2.3 From Boiling Point down to the Glass Transition - Dynamics of Molecular Liquids Described by a Generalized Angell Plot [Pub. 3]

This Publication is an overview of the measurements, ideas and results obtained during the last years. It contains the findings of both aforementioned publications, together with some new results.

Broad band LS and DS spectra are compared to each other revealing significant differences in the high-frequency range where secondary relaxation processes occur. We showed that the spectral shape of the α -process is the same when different spectroscopic methods are applied, but at high frequencies, the amplitude (of the excess wing) differs by a factor of about three. We also showed the absence of the β -process, which is clearly detected by DS, in the DLS spectra. We conclude that the excess wing is a different spectral feature than the β -process and it exhibits quite universal features whereas relaxation strength and spectral width of the β -relaxation vary and depend on the method.

Another new idea was to use the separation of the activation energy of $\tau(T)$ in a constant, “single particle” contribution E_∞ and an exponentially temperature dependent, “cooperative” contribution $E_{\text{coop}}(T)$ for an estimation of the number of correlated particles $N_{\text{corr}}(T)$. This is following the idea of N. Fatkullin that

$$N_{\text{corr}} = \frac{E_A(T)}{kT_g} \quad (3.3)$$

The result is shown in Figure 3.1. In a physically reasonable way, $N_{\text{corr}}(T)$ changes from about 1 at high temperatures up to about 300 at about T_g . This is quite similar to results from third-order non-linear dielectric susceptibility.[125] Here it has to be added that in [Pub. 3], we divided by T instead of T_g as a reference energy scale. After discussions with G. Tarjus, we now believe that T_g is the proper scaling parameter. This leads to a minor shift at high temperatures, but all the conclusions drawn stay the same.

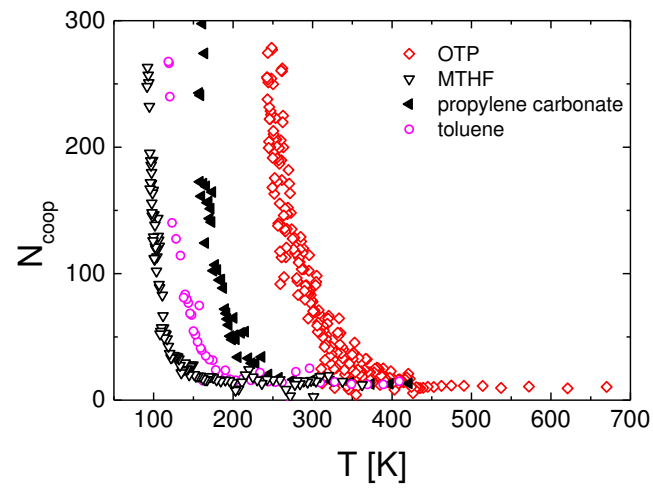


Figure 3.1 Estimate of the number N_{coop} of cooperatively moving molecules as a function of temperature by applying eq. (3.3). Figure adapted from [Pub. 3].

3.2.4 Relaxation Stretching, Fast Dynamics and Activation Energy: a Comparison of Molecular and Ionic Liquids as Revealed by Depolarized Light Scattering [Pub. 4]

We compared the spectra of different liquids, which are qualitatively similar, but quantitatively characterized by parameters like β_{CD} , l^* and $1-f$. These are correlated among each other and with parameters describing the temperature dependence of the correlation time τ . The results of this Publication can be summarized as follows:

- The long-time tail of the correlation function can be described by a Kohlrausch function and the α -scaling, *i. e.* frequency-temperature superposition (FTS) holds. This must not be seen as perfect agreement of the spectra, but as the existence of a common envelope, which the data follow the longer, the lower the temperature is.
- The minimum scaling also holds (as a common envelope), but its high frequency exponent shows deviations from MCT forecast.
- The excess wing was identified in the pulse-response representation of our data, including PCS data.
- Based on the DLS spectra, an inertial quantity l^* , which is temperature independent at high temperatures and agrees with the scale of molecular moments of inertia, was determined. As expected, it correlates with the molar mass M .
- No further correlations between parameters have been found. In particular, the stretching parameter β_{CD} does not correlate with the fragility m , even though this was reported.[126]
- None of the evaluated parameters shows significant differences between molecular liquids and RTIL. From the view of DLS spectra, one cannot distinguish between them.
- The time constants we found for the RTIL match those from dielectric spectroscopy.

3.2.5 Depolarized light scattering spectra of molecular liquids: Described in terms of mode coupling theory [Pub. 5]

We analyzed DLS spectra in the frame work of mode coupling theory. Eight susceptibility spectra are fitted to the numerical solution of the schematic F_{12} model of MCT and the validity of the asymptotic laws is discussed. The results drawn in this Publication can be summarized as follows:

- The F_{12} model is able to quantitatively describe the spectra up to the boiling point, where the main (structural) relaxation and the contribution of the microscopic (vibrational) dynamics have essentially merged, and down to the moderately super-cooled liquid where glassy dynamics is established.
- The parameters of the F_{12} model show smooth temperature dependence, allowing for extraction of T_c and extrapolation to temperature close to T_c .
- The value of MCT width parameter b , obtained by combining equations (2.11) and (2.19), match the β_{CD} values from Cole-Davidson fits to the experimental data.
- The experimentally extracted values of ω_{min} , ω_{max} and χ''_{min} follow the asymptotic scaling laws. But according to these asymptotic scaling laws one expects a power-law behavior of the minimum coordinates with a slope around 0.35. Instead, in all our experimental spectra we found a value of around 0.50.
- By a phenomenological analysis we show that $1 - f_{rel}$ exhibits the cusp like anomaly forecast by MCT, allowing the extraction of T_c .
- The critical temperatures T_c determined by the scaling laws, the fits by the F_{12} model and the phenomenological analysis show significant, systematic differences.
- The appearance of the excess wing around $\tau \cong 10^{-9}$ s is shown by plotting maximum vs. minimum position.

4 Publications

List of included publications as referred to in this thesis

- Pub. 1** From boiling point to glass transition temperature: Transport coefficients in molecular liquids follow three-parameter scaling
B. Schmidtke, N. Petzold, R. Kahlau, M. Hofmann, E. A. Rössler
Physical Review E **86**, 041507 (2012).
- Pub.2** Reorientational dynamics in molecular liquids as revealed by dynamic light scattering: From boiling point to glass transition temperature
B. Schmidtke, N. Petzold, R. Kahlau, E. A. Rössler
The Journal of Chemical Physics **139**, 084504 (2013).
- Pub. 3** From Boiling Point down to the Glass Transition - Dynamics of Molecular Liquids Described by a Generalized Angell Plot
B. Schmidtke, N. Petzold, M. Flämig, E. A. Rössler
Article in *Fragility of Glass-forming Liquids*, Editors: A. Lindsay Greer, Kenneth Kelton, and Srikanth Sastry, Hindustan Book Agency, (2013).
- Pub. 4** Relaxation stretching, fast dynamics and activation energy: a comparison of molecular and ionic liquids as revealed by depolarized light scattering
B. Schmidtke, N. Petzold, B. Pötzschner, H. Weingärtner, E. A. Rössler
The Journal of Physical Chemistry B **118**, 7108 (2014).
- Pub.5** Depolarized light scattering spectra of molecular liquids: Described in terms of mode coupling theory
B. Schmidtke, E. A. Rössler
The Journal of Chemical Physics, **141**, 044511 (2014).

Individual contributions to joint publications

- Pub. 1** I conducted the experiments for determination of time constants by DM/TFPI. PCS data by N. Petzold and dielectric data by R. Kahlau were included. I performed all analysis during my Ph.D. studies.
- Pub. 2** I measured the spectra shown in Fig. 1(a) and half the temperatures of the one in Fig. 1(b). The PCS decays were measured by N. Petzold. The additional time constants used were already published in Pub. 1. I performed all analysis during my Ph.D. studies.
- Pub. 3** I measured the spectra shown in Fig. 1(a) and half the temperatures from the one in Fig. 1(b). The PCS decays were measured by N. Petzold, Field Cycling ^1H NMR experiments were performed by M. Flämig, dielectric experiments were performed by R. Kahlau. The additional time constants used were already published in Pub. 1. I performed all analysis during my Ph.D. studies.
- Pub. 4** I measured parts of the spectra shown in Fig. 1 and most shown in Fig. 2. I conducted the experiments for determination of time constants by DM/TFPI. I performed all analysis during my Ph.D. studies.
- Pub. 5** I measured the spectra of EAN and about half the temperatures of toluene shown in Fig. 1 and most of the others used for the analysis. I made the MCT fits using a program provided by Th. Voigtmann. I performed all analysis during my Ph.D. studies.

Other publications

- Time resolved measurement of longitudinal mode competition in 405 nm (Al,In)GaN laser diodes
B. Schmidtke, H. Braun, U. T. Schwarz, D. Queren, M. Schillgalies, S. Lutgen, U. Strauß
Phys. Status Solidi C 6, No. S2, S860– S863 (2009).
- High power broad ridge (Al,In)GaN laser diodes: Spatial and spectral stability
H. Braun, S. Rogowsky, B. Schmidtke, U. T. Schwarz, S. Brüninghoff, A. Lell, U. Strauß
Phys. Status Solidi A 206, No. 6, 1211–1214 (2009).
- Iso-Frictional Mass Dependence of Diffusion of Polymer Melts Revealed by ^1H NMR Relaxometry
R. Meier, A. Herrmann, M. Hofmann, B. Schmidtke, B. Kresse, A. F. Privalov, D. Kruk, F. Fajara, E. A. Rössler
Macromolecules, 46, 5538–5548 (2013).
- Evolution of the dynamic susceptibility in molecular glass formers: Results from light scattering, dielectric spectroscopy, and NMR
N. Petzold, B. Schmidtke, R. Kahlau, D. Bock, R. Meier, B. Micko, D. Kruk, E. A. Rössler
The Journal of Chemical Physics 138, 12A510 (2013)
- Dynamics of asymmetric binary glass formers. I. A dielectric and nuclear magnetic resonance spectroscopy study
R. Kahlau, D. Bock, B. Schmidtke, E. A. Rössler
The Journal of Chemical Physics 140, 044509 (2014).
- Dynamic heterogeneities in glass forming systems
D. Bock, N. Petzold, R. Kahlau, S. Gradmann, B. Schmidtke, N. Benoit, E. A. Rössler
Journal of Non-Crystalline Solids 407, 88–97 (2015).
- Temperature Dependence of the Segmental Relaxation Time of Polymers Revisited
B. Schmidtke, M. Hofmann, A. Lichtinger, E.A. Rössler
Macromolecules, in print (2015).

Publication 1

From boiling point to glass transition temperature: Transport coefficients in molecular liquids follow three- parameter scaling

B. Schmidtke, N. Petzold, R. Kahlau, M. Hofmann, E. A. Rössler

Physical Review E **86**, 041507 (2012).

Copyright 2012 by The American Physical Society

DOI: 10.1103/PhysRevE.86.041507

From boiling point to glass transition temperature: Transport coefficients in molecular liquids follow three-parameter scaling

B. Schmidtke, N. Petzold, R. Kahlau, M. Hofmann, and E. A. Rössler*

Universität Bayreuth, Experimentalphysik II, D-95440 Bayreuth, Germany

(Received 15 March 2012; revised manuscript received 3 August 2012; published 19 October 2012)

The phenomenon of the glass transition is an unresolved problem in condensed matter physics. Its prominent feature, the super-Arrhenius temperature dependence of the transport coefficients, remains a challenge to be described over the full temperature range. For a series of molecular glass formers, we combined $\tau(T)$ collected from dielectric spectroscopy and dynamic light scattering covering a range 10^{-12} s $< \tau(T) < 10^2$ s. Describing the dynamics in terms of an activation energy $E(T)$, we distinguish a high-temperature regime characterized by an Arrhenius law with a constant activation energy E_∞ and a low-temperature regime for which $E_{\text{coop}}(T) \equiv E(T) - E_\infty$ increases exponentially while cooling. A scaling is introduced, specifically $E_{\text{coop}}(T)/E_\infty \propto \exp[-\lambda(T/T_A - 1)]$, where λ is a fragility parameter and T_A a reference temperature proportional to E_∞ . In order to describe $\tau(T)$ still the attempt time τ_∞ has to be specified. Thus, a single interaction parameter E_∞ describing the high-temperature regime together with λ controls the temperature dependence of low-temperature cooperative dynamics.

DOI: [10.1103/PhysRevE.86.041507](https://doi.org/10.1103/PhysRevE.86.041507)

PACS number(s): 64.70.pm, 77.22.Gm, 78.35.+c

I. INTRODUCTION

Although of fundamental importance and extensively investigated, the glass transition phenomenon is far from being understood. Its most prominent feature is the super-Arrhenius temperature dependence of transport coefficients such as viscosity or correlation time τ , which is observed when a liquid is strongly supercooled. While a simple (molecular) liquid well above its melting point T_m exhibits a viscosity on the order of 10^{-3} Pa s, upon supercooling it may finally reach values of 10^{12} Pa s which are typical for solids. The corresponding temperature is defined as glass transition temperature T_g . The slowing down of dynamics is accompanied by only a slight and smooth change in structure. This has led to the interpretation that the glass transition is a kinetic transition and several theoretical approaches have been developed, yet none is fully accepted [1–4]. In particular, it remains a great challenge of any theory of the liquid state to provide an interpolation of $\tau(T)$, which covers the full range from the boiling point down to T_g .

Often the empirical Vogel-Fulcher-Tammann formula (VFT), $\lg \tau/\tau_\infty = D/(T - T_0)$, is applied to fit experimental data. One of the problems faced when applying VFT is that its parameters depend strongly on the fitting interval and it fails when relaxation data well above T_m are included. Regarding the divergence of the correlation time implied by VFT at $T_0 < T_g$, doubts have also been raised [5]. Numerous further formulas have been proposed attempting to fit $\tau(T)$, but none is fully satisfying. Another route of searching for “corresponding states” of liquids relies on scaling, for example, the low-temperature regime by introducing some crossover temperature [6–9]. Yet, in the different approaches the physical meaning of the crossover temperature is quite different, and it is difficult to extract unambiguously a crossover temperature.

Inspecting the experimental situation it turns out that, although extensively studied close to T_g , molecular glass

formers are not sufficiently well investigated in the high-temperature regime above T_m . With a few exceptions, most tests of interpolating $\tau(T)$ are restricted to time constants above about 10^{-9} s, actually ignoring a temperature range of up to 300 K until the high-temperature limit $\tau_\infty \cong 10^{-12}$ s is essentially reached. The most popular approach probing molecular reorientation is dielectric spectroscopy [10–12], but for technical reasons most such experiments do not cover frequencies above a few gigahertz. Correlation times down to 10^{-12} s are now easily available when glass formers are studied by depolarized dynamic light scattering (LS) using a tandem-Fabry-Perot interferometer (TFPI) and a double monochromator (DM) [13–17]. We have combined LS, including also photon correlation spectroscopy (PCS) data [17] measured up to 440 K of a series of 17 molecular liquids with the data obtained by dielectric spectroscopy, thus covering, in most cases, the entire temperature range needed to attempt a complete description of $\tau(T)$, i.e., which includes both the high- as well as the low-temperature regime of molecular liquids. As different rank reorientational correlation functions are probed by DS and LS, one expects some difference in the absolute values of $\tau(T)$, which, however, can be neglected on a logarithmic scale. For example, comparing $\tau(T)$ obtained from DS and LS, a factor of 1.65 among the time constant has been reported [16]. The time constants $\tau(T)$ are extracted from the DS and LS susceptibility spectra by standard line-shape analysis described in Refs. [10–13, 15, 17–19]. Looking for a minimal number of system-specific parameters controlling $\tau(T)$ in the range 10^{-12} – 10^2 s, we will show that actually three parameters are sufficient.

II. RESULTS

Figure 1(a) displays, in an Arrhenius representation, dielectric correlation times collected in our group (open symbols) [10, 15, 18–22] together with few other literature data for glycerol [11], benzophenone [23], salol [24], propylene carbonate [25], *n*-butyl benzene [26], and iso-propylene benzene [27, 28]. In addition, we have included our data together with previously published LS data [14–17] (full symbols)

*Corresponding author.

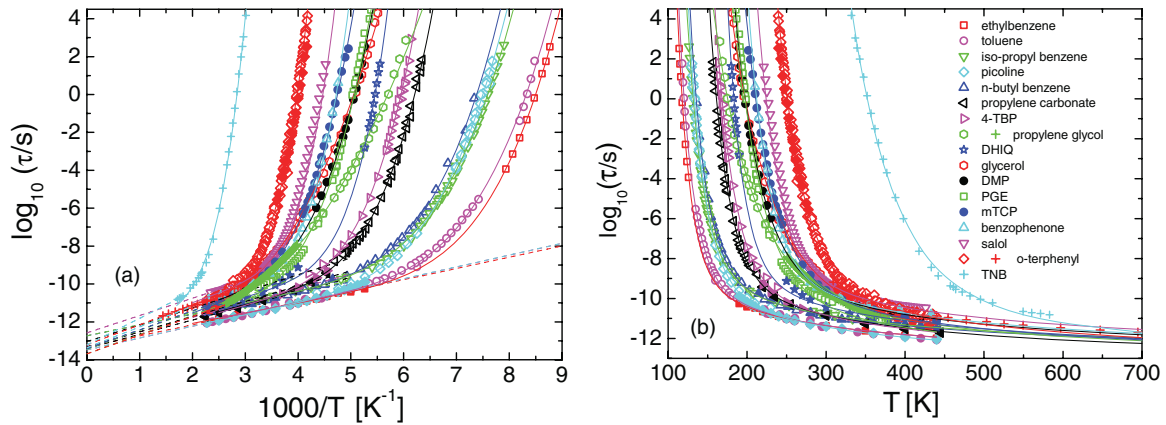


FIG. 1. (Color online) Reorientational correlation times of molecular liquids obtained by dielectric spectroscopy (open symbols) [10,18–21] and dynamic light scattering (full symbols) (this work and [14–17]); 4-TBP: 4-*tert*-butyl pyridine, DHIQ: decahydroisoquinoline, DMP: dimethyl phthalate, PGE: monoepoxide phenyl glycidyl ether, *m*-TCP: *m*-tricresyl phosphate; data for *n*-butyl benzene from [26,29], iso-propylene benzene from [27,28,35]; viscosity data for *o*-terphenyl [31], trisnaphthyl benzene (TNB) [33], and propylene glycol [34] (crosses); for toluene, ^2H NMR data [36] have been included; straight dashed lines: high-temperature Arrhenius behavior; solid lines: full fit by Eqs. (1) and (3). Corresponding T_g values are listed in Table I.

together with literature LS data for *n*-butyl benzene [29]. In the cases of dimethyl phthalate (DMP) and *m*-tricresyl phosphate (*m*-TCP), we only use LS data as we collected both TFPI/DM and PCS data [30]. It is obvious that adding the LS data (solid symbols in Fig. 1) extends the temperature range significantly to be included in a full-scale description of $\tau(T)$, a fact better seen when the data are plotted as a function of temperature [Fig. 1(b)]. Even including the LS data, however, one reaches correlation times on the order of 10^{-12} s at our experimental high-temperature limit of 440 K only in the case of the low- T_g liquids (say, $T_g < 180$ K). For the systems with high T_g this limit is not reached. An exception is *o*-terphenyl ($T_g = 245$ K), for which viscosity data [31] are available up to almost 700 K, which is actually above the boiling point ($T_b = 605$ K) [32] and allows us to cover the high-temperature regime also for this high- T_g system. Here, with regard to our LS data measured up to 440 K, still another 260 K have to be covered to reach 10^{-12} s, finally. As another high- T_g system we included viscosity data of $\alpha\alpha\beta$ -trisnaphthyl benzene (TNB; $T_g = 343$ K) [33], additional data for propylene glycol [34], and iso-propylene benzene [35].

It is well known from transport data in low-viscosity (non-glass-forming) liquids that their temperature dependence is described by an Arrhenius law [37]. This may also be anticipated when inspecting the data in Fig. 1(a). At high temperatures a simple Arrhenius law appears to describe the data well, whereas the apparent activation energy $E(T)$ strongly increases at lower temperatures. The analysis of Stickel *et al.* [38] has shown that for molecular glass formers the Arrhenius regime has been reached by dielectric experiments in some cases. However, the analysis included only molecular rates below 10^{10} Hz, which is not always sufficient to reach the high-temperature range. In Fig. 2 we plot the apparent activation energy $E(T) = \partial \ln(\tau) / \partial(1/T)$ at the highest temperatures investigated as revealed by our LS data. Although some scatter shows up as a derivative is involved, in all cases the activation energy shows a trend to level off

at the highest temperatures. In the case of low- T_g liquids the Arrhenius behavior is well established over 100–200 K. For example, $E(T)$ is essentially constant above 200 K for ethyl benzene, while for *o*-terphenyl for which viscosity data are available up to the boiling point the Arrhenius behavior is observed only above 500 K. Regarding the nonfragile glass formers glycerol and propylene glycol, the Arrhenius regime is not clearly reached but again a trend toward $E(T) = E_\infty = \text{const.}$ is observed in both cases. This also holds for some other fragile high- T_g systems like salol. Thus, although we significantly extended the temperature range studied so far, only an estimate may be available for the activation energy E_∞ in some liquids. In order to facilitate estimating E_∞ in these cases, we assumed a pre-exponential time τ_∞ listed in Table I, which actually does not significantly vary for the considered liquids [cf. Fig. 1(b)]. Together with the experimental value of τ at highest temperatures, this allows some reasonable estimate of E_∞ for nonfragile glass formers. The optimization

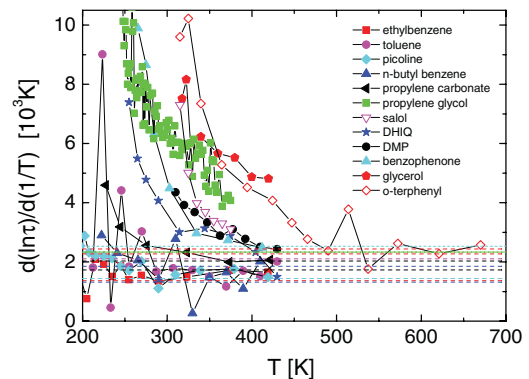


FIG. 2. (Color online) Apparent activation energy $E(T) = \partial \ln(\tau) / \partial(1/T)$ of the temperature dependence of $\tau(T)$ at highest temperatures, as revealed by light scattering. A trend of $E(T)$ to become constant is recognized; dashed lines indicate values of E_∞ used for the analysis (cf. Table I).

TABLE I. Parameters of the analysis: glass transition temperature T_g [defined by $\tau_\alpha(T_g) = 100$ s], high-temperature activation energy E_∞ , reference temperature T_A corresponding to the optimization, generalized fragility parameter λ , logarithm of pre-exponential factor τ_∞/s .

Sample	T_g [K]	E_∞ [K]	T_A [K]	λ	$\lg \tau_\infty/s$	T_A/T_g
Ethyl benzene	115	1369	128	7.67	-13.34	1.11
Toluene	117	1440	131	7.15	-13.49	1.12
<i>n</i> -Butyl benzene	131	1315	150	6.46	-12.74	1.15
Iso-propyl benzene	128	1342	145	6.44	-12.74	1.13
α -Picoline	129	1438	148	6.6	-13.47	1.15
Propylene carbonate	157	1729	177	7.04	-13.41	1.13
4- <i>tert</i> -Butyl pyridine (4-TBP)	164	1761	185	7.3	-13.30	1.13
Propylene glycol	168	2332	205	3.32	-13.69	1.22
Decahydroisoquinoline (DHIQ)	180	1851	201	7.37	-13.34	1.12
Glycerol	188	2271	235	3.56	-13.69	1.25
Dimethyl phthalate (DMP)	191	2029	221	5.66	-13.04	1.16
Monoepoxide phenyl glycidyl ether (PGE)	194	2321	215	7.08	-13.45	1.11
<i>m</i> -Tricresyl phosphate (m-TCP)	205	2301	235	6.21	-13.42	1.15
Benzophenone	207	2530	227	8.87	-13.37	1.10
Salol	218	2104	242	8.5	-12.58	1.11
<i>o</i> -Terphenyl	245	2441	274	8.26	-13.22	1.12
Trinaphthyl benzene (TNB)	343	3232	390	8.09	-13.22	1.14

procedure presented in the following takes specifically into account that E_∞ cannot be determined unambiguously in some of the liquids considered.

Although the energy E_∞ is an apparent quantity and must not be connected to some single-particle barrier in the liquid, we take the Arrhenius high-temperature dependence of $\tau(T)$ as an empirical fact and as a starting point of our analysis. Explicitly, we assume

$$\tau(T) = \tau_\infty \exp[(E_\infty + E_{\text{coop}}(T))/T], \quad (1)$$

where the apparent activation energy $E(T)$ is decomposed into a temperature-independent part E_∞ and a temperature-dependent part $E_{\text{coop}}(T)$. The quantity $E_{\text{coop}}(T)$ reflects the cooperative dynamics becoming dominant at low temperature, and its properties have been discussed by several authors [3,4,39–41]. The corresponding values E_∞ and τ_∞ are listed in Table I.

In Fig. 3(a), by plotting $T \lg(\tau/\tau_\infty) - E_\infty$ the quantity $E_{\text{coop}}(T)$ is displayed as a function of temperature. The high-temperature regime is now characterized by E_{coop} being essentially zero, while at low temperatures $E_{\text{coop}}(T)$ strongly increases for most liquids in a rather similar way, except for the nonfragile liquids glycerol and propylene glycol. In Fig. 3(b) $E_{\text{coop}}(T)$ is plotted on a logarithmic scale. Straight lines are observed for the low- T_g systems. In the case of the high- T_g systems and particularly for the nonfragile liquids, the curves bent over at low values of E_{coop} . Most probably this is due to an underestimated E_∞ . This once again points to the principal difficulty of determining E_∞ correctly. Moreover, we are faced with the problem of analyzing $E_{\text{coop}}(T)$ containing the error of a not-correctly-chosen E_∞ in addition to scatter reflecting experimental errors in $\tau(T)$. Regardless, we assume that $E_{\text{coop}}(T)$ is a simple exponential function of temperature; explicitly,

$$E_{\text{coop}}(T) \propto \exp[-\lambda(T/T_A - 1)]. \quad (2)$$

For reasons which will become clear below, we have introduced two parameters: a reference temperature T_A and a generalized fragility parameter λ which controls the “steepness” of $E_{\text{coop}}(T)$ in Fig. 3(b). Together with E_∞ and τ_∞ , four parameters are needed to describe the full temperature dependence of $\tau(T)$ in the present state of analysis, and so far we are free to choose any reference temperature T_A defining an “isoenergetic” point.

Here the question arises whether there is some connection between the reference temperature T_A and the high-temperature activation energy E_∞ . For this purpose we first reinspect Fig. 3(b). The quantity $E_{\text{coop}}(T = T_g)$, i.e., the energy at T_g , is higher, the higher T_g is. A trend already anticipated in Fig. 1(a). Indeed, the ratio $E_{\text{coop}}(T_g)/T_g$ appears to be roughly constant [cf. Fig. 4(a)], but this is not surprising as it follows from the definition of $T \lg(\tau/\tau_\infty) - E_\infty$, with E_∞ being a relatively small quantity. One may speculate whether $E_\infty \propto T_g$ holds. This is also checked in Fig. 4(a). Indeed, both ratios $E_{\text{coop}}(T_g)/T_g$ and E_∞/T_g appear to be constant, although some scatter/trend is observed. As T_g is an “isodynamic point” chosen arbitrarily, it is not expected to be a physically relevant temperature, but the correlation observed in Fig. 4(a) suggests that the temperature dependence of the low-temperature dynamics may be linked to the high-temperature activation energy E_∞ , explicitly $T_A \propto E_\infty$, and the four-parameter description $(\tau_\infty, E_\infty, \lambda, T_A)$ could possibly be reduced to a three-parameter description.

In order to find the relationship among T_A and E_∞ , we display the quantity $E_{\text{coop}}(T)/E_\infty$ as a function of the reduced temperature T/E_∞ in a semilogarithmic plot [cf. Fig. 4(b)]. Again, straight lines of different slopes are observed, suggesting that a common intersection exists possibly in the range $0.05 > T/E_\infty > 0.15$. Given the experimental uncertainty of E_∞ , this intersection may be smeared out. In order to find T_A in the range $T_g < T_A < E_\infty$, we take recourse to an optimization procedure. We fit $E_{\text{coop}}(T)$ in Fig. 3(a) for

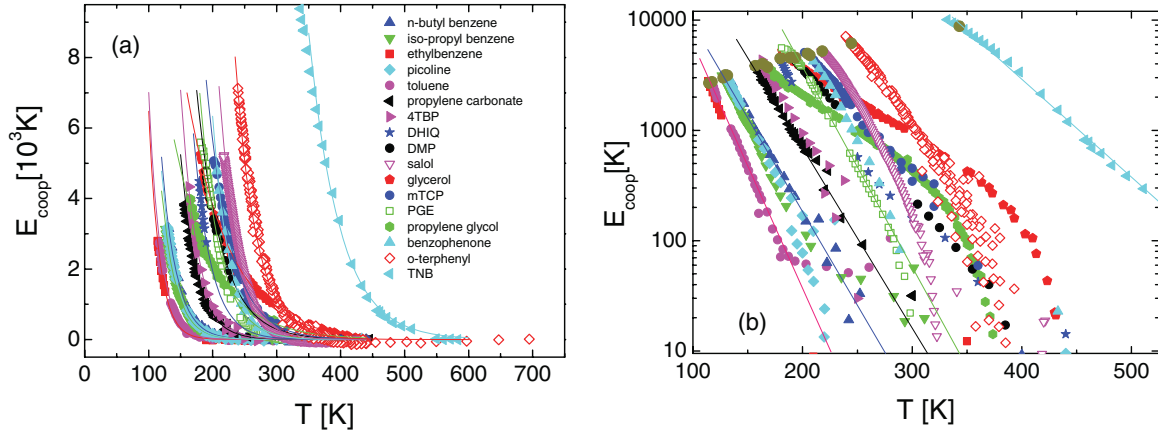


FIG. 3. (Color online) (a) Quantity $E_{\text{coop}}(T)$ [cf. Eq. (1)] as a function of temperature. (b) Data in a semilogarithmic plot; straight lines signal exponential dependence in particular for low- T_g liquids. Marked points indicate $E_{\text{coop}}(T_g)$. For high- T_g and nonfragile liquids the curves bent over at low E_{coop} values are probably due to an underestimated value of E_{∞} .

all systems by the expression

$$E_{\text{coop}}/E_{\infty} = a \exp \left[-\lambda \left(\frac{T}{bE_{\infty}} - 1 \right) \right], \quad (3)$$

where a and b are universal (global) parameters to be determined under the condition that the correlation between the experimental and fitted values of E_{∞} [by applying Eq. (3) to the data in Fig. 3(a)] becomes best. Our search yields the result that $E_{\text{coop}}(T_A) \cong E_{\infty}$ ($a \cong 1$) and $T_A \cong 0.104E_{\infty}$ ($b \cong 0.104$). The inset in Fig. 5(b) shows a satisfying correlation between the optimized E_{∞}^{opt} and the experimental values of E_{∞} , confirming our procedure. In Fig. 5(a) we show $E_{\text{coop}}(T)/E_{\infty}^{\text{opt}}$ vs $T/E_{\infty}^{\text{opt}}$, where the nonfragile liquids glycerol and propylene glycol show a significantly different behavior reflected by a much lower generalized fragility parameter λ . The values obtained for T_A and λ are included in Table I. One may call Fig. 5(a) [and Fig. 4(b)] a generalized Angell plot where reduced relaxation data [here $E_{\text{coop}}(T)/E_{\infty}$] are plotted vs reduced temperature T/E_{∞} instead of vs T/T_g , as in the original Angell plot [42]. In other words, the physically well

defined (but in some glass formers experimentally difficult to access) quantity E_{∞} defines the energy scale of the glass transition phenomenon.

In Fig. 5(b) a master curve is shown by plotting $E_{\text{coop}}(T)/E_{\infty}^{\text{opt}}$ vs $\lambda(T/T_A - A)$, i.e., the fragility parameter λ is taken to scale the reduced temperature axis. Indeed, all data can be collapsed to a single straight line. In Figs. 1(a) and 1(b) very satisfying three-parameter ($E_{\infty}, \lambda, \tau_{\infty}$) fits of $\tau(T)$ by Eqs. (1) and (3) are shown (using the universal parameters a and b), which cover all the available data essentially from the boiling point down to T_g .

III. DISCUSSION AND CONCLUSION

Concluding, we propose a three-parameter interpolation of the complete temperature dependence of transport quantities in molecular liquids which can be easily supercooled, i.e., when time constants in the range of 10^{-12} – 10^2 s are covered. Here one has to exclude diffusion data, as they show a “decoupling phenomenon” close to T_g [43]. The decomposition along Eq. (1) is not unique, and our sole justification is the success

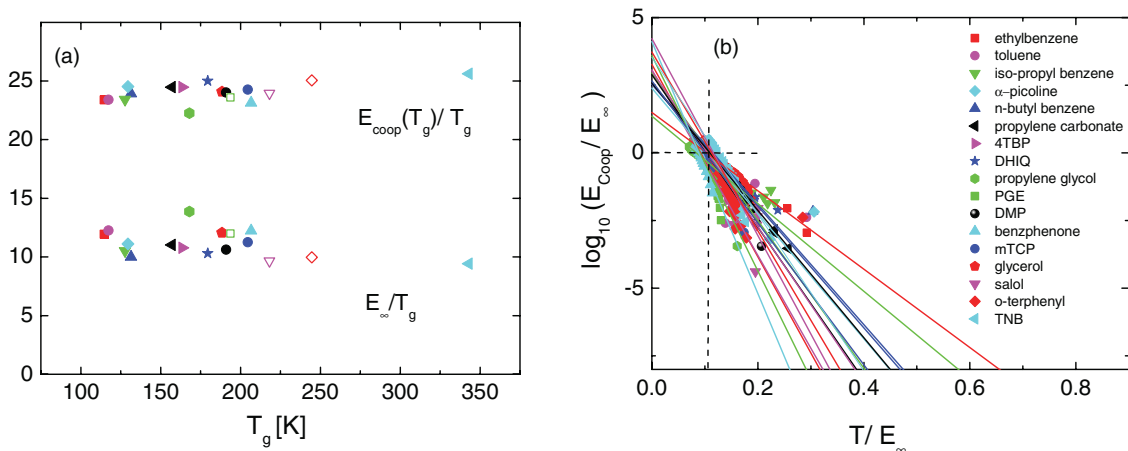


FIG. 4. (Color online) (a) Correlation between $E_{\text{coop}}(T = T_g)$ and E_{∞} , respectively, with the glass transition temperature T_g . (b) Reduced energy $E_{\text{coop}}(T)/E_{\infty}$ vs reduced temperature T/E_{∞} , dashed lines mark intersection after optimization [cf. Fig. 5(a)].

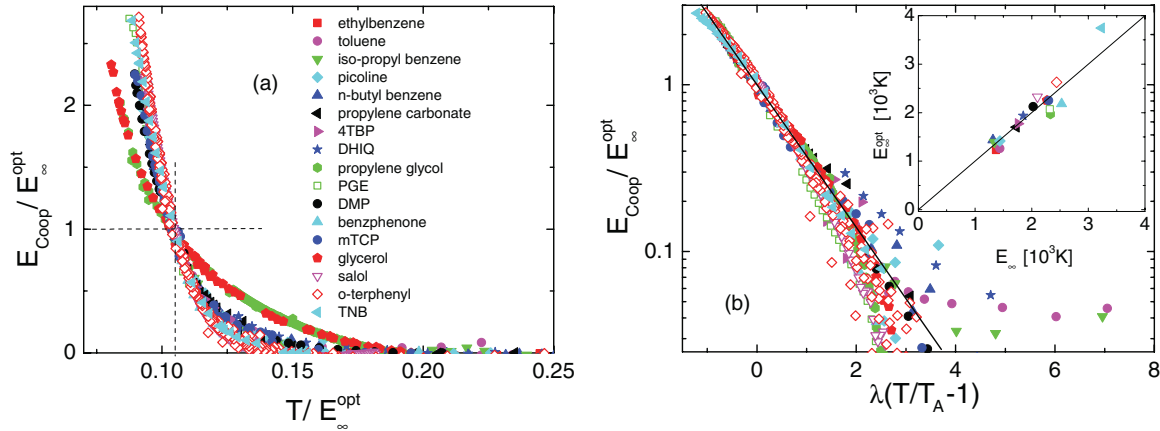


FIG. 5. (Color online) (a) $E_{\text{Coop}}/E_{\infty}^{\text{opt}}$ as a function of the reduced temperature $T/E_{\infty}^{\text{opt}}$ with E_{∞}^{opt} obtained by the optimization strategy (values of T_A and fragility parameter λ given in Table I). (b) Corresponding master curve obtained by introducing the fragility parameter λ and $T_A = 0.104 E_{\infty}^{\text{opt}}$ (cf. Table I); inset: correlation between E_{∞}^{opt} and the experimentally determined E_{∞} .

of the corresponding scaling, a minimal set of system-specific parameters, and furthermore, a simple exponential describes $E_{\text{Coop}}(T)$. We interpret the quantity E_{∞} extracted from the high-temperature transport data as an interaction parameter which, together with the single fragility parameter λ , controls the low-temperature behavior of $\tau(T)$. We emphasize that λ is defined by the “steepness” of $E_{\text{Coop}}(T/T_A)$ in contrast to the conventional fragility parameter m defined via $\tau(T/T_g)$. Thus, current attempts to relate m with some other physical properties have to be reconsidered.

We note a scaling of the kind of Eq. (3) was already proposed by the theoretical work of Kivelson, Tarjus, and co-workers [3,39–41] and a similar one by experimental studies [44]. Yet, to our knowledge, no one made a systematic study on a series of molecular liquids including high-temperature data which, as mentioned, have been rare. Important to note, the crossover temperature discussed by Kivelson *et al.* is connected to the presumable appearance of cooperative dynamics well above T_m (the so-called onset temperature), whereas the present T_A turns out to be right in the middle between T_g and T_m and thus possibly close to T_c of the mode coupling theory [2]. We note that, as an optimization procedure is applied, the universal parameters a and b depend on the quality of the experimental data, and actually, the optimization minimum is rather broad. As mentioned, attempts to scale the $\tau(T)$ data for glass formers have usually started from the low-temperature side; for instance, the time constants close to T_g have been collapsed to provide a single master curve by scaling out two parameters, namely, T_g and the fragility index m , and which works up to a crossover temperature which lies near $1.2T_g$ [7]. At higher temperatures individual curves

have been found, indicating that there a different transport mechanism takes over. In contrast, the present approach starts from the high-temperature side where an Arrhenius law is well documented, and again, a two-parameter scaling applies when the influence of the high-temperature dynamics is separated from the $\tau(T)$ data. In both cases a similar crossover temperature is disclosed. All in all, the present finding is of great relevance for the future theory of the glass transition phenomenon associated with the super-Arrhenius temperature dependence of the correlation time, which sets in well above the melting point and is thus an important feature of any liquid.

As we propose a universal description of $\tau(T)$ for molecular liquids, this also allows for some forecasts. For example, Capaccioli and Ngai [45] recently reiterated the controversy of providing a reliable estimate of T_g of water. They suggested $T_g = 136$ K as the best value. Taking this value for granted, we fitted our formula to the $\tau(T)$ data from [46], which the authors also used. In this way, we are able to extract the fragility parameter $\lambda = 2.6$ (referring to $m = 37$), which is close to that of glycerol and propylene glycol, both of which are nonfragile. As expected, water is a hydrogen bond network, forming liquid similar to glycerol and thus is not a fragile glass former. Actually, Capaccioli and Ngai estimated $m = 44$, which is in good agreement with our prediction.

ACKNOWLEDGMENTS

The authors thank D. Kruk, A. Bourdick, and B. Pötzschner for helpful discussions, and the financial support of Deutsche Forschungsgemeinschaft (DFG) through Projects RO 907/11 and RO 907/15 is appreciated.

- [1] T. R. Kirkpatrick, D. Thirumalai, and P. G. Wolynes, *Phys. Rev. A* **40**, 1045 (1989).
 [2] W. Götze and L. Sjögren, *Rep. Prog. Phys.* **55**, 241 (1992).
 [3] G. Tarjus, S. A. Kivelson, Z. Nussinov, and P. Viot, *J. Phys.: Condens. Matter* **17**, R1143 (2005).
 [4] L. Berthier and G. Biroli, *Rev. Mod. Phys.* **83**, 587 (2011).

- [5] T. Heckscher, A. I. Nielsen, N. B. Olsen, and J. C. Dyre, *Nat. Phys.* **4**, 737 (2008).
 [6] E. Rössler, *J. Chem. Phys.* **92**, 3725 (1990).
 [7] E. Rössler, K.-U. Hess, and V. Novikov, *J. Non-Cryst. Solids* **223**, 207 (1998).
 [8] E. J. Saltzmann and K. S. Schweizer, *J. Chem. Phys.* **121**, 2001 (2004).

- [9] Y. Elmatad, J. P. Garrahan, and D. Chandler, *J. Phys. Chem. B* **113**, 5563 (2009).
- [10] A. Kudlik, S. Benkhof, T. Blochowicz, C. Tschirwitz, and E. Rössler, *J. Mol. Struct.* **479**, 201 (1999).
- [11] P. Lunkenheimer, U. Schneider, R. Brand, and A. Loidl, *Contemp. Phys.* **41**, 15 (2000).
- [12] F. Kremer and A. Schönhal, *Broadband Dielectric Spectroscopy* (Springer, Berlin, 2003).
- [13] H. Z. Cummins, G. Li, Y. H. Hwang, G. Q. Shen, W. M. Du, J. Hernandez, and N. J. Tao, *Z. Phys. B* **103**, 501 (1997).
- [14] J. Wiedersich, N. V. Surovtsev, V. N. Novikov, E. Rössler, and A. P. Sokolov, *Phys. Rev. B* **64**, 064207 (2001).
- [15] S. V. Adichtchev, S. Benkhof, T. Blochowicz, V. N. Novikov, E. Rössler, C. Tschirwitz, and J. Wiedersich, *Phys. Rev. Lett.* **88**, 055703 (2002).
- [16] A. Brodin and E. A. Rössler, *Eur. Phys. J. B* **44**, 3 (2005).
- [17] N. Petzold and E. A. Rössler, *J. Chem. Phys.* **133**, 124512 (2010).
- [18] T. Blochowicz, Ch. Tschirwitz, St. Benkhof, and E. A. Rössler, *J. Chem. Phys.* **118**, 7544 (2003).
- [19] T. Blochowicz, A. Brodin, and E. A. Rössler, *Adv. Chem. Phys.* **133**, 127 (2006).
- [20] T. Blochowicz, C. Gainaru, P. Medick, C. Tschirwitz, and E. A. Rössler, *J. Chem. Phys.* **124**, 134503 (2006).
- [21] J. Hintermeyer, A. Herrmann, R. Kahlau, C. Goiceanu, and E. A. Rössler, *Macromolecules* **41**, 9335 (2008).
- [22] C. Gainaru, R. Kahlau, E. A. Rössler, and R. Böhmer, *J. Chem. Phys.* **131**, 184510 (2009).
- [23] P. Lunkenheimer, L. C. Pardo, M. Köhler, and A. Loidl, *Phys. Rev. E* **77**, 031506 (2008).
- [24] F. Stickel, E. W. Fischer, and R. Richert, *J. Chem. Phys.* **104**, 2043 (1996).
- [25] K. L. Ngai, P. Lunkenheimer, C. León, U. Schneider, R. Brand, and A. Loidl, *J. Chem. Phys.* **115**, 1405 (2001).
- [26] L. Andrussov, in *Eigenschaften der Materie in ihren Aggregatzuständen: Transport-Phänomene I*, Landolt-Börnstein II5a (Springer, Berlin, 1969).
- [27] A. I. Nielsen, T. Christensen, B. Jakobsen, K. Niss, N. B. Olsen, R. Richert, and J. C. Dyre, *J. Chem. Phys.* **130**, 154508 (2009).
- [28] C. Gangasharan and S. S. N. Murthy, *J. Chem. Phys.* **99**, 9865 (1993).
- [29] S. Wiebel, Doctoral thesis, Technische Universität München, 2003.
- [30] N. Petzold and E. A. Rössler (unpublished).
- [31] G. Friz, G. Kuhlbörsch, R. Nehren, and F. Reiter, *Atomkernenergie* **13**, 25 (1968).
- [32] *CRC Handbook of Chemistry and Physics*, 78th ed. (CRC Press, Boca Raton, FL, 1997).
- [33] D. J. Plazek and J. H. Magill, *J. Chem. Phys.* **45**, 3038 (1966).
- [34] Data from https://dow-answer.custhelp.com/app/answers/detail/a_id/7457/~propylene-glycols-viscosity-information, © Copyright The Dow Chemical Company (2011).
- [35] A. J. Barlow, J. Lamb, and A. J. Matheson, *Proc. R. Soc. London, Ser. A* **292**, 322 (1966).
- [36] E. Rössler and H. Sillescu, *Chem. Phys. Lett.* **112**, 94 (1984).
- [37] E. A. Moelwyn-Hughes, *Physikalische Chemie* (Thieme, Stuttgart, 1970).
- [38] F. Stickel, E. W. Fischer, and R. Richert, *J. Chem. Phys.* **104**, 2043 (1996).
- [39] Ch. Alba-Simionesco, D. Kivelson, and G. Trajus, *J. Chem. Phys.* **116**, 5033 (2002).
- [40] S. Sastry, *PhysChemComm* **3**, 79 (2000).
- [41] D. Kivelson, S. A. Kivelson, X. L. Zhao, Z. Nussinov, and G. Tarjus, *Physica A* **219**, 27 (1995).
- [42] C. A. Angell, in *Relaxation in Complex Systems*, edited by K. L. Ngai and G. B. Wright (US Dept. of Commerce, Springfield, 1985).
- [43] F. Fujara, B. Geil, H. Sillescu, and G. Fleischer, *Z. Phys. B* **88**, 195 (1992).
- [44] C. Dreyfus, A. Le Grand, J. Gapinski, W. Steffen, and A. Patkowski, *Eur. Phys. J. B* **42**, 309 (2004).
- [45] S. Capaccioli and K. Ngai, *J. Chem. Phys.* **135**, 104504 (2011).
- [46] G. Monaco, A. Cunsolo, G. Ruocco, and F. Sette, *Phys. Rev. E* **60**, 5505 (1999).

Publication 2

Reorientational dynamics in molecular liquids as revealed by dynamic light scattering: From boiling point to glass transition temperature

B. Schmidtke, N. Petzold, R. Kahlau, E. A. Rössler

The Journal of Chemical Physics **139**, 084504 (2013).

Copyright 2013 by The American Institute of Physics Publishing LLC

DOI: 10.1063/1.4817406

Reorientational dynamics in molecular liquids as revealed by dynamic light scattering: From boiling point to glass transition temperature

B. Schmidtke, N. Petzold, R. Kahlau, and E. A. Rössler
Experimentalphysik II, Universität Bayreuth, D-95444 Bayreuth, Germany

(Received 28 May 2013; accepted 19 July 2013; published online 26 August 2013)

We determine the reorientational correlation time τ of a series of molecular liquids by performing depolarized light scattering experiments (double monochromator, Fabry-Perot interferometry, and photon correlation spectroscopy). Correlation times in the range 10^{-12} s–100 s are compiled, i.e., the full temperature interval between the boiling point and the glass transition temperature T_g is covered. We focus on low- T_g liquids for which the high-temperature limit $\tau \cong 10^{-12}$ s is easily accessed by standard spectroscopic equipment (up to 440 K). Regarding the temperature dependence three interpolation formulae of $\tau(T)$ with three parameters each are tested: (i) Vogel-Fulcher-Tammann equation, (ii) the approach recently discussed by Mauro *et al.* [Proc. Natl. Acad. Sci. U.S.A. **106**, 19780 (2009)], and (iii) our approach decomposing the activation energy $E(T)$ in a constant high temperature value E_∞ and a “cooperative part” $E_{\text{coop}}(T)$ depending exponentially on temperature [Schmidtke *et al.*, Phys. Rev. E **86**, 041507 (2012)]. On the basis of the present data, approaches (i) and (ii) are insufficient as they do not provide the correct crossover to the high-temperature Arrhenius law clearly identified in the experimental data while approach (iii) reproduces the salient features of $\tau(T)$. It allows to discuss the temperature dependence of the liquid’s dynamics in terms of a $E_{\text{coop}}(T)/E_\infty$ vs. T/E_∞ plot and suggests that E_∞ controls the energy scale of the glass transition phenomenon. © 2013 AIP Publishing LLC. [<http://dx.doi.org/10.1063/1.4817406>]

I. INTRODUCTION

Describing and understanding the temperature dependence of transport quantities such as viscosity and diffusion as well as structural correlation time τ of molecular liquids is an unsolved problem.^{1–7} In particular, extending the temperature range to the super-cooled regime, a super-Arrhenius temperature dependence is observed in which transport quantities change by many orders of magnitude within a narrow temperature interval. Numerous phenomenological descriptions of $\tau(T)$ have been proposed; yet, most of them cover only a limited temperature range. While a molecular liquid well above its melting point T_m exhibits a viscosity on the order of 10^{-3} Pa s, upon super-cooling it finally reaches values of 10^{12} Pa s (provided crystallization can be avoided) which are typical of solids. The corresponding temperature is defined as glass transition temperature T_g . The slowing-down of dynamics in such glass formers is accompanied by a smooth change in structure and the glass transition is interpreted as a kinetic phenomenon. Several theoretical approaches have been developed, yet none is fully accepted.^{3,8–10} In particular, no full description of $\tau(T)$ is offered from this side.

It turns out that, although extensively studied below T_m , molecular glass formers are not well investigated in the high-temperature regime above T_m . With a few exceptions most tests of interpolating $\tau(T)$ are restricted to time constants above 10^{-10} s– 10^{-9} s actually ignoring a large temperature range until the high-temperature limit $\tau_\infty \cong 10^{-12}$ s is reached. For example, a popular approach for probing molecular reorientation is dielectric spectroscopy (DS),^{11–13} but in most cases such experiments do not cover frequencies above

a few GHz. Correlation times down to 10^{-12} s are now easily available when glass formers are studied by depolarized light scattering (LS) using tandem-Fabry-Perot interferometer (TFPI) and double monochromator (DM).^{14–18} In a recent publication, we have reported the results of such a LS study on a series of molecular liquids.⁴ The data $\tau(T)$ have been combined with those obtained from photon correlation spectroscopy (PCS) and DS and thus cover the entire temperature range from the boiling point down to T_g needed to attempt a full description of $\tau(T)$.

Often the empirical Vogel-Fulcher-Tammann (VFT) formula¹⁹ is applied to fit experimental data. However, its parameters depend strongly on the fitting interval and it fails when relaxation data well above T_m have to be interpolated. Recently, a three-parameter formula has been introduced by Mauro *et al.*²⁰ which appears to work over a larger temperature interval.²¹ As an empirical formula it was already proposed by Waterton in 1932.²² Here, the simple Arrhenius law is (formally) generalized by introducing an exponential temperature dependence of the activation energy. Actually, it is based on a particular temperature dependence of the configuration entropy of a liquid. The approach bears some similarity with our recent attempt⁴ in which, following ideas of Kivelson *et al.*²³ and Sastry,²⁴ the activation energy $E(T)$ is decomposed into a temperature independent part E_∞ describing the high-temperature regime well above the melting point T_m and a quantity $E_{\text{coop}}(T) \equiv E(T) - E_\infty$ reflecting “cooperative dynamics” dominating in the low-temperature regime close to T_g . The quantity $E_{\text{coop}}(T)$ appears to follow an exponential temperature dependence.⁴ Analyzing the data of the below mentioned series of molecular liquids, we have introduced

a “generalized” Angell plot displaying $E_{\text{coop}}(T)/E_{\infty}$ vs. T/E_{∞} , and looking for a minimal number of system-specific parameters controlling $\tau(T)$ in the range 10^{-12} s– 10^2 s, three parameters turn out to be sufficient. Thus, instead of T_g the energy scale of the glass transition phenomenon might be set by the experimentally accessible quantity E_{∞} . Having at hand such data, it is one aim of the present contribution to compare the different approaches provided by VFT, Mauro *et al.*,²⁰ and our own one.

In our previous work⁴ we reported only the $\tau(T)$ data without presenting the corresponding DM/TFPI spectra or PCS decays and not describing their analysis; this will be done here. As the boiling point T_b is reached, the susceptibility spectra (obtained from LS) collapse to a single broad relaxation including α -peak and the so-called microscopic peak. Thus, it is not straightforward to extract the actual time constant of the α -relaxation, and it will be done here in a model independent way. The best chance to find a fully satisfying description of $\tau(T)$ will be provided by experimental data on low- T_g glass formers, where time constants between T_b and T_g are easily accessed by standard LS apparatus. We present DM/TFPI spectra and PCS decay curves also on the glass former 2-methyl tetrahydrofuran (MTHF) for which a temperature range 92 K–440 K is covered, and we complement our previously published data^{16–18,25–27} to include temperatures up to 440 K. The values of T_g show a variation of a factor of almost four. Most importantly, we find clear indication that all liquids display a trend of an Arrhenius temperature dependence at highest temperatures, in the case of MTHF it is observed over a range of 250 K. Although the high-temperature activation energy cannot be attributed to some single-particle barrier in the liquid, the Arrhenius law at high temperatures has to be taken as a matter of fact and any description of $\tau(T)$ has to contain this limiting behavior. Yet, also, the aforementioned analyses, e.g. the Mauro *et al.* formula,^{20,21} have not included high-temperature data. The data analyzed in the present work allow for the conclusion that in general the interpolations by Mauro *et al.*²⁰ and by VFT (in the latter case a well-known fact) are not appropriate to fully interpolate the $\tau(T)$. Still, the approach by Mauro *et al.*²⁰ provides satisfying interpolations in some cases as well as the VFT equation does. Our recently introduced approach⁴ appears to fit the data between T_b and T_g in all cases, and will be discussed in detail.

II. EXPERIMENTAL DETAILS

The samples were commercially available (Sigma-Aldrich) and were investigated without further purification. The sample was vacuum distilled right into glass tubes with an inner diameter of 8 mm. After degassing of the sample the tubes were flame sealed. For measurements with TFPI and DM the sample was either mounted in a self-built furnace or a CryoVac continuous-flow (liquid nitrogen) cryostat. As light source we used a vertically polarized Coherent Verdi-V2 laser at a wavelength of 532 nm and 200 mW optical power. Measurements with TFPI (JRS Scientific, triple-pass tandem Etalon) and DM (Jobin Yvon, U1000) were performed in parallel. TFPI was operating at horizontal polarization in almost backscattering geometry whereas the DM was

operating at orthogonal geometry. For details, the reader is referred to Wiedersich *et al.*¹⁵ The TFPI-measurements were done with three different free spectral ranges and the DM-measurements with two combinations of slits and frequency intervals. The parts are then adjusted in amplitude to match together and form a smooth spectral density $S(\nu)$. For performing a Fourier transformation, an algorithm based on the Filon algorithm has been used, because the arbitrary spaced data points are incompatible with the fast Fourier algorithm.

For PCS measurements the samples were mounted in a cold-finger (Advanced Research Systems). The incident light again was vertically polarized. Scattered intensity was gathered at an angle of 90° at horizontal polarization using a single mode fiber. The fiber was then connected via a 50/50-splitter with two avalanche photo diodes (Perkin Elmer). Both signals were cross-correlated with an ALV 6010 correlator with a shortest lag time of $\tau \approx 6$ ns.

We investigated 13 different molecular liquids by DM/TFPI, and four of them in addition by PCS. Some of the DM/TFPI as well as PCS spectra were already published in parts before.^{16–18,25–27} In particular, we complemented all our previous data to include temperatures up to 440 K. One system (monoepoxide phenyl glycidyl ether) is only characterized by dielectric spectroscopy, and for further four ones, the time constant $\tau(T)$ are taken from the literature. The systems, their T_g , and fit parameters referring to Eq. (3), are listed in Table I. For reasons of lucidity only a selection of DM/TFPI spectra and PCS decays are shown.

III. RESULTS AND DISCUSSION

Figure 1(a) shows depolarized LS susceptibility spectra of MTHF ($T_g = 92$ K, $T_m = 137$ K, $T_b = 352$ K²⁸) as obtained by combing spectra from DM and TFPI measurements in the temperature range 135 K–440 K. The highest temperature is somewhat above the (ambient pressure) boiling point. The experimentally measured spectral density $S(\nu)$ was converted to the susceptibility representation via $\chi''(\nu) = (1 + n(\nu))^{-1} S(\nu)$ where $n(\nu)$ is the Bose factor. The spectra are normalized to an equal integrated intensity of Raman bands which have turned out to show virtually no temperature dependence. The liquid MTHF has a low scattering power due to its low molecular electronic polarizability, and the signal-to-noise ratio is rather low compared to that of ethyl benzene⁷ or *o*-terphenyl (OTP).¹⁸ At low temperatures and low frequencies the primary or α -relaxation is well recognized as a separate asymmetrically broadened peak in addition to the microscopic (vibrational) peak around 2 THz. In between, a minimum is observed in the susceptibility. While heating, the α -process shifts to higher frequencies and approaches the microscopic peak. At highest temperatures, both peaks have virtually merged to become a somewhat broadened single peak. Very similar results are observed for dimethyl phthalate (DMP; $T_g = 191$ K, $T_m = 233$ K, $T_b = 565$ K;²⁹ cf. Fig. 1(b)). As T_g of DMP is significantly higher than that of MTHF, the α -relaxation and the microscopic dynamics have not yet merged at 440 K. We note, that applying a detailed spectral analysis including the contribution of the fast dynamics, the stretching of the α -relaxation turns out to be

TABLE I. Molecular liquids investigated and parameters of the analysis: glass transition temperature T_g ; high-temperature activation energy E_∞ as determined by an Arrhenius fit; and E_∞ , fragility parameter μ , and logarithm of pre-exponential factor τ_∞ all obtained by applying fits with Eq. (3). Abbreviations used and the methods with which the system is characterized in the present work are given in brackets (when taken from the literature: lit.). References to the corresponding literature are given in the appropriate figures.

Sample	T_g (K)	E_∞ Arrhenius (K)	E_∞ fit (K)	μ	$\lg \tau_\infty$ (s)
2-Methyl tetrahydrofuran (MTHF; DM/TFPI, PCS)	92	1169	1020	80	-13.43
Ethyl benzene (DM/TFPI)	115	1369	1229	74	-13.34
Toluene (DM/TFPI)	117	1440	1258	59	-13.49
<i>n</i> -Butyl benzene (lit.)	131	1315	1440	62	-12.74
Iso-propyl benzene (lit.)	128	1342	1392	62	-12.74
α -Picoline (DM/TFPI)	129	1438	1421	63	-13.47
Propylene carbonate (DM/TFPI)	157	1729	1699	68	-13.41
4-Tert-butyl pyridine (4-TBP; DM/TFPI)	164	1761	1776	70	-13.30
Propylene glycol (lit.)	168	2332	1968	32	-13.69
Decahydroisoquinoline (DHIQ; DM/TFPI)	180	1851	1930	71	-13.34
Glycerol (DM/TFPI)	188	2271	2256	34	-13.69
Dimethyl phthalate (DMP; DM/TFPI/PCS)	191	2029	2122	54	-13.04
Monoepoxide phenyl glycidyl ether (PGE; DS)	194	2321	2064	68	-13.45
<i>m</i> -Tricresyl phosphate (<i>m</i> -TCP; DM/TFPI/PCS)	205	2301	2256	60	-13.42
Benzophenone (DM/TFPI)	207	2530	2179	85	-13.37
Salol (DM/TFPI)	218	2104	2323	82	-12.58
<i>o</i> -Terphenyl (DM/TFPI/PCS)	245	2441	2630	79	-13.22
Trinaphthyl benzene (TNB; lit.)	343	3232	3744	78	-13.22

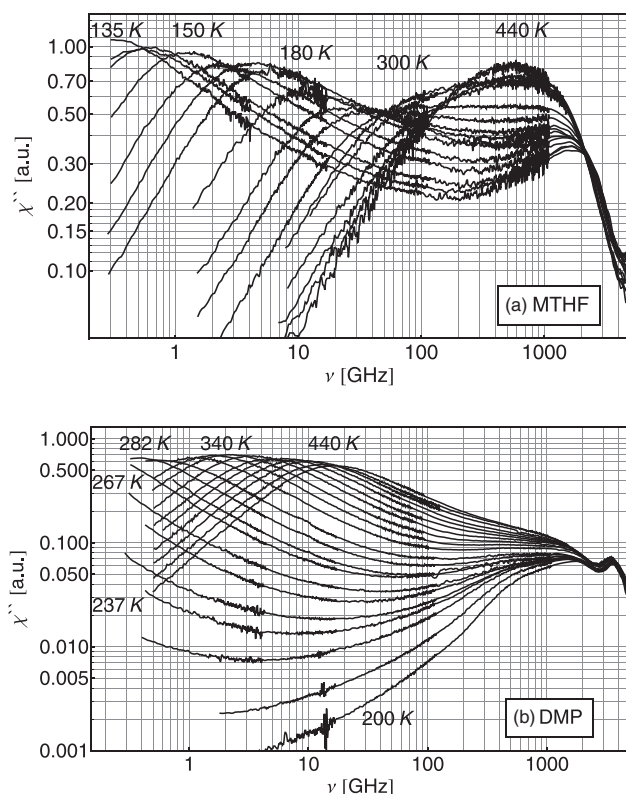


FIG. 1. (a) Susceptibility spectra of 2-methyl tetrahydrofuran (MTHF; $T_g = 92$ K, $T_m = 137$ K, and $T_b = 352$ K) obtained by applying DM/TFPI for different temperatures in K: 135, 140, 145, 150, 160, 170, 180, 200, 220, 240, 270, 300, 320, 350, 380, 410, and 440. (b) Corresponding spectra of dimethyl phthalate (DMP; $T_g = 191$ K, $T_m = 233$ K, $T_b = 565$ K) at temperatures in K: 200, 215, 230, 237, 245, 252, 260, 267, 275, 282, 290, 305, 315, 325, 340, 355, 370, 385, 400, 420, and 440.

essentially temperature independent. No evidence of crossover to a Debye spectral form is found.¹⁸ These findings are virtually observed for all the liquids studied here.⁷

Extracting the time constant $\tau(T)$ at low temperatures is easily carried out by interpolating the α -relaxation peak with a Cole-Davidson (CD) function.³⁰ Then, the spectra normalized by the amplitude χ_α° of the α -process are plotted as a function of the reduced frequency $\omega\tau$ (cf. Figure 2(a)). At the highest temperatures, when the α -peak and the microscopic dynamics have more or less merged, the spectra are rescaled to provide a common low-frequency envelope, explicitly $\chi''/\chi_\alpha^\circ = \omega\tau$ holds as needed for a simple liquid. As a crosscheck, the amplitude χ_α° follows the temperature dependence established at low temperatures up to highest temperatures in a regular smooth way, cf. inset in Fig. 2(a). The corresponding results for DMP are shown in Fig. 2(b). By this scaling procedure the time constants can be extracted in a model independent way. The time constant $\tau(T)$ for MTHF is plotted in Fig. 4 together with results reported by other methods and also in Fig. 5 where it is compared to the data compiled for three other liquids including DMP. In Fig. 10 all our data for the 18 liquids investigated are displayed, and the results will be discussed below.

In Fig. 3(a) we show the results for MTHF from our PCS set-up¹⁸ covering a temperature range from 92 K to 107 K. The measured intensity correlation functions were normalized and transformed utilizing the Siegert relation into the field correlation function, respectively, the intermediate scattering function $\Phi(t) = \sqrt{\langle(I(t)I_0)\rangle/\langle I^2 - 1\rangle}/c$ with the coherence factor c .³¹ Upon cooling the long-time tail of the α -relaxation enters the explored time window until the entire non-exponential decay curve is observed at temperatures

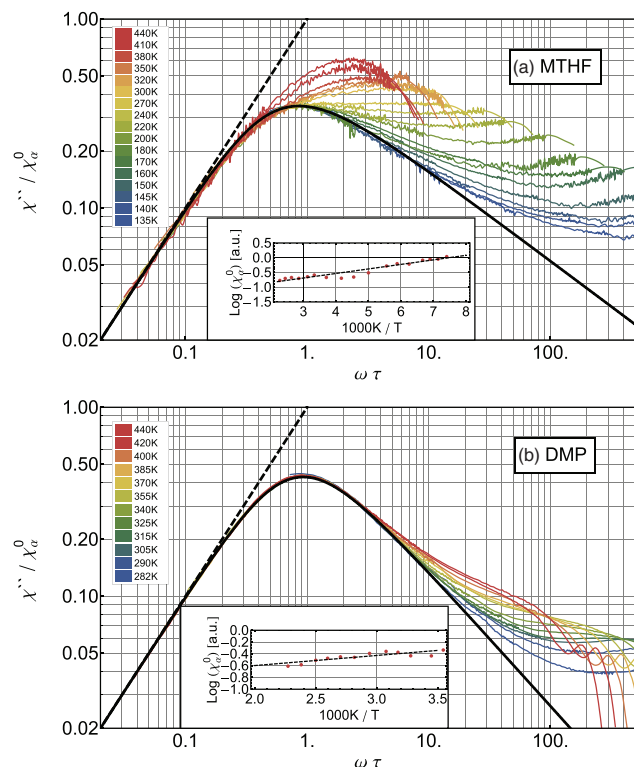


FIG. 2. (a) Susceptibility master curve of 2-methyl tetrahydrofuran (MTHF) obtained by rescaling the spectra of Fig. 1(a); solid line: Cole-Davidson (CD) function with $\beta = 0.48$; dashed line: low-frequency limiting behavior $\chi''/\chi_\alpha^0 = \omega\tau$; inset: amplitude χ_α^0 of α -relaxation as revealed by constructing the master curve showing a smooth change with temperature. (b) Corresponding spectra (cf. Fig. 1(b)) and amplitude χ_α^0 for dimethyl phthalate (DMP); CD fit with $\beta = 0.72$ is shown as solid line.

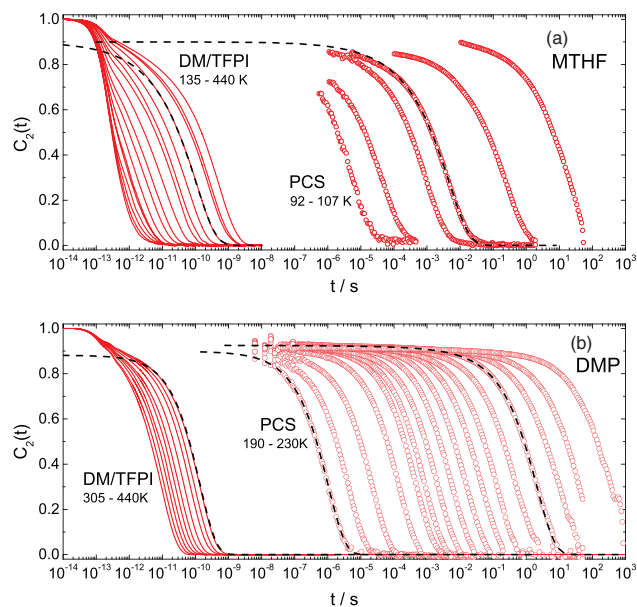


FIG. 3. Reorientational correlation function $C_2(t)$ of (a) 2-methyl tetrahydrofuran (MTHF) and of (b) dimethyl phthalate (DMP) obtained from PCS (open circles) and from DM/TFPI (after Fourier transformation; lines). Fits by the time domain expression of the generalized Cole-Davidson function³³ (dashed lines).

close to T_g . We included the DM/TFPI decay curves from Fig. 1 (after Fourier transforming) which extend the dynamic window to highest temperatures (up to 440 K). Again, due to the low scattering power of MTHF, the PCS correlation decay is probed over a rather narrow time window and the amplitude had to be corrected to match the DM/TFPI data. In contrast, in the case of DMP a much better data set is obtained, cf. Fig. 4(b). Apparently no change with temperature in amplitude as well as stretching is recognizable up to highest temperatures. After having established its bimodal shape well above the melting point, essentially no further change is recognizable in the reorientational correlation function while cooling down to T_g . Subtle features like the emergence of the so-called excess wing can only be identified (by bare eyes) after transforming the data into the frequency domain.⁷ At high-temperatures one can clearly see how the stretched long-time decay “grows out” of the microscopic peak when the temperature is decreased, i.e., a new relaxation feature characteristic of glassy dynamics emerges well above the melting point. Finally, we note that a slow β -process identified in the dielectric spectra of DMP is not probed by PCS.^{7,32}

In order to extract time constants and stretching parameters the decays are interpolated by the time domain expression of the Cole-Davidson function or the more general function introduced by Kahlau *et al.*³³ (see Appendix B). An excess wing can be taken into account for modeling the crossover to the relaxation plateau, but it has virtually no influence on the value of the time constants of the α -process.⁷ The corresponding time constants of MTHF are included in Figs. 4, 5, and 10, and those of DMP in the Figs. 5 and 10.

Figure 4 compares our results $\tau(T)$ for MTHF as obtained by the different techniques: DM/TFPI, PCS, DS,^{34,35} stimulated echo decay of nuclear magnetic resonance spectroscopy (NMR)³⁴ and diffusion³⁴ as a function of reciprocal temperature. The data agree very well, no systematic change is observed among the different methods although single-particle as well as collective reorientational correlation functions of different rank as well as diffusion data are probed. Except the PCS data show some small deviations at high temperatures. We note that a very large temperature interval of about 350 K is covered and time constants down to

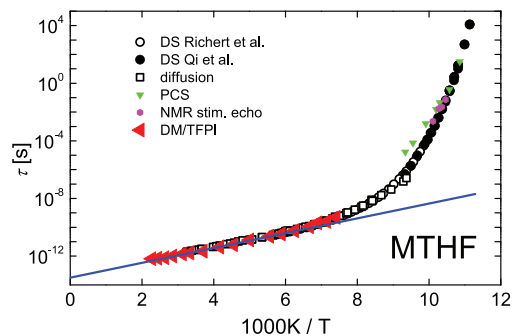


FIG. 4. τ of 2-methyl tetrahydrofuran (MTHF; $T_g = 92$ K, $T_m = 137$ K, and $T_b = 352$ K) obtained from different techniques (as indicated); present work (DM/TFPI and PCS) dielectric spectroscopy (DS),^{34,35} diffusion coefficient (shifted),³⁴ and NMR (stimulated echo decay).³⁴ Solid line indicates Arrhenius law at high temperatures.

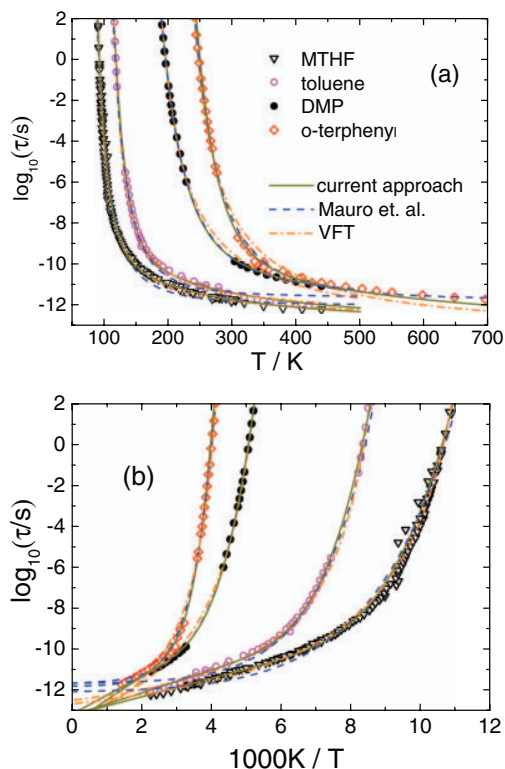


FIG. 5. Reorientational correlation time of 2-methyl tetrahydrofuran (MTHF), toluene, dimethyl phthalate (DMP), and *o*-terphenyl (OTP) plotted versus temperature (a) and versus inverse temperature (b); interpolation by VFT-equation (Eq. (1)), Mauro *et al.*²⁰ (Eq. (2)), and current approach (Eq. (3)).

about 5×10^{-13} s are shown. At high temperatures an Arrhenius behavior can be clearly anticipated (solid line).

In Fig. 5 we display the data $\tau(T)$ for two other liquids, namely, *o*-terphenyl ($T_g = 244$ K, $T_m = 328$ K, $T_b = 605$ K),^{14,18,36–40} and toluene ($T_g = 118$ K, $T_m = 178$ K, $T_b = 384$ K),^{11,41} together with those from MTHF and DMP. The liquids exhibit a significant variation in T_g and are studied up to rather high temperatures. In this case we do not distinguish any longer among the results from different techniques (cf. caption of Fig. 10). In order to test the quality of often applied interpolation formulae the data in the entire temperature range investigated are interpolated by the following expressions, referring to the VFT,¹⁹ the Mauro *et al.*²⁰ expression, and our current approach:⁴

(i) VFT:

$$\tau = \tau_\infty \exp[D/(T - T_0)]. \quad (1)$$

(ii) Mauro *et al.*:²⁰

$$\tau = \tau_\infty \exp[K/T \exp(C/T)]. \quad (2)$$

(iii) Our current approach:

$$\begin{aligned} \tau &= \tau_\infty \exp[(E_\infty + E_{coop})/T] \\ &= \tau_\infty \exp[E_\infty/T(1 + \exp(-\mu(T/E_\infty - b)))]. \quad (3) \end{aligned}$$

The three parameters showing up in approach (i) (τ_∞ , D , and T_0) and (ii) (τ_∞ , K , and C) are assumed to be mere fit parameters. Actually also in the case of our approach (iii) a three-parameter (τ_∞ , E_∞ , and μ) interpolation is implied since the parameter $b = T_A/E_\infty \cong 0.10$ may be taken to be constant for all the molecular liquids studied here and this is done for all the following fits. Here, the temperature T_A refers to a common point in the plot E_{coop}/E_∞ vs. T/E_∞ (cf. below). In Appendix A our approach is again rationalized (cf. also Ref. 4). As will be demonstrated, the parameter μ has the meaning of a generalized fragility parameter. We note that in our previous work^{4,7} we used the parameter $\lambda = \mu b$. Choosing μ instead of λ leads to values for the fragility which are on the same order of magnitude as the conventionally defined fragility index m (cf. Fig. 9).

In Fig. 5 the rotational time constants τ are plotted as a function of temperature and inverse temperature, respectively. In the case of the high- T_g system *o*-terphenyl the approaches by VFT and by Mauro *et al.*²⁰ fail to interpolate the data in particular at high temperatures. Yet, VFT works rather well for the low- T_g liquid MTHF for which again the Mauro *et al.*²⁰ approach fails. In contrast, our current approach interpolates the data rather well in all cases. We again want to emphasize that the parameter b was set to the universal value of 0.10. As already mentioned, the high-temperature behavior is well reproduced by an Arrhenius law, in the case of MTHF, it is observed over more than 250 K. Consequently, in such well studied systems the high-temperature activation energy E_∞ can be assessed model independently.

To inspect the temperature dependence of $\tau(T)$ in more detail we show in Fig. 6(a) the apparent activation energy as given by the derivative of $\ln \tau$ with respect to the reciprocal temperature $1/T$. This is calculated point by point and then averaged over three neighboring points to reduce scatter produced by performing the derivation. The liquids MTHF, toluene, propylene carbonate, propylene glycol, and OTP are considered. Again, the derivative data are shown as a function of inverse temperature (a) and as a function of temperature (b). In both representations evidence is found that the apparent activation energy becomes finally constant at highest temperatures. The three approaches ((1)–(3)) provide specific analytic expressions for the temperature dependence of $E_A(T)$ (cf. Appendix B) which are used to interpolate the experimental data. Again, the quality of the fits depends on the fact whether T_g is high or low. While the Mauro *et al.*²⁰ approach, which essentially yields a linear behavior of $E_A(1/T)$, well interpolates most of the *o*-terphenyl data except for highest temperatures, it severely fails for low- T_g liquids. Here, the VFT equation works somewhat better. But in any case, the final high-temperature behavior is not described by approach (i) as well as (ii) what is best seen in Fig. 6(b) displaying $E_A(T)$. The present approach (iii) captures all salient features of $\tau(T)$; in particular, the crossover to E_∞ at highest temperatures is well reproduced. Regarding the non-fragile glass former propylene glycol all three approaches work well, and this is also the case for glycerol.^{4,21} As the high-temperature regime with constant activation energy is not reached no decision regarding the quality of the interpolation can be drawn here.

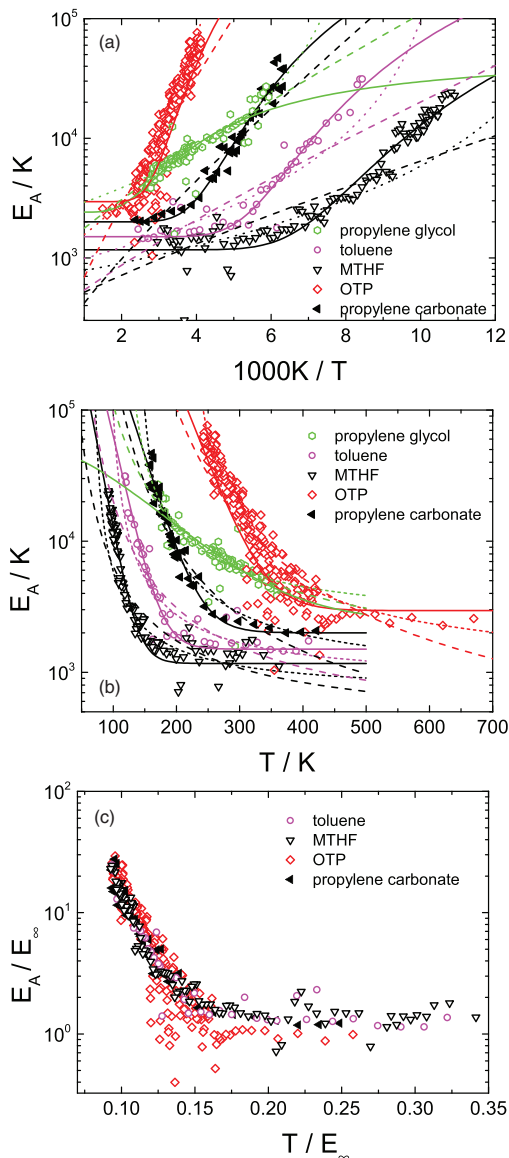


FIG. 6. Apparent activation energy $E_A(T)$ for selected molecular liquids as function of (a) temperature and (b) inverse temperature, dotted lines: VFT (Eq. (1)), dashed lines: Mauro *et al.*²⁰ (Eq. (2)), and solid lines: our current model (Eq. (3)) (cf. Appendix B). (c) Reduced activation energy $E_A(T)/E_\infty$ vs. T/E_∞ .

Another feature is recognized in Fig. 6(b). It appears that the lower E_∞ (plateau in Fig. 6(b)), the more the onset of cooperative dynamics shifts to lower temperatures. In other words, T_A (see Appendix A) and E_∞ appear to be correlated. Thus, we plotted the reduced activation energy $E_A(T)/E_\infty$ vs. T/E_∞ in Fig. 6(c). Within the scatter of the data a universal dependence is observed. MTHF and OTP, for example, systems with rather different T_g as well as E_∞ display very similar behavior. Not surprising, fragility parameters m are quite alike in these systems (cf. below and Table I). Here, propylene glycol has been excluded as E_∞ is not reached.

In order to estimate E_∞ for all the systems studied it is extracted from an Arrhenius fit of the high-temperature data in Fig. 10. Of course, in some cases this provides only a rough estimate for E_∞ as still sufficient high-temperature data are

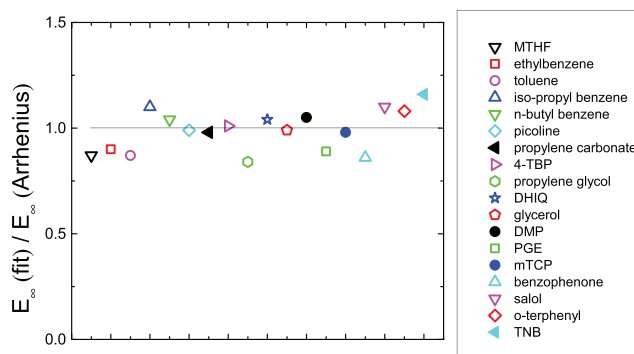


FIG. 7. Quotient of the parameter E_∞ from the free three-parameter fits shown in Fig. 10 and the experimentally observed activation energy E_∞ at high temperatures (Arrhenius).

not available. In Fig. 7 the quotient of the parameters E_∞ from the free three-parameter fits with Eq. (3) shown in Fig. 10 and the experimentally found high-temperature activation energy E_∞ (Arrhenius) is displayed for the different systems studied. The uppermost deviation from unity is in the order of 15%, and is for most systems smaller. This is in the range of the experimental uncertainty in determining E_∞ from the time constants $\tau(T)$ as well as from the high-temperature Arrhenius fit. It proves that the parameter E_∞ in Eq. (3) represents the activation energy at high temperatures.

Figure 8 presents the reduced quantity $E_{coop}(T)/E_\infty$ as given by plotting $(T \ln \tau / \tau_\infty - E_\infty) / E_\infty = E_{coop}(T)/E_\infty$ versus T/E_∞ for four selected systems, which cover a wide range of μ parameters.^{4,7} The values of the parameters E_∞ and τ_∞ , which are needed to calculate $E_{coop}(T)$ are taken from the three-parameter fits to the $\tau(T)$ data shown in Fig. 10. This “generalized Angell plot”^{4,7} takes E_∞ instead of the conventionally defined T_g as energy scale of the glass transition. Exponential temperature dependence is observed in good approximation justifying our formula. Again, the curves of MTHF and OTP are very similar, and they intersect with the curve of propylene glycol at $E_{coop}(T_A)/E_\infty \cong 1$. We repeat to note that the energy scale E_∞ might be well defined for all molecular liquids, though it is hard to access as one needs $\tau(T)$ at high temperatures compared to T_g . Thus low- T_g systems are better suited for the separation of $E_{coop}(T)$ and E_∞ . Therefore the bending down of the curve for propylene glycol might be attributed to an imperfect estimation of E_∞ which, as discussed, in the case of non-fragile glass formers is indeed experimentally difficult to access.

The parameter μ introduced in approach (iii) has been called a generalized fragility;⁴ it can directly be read off as the slope of $E_{coop}(T/E_\infty)/E_\infty$ in Fig. 8(b), and it is expected to be correlated to the “steepness” of $\lg \tau = f(T_g/T)$ which conventionally is defined by the fragility index $m = \left. \frac{\partial \lg(\tau)}{\partial (T_g/T)} \right|_{T=T_g}$. Although no clear cut relation between μ and m can be given, still a correlation is found in Fig. 9 justifying the notion of generalized fragility for μ . Noteworthy, two systems show strong deviations from the correlation displayed in Fig. 9, namely decahydroisoquinoline (DHIQ) and toluene. In contrast to the rest of the systems both liquids exhibit a strong

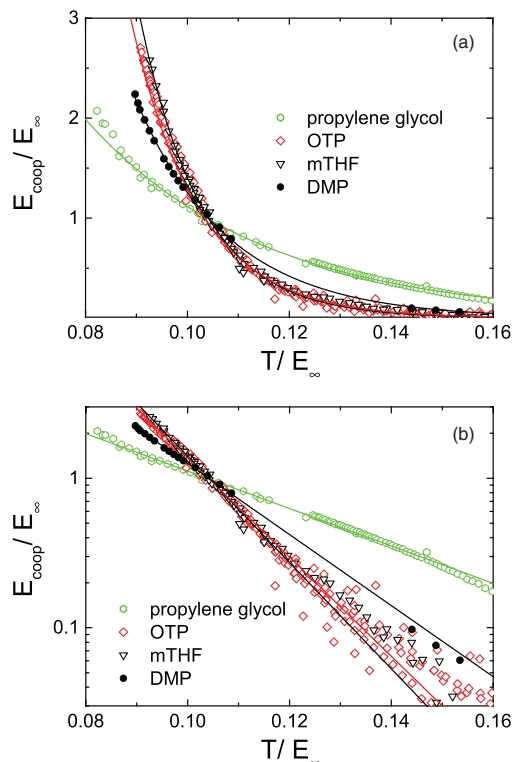


FIG. 8. (a) $E_{\text{coop}}(T)/E_{\infty}$ versus T/E_{∞} obtained by fitting $\tau(T)$ data interpolated by an exponential function (solid lines) for the three systems 2-methyl tetrahydrofuran (MTHF), *o*-terphenyl (OTP), and propylene glycol. (b) Same data on logarithmic scale; straight lines illustrate an exponential temperature dependence.

secondary relaxation (β -process), and the separation of the spectral contributions of α - and β -process and consequently a reliable estimate of $\tau(T)$ may not be straightforward. Except for the two hydrogen bond network forming liquids glycerol and propylene glycol μ or m does not vary significantly, and it is not clear so far whether there are examples of molecular glass formers which exhibit fragility between the limit of glycerol/propylene glycol and the group of van der Waals liquids like OTP.

In Fig. 12 (in Appendix D) a possible correlation between the parameters E_{∞} and μ is tested. Clearly, no correlation is found, meaning that the parameters are independent of each

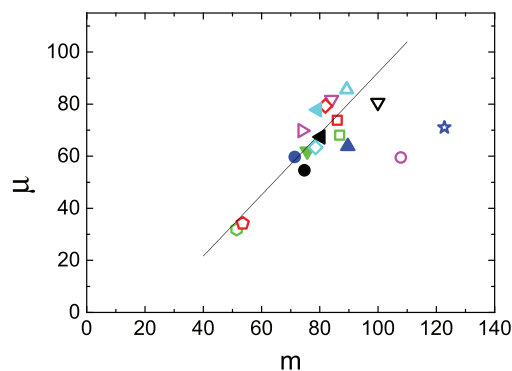


FIG. 9. Correlation between the generalized fragility parameter μ and the conventionally defined fragility index m ; color code as in Fig. 7.

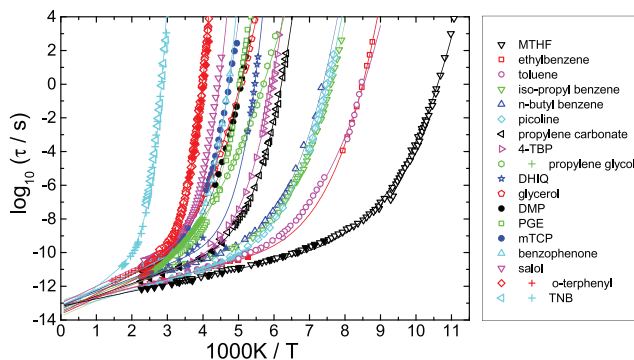


FIG. 10. Reorientational correlation times of the molecular liquids (for abbreviations see Table I) obtained by depolarized light scattering including DM/TFPI and PCS (full symbols; present work and Refs. 16–18 and 25–27) and from our dielectric database (open symbols).^{11,43–46} For the following systems additional data are used: OTP,^{14,37–39} MTHF;^{34,35} *n*-butyl benzene;^{47,48} iso-propylene benzene;^{49–51} trinitrophenyl benzene (TNB).⁵² Viscosity data (rescaled): for OTP,³⁶ TNB,⁵³ and propylene glycol⁵⁴ (crosses); for toluene ²H NMR data⁴¹ have been included; solid lines: fit by the current approach (Eq. (3)).

other and we need at least another parameter in addition to τ_{∞} and E_{∞} for describing the increase of the time constants close to T_g . We note that based on the validity of the VFT equation a correlation $E_{\infty} \propto T_g/m$ was proposed for a series of molecular as well as network glass formers,⁴² which is not found in our data. Actually, it is difficult to test because of the relatively small variation of m in our dataset for molecular liquids. Accessing the high-temperature activation energy E_{∞} in network forming glasses such as GeO_2 ($T_g = 800$ K) appears almost impossible. The authors restricted their analysis to reduced temperatures $T/T_g < 2.5$ while, e.g., for MTHF our present analysis covers a range $T/T_g < 4.5$.

Finally, we display in Fig. 10 all the data compiled by our light scattering equipment and complemented in some cases by the results of other techniques like dielectric spectroscopy (partly from our group), viscosity, and diffusion. They are almost perfectly interpolated by applying Eq. (3). For the first time, a complete fit of $\tau(T)$ from the boiling point down to T_g has become possible.

IV. CONCLUSION

Combining different light scattering techniques (DM, TFPI, and PCS), the evolution of the susceptibility spectra has been measured for a series of molecular glass formers and for temperatures between the boiling point ($T \leq 440$ K) and T_g . The corresponding T_g values range from 92 K to 333 K. The time constants presented agree well with those obtained from other techniques when available. In the case of the low- T_g liquids a broad high-temperature interval has been identified for which $\tau(T)$ is well described by an Arrhenius temperature dependence. Here, structural and microscopic dynamics have essentially merged, i.e., a two-step correlation function is not observed any longer, and time constants down to 10^{-12} s (in some cases even below) have been extracted in a model independent way. A trend to crossover to Arrhenius high-temperature dependence well above the melting point is also found for systems with higher T_g and also for the

non-fragile liquids glycerol and propylene glycol. Yet, the high-temperature activation energy E_∞ cannot be accessed reliably in these cases.

Having at hand correlation times in the range $10^{-12} \leq \tau/s \leq 100$ which cover the entire regime of the liquid's dynamics, i.e., from simple liquid to glassy dynamics, we have tested different formulae currently applied to interpolate $\tau(T)$. We note that most such tests so far have been restricted to $\tau > 10^{-10}$ s due to missing high-temperature data. While the formulae of VFT and Mauro *et al.*²⁰ fail to describe the crossover to Arrhenius law at high temperatures correctly, our previously introduced description⁴ works well in all cases. It decomposes the activation energy $E(T)$ in a temperature independent high-temperature contribution E_∞ and a temperature dependent part $E_{coop}(T)$. The latter follows essentially an exponential temperature dependence. Introducing a generalized Angell plot, namely $E_{coop}(T)/E_\infty$ vs. T/E_∞ , indicates the possibility that a common intersection point for the data of the group of liquids defines a crossover temperature T_A , for which $T_A/E_\infty = b$ is a universal constant and which renders our approach describing $\tau(T)$ a three-parameter formula. Still a reliable decomposition of E_∞ and $E_{coop}(T)$ is only possible provided that sufficient high-temperature data are available and only for high-fragility systems. Thus, the parameter b as well as a (cf. Eq. (A1)) refer to an average over the ensemble of liquids investigated here and may change with future experimental data. The different molecular glass formers distinguish themselves by a (generalized) fragility parameter μ which actually varies only weakly except for glycerol and propylene glycol. Once again we emphasize that the experimentally observed E_∞ must not be mistaken with some energy barrier in the liquid. Yet, the Arrhenius law revealed at high temperatures has to be taken into account by liquid theories. Furthermore, our attempt suggests that the high-temperature activation energy E_∞ defines the energy scale of the glass transition phenomenon. Thus, it appears that high-temperature and glassy dynamics in liquids are linked phenomena.

ACKNOWLEDGMENTS

Financial support of Deutsche Forschungsgemeinschaft (DFG) through Project Nos. RO 907/11 and RO 907/15 is appreciated.

APPENDIX A: MOTIVATION OF CURRENT APPROACH

Here we want to give a short motivation of our current approach (iii) (cf. also Ref. 4). We have started with the decomposition of the activation energy in a constant and a temperature dependent part:

$$\tau = \tau_\infty \exp\left(\frac{E_\infty + E_{coop}(T)}{T}\right),$$

and have noticed that $E_{coop}(T)/E_\infty$ vs. T/E_∞ ("generalized Angell plot") can be well described by an exponential function.

Thus, one can write

$$\ln \frac{E_{coop}(T)}{E_\infty} = -\mu \left(\frac{T}{E_\infty} - \frac{T_A}{E_\infty} \right) + \ln a, \quad (\text{A1})$$

where a parameter a , a reference temperature T_A , and a generalized fragility μ have been introduced. For a given system we are free to choose any T_A . In contrast to theoretical forecasts, e.g., by the frustration based theories,^{10,23} a crossover temperature (sometimes called onset temperature) cannot be identified by the mathematical function applied to interpolate $E_{coop}(T)$. Looking at $\tau(T)$ data of an ensemble of substances, however, the values of T_A appear to correlate with E_∞ and the quality of the correlation depends on the choice of a . This implies that the different curves $E_{coop}(T)/E_\infty$ have a common intersection at $T_A = b E_\infty$. It has turned out that $b \cong 0.10$ and $a \cong 1$ provide the best global interpolation. Yet, since the experimental value E_∞ as well as $\tau(T)$ data bear some uncertainty, the value of a and b cannot be specified beyond a certain limit. In addition, as most of the liquids investigated have similar fragilities, these uncertainties lead to a rather smeared out intersection point in the generalized Angell plot. Including more high quality data of glass formers with high variation in fragility will help to better define the parameters a and b – or to reject the assumption of a common intersection points of the plot $E_{coop}(T)/E_\infty$ vs. T/E_∞ .

For a data set of a given liquid, in principle, Eq. (3) can be taken also as a four parameter description. In addition to the parameters τ_∞ , E_∞ , and μ , the quantity b can be included in a free fit. In Fig. 11 the quality of the four parameter fit vs. the three parameter fit is compared for the investigated systems. As a measure of the error, the difference on logarithmic scale has been squared and averaged over all available data points for each liquid. As one can see, for most liquids, the fit quality does not increase significantly, a three parameter description is sufficient. Here we deliberately do not compare our approach to the competing models, as one could argue that even our three parameter description has more degrees of freedom (due to the global parameter b) than the approach by Mauro *et al.*²⁰ and VFT.

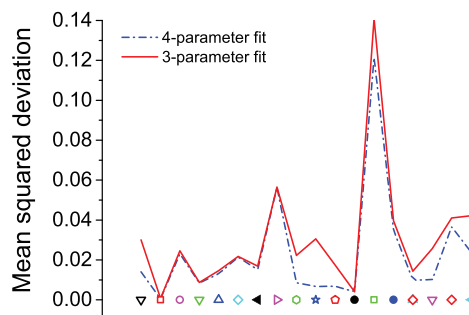


FIG. 11. Interpolation of $\tau(T)$ data: Mean squared deviations (on log-scale, cf. text) between the three (solid red line) and the four parameter fit (dashed blue line) of Eq. (3). Symbols according to the color code in Fig. 8. For most systems no benefit from an additional parameter is observed.

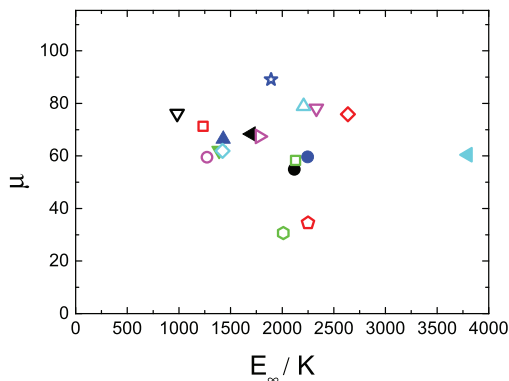


FIG. 12. Parameter μ plotted vs. E_∞ (approach (iii)). No correlation is observed; color code as in Fig. 7.

APPENDIX B: FUNCTION APPLIED FOR PCS FITS

For modeling the decays of the correlation function measured by PCS, the function introduced by Kahlau *et al.*³³ was applied. Explicitly, it is given by $\phi_g(t) = \frac{\Gamma(\frac{t}{\tau_g}, (\frac{t}{\tau_g})^\nu)}{\Gamma(\frac{t}{\tau_g})}$, where $\Gamma(\beta) = \int_0^\infty x^{\beta-1} \exp(-x) dx$ denotes the Gamma function and

$$\begin{aligned} \frac{\partial \ln \tau}{\partial 1/T} &= \frac{\partial}{\partial 1/T} \left(\ln \tau_\infty + \frac{E_\infty}{T} \left(1 + \exp \left(-b\mu \left(\frac{T}{bE_\infty} - 1 \right) \right) \right) \right) \\ &= E_\infty \left(1 + b\mu \frac{T}{bE_\infty} + \exp \left(b\mu \left(\frac{T}{bE_\infty} - 1 \right) \right) \right) \exp \left(-b\mu \left(\frac{T}{bE_\infty} - 1 \right) \right). \end{aligned}$$

APPENDIX D: TESTING CORRELATION BETWEEN μ AND E_∞

Figure 12 tests the correlation between the fragility parameter μ and E_∞ . Actually, none is found.

- ¹K. Binder, and W. Kob, *Glassy Materials and Disordered Solids* (World Scientific, 2005).
- ²J. Dyre, *Rev. Mod. Phys.* **78**, 953 (2006).
- ³L. Berthier and G. Biroli, *Rev. Mod. Phys.* **83**, 587 (2011).
- ⁴B. Schmidtke, N. Petzold, R. Kahlau, M. Hofmann, and E. A. Rössler, *Phys. Rev. E* **86**, 041507 (2012).
- ⁵M. D. Ediger and P. Harrowell, *J. Chem. Phys.* **137**, 080901 (2012).
- ⁶R. Richert, in *Structural Glasses and Supercooled Liquids*, edited by P. G. Wolynes and V. Lubchenko (Wiley, Hoboken, 2012), p. 1.
- ⁷N. Petzold, B. Schmidtke, R. Kahlau, D. Bock, R. Meier, B. Micko, D. Kruk, and E. A. Rössler, *J. Chem. Phys.* **138**, 12A510 (2013).
- ⁸T. R. Kirkpatrick, D. Thirumalai, and P. G. Wolynes, *Phys. Rev. A* **40**, 1045 (1989).
- ⁹W. Götze and L. Sjögren, *Rep. Prog. Phys.* **55**, 241 (1992).
- ¹⁰G. Tarjus, S. A. Kivelson, Z. Nussinov, and P. Viot, *J. Phys.: Condens. Matter* **17**, R1143 (2005).
- ¹¹A. Kudlik, S. Benkhof, T. Blochowicz, C. Tschirwitz, and E. Rössler, *J. Mol. Struct.* **479**, 201 (1999).
- ¹²P. Lunkenheimer, U. Schneider, R. Brand, and A. Loidl, *Contemp. Phys.* **41**, 15 (2000).
- ¹³F. Kremer and A. Schönhal, *Broadband Dielectric Spectroscopy* (Springer, Berlin, 2003).

$\Gamma(\beta, y) = \int_y^\infty x^{\beta-1} \exp(-x) dx$ the upper incomplete Gamma function.

APPENDIX C: APPARENT ACTIVATION ENERGIES OF DIFFERENT APPROACHES

The fits to the temperature dependent activation energies $E(T)$ displayed in Fig. 5 are done by using the derivative of the natural logarithm of the model function with respect to the inverse temperature. These derivatives are analytically and are explicitly given by the following expressions:

(i) VFT-equation:

$$\frac{\partial \ln \tau}{\partial 1/T} = \frac{\partial}{\partial 1/T} \left(\ln \tau_\infty + \frac{D}{T - T_0} \right) = \frac{DT^2}{(T - T_0)^2}.$$

(ii) Formula by Mauro *et al.*:²⁰

$$\begin{aligned} \frac{\partial \ln \tau}{\partial 1/T} &= \frac{\partial}{\partial 1/T} \left(\ln \tau_\infty + \frac{K}{T} \exp \left(\frac{C}{T} \right) \right) \\ &= \frac{K}{T} \exp \left(\frac{C}{T} \right) (C + T). \end{aligned}$$

(iii) Our current approach:

- ¹⁴H. Z. Cummins, G. Li, Y. H. Hwang, G. Q. Shen, W. M. Du, J. Hernandez, and N. J. Tao, *Z. Phys. B* **103**, 501 (1997).
- ¹⁵J. A. H. Wiedersich, N. V. Surovtsev, V. N. Novikov, and E. Rössler, *Phys. Rev. B* **64**, 064207 (2001).
- ¹⁶S. Adichtchev, S. Benkhof, T. Blochowicz, V. N. Novikov, E. Rössler, C. Tschirwitz, and J. Wiedersich, *Phys. Rev. Lett.* **88**, 055703 (2002).
- ¹⁷A. Brodin and E. A. Rössler, *Eur. Phys. J. B* **44**, 3 (2005).
- ¹⁸N. Petzold and E. A. Rössler, *J. Chem. Phys.* **133**, 124512 (2010).
- ¹⁹H. Vogel, *Phys. Z.* **22**, 645 (1921); G. S. Fulcher, *J. Am. Ceram. Soc.* **8**, 339 (1925); G. Tammann and W. Hesse, *Z. Anorg. Allg. Chem.* **156**, 245 (1926).
- ²⁰J. C. Mauro, Y. Yue, A. J. Ellison, P. K. Gupta, and D. C. Allan, *Proc. Natl. Acad. Sci. U.S.A.* **106**, 19780 (2009).
- ²¹P. Lunkenheimer, S. Kastner, M. Köhler, and A. Loidl, *Phys. Rev. E* **81**, 051504 (2010).
- ²²S. C. Waterton, *J. Soc. Glass Technol.* **16**, 244 (1932).
- ²³D. Kivelson, S. A. Kivelson, X. L. Zhao, Z. Nussinov, and G. Tarjus, *Physica A* **219**, 27 (1995).
- ²⁴S. Sastry, *PhysChemComm* **3**, 79 (2000).
- ²⁵A. Brodin and E. A. Rössler, *J. Chem. Phys.* **125**, 114502 (2006).
- ²⁶A. Brodin and E. A. Rössler, *J. Chem. Phys.* **126**, 244508 (2007).
- ²⁷J. Wiedersich, N. Surovtsev, and E. A. Rössler, *J. Chem. Phys.*, **113**, 1143 (2000).
- ²⁸K. A. Kobe, A. E. Ravicz, and S. P. Vohra, "Critical properties and vapor pressures of some ethers and heterocyclic compounds," *J. Chem. Eng. Data* **1**, 50-56 (1956).
- ²⁹W. M. Haynes, *CRC Handbook of Chemistry and Physics* (Taylor & Francis, New York, 2012).

- ³⁰C. J. Böttcher and P. Bordewijk, *Theory of Electric Polarization* (Elsevier, Amsterdam, 1980), Vol. 2, p. 1978.
- ³¹B. J. Berne and R. Pecora, *Dynamic Light Scattering: With Applications to Chemistry, Biology and Physics* (Wiley, New York, 1976).
- ³²A. Brodin, E. A. Rössler, R. Bergman, and J. Mattsson, *Eur. Biophys. J. B* **36**, 349 (2003).
- ³³R. Kahlau, D. Kruk, V. N. Novikov, and E. A. Rössler, *J. Phys.: Condens. Matter* **22**, 365101 (2010).
- ³⁴F. Qi, T. El Goresy, R. Böhmer, A. Döss, G. Diezemann, G. Hinze, H. Sillescu, T. Blochowicz, C. Gainaru, E. A. Rössler, and H. Zimmermann, *J. Chem. Phys.* **118**, 7431 (2003).
- ³⁵R. Richert, F. Stickel, R. S. Fee, and M. Maroncelli, *Chem. Phys. Lett.* **229**, 302 (1994).
- ³⁶G. Friz, G. Kuhlbörsch, R. Nehren, and F. Reiter, *Atomkernenergie* **13**, 25 (1968).
- ³⁷W. Steffen, A. Patkowski, H. Glaeser, G. Meier, and E. W. Fischer, *Phys. Rev. E* **49**, 2992 (1994).
- ³⁸G. Fytas, C. H. Wang, D. Lilge, and T. Dorfmueller, *J. Chem. Phys.* **75**, 4247 (1981).
- ³⁹Y. H. Hwang and G. Q. Shen, *J. Phys.: Condens. Matter* **11**, 1453 (1999).
- ⁴⁰R. Richert, *J. Chem. Phys.* **123**, 154502 (2005).
- ⁴¹E. Rössler and H. Sillescu, *Chem. Phys. Lett.* **112**, 94 (1984).
- ⁴²V. N. Novikov, Y. Ding, and A. P. Sokolov, *Phys. Rev. E* **71**, 061501 (2005).
- ⁴³T. Blochowicz, Ch. Tschirwitz, St. Benkhof, and E. A. Rössler, *J. Chem. Phys.* **118**, 7544 (2003).
- ⁴⁴T. Blochowicz, A. Brodin, and E. A. Rössler, *Adv. Chem. Phys.* **133**, 127 (2006).
- ⁴⁵T. Blochowicz, C. Gainaru, P. Medick, C. Tschirwitz, and E. A. Rössler, *J. Chem. Phys.* **124**, 134503 (2006).
- ⁴⁶J. Hintermeyer, A. Herrmann, R. Kahlau, C. Goiceanu, and E. A. Rössler, *Macromolecules* **41**, 9335 (2008).
- ⁴⁷S. Wiebel, Ph.D thesis, Technische Universität München, 2003.
- ⁴⁸L. Andrussov, "Transportphänomene I," in *Eigenschaften der Materie in ihren Aggregatzuständen*, Landolt-Börnstein II5a (Springer, Berlin, 1969).
- ⁴⁹A. J. Barlow, J. Lamb, and A. J. Matheson, *Proc. R. Soc. London, Ser. A* **292**, 322 (1966).
- ⁵⁰A. I. Nielsen, T. Christensen, B. Jakobsen, K. Niss, N. B. Olsen, R. Richert, and J. C. Dyre, *J. Chem. Phys.* **130**, 154508 (2009).
- ⁵¹C. Gangasharan and S. S. N. Murthy, *J. Chem. Phys.* **99**, 9865 (1993).
- ⁵²R. Richert, K. Duvvuri, and L. T. Duong, *J. Chem. Phys.* **118**, 1356 (2003).
- ⁵³D. J. Plazek and J. H. Magill, *J. Chem. Phys.* **45**, 3038 (1966).
- ⁵⁴See https://dow-answer.custhelp.com/app/answers/detail/a_id/7457/~propylene-glycols—viscosity-information for information about the viscosity of propylene glycol. Copyright © 2011 The Dow Chemical Company.

Publication 3

From Boiling Point down to the Glass Transition - Dynamics of Molecular Liquids Described by a Generalized Angell Plot

B. Schmidtke, N. Petzold, M. Flämig, E. A. Rössler

Article in *Fragility of Glass-forming Liquids*, Editors: A. Lindsay Greer,
Kenneth Kelton, and Srikanth Sastry, Hindustan Book Agency, New Delhi, India (2013).

Copyright 2013 by Hindustan Book Agency, New Delhi, India

ISBN-13: 978-9380250618

From Boiling Point Down to the Glass Transition – Dynamics of Molecular Liquids Described by a Generalized Angell Plot

**Bernd Schmidtke, Nicolaus Petzold, Max Flämig and
Ernst A. Rössler**

We discuss the temperature dependence of the reorientational correlation time τ of a series of molecular liquids by performing thorough depolarized light scattering (LS) experiments (double monochromator, tandem Fabry-Perot interferometry and photon correlation spectroscopy) as well as dielectric spectroscopy (DS) studies. Focus is on low- T_g liquids for which the high-temperature limit $\tau \cong 10^{-12}$ s is easily accessed. The broad band LS and DS spectra are compared to each other revealing significant differences in the high-frequency range where secondary relaxation processes occur. Correlation times in the range 10^{-12} s – 100 s are extracted, i.e., the full temperature interval between the boiling point and the glass transition temperature T_g is covered monitoring the crossover from simple liquid to glassy dynamics. Regarding the temperature dependence of $\tau(T)$ a three parameter description is introduced which decomposes the activation energy $E(T)$ in a constant high-temperature value E_{coop} and a “cooperative part” $E_{\text{coop}}(T)$ depending exponentially on temperature. It allows to discuss the temperature dependence of the liquid’s dynamics in terms of a plot $E_{\text{coop}}(T)/E_{\infty}$ vs. T/E_{∞} , and it is suggested that E_{∞} (instead of the conventionally defined

T_g) controls the energy scale of the glass transition phenomenon. The slope in this “generalized plot” may provide an absolute measure of fragility.

6.1 Introduction

Describing and understanding the temperature dependence of transport quantities of molecular liquids such as viscosity and diffusion as well as the structural correlation time τ is an unsolved problem. [1–8] In particular, extending the temperature range to the super-cooled regime, a super-Arrhenius temperature dependence is observed in which transport quantities change by many orders of magnitude within a narrow temperature interval. Numerous phenomenological interpolations of $\tau(T)$ offered from this side. [3, 9, 10]

Although extensively studied below T_m , molecular glass formers are not well investigated in the high-temperature regime above T_m . With a few exceptions most tests of interpolating $\tau(T)$ are restricted to time constants above about $10^{-10}s - 10^{-9}s$ actually ignoring a large temperature range until the high-temperature limit $\tau_\infty \cong 10^{-12}s$ is reached. Correlation times characterizing reorientational dynamics down to $10^{-12}s$ are now easily available when liquids are studied by depolarized light scattering (LS) using tandem-Fabry-Perot interferometer (TFPI) and double monochromator (DM). [4, 8, 11–15] The data $\tau(T)$ can be combined with those obtained from photon correlation spectroscopy (PCS) and dielectric spectroscopy and thus cover the entire temperature range from the boiling point down to T_g , needed to attempt a full description of $\tau(T)$.

In the present contribution, DM/TFPI susceptibility spectra of a series of (simple) molecular liquids are combined with state-of-the-art PCS spectra. Thereby broad band susceptibility spectra become accessible which can compete with those of dielectric spectroscopy. [16–20] A direct comparison of their evolution while cooling the liquid will be carried out. Only by combining information compiled by different methods will give a clear phenomenological picture of the cooperative dynamics in dense liquids. Our review includes the discussion of data on low- T_g liquids for which the high-temperature regime well above T_m is easily be accessed experimentally ($T \leq 440K$). This allows us to monitor the crossover from simple liquid dynamics well above T_m to glassy dynamics close to T_g . In particular we will demonstrate that all liquids exhibit a trend to an Arrhenius temperature dependence at high temperatures above T_m .

Having at hand time constants $\tau(T)$ which cover the full temperature range from boiling point down to T_g , we discuss our recently introduced three-parameter description. Following ideas of Kivelson et al. [10, 21] and Sastry, [22] the activation energy $E(T)$ is decomposed into a temperature independent part E_∞ describing the high-temperature regime well above the melting point T_m , and a quantity $E_{coop} = E(T) - E_\infty$ reflecting “cooperative dynamics”, dominating in the low-temperature regime close to T_g . The temperature dependence of $E_{coop}(T)$ is presented, and a “generalized Angell plot” displaying $E_{coop}(T)/\infty$

vs. T/E_∞ is introduced. Thus, instead of T_g the energy scale of the glass transition phenomenon is set by the experimentally accessible quantity E_∞ . Moreover, from the activation energy $E(T)$ an estimate of an increasing number of cooperatively moving molecules is given.

6.2 Evolution of the Dynamic Susceptibility

The glass former with the lowest T_g value studied is 2-methyl tetrahydrofuran (MTHF, $T_g = 92$ K, $T_m = 137$ K, $T_b = 352$ K). Figure 6.1 (a) shows susceptibility spectra of MTHF as obtained by DM and TFPI measurements in the temperature range 135 K – 440 K. The highest temperature is somewhat above the (ambient pressure) boiling point. At low temperatures and low frequencies the primary or α -relaxation is well recognized as a separate, asymmetrically broadened peak in addition to the microscopic (vibrational) peak around 2 THz. In between a minimum is observed in the susceptibility. While heating, the α -process shifts to higher frequencies and approaches the microscopic peak. At highest temperatures both peaks have virtually merged to become a somewhat broadened single peak. The single-peak susceptibility observed above say 240 K we take as an indication that glassy dynamics have disappeared and that the liquid has become a simple liquid (cf. also below). Similar results are observed for dimethyl phthalate (DMP; $T_g = 191$ K, $T_m = 233$ K, $T_b = 565$ K); cf. Figure 6.1 (b)). As T_g of DMP is significantly higher than that of MTHF, the α -relaxation and the microscopic dynamics have not yet fully merged at 440 K. The liquid MTHF has a low scattering power due to its low molecular electronic polarizability and the signal-to-noise ratio in the spectra is rather low compared to that of DMP. In a detailed line-shape analysis including the fast dynamics the stretching of the α -relaxation turns out to be essentially temperature independent, i.e., frequency-temperature superposition applies. No evidence of a crossover to a Debye spectral form is found. [13–15] These findings are virtually observed for all of the liquids studied. [7]

The DM/TFPI spectra can be interpolated by the schematic F_{12} model of mode coupling theory (MCT). [23] In Figure 6.1 the corresponding fits (solid lines) are displayed clearly demonstrating that MCT can even describe the crossover to simple liquid dynamics at highest temperatures as previously demonstrated for benzene. [24] We note that in all cases the fits are not in the asymptotic regime for which the simple power-law interpolations apply.

Extracting the time constant $\tau(T)$ at low temperatures is easily carried out by interpolating the α -relaxation peak with a Cole-Davidson function. [25] At high temperatures when α - and microscopic peak have merged we apply the following procedure. The low-temperature spectra normalized by the amplitude χ_α^o of the α -process are plotted as a function of the reduced frequency $\omega\tau$ (cf. Figure 6.2). At high temperatures the spectra are rescaled to provide a common low-frequency envelope, explicitly $\chi''/\chi_\alpha^o = \omega\tau$ holds as needed for a simple liquid in the low-frequency regime. As a crosscheck, the amplitude

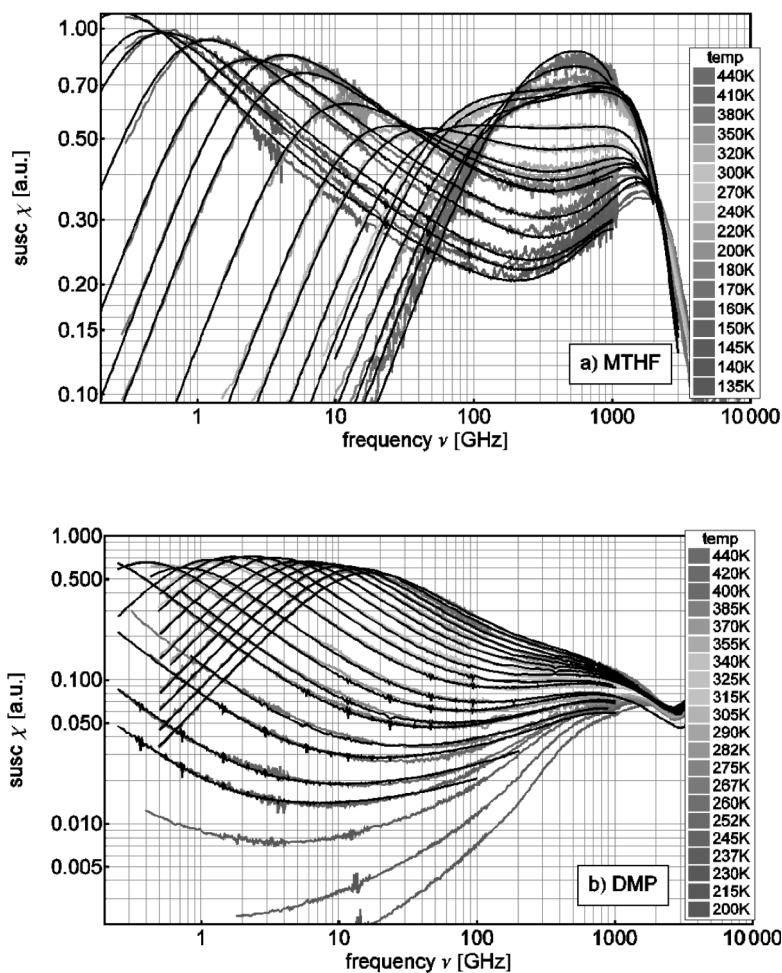


Figure 6.1: (a) Susceptibility spectra of 2-methyl tetrahydrofuran (MTHF : $T_g = 92K$, $T_m = 137K$ and $T_b = 352K$) obtained by applying DM/TFPI for different temperatures. (b) Corresponding spectra of dimethyl phthalate (DMP; $T_g = 191K$, $T_m = 233K$ and $T_b = 565K$). Black lines: interpolations by mode coupling theory.

χ_α^o follows the temperature dependence established at low temperatures up to highest temperatures in a regular smooth way, *cf.* insert Figure 6.2. By this scaling procedure the time constants can be extracted in a model independent way. The time constant $\tau(T)$ for MTHF is plotted in Figure 6.6 together with results reported by other methods, where it is compared to the data compiled for three other liquids including DMP. In Figure 6.7 all our data for the 18

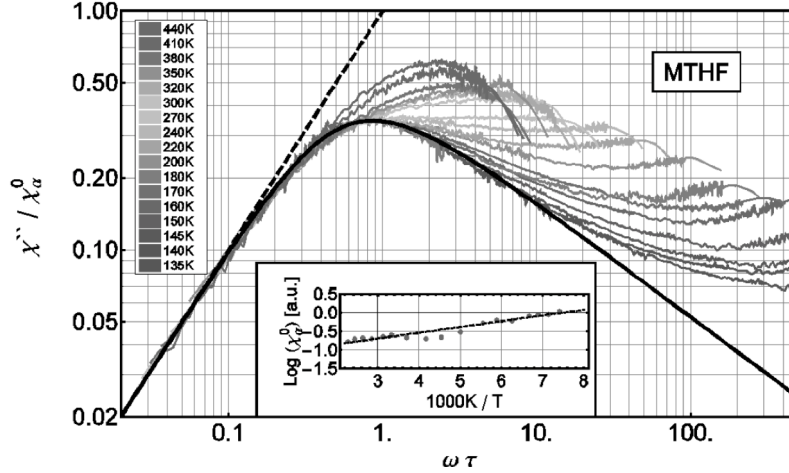


Figure 6.2: Susceptibility master curve of 2-methyl tetrahydrofuran (MTHF) obtained by rescaling the spectra of 6.1(a); solid line: Cole-Davidson function with $\beta = 0.48$; dashed line: low-frequency limiting behavior $\chi''/\chi_\alpha^0 = \omega\tau$; insert: amplitude χ_α^0 of α -relaxation as revealed by constructing the master curve showing a smooth change with temperature; adapted with permission from [8].

liquids investigated including also some from DS [16–18,20] are displayed, and the results will be discussed below.

In Figure 6.3(a) we show the results for MTHF from our PCS setup. [15] The measured intensity correlation functions were normalized and transformed utilizing the Siegert relation into the field correlation function, respectively the intermediate scattering function. [26] Upon cooling the long-time tail of the α -relaxation enters the explored time window until the entire non-exponential decay is observed at temperatures close to T_g . We included the DM/TFPI decays from Fig 6.1(a) (after Fourier transforming), which extend the dynamic window to highest temperatures (up to 440 K). Again, due to the low scattering power the PCS correlation decay is probed over a rather narrow time window. In contrast, in the case of m-tricresyl phosphate (m-TCP) a much better data set is obtained, *cf.* Figure 6.3(b). Apparently no change with temperature in amplitude as well as stretching is recognizable up to high temperatures as is demonstrated in Figure 6.3(b) for m-TCP. After having established its bimodal shape well above the melting point essentially no further change is recognizable in the reorientational correlation function while cooling down to T_g . At highest temperatures one can clearly see how the stretched long-time decay “grows out” of the microscopic decay when the temperature is decreased, *i.e.*, a new relaxation mode characteristic of glassy dynamics emerges well above the melting point. [7,8] We note that subtle features like the emergence of the so-called excess wing can only be identified (by bare eyes) after transforming the data into the frequency domain (*cf.* below). [7] In order to extract time

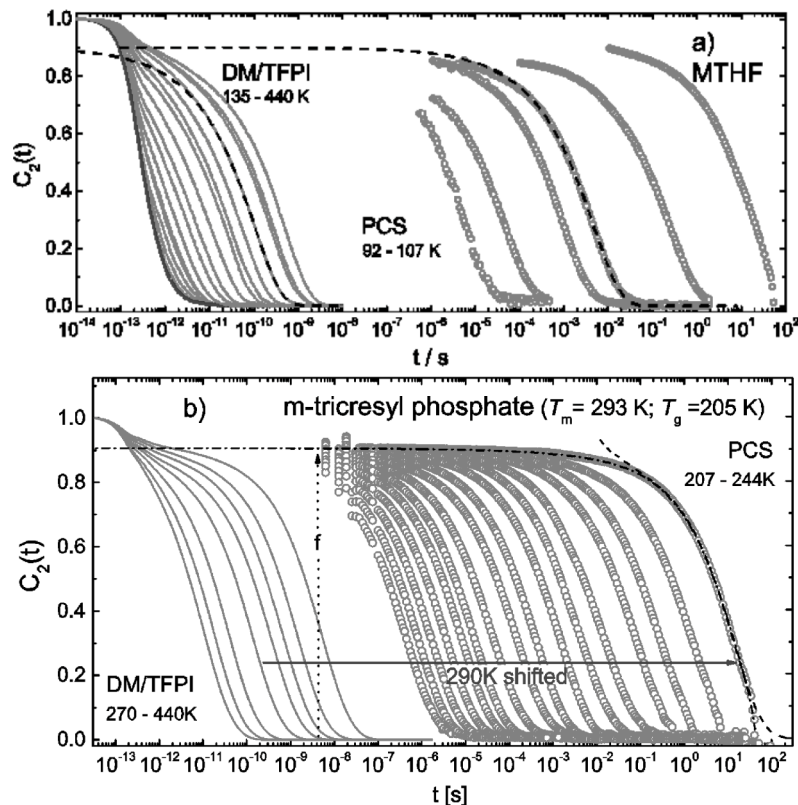


Figure 6.3: Reorientational correlation function $C_2(t)$ of (a) 2-methyl tetrahydrofuran (MTHF), obtained by PCS and DM/TFPI (after Fourier transformation; lines) (b) analogous results for m-tricresyl phosphate. Fits by time domain expression of the generalized Cole-Davidson function [28] (dashed and dashed-dotted lines respectively); solid blue line: correlation function at $T = 290$ K shifted to coincide with that at $T = 207$ K; dotted line: amplitude f of α -process; adapted with permission from ref. [7, 8]

constants and stretching parameters the decays are interpolated by the time domain expression of the Cole-Davidson function or the more general function introduced by us. [28] The corresponding time constants of MTHF and m-TCP are included in Figs. 6.6 or 6.7.

Having measured the response function by LS as well as by DS a direct comparison becomes possible. This is done in Figure 6.4 for the case of m-TCP [7] and glycerol, [30] for which master curves $\chi''(\omega\tau)$ are displayed. The results from field-cycling (FC) ^1H NMR relaxometry are included. [30] The latter technique probes the frequency dependence of the spin-lattice relaxation time T_1 which is connected to the spectral density of the dipolar correlation

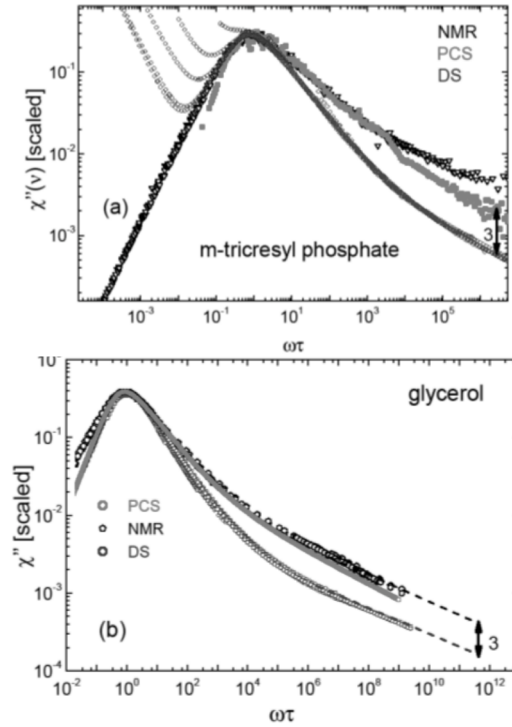


Figure 6.4: (a) Comparing susceptibilities of m-tricresyl phosphate as obtained from PCS (red squares), from Field Cycling (FC) ^1H NMR (black triangles) and dielectric spectroscopy (blue diamonds); (b) master curves of glycerol compiled from FC ^1H NMR (pentagons), [32] dielectric spectroscopy (diamonds) [30] and PCS (circles); [29] dashed lines: interpolations by a Cole-Davidson function together with a high-frequency power-law; arrow indicates factor 3 between the amplitude of the excess wing.

function. [31] Dielectric spectroscopy probes a rank-one correlation function $C_{(1)}(t)$ while LS and NMR probe a rank-two function $C_{(2)}(t)$. The latter two agree rather well, whereas the dielectric susceptibility in both liquids exhibits a narrower susceptibility spectrum. At highest frequencies in the regime of what is called the excess wing, as power-law behavior with an exponent $\gamma \cong 0.2$ is found and its amplitude differs by a factor of about three while the exponent of the excess wing appears to be the same. A relation $\chi''_{(2)}(\omega) = 3\chi''_{(1)}(\omega)$ results when assuming that the reorientation proceeds via small angle steps. [30,33,34] In other words, as is also confirmed by NMR studies, [35] the excess wing is a highly hindered precursor of the α -process, and appears to be a generic feature of molecular liquids, and due to its larger amplitude is actually better recognized by a rank-two correlation function like that probed by light scattering or NMR.

In the case of m-TCP, FC ^1NMR probes an additional relaxation process which at high-frequencies yields an upward trend in the data probably due to phenyl ring rotation.

Whether the width of α -relaxation peak itself depends on the rank of the correlation function cannot be clearly decided without a model of decomposing α - and excess wing relaxation. An additive model for the α -relaxation spectrum and a power-law contribution for the excess wing allows to interpolate DS and LS susceptibility assuming a temperature independent stretching parameter for the α -process (cf. Figure 6.4b). [7, 30] In any case, this points to the problem of determining the stretching of the α -process close to T_g where the presence of secondary processes like the excess wing or even a well resolved β -process (cf. below) affects a clear-cut spectral analysis. Analyzing step-response functions directly in the time domain one could argue that fitting the decay essentially provides information on the long-time decay attributed to the α -relaxation. Yet, we have shown that also in the time domain the different stretching of the α -process as probed by different techniques may be attributed to a stronger spectral weight of the excess wing in the LS signal. [7]

Many glass formers show in addition or instead of an excess wing a secondary relaxation peak (β -process). In Figure 6.5 we compare our dielectric spectra with our PCS results for DMP after transforming the PCS time domain data into the frequency domain at comparable temperatures. [7] No β -process is recognized by LS, yet a well resolved excess wing is found with an exponent $\gamma \cong 0.2$, in agreement with our previous DS results. [36] Similar results are reported for other liquids. [36, 38] We conclude that the excess wing is a different phenomenon than the β -process and it exhibits quite universal features whereas relaxation strength and spectral width of the β -relaxation vary and depend on the probing technique. [7]

6.3 Temperature Dependence of the Time Constants

Let us now return to the temperature dependence of the time constants τ compiled for a series of molecular liquids. In Figure 6.6 we display $\tau(T)$ for MTHF, DMP, o-terphenyl ($T_g = 244$ K, $T_m = 328$ K, $T_b = 605$ K) [11, 15, 39–43] and toluene ($T_g = 118$ K, $T_m = 178$ K, $T_b = 384$ K). [15, 44] The liquids exhibit a significant variation in T_g and are well studied up to rather high temperatures. We do not distinguish among the results from different techniques. The results for all the eighteen liquids are collected in Figure 6.7 (note color code for all figures in Figure 6.7). At high temperatures an Arrhenius behavior can be clearly anticipated in all cases (dashed lines in Figure 6.6) which in the case of MTHF covers about 200 K. We note that the crossover to the high-temperature dynamics is difficult to detect in the evolution of the susceptibility spectra (cf. Figure 6.1(a)). The crossover from bimodal to monomodal decay (cf. Figure 6.3) occurs in a narrow interval of correlation times ($\tau \sim 10^{-11}$ s), while it is difficult to identify a clear cut crossover temperature (“onset temper-

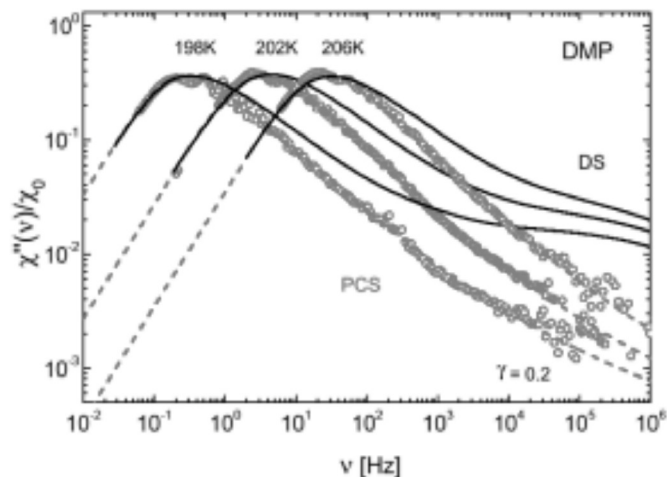


Figure 6.5: Comparison of the susceptibility of dimethyl phthalate (DMP) from photon correlation spectroscopy (PCS) [37] and from dielectric spectroscopy (DS); the slow β -process is not probed by PCS, instead an excess wing is observed; adapted with permission from ref. [7].

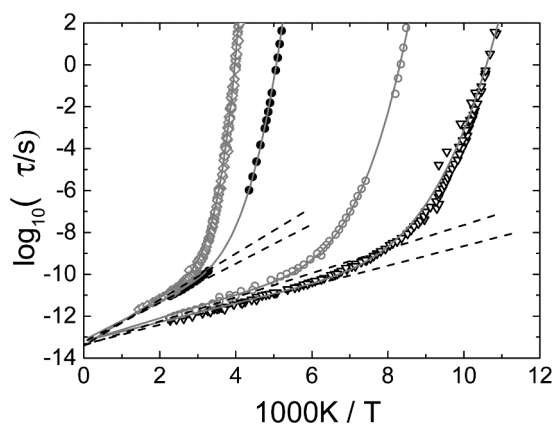


Figure 6.6: Reorientational correlation time of 2-methyl tetrahydrofuran (MTHF), toluene, dimethyl phthalate (DMP) and o-terphenyl (OTP) plotted versus inverse temperature; interpolation by current approach (solid lines); dashed lines: Arrhenius high temperature behavior; color code: *cf.* Figure 6.7.

ature”). Actually the crossover to “normal” liquid dynamics with a single-step correlation function is only observed when the liquid is heated well above T_m actually approaching T_b . Most “laboratory” liquids display traces of glassy dynamics.

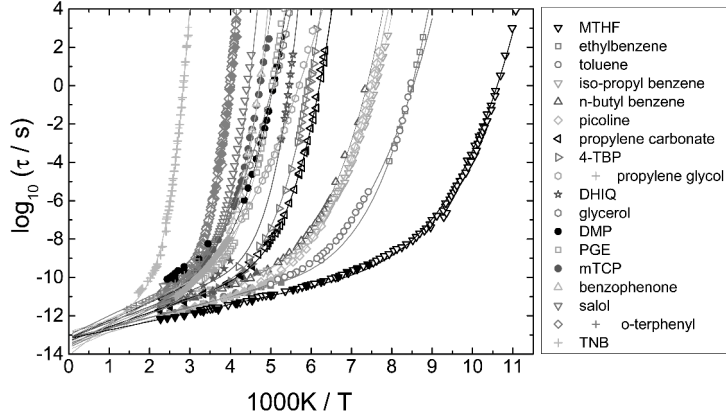


Figure 6.7: Reorientational correlation times of molecular liquids from light scattering (full symbols) and from dielectric data base (open symbols); solid lines: fit by the current approach (eq. 2); (for abbreviations and literature see ref. [7,8]); adapted with permission from ref. [8].

To inspect the temperature dependence of $\tau(T)$ in more detail we show in Figure 6.8(a) the apparent activation energy $E_A(T)$ (not to be confused with $E(T)$) in eq.6.1, below) as given by the derivative of $\ln \tau$ with respect to the reciprocal temperature $1/T$. The liquids MTHF, propylene carbonate, propylene glycol and OTP are considered, and the derivative data are shown as a function of inverse temperature. Clear evidence is found that the apparent activation energy becomes finally constant at highest temperatures. In the case of the non-fragile liquid propylene glycol not sufficient high-temperature data is available to demonstrate the crossover to constant activation energy. Another feature is recognized in Figure 6.8(a). It appears that the lower E_∞ (plateau in Figure 6.8(a)), the more the onset of cooperative dynamics, i.e., a possibly existing crossover temperature, shifts to lower temperatures. Thus, we plotted the reduced activation energy $E_A(T)/E_\infty$ vs. T/E_∞ in Figure 6.8(b). Within the scatter of the data a universal dependence is observed. For example, MTHF and OTP, liquids with rather different T_g as well as E_∞ display similar behavior. Not surprisingly, fragility parameters m are quite alike in these systems.

None of the existing approaches (including the recently discussed approach by Mauro et al. [45]) are suitable for interpolation of $\tau(T)$ over the entire temperature interval from T_g up to T_b ; in particular the crossover to Arrhenius behavior is not well reproduced. Recently, we have introduced an approach already discussed by Kivelson and coworkers [21] as well as by Sastry [22], which starts with a decomposition of the activation energy into a constant high-temperature part E_∞ and a temperature dependent part $E_{coop}(T)$:

$$\tau = \tau_\infty \exp\left(\frac{E_\infty + E_{coop}(T)}{T}\right) \quad (6.1)$$

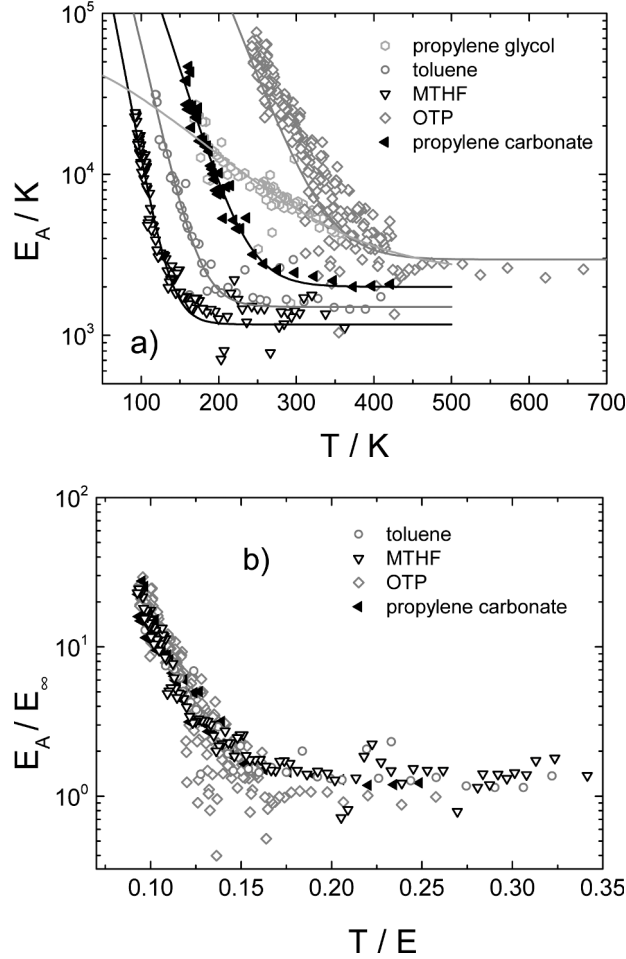


Figure 6.8: (a) Activation energy $E_A(T)$ for selected molecular liquids as function of inverse temperature, solid lines: fits by current model (eq.6.3). (b) Reduced activation energy $E_A(T)/E_\infty$ vs. T/E_∞ ; adapted with permission from ref. [8].

Singling out $E_{coop}(T)$ it is noticed that $E_{coop}(T)$ can be described well by an exponential function in T . In particular, one can write

$$\ln \frac{E_{coop}(T)}{E_\infty} = -\mu \left(\frac{T}{E_\infty} - \frac{T_A}{E_\infty} \right) + \ln a \quad (6.2)$$

where a parameter a , a reference temperature T_A , and a generalized fragility μ have been introduced.

For a given system we are free to choose any T_A and a corresponding a . Looking at $\tau(T)$ data of an ensemble of molecular liquids, however, the values

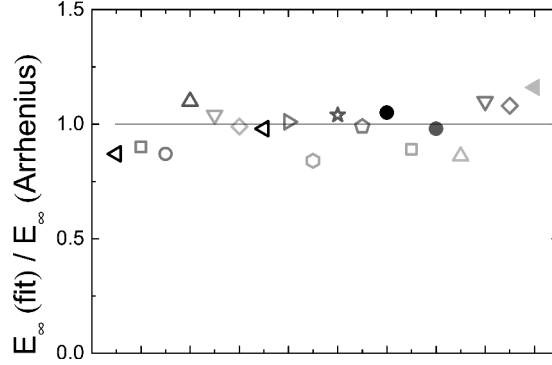


Figure 6.9: Quotient of the parameters E_∞ from the free three-parameter fits shown in Figure 6.7 and the experimentally observed activation energy E_∞ at high temperatures (Arrhenius law); adapted with permission from ref. [8].

of T_A appear to correlate with E_∞ (cf. Fig. 6.8(a)) and the quality of the correlation depends on the choice of a . This implies that the different curves $E_{coop}(T)/E_\infty$ have a common intersection at $T_A = bE_\infty$. It has turned out that $b \cong 0.10$ and $a \cong 1$ provide the best global interpolation. Yet, since the experimental value E_∞ as well as $\tau(T)$ data bear some uncertainty the value of a and b cannot be specified beyond a certain limit. Including more high quality data of glass formers with high variation in fragility will help to better define the parameters a and b – or to reject the assumption of a common intersection point in the plot $E_{coop}(T)/E_\infty$ vs. T/E_∞ . We note that in contrast to theoretical forecasts, *e.g.*, by the frustration based theories, [10,21] for a given liquid an onset temperature cannot be identified by the mathematical function applied to interpolate $E_{coop}(T)$.

In order to estimate E_∞ for all the systems studied, the quantity is extracted from an Arrhenius fit of the high-temperature data in Fig.6.7. In Figure 6.9 the quotient of the parameters E_∞ from the free three-parameter fits with eq. 2 (assuming $b = 0.1$) and the experimentally found high-temperature activation energy E_∞ (Arrhenius) is displayed for the different systems studied. The uppermost deviation from unity is about 15 %, for most systems it is even smaller. This is in the range of the experimental uncertainty in determining E_∞ from the time constants τ as well as from the high-temperature Arrhenius fit. It proves that the parameter E_∞ in eq. (2) represents the activation energy at high temperatures, and thus justifies our approach.

Figure 6.10 presents the reduced activation quantity $E_{coop}(T)/E_\infty$ as given by plotting $(T \ln \tau / \tau_\infty - E_\infty) / E_\infty = E_{coop}(T) / E_\infty$ versus T/E_∞ for four selected systems, which cover a wide range of μ parameters. [4, 7] Exponential temperature dependence is observed in good agreement justifying the exponential dependence of E_{coop} in T . The values of the parameters E_∞ and

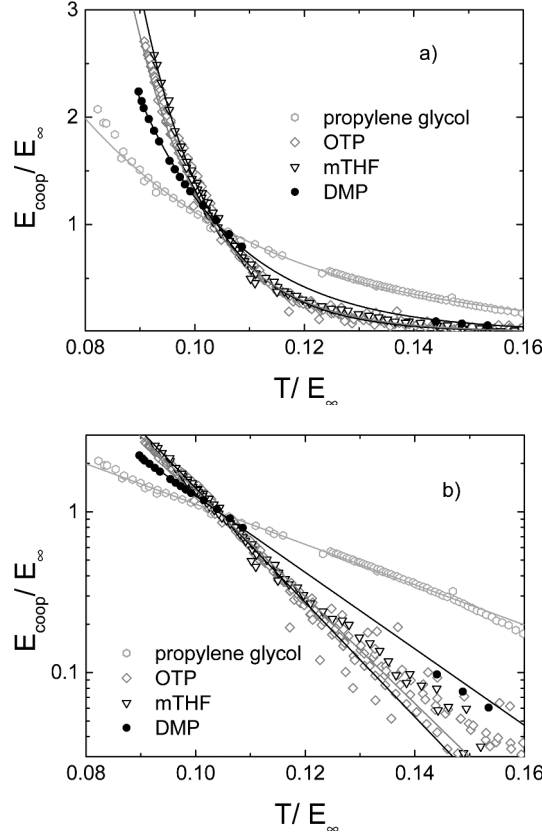


Figure 6.10: (a) E_{coop}/E_{∞} versus T/E_{∞} obtained by fitting $\tau(T)$ data interpolated by an exponential function (solid lines) for the three systems 2-methyl tetrahydrofuran (MTHF), o-terphenyl (OTP) and propylene glycol. (b) Same data on logarithmic scale; straight lines illustrate an exponential temperature dependence; adapted with permission from ref. [8].

τ_{∞} , which are needed to calculate $E_{coop}(T)$ are taken from the three-parameter fits to the $\tau(T)$ data shown in Figure 6.7. The representation of the data in Figure 6.10 has been called a “generalized Angell plot” [4, 7] it takes E_{∞} instead of the conventionally defined T_g as energy scale of the glass transition phenomenon. Again, the curves of MTHF and OTP are very similar, and they intersect with the curve of propylene glycol at $E_{coop}(T_A)/E_{\infty} \cong 1$.

We note that the energy scale E_{∞} might be well defined for all molecular liquids, though it is hard to assess as one needs $\tau(T)$ at high temperatures compared to T_g . Thus low- T_g systems are better suited for the separation of $E_{coop}(T)$ and E_{∞} . Therefore the bending down (cf. Figure 6.11) of the curve for propylene glycol might be attributed to an imperfect estimation of E_{∞} which,

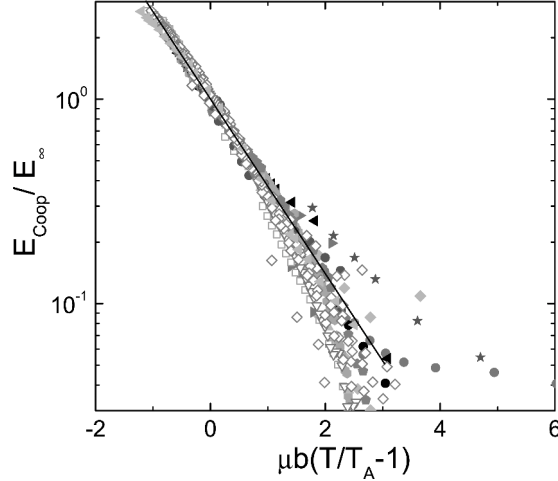


Figure 6.11: Reduced activation energy $E_{coop}(T)/E_{\infty}$ plotted vs. a reduced temperature scale to provide a master curve for all molecular liquids investigated; color code as in Figure 6.7.

as discussed, in the case of non-fragile glass formers is indeed experimentally difficult to access.

Equation 6.2 allows representing the E_{coop} data in form of the master curve when plotting E_{coop}/E_{∞} as a function of the rescaled reduced temperature T/E_{∞} . This is demonstrated in Figure 6.11. The data points follow a common straight line in fair agreement.

The parameter μ introduced in eq. 6.2 has been called a generalized fragility; [4, 8] it can directly be read off as the slope of $E_{coop}(T)/E_{\infty}$ in Figure 6.10(b), and it is expected to be correlated to the “steepness” of $\ln \tau = f(T_g/T)$ which conventionally is defined by the fragility index m . Although no clear cut relation between μ and m can be given, still a correlation is found in Figure 6.12 justifying the notion generalized fragility for μ . Noteworthy, two systems show strong deviations from the correlation displayed in Figure 6.12, namely decahydroisoquinoline (DHIQ) and toluene. In contrast to the rest of the systems both liquids exhibit a strong secondary relaxation (β -process), and the separation of the spectral contributions of α - and β -process and consequently a reliable estimate of $\tau(T)$ may not be straight forward. Except for the two hydrogen bond network forming liquids glycerol and propylene glycol μ does not vary significantly.

6.4 Estimate of Number of Correlated Molecules

Given that $E_{coop}(T)$ reflects the number of cooperatively moving molecules, which is expected to grow upon cooling, following a recent idea of N. Fatkullin

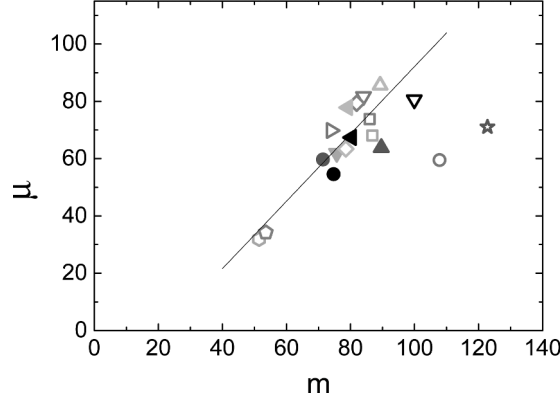


Figure 6.12: Correlation between the generalized fragility parameter μ and the conventionally defined fragility index m ; color code as in Figure 6.7; adapted with permission from ref. [8].

[46] one may estimate the number N_{corr} by assuming that $E_A = \in N_{coop}(T)$ and further that $\epsilon \sim kT$ holds. Thus, one gets

$$N_{corr} = E_A(T)/kT \quad (6.3)$$

The result shown in Figure 6.13 shows a physically reasonable behavior, as at high temperatures, N_{coop} is close to one and rise up to about 300 when the liquid is cooled down to T_g . This result is similar to what has been reported very recently by the Augsburg group measuring the third-order non-linear dielectric susceptibility. [47] The latter allows to directly extracting N_{coop} . The authors have found that the apparent activation energy $E_A(T)$ scales with $N_{coop}(T)$.

6.5 Conclusion

Combining different light scattering techniques (DM, TFPI and PCS), the evolution of the susceptibility spectra has been measured for a series of molecular glass formers and for temperatures between the boiling point ($T \leq 440$ K) and T_g . The T_g values range from 92 K to 333 K. Comparing the obtained broad band LS spectra with those from dielectric spectroscopy significant differences are observed regarding the secondary processes such as excess wing and β -process occurring at high frequencies. In the case of the low- T_g liquids a broad high-temperature interval has been identified for which the extracted time constants of the α -process $\tau(T)$ are well described by an Arrhenius temperature dependence down to $\tau \cong 10^{-12}$ s. Here, structural and microscopic dynamics have essentially merged, *i.e.*, a two-step correlation function, typical for glassy dynamics, is not observed any longer, yet a clear cut onset temperature cannot easily be identified. A trend to a crossover to Arrhenius high-temperature dependence well above the melting point is also found for systems with higher T_g

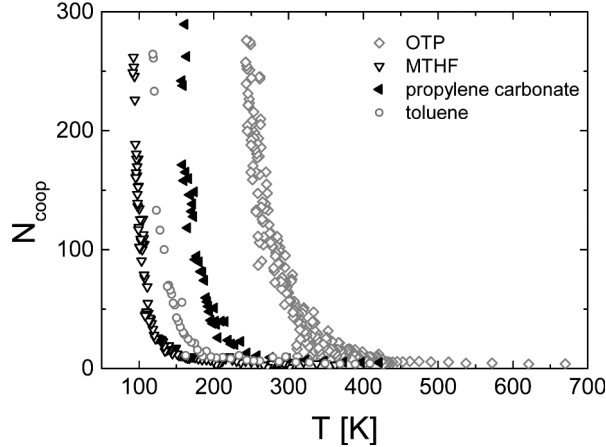


Figure 6.13: Estimate of the number N_{coop} of cooperatively moving molecules as a function of temperature by applying Eq. 6.3.

and also for the non-fragile liquids, but the high-temperature activation energy E_∞ cannot be accessed reliably in these cases.

Having at hand correlation times ranging from $10^{-12} \leq \tau/s \leq 100$ which cover the entire regime of the liquid's dynamics, *i.e.*, from simple liquid to glassy dynamics, we have introduced a three-parameter description to interpolate $\tau(T)$. We note that most functions interpolating $\tau(T)$ so far have been restricted to $\tau > 10^{-10}$ s due to missing high-temperature data. The present approach decomposes the activation energy $E(T)$ in a temperature independent high-temperature contribution E_∞ and a temperature dependent part $E_{coop}(T)$, the latter follows essentially an exponential temperature dependence. Introducing a generalized Angell plot, namely E_{coop}/E_∞ vs. T/E_∞ indicates the possibility that a common intersection point for the data of the group of liquids defines a crossover temperature T_A , for which $T_A / E_\infty = b$ is a universal constant. Still a reliable decomposition of E_∞ and $E_{coop}(T)$ is only possible provided that sufficient high-temperature data are available and only for high-fragility systems. Thus, the parameter b as well as a (cf. eq. 6.2) refers to an average over the ensemble of liquids investigated here and may change with future experimental data. The different molecular glass formers distinguish themselves by a (generalized) fragility parameter μ , which actually varies only weakly except for glycerol and propylene glycol. We emphasize that the experimentally observed E_∞ must not be associated with some energy barrier in the liquid. Yet, the Arrhenius law revealed at high temperatures has to be taken into account by any liquid theory. Our attempt suggests that the high-temperature activation energy E_∞ defines the energy scale of the glass transition phenomenon. Thus, simple liquid dynamics and glassy dynamics appear to be connected.

Acknowledgements

Financial support by Deutsche Forschungsgemeinschaft (DFG) through project RO 907/11 and RO 907/15 is appreciated.

References

- [1] K. Binder, and W. Kob, *Glassy Materials and Disordered Solids*, World Scientific, New Jersey (2005).
- [2] J. Dyre, *Rev. Mod. Phys.* **78**, 953 (2006).
- [3] L. Berthier, and G. Biroli, *Rev. Mod. Phys.* **83**, 587 (2011).
- [4] B. Schmidtke, N. Petzold, R. Kahlau, M. Hofmann, and E.A. Rössler, *Phys. Rev. E* **86**, 041507 (2012).
- [5] M.D. Ediger, and P. Harrowell, *J. Chem. Phys.* **137**, 080901 (2012).
- [6] R. Richert, in *Structural Glasses and Supercooled Liquids*, edited by P.G. Wolynes, and V. Lubchenko Wiley, Hoboken, 2012, p. 1.
- [7] N. Petzold, B. Schmidtke, R. Kahlau, D. Bock, R. Meier, B. Micko, D. Kruk, and E. A. Rössler, *J. Chem. Phys.* **138**, 12A510 (2013).
- [8] B. Schmidtke, N. Petzold, R. Kahlau, and E. A. Rössler, *J. Chem. Phys.* **139**, 084504 (2013).
- [9] W. Götze, and L. Sjögren, *Rep. Prog. Phys.* **55**, 241 (1992).
- [10] G. Tarjus, S.A. Kivelson, Z. Nussinov, and P. Viot, *J. Phys.: Condens. Matter* **17**, R1143 (2005).
- [11] H.Z. Cummins, G. Li, Y.H. Hwang, G.Q. Shen, W.M. Du, J. Hernandez, and N.J. Tao, *Z. Phys. B* **103**, 501 (1997).
- [12] J.A.H. Wiedersich, N.V. Surovtsev, V.N. Novikov, E. Rössler, *Phys. Rev. B* **64**, 064207 (2001).
- [13] S. Adichtchev, S. Benkhof, T. Blochowicz, V.N. Novikov, E. Rössler, C. Tschirwitz, and J. Wiedersich, *Phys. Rev. Lett.* **88**, 55703 (2002).
- [14] A. Brodin, E.A. Rössler, *Eur. Phys. J. B* **44**, 3 (2005).
- [15] N. Petzold, E.A. Rössler, *J. Chem. Phys.* **133**, 124512 (2010).
- [16] A. Kudlik, S. Benkhof, T. Blochowicz, C. Tschirwitz, E. Rössler, *J. Mol. Struct.* **479**, 201 (1999).
- [17] P. Lunkenheimer, U. Schneider, R. Brand, A. Loidl, *Contemp. Phys.* **41**, 15 (2000).
- [18] F. Kremer, A. Schnhals, *Broadband dielectric spectroscopy*, Springer, Berlin (2003).

- [19] T. Blochowicz, C. Tschirwitz, S. Benkhof, E.A. Rössler, *J. Chem. Phys.* **118**, 7544 (2003).
- [20] T. Blochowicz, C. Gainaru, P. Medick, C. Tschirwitz, E.A. Rössler, *J. Chem. Phys.* **124**, 134503 (2006).
- [21] D. Kivelson, S. A. Kivelson, X. L. Zhao, Z. Nussinov, and G. Tarjus, *Physica A* **219**, 27 (1995).
- [22] S. Sastry, *PhysChemComm.* **3**, 79 (2000).
- [23] W. Götze and Th. Voigtmann, *Phys. Rev. E* **61**, 4133 (2000).
- [24] S. Wiebel and J. Wuttke, *New J. Phys.* **4**, 56 (2002).
- [25] C.J. Böttcher and P. Bordewijk, *Theory of Electric Polarization vol 2* (Amsterdam: Elsevier), p 1978, (1980).
- [26] B. J. Berne and R. Pecora, *Dynamic Light Scattering: With Applications to Chemistry, Biology and Physics*, Wiley, New York, (1976).
- [27] A. Brodin, E.A. Rössler, R. Bergman, and J. Mattsson, *European Physics J. B* **36**, 349 (2003).
- [28] R. Kahlau, D. Kruk, V. N. Novikov, and E. A. Rössler, *J. Phys.: Condens. Matter* **22**, 365101, (2010).
- [29] R. Böhmer, and C.A. Angell, *Phys. Rev. B* **45**, 10091 (1992).
- [30] C. Gainaru, O. Lips, A. Troshagina, R. Kahlau, A. Brodin, F. Fujara, and E.A. Rössler, *J. Chem. Phys.* **128**, 174505 (2008).
- [31] R. Meier, D. Kruk, and E. A. Rössler, *ChemPhysChem.* **14**, 3071 (2013).
- [32] A. Brodin, L. Börjesson, D. Engberg, L.M. Torell, and A.P. Sokolov, *Phys. Rev. B* **53**, 11511 (1996).
- [33] M.J. Lebon, C. Dreyfus, Y. Guissani, R.M. Pick, and H.Z. Cummins, *Z. Phys. B* **103**, 433 (1997).
- [34] T. Blochowicz A. Kudlik, S. Benkhof, J. Senker, E. Rössler, and G. Hinze, *J. Chem. Phys.* **110**, 12011 (1999).
- [35] M. Vogel, P. Medick, and E.A. Rössler, *Ann. Rep. NMR Spectr.* **56**, 231 (2005).
- [36] C. Gainaru, R. Kahlau, E.A. Rössler, and R. Böhmer, *J. Phys. Chem.* **131**, 184510 (2009).
- [37] N. Petzold, and E.A. Rössler, unpublished results.
- [38] L. Comez, D. Fioretto, L. Palmieri, L. Verdini, P.A. Rolla, J. Gapinski, T. Pakula, A. Patkowski, W. Steffen, and E.W. Fischer, *Phys. Rev. E* **60**, 3086 (1999).

- [39] G. Friz, G. Kuhlbörsch, R. Nehren, and F. Reiter, *Atomkernenergie* **13**, 25 (1968).
- [40] W. Steffen, A. Patkowski, H. Glaeser, G. Meier, E.W. Fischer, *Phys. Rev. E* **49**, 2992 (1994).
- [41] G. Fytas, C. H. Wang, D. Lilge, and T. Dorfmueller, *J. Chem. Phys.* **75**, 4247 (1981).
- [42] Y. H. Hwang and G. Q. Shen, *J. Phys.: Condens. Matter* **11**, 1453 (1999).
- [43] R. Richert, *J. Chem. Phys* **123**, 154502 (2005).
- [44] E. Rössler and H. Sillescu, *Chem. Phys. Lett* **122**, 94 (1984).
- [45] J. C. Mauro, Y. Yue, A. J. Ewqllison, P. K. Gupta, and D. C. Allan, *Proc. Natl. Acad. Sci. U.S.A.* **106**, 19780 (2009).
- [46] N. Fatkullin, *private communication*.
- [47] Th. Bauer, P. Lunkenheimer, S. Kastner, and A. Loidl, *Phys. Rev. Lett.* **110**, 107603 (2013).

Publication 4

Relaxation Stretching, Fast Dynamics and Activation Energy: A Comparison of Molecular and Ionic Liquids as Revealed by Depolarized Light Scattering

B. Schmidtke, N. Petzold, B. Pötzschner, H. Weingärtner, E. A. Rössler

The Journal of Physical Chemistry B 118, 7108 - 7118 (2014).

Copyright 2014 by The American Chemical Society

DOI: 10.1021/jp412297u

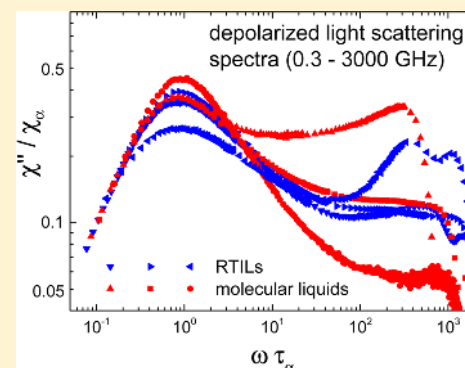
Relaxation Stretching, Fast Dynamics, and Activation Energy: A Comparison of Molecular and Ionic Liquids as Revealed by Depolarized Light Scattering

B. Schmidtke,[†] N. Petzold,[†] B. Pötzschner,[†] H. Weingärtner,[‡] and E. A. Rössler^{*,†}

[†]Experimentalphysik II, Universität Bayreuth, D-95444 Bayreuth, Germany

[‡]Physikalische Chemie II, Ruhr-Universität Bochum, D-44780 Bochum, Germany

ABSTRACT: Depolarized light scattering (DLS) spectra of a series of 16 molecular and 6 room temperature ionic liquids are investigated by applying tandem-Fabry-Pérot interferometry, double monochromator, and photon correlation spectroscopy. Temperatures up to well above the melting point, in some cases, even up to the boiling point, are covered, and all liquids can be supercooled. The accessed time constants are between 1 ps and 10 ns; in some cases, even longer times are reached. The susceptibility spectra and likewise the corresponding reorientational correlation functions are characterized by stretching parameter β_{CD} (0.32–0.80) for the long-time decay (α -process), strength of fast dynamics $1 - f$, and time scale at shortest times expressed by $k_B T / I^*$ with the apparent quantity I^* reflecting essentially inertia effects. An additional (intermediate) power-law regime (or excess wing in the frequency domain) between fast dynamics and the α -process has to be taken into account. For a given system the spectral parameters are virtually temperature independent up to the boiling point, i.e., frequency–temperature superposition applies for the α -process. Among the liquids, the quantity I^* correlates with molecular mass, and the larger $1 - f$, the smaller the inertial quantity I^* . No correlation among $1 - f$ and β_{CD} is revealed. Testing for correlation of β_{CD} or $1 - f$ with parameters describing the temperature dependence of the correlation time τ_ω , namely, high-temperature activation energy E_∞ , fragility m , or glass transition temperature T_g , no significant correlation is found. Regarding molecular vs ionic liquids, no relevant difference in the evolution of their DLS spectra is observed.



I. INTRODUCTION

After more than two decades of extensive research the generic properties of the dynamics involved in the glass transition phenomenon have been revealed and can be summarized as follows.^{1–9} When cooling a liquid, (i) a two-step correlation function characterizing density as well as orientational fluctuations (in molecular liquids) emerges with a long-time decay (α -process) showing (ii) relaxation stretching. At least in the high-temperature regime not too close to the glass transition temperature T_g , the stretching does not change with temperature, i.e., (iii) time– (or frequency–) temperature superposition (FTS) applies. The time constant τ_α of the long-term relaxation follows (iv) a super-Arrhenius temperature dependence. Such “glassy dynamics” are established well above the melting point (T_m) and simple liquid dynamics with monomodal correlation function and time constants following an Arrhenius law are only observed when approaching the boiling point T_b .^{10,11} Clearly, glassy dynamics previously only reported for temperatures below T_m are not restricted to the supercooled regime of a liquid.

Concerning quantitative aspects of the relaxation, understanding is still poor. For example, a full description of $\tau_\alpha(T)$ starting from the boiling point down to T_g is still missing (see, however, refs 10,11). Also, the strength of the change of $\tau_\alpha(T)$, usually cast in terms of the fragility index m , is neither

understood. Regarding relaxation stretching quantified, e.g., by a parameter β_K of the Kohlrausch function, the values vary over an interval of, e.g., $0.4 < \beta_K < 1.0$, and after inspecting a large number of glass formers, it has been suggested that the lower β_K is, the larger the fragility m is.¹² Ever since this correlation has been published it also has been challenged. For example, a recent study claims that β_K follows a more or less narrow distribution peaked around $\beta_K = 0.50$.¹³ Usually, the stretching is estimated from the high-frequency flank of the susceptibility spectra analyzed close to T_g by applying some model function or by inspecting some derivative of the high-frequency flank. Here, the problem is that a straightforward spectral analysis is hampered by the appearance of secondary relaxation processes, namely, excess wing and/or β -relaxation peak, and a model is needed to disentangle primary and secondary relaxations.¹⁴ The influence of secondary relaxations may also explain that apparently FTS often fails close to T_g .⁵ In addition, the correlation plots reported rely almost exclusively on scrutinizing dielectric spectra, and it is not clear to what extent, e.g., relaxation stretching, depends on the probing technique.

Received: December 16, 2013

Revised: May 21, 2014

Published: May 23, 2014

In a recent survey by photon correlation spectroscopy (PCS) it has been demonstrated that analyzing the data in the time domain essentially no change with temperature is observed in the relaxation stretching, and subtle changes caused by the excess wing are only revealed when the data are converted to the frequency domain.¹⁵ Yet, a stronger relaxation strength of the excess wing can explain the apparently stronger stretching observed for depolarized light scattering (DLS) compared to dielectric data. Moreover, it appears that the β -relaxation is not observed by DLS,^{15–17} a phenomenon not understood so far. In order to avoid separating primary and secondary relaxation close to T_g , an analysis of the relaxation stretching observed at higher temperatures is worthwhile doing. This is captured in the DLS spectra collected by tandem-Fabry-Pérot interferometry (TFPI) in combination with a double monochromator (DM). In the present study we analyze DLS spectra and their corresponding correlation function $C_2(t)$ (after Fourier transformation) of a series of molecular and ionic liquids which show a strong variation of their spectral parameters, such as relaxation stretching, relaxation strength of the fast dynamics, and short-time expansion of the corresponding reorientational correlation function. Thus, we assume that interaction induced scattering can be ignored and $C_2(t)$ reflects the correlation function of the second Legendre polynomial.^{18,19} For extending the time scale, data from PCS are included. The glass formers are studied up to temperatures well above T_m , in some cases even up to the boiling point. Correlations among the spectral parameters as well as with parameters describing the temperature dependence of $\tau_\alpha(T)$ like high-temperature activation energy E_∞ or fragility m are considered. As the determination of the rotational time constants for the molecular liquids studied has been reported in detail in our preceding publications,^{10,11,15} this will not be treated here, yet they are used to calculate the values of the fragility m and the high-temperature activation energy E_∞ . Regarding the ionic liquids investigated we present the corresponding time constants, and our results are discussed in comparison with those reported by optical Kerr effect (OKE)^{20–25} and dielectric spectroscopy.^{26–28} In a forthcoming contribution the collected DLS spectra will be analyzed in the frame of mode coupling theory (MCT), in particular, within the F_{12} model which allows an analysis beyond applying the “asymptotic laws” of MCT. As it turns out the DLS spectra can be quantitatively interpolated up to the boiling point.

II. EXPERIMENTAL DETAILS

Most samples were commercially available (Sigma-Aldrich) and were investigated without special purification. A sample was vacuum-distilled right into a glass tube with an inner diameter of 8 mm. Four ionic liquids were provided by io-li-tec (IoLiTec Ionic Liquids Technologies GmbH, Salzstrasse 184, D-74076 Heilbronn). After degassing the sample the tubes were flame-sealed. For measurements with a tandem-Fabry-Pérot interferometer (TFPI) and double monochromator (DM) the sample was either mounted in a self-built furnace or a CryoVac continuous-flow (liquid nitrogen) cryostat. As light source we used a vertically polarized Coherent Verdi-V2 laser at a wavelength of 532 nm and 200 mW optical power. Measurements with TFPI (JRS Scientific, triple-pass tandem Etalon) and DM (Jobin Yvon, U1000) were performed in parallel. TFPI was operated at horizontal polarization in almost backscattering geometry whereas the DM was applied at orthogonal geometry. For details, the reader is referred to refs 1,29,30. The TFPI measurements were done with three different free spectral

ranges and the DM measurements with two combinations of slits and frequency intervals. The overlapping spectral parts are then adjusted in amplitude to match together and form a smooth spectral density $S(\nu)$. For performing Fourier transformation, an algorithm based on the Filon algorithm was used. The spectral density $S(\nu)$ was converted to the susceptibility representation via $\chi''(\nu) = (1 + n(\nu))^{-1}S(\nu)$ with $n(\nu)$ being the Bose factor.

To determine time constants and relaxation strengths in the frequency domain, we used fits by a Cole-Davidson (CD) function³¹

$$\chi''(\omega) = \chi_\alpha \text{Im}\{(1 - i\omega\tau_{\text{CD}})^{-\beta_{\text{CD}}}\} \quad (1)$$

as it works better than a Kohlrausch function³² in most cases. We also used a so-called hybrid function,^{33,34} which consists of a CD part and a power-law describing part of the fast dynamics; explicitly

$$\chi''(\omega) = A \text{Im}\{(1 - i\omega\tau_{\text{CD}})^{-\beta_{\text{CD}}} + i\omega B(\tau_{\text{CD}}^{-1} - i\omega)^{a-1}\} \quad (2)$$

where A and B are prefactors. Thus, α -peak and susceptibility minimum are fully interpolated. The time constant τ_α is given by $\tau_\alpha = \beta_{\text{CD}}\tau_{\text{CD}}$. We investigated a series of 22 liquids, which consist of 16 molecular glass formers and 6 room temperature ionic liquids (RTIL) by DM/TFPI. Some of the DM/TFPI as well as PCS spectra were already published.^{28,30,34–38} Some of the RTIL were slightly colored due to unknown impurities which led to a background signal in the DLS spectra, seen at high frequencies, e.g., in Figure 1d. The systems studied, their molar mass M , T_g , fragility m , and other fit parameters are listed in Table 1, together with values taken from ref 11. There, the temperature range ΔT is also given, for which the α -peak was studied. For certain liquids, not all parameters were available; therefore, data of these liquids do not appear in Figures 9 and 10. The data symbols of the molecular liquids are connected to filled icons, whereas those of the RTIL are represented by open symbols.

III. RESULTS

In Figure 1 DLS susceptibility spectra of the three selected molecular glass formers salol³⁶ (see also ref 43), toluene (see also ref 44), DHIQ, and the ionic liquid EAN are shown as compiled by applying TFPI and DM. For reasons of clarity only a selection of spectra are shown. At low temperatures and low frequencies the primary or α -relaxation is well recognized for all liquids as a separate, asymmetrically broadened peak in addition to the microscopic (vibrational) peak in the THz regime; in between, a minimum is observed. While heating, the α -process shifts to high frequencies and approaches the vibrational excitation (comprising boson and microscopic peak). Finally, at highest temperatures, in the case of toluene and DHIQ both peaks have virtually merged to become a somewhat broadened single peak. For toluene, as well as ethylbenzene ($T_b = 409 \text{ K}$)¹⁵ and 2-methyl tetrahydrofuran ($T_b = 352 \text{ K}$) (corresponding spectra¹¹ not shown here, but analyzed) such merging is observed close to the (ambient pressure) boiling point T_b . The glass transition temperature T_g of the other liquids is significantly higher than that of toluene; therefore, the α -relaxation and the microscopic dynamics have not yet merged at the highest temperatures measured. The Raman lines, which show up at frequencies above a few terahertz, are not of interest here, as they contain no information on molecular dynamics.

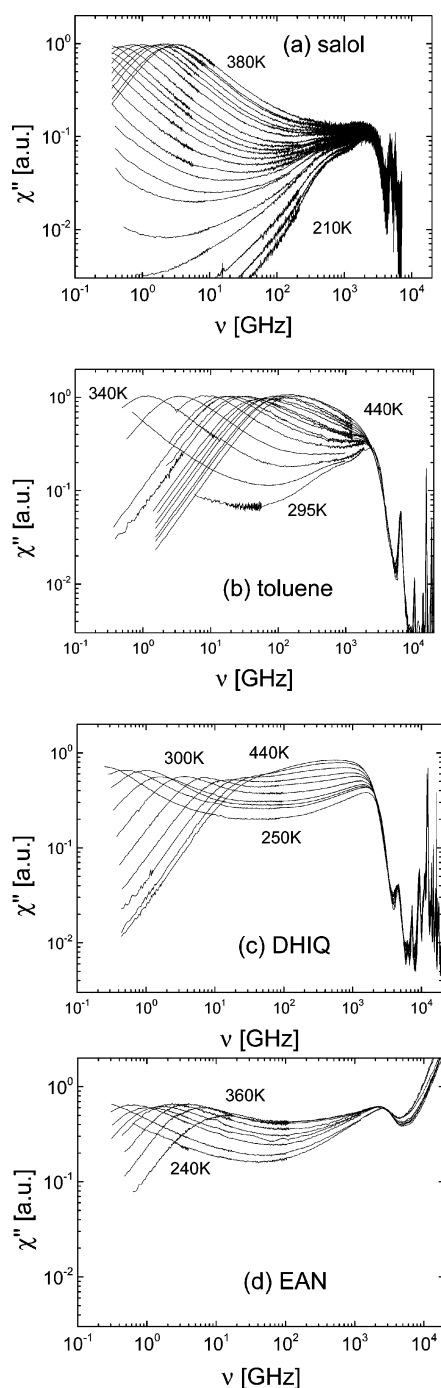


Figure 1. Susceptibility spectra of three molecular and one ionic liquid (EAN) as obtained by depolarized light scattering; all spectra are shown on the same scales. (a) salol 210–380 K ($T_b = 446$ K); (b) toluene 295–440 K ($T_b = 384$ K); (c) DHIQ 250–440 K ($T_b = 475$ K); (d) EAN 240–360 K ($T_b = 513$ K).³⁹

Even though they are looking quite similar at first glance the susceptibility spectra of the different liquids differ in some important details. For example, the relative spectral weight of the α -relaxation peak compared to that of the fast dynamics (comprising boson and microscopic peak) varies significantly. While for salol and toluene the α -peak is relatively strong, it is rather weak for EAN and DHIQ. These differences are best recognized in Figure 2, where the normalized spectra of all liquids taken at comparatively low temperature, yet still displaying a full α -peak in the present frequency window, are

plotted as a function of reduced frequency $\omega\tau_\alpha$. This means we chose an isodynamic point where the time constant of the α -process is on the order of 1 ns. The amplitude of the α -relaxation peak χ_α was determined via a CD fit by eq 1. Thereby, for all liquids a common low-frequency envelope, explicitly $\chi''/\chi_\alpha = \omega\tau_\alpha$ is found, and the different width of the α -relaxation is directly reflected in the height of its peak. More explicitly, the lower the α -peak, the flatter its high-frequency flank which corresponds to stronger relaxation stretching. A variation by about a factor of 2 is found which leads to a span of stretching parameters β_{CD} from about 0.32 up to 0.80, when a CD function is applied (cf. below). In addition, even though the figure appears a bit crowded, one clearly recognizes a strong variation in the height of the microscopic peak. For example, the amplitude of the α -process in comparison to the microscopic peak changes by a factor of about 10 between the extreme cases salol and DHIQ.

In order to determine the stretching parameter β_{CD} we show in Figure 3 the normalized spectra χ''/χ_α vs reduced frequency $\omega\tau_\alpha$ for toluene and EAN as given for different temperatures; here χ_α is again the relaxation strength of the α -process. Details on this scaling procedure are found in our recent publication.¹¹ As mentioned, by performing this scaling the low-frequency slope is identical with $\chi''/\chi_\alpha = \omega\tau_\alpha$. Yet, the data do not need to agree at the α -peak maximum. The lower the temperature, the better the high-frequency flank of the primary relaxation peak is resolved. In the case of toluene, the best interpolation of the envelope is given by a CD function³¹ with $\beta_{CD} = 0.64$. At the lowest temperature we show the result of fitting with a hybrid function (cf. Experimental Section, eq 2) which in addition takes into account a fast dynamics contribution in the form of a power-law $\chi'' \propto \nu^a$ and thus allows interpolation of the region around the susceptibility minimum. The hybrid fit (for toluene) works best with $\beta_{CD} = 0.68$, which is slightly higher than that of a pure CD fit. We note that, at high temperatures, when the α -peak and microscopic peak have merged, a hybrid function cannot interpolate the spectra any longer, yet it appears that a new envelope shows up, a phenomenon also reported for benzene.⁴⁵ This is indicated by the dashed line in Figure 3a. In the case of EAN, we get $\beta_{CD} = 0.39$ for the CD function and $\beta_{CD} = 0.42$ for the hybrid function fit. This kind of “ α -scaling” has been done for all the systems and the parameter β_{CD} obtained from the pure CD interpolation is collected in Table 1 and displayed in Figures 9 and 10, where they are compared to other parameters of the spectra as well as to quantities describing the temperature dependence of the time constants $\tau_\alpha(T)$ (cf. below). As already noted, a range of $0.32 \leq \beta_{CD} \leq 0.80$ is found for the 22 liquids studied (cf. Table 1).

We note that in most cases the exponent a , characterizing the fast dynamics, does not comply with the prediction of the asymptotic laws of the MCT.⁴⁶ Usually the value is too high, yet, in the case of a weak microscopic (and boson) peak such as in toluene (cf. Figure 3a) or salol (cf. Figure 1a), the MCT interpolation of the susceptibility works well, i.e., the exponent a and β_{CD} can be fixed via the so-called exponent parameter λ (cf. also Figure 4a) by

$$\lambda = \frac{\Gamma(1-a)^2}{\Gamma(1-2a)} = \frac{\Gamma(1+\beta_{CD})^2}{\Gamma(1+2\beta_{CD})} \quad (3)$$

The features of the susceptibility minimum are once again inspected in Figure 4 where the “minimum scaling” is displayed for salol and ethylbenzene, i.e., the spectra are rescaled in such a

Table 1. Molecular and Ionic Liquids Investigated and Parameters of the Analysis: Molar Mass M Given in $[\text{g mol}^{-1}]$, Glass Transition Temperature T_g [K], Fragility Index m , Cole-Davidson (Stretching) Parameter β_{CD} , High-Temperature Activation Energy E_∞ [K],¹⁰ Amplitude $1 - f$ of the Fast Dynamics, Effective Momentum of Inertia I^* [10^{-45} kg m^2] Calculated via eq 6 and the Temperature Range ΔT [K] Studied

	name (abbreviation)	M	T_g	m	β_{CD}	E_∞	$1-f$	I^*	ΔT
●	2-methyl tetrahydrofuran (MTHF)	86.1	92	100	0.48	1169	0.20	0.50	140 - 440
▲	glycerol	92.1	188	54	0.45	2271	0.13	---	315 - 330
▼	toluene	92.1	117	108	0.66	1440	0.17	0.68	180 - 440
◀	picoline	93.1	129	79	0.65	1438	0.17	---	190 - 440
▶	propylene carbonat	102.1	157	80	0.67	1729	0.15	1.27	235 - 445
■	ethylbenzene	106.2	115	86	0.55	1369	0.09	1.29	170 - 440
○	ethylammonium nitrate (EAN)	108.1	182 ³⁹	---	0.42	2790	0.32	0.50	260 - 360
△	lithium chloride (LiCl:5H ₂ O)	132.5	129	---	0.32	2294	0.23	---	214 - 320
◆	4-tert-butyl pyridine (4-TBP)	135.2	164	74	0.54	1761	0.20	1.35	230 - 270
★	decaline	138.3	134.7 ⁴⁰	147 ⁴⁰	0.67	---	0.36	0.96	310
●	decahydroisoquinoline (DHiQ)	139.2	179	123	0.54	1851	0.38	0.92	250 - 440
▲	trimethyl phosphate (TMP)	140.1	136	81	0.39	1573	0.35	0.35	230 - 440
▼	benzophenone	182.2	207	90	0.71	2954	0.10	1.58	290 - 440
▶	dimethyl phthalate (DMP)	194.2	191	75	0.73	2029	0.11	1.47	290 - 440
◀	salol	214.2	218	84	0.78	2104	0.12	2.75	320 - 380
▽	1,3-dimethylimidazolium dimethylphosphate (MMIM MMPO ₄)	222.2	203	95	0.50	3065	0.13	---	320 - 420
■	tripropyl phosphate (TPP)	224.2	131	46	0.40	---	0.26	0.86	350 - 400
◆	o-terphenyl (OTP)	230.3	245	82	0.65	2441	0.11	1.22	330 - 440
◁	1-butyl-3-methylimidazolium hexafluorophosphate (BMIM-PF ₆)	284.2	194	44	0.61	---	0.23	---	360 - 380
★	m-tricresyl phosphate (m-TCP)	368.4	205	71	0.41	2301	0.04	2.28	300 - 440
▷	1-ethyl-3-methylimidazolium bis(trifluoromethylsulfonyl)imide (EMIM imide)	391.3	186 ⁴¹	---	0.39	2476	---	---	300 - 440
◻	1-butyl-3-methylimidazolium bis(trifluoromethylsulfonyl)imide (BMIM imide)	419.4	182 ⁴²	---	0.40	---	---	---	350 - 400

way that a common envelope of the minimum between the α -process and the microscopic peak results. Indeed, the common envelope applies up to high temperatures and the shape of the envelope can be approximated by a sum of two power-laws. The latter is actually an approximation of the hybrid function in the region of the susceptibility minimum. The exponents obtained by this fit do not need to be equal to those of the α -scaling (cf. Figure 3) for reasons that will become clear below. Here, we compare a free interpolation with that of the forecast by MCT. As already discussed, in the case of salol the power-law interpolation of the minimum is compatible with that of MCT; however, for ethylbenzene with its strong microscopic peak (and broad α -relaxation), the asymptotic MCT prediction

does not adequately interpolate the data. Below about 155 K the minimum scaling clearly fails for ethylbenzene (shown in blue). The minimum becomes increasingly flatter through a decrease of the slope of its low-frequency flank. As in our preceding work,^{15,36,37} we interpret this flattening of the minimum as a sign of the emergence of the excess wing (or intermediate power-law, see below). The excess wing is usually identified by dielectric spectroscopy on the high-frequency flank of the α -relaxation and described by a power-law $\chi'' \propto \nu^{-\gamma}$ with an exponent around $\gamma \cong 0.2 < \beta_{\text{CD}}$ (included in Figure 4b). Given the validity of the minimum scaling at high temperatures one can conclude that α -process and fast dynamics do not change their spectral shapes and amplitudes.

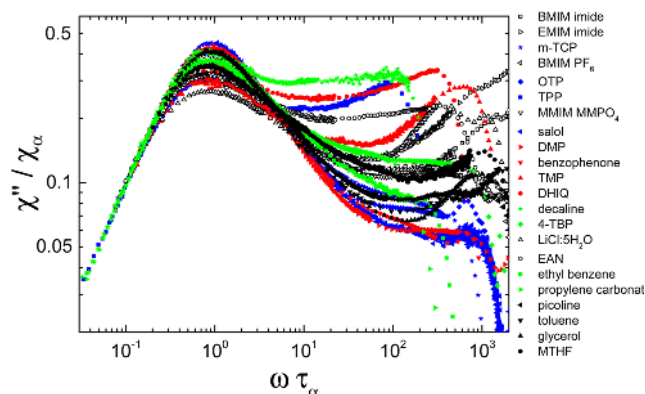


Figure 2. Susceptibility spectra of 22 molecular and ionic liquids (cf. Table 1) normalized by the intensity of the α -process and plotted versus the rescaled frequency $\omega\tau_\alpha$. Pronounced differences are recognized regarding the width of the α -relaxation and the relative amplitude of the microscopic peak.

So far, we have investigated the dynamics of the liquids in the frequency domain. Now we will continue our analysis in the time domain. Figure 5 shows the cosine Fourier transforms of the spectral densities corresponding to the susceptibilities displayed in Figure 1 for toluene and DHIQ. As mentioned, we assume that a rotational correlation function of rank-two is probed. At shortest times, the correlation loss starts with an essentially temperature independent time scale followed by a decay down to a plateau, and finally the α -process takes the rest of the correlation. In the two examples shown, we see a significant difference in the relaxation stretching and in the height of plateau f which reflects the strength of the α -relaxation.

Instead, by CD function, the correlation function $C_2(t)$ can also be approximated by a stretched exponential (Kohlrausch) function at long times at which the α -process dominates; explicitly

$$C_2(t) = f \exp\left(-\left(\frac{t}{\tau_K}\right)^{\beta_K}\right) \quad (4)$$

As mentioned, the amplitude f describes the strength of the α -process also known as non-ergodicity parameter. The Kohlrausch parameter τ_K is related to the (mean) correlation time τ_α via $\tau_\alpha = \tau_K \Gamma(1/\beta_K)/\beta_K$, where Γ denotes the gamma

function. The Kohlrausch function can be linearized by plotting $C_2(t)$ on logarithmic scales versus $(t/\tau_K)^{\beta_K}$ as shown in Figure 6. The values of β_K are system specific but not temperature dependent, and parallel straight lines are found at long times for the different systems. In the case of DHIQ some deviations from the straight line occur, yet, as displayed in the inset of Figure 6, the variation in β_K is about 5% and has no clear temperature trend. The only relevant difference the systems show is the amplitude of the straight line which reflects different f . This plot directly demonstrates three features already partly obvious from α - and minimum scaling. (i) The relaxation stretching does not change with temperature, thus FTS applies. (ii) Relaxation stretching is observed up to highest temperatures close to the boiling point. No crossover to an exponential relaxation is recognized. (iii) Also, the amplitude f is temperature independent, yet as for β_K it varies among the different systems, and below we investigate their correlation with other quantities characterizing the glass transition. All in all, these relaxation features define what is called “glassy dynamics”, and they are observed almost up to the boiling point. At such high temperatures, actually the bimodal shape of the correlation function is almost lost as microscopic dynamics and α -process have more or less merged. The values of β_K are about 0.1–0.2 higher than the corresponding β_{CD} values, in agreement with a comparison of CD and Kohlrausch function carried out by Lindsey and Patterson.⁴⁷

Figure 7 shows the rescaled pulse-response representation of the DLS data for the liquids m-TCP, toluene, salol, and DMP on a reduced time scale t/τ_α . The pulse-response is calculated from the correlation function $C_2(t)$ via

$$F_p(t) \propto -\frac{dC_2(t)}{dt} \quad (5)$$

This representation of the data is directly measured by OKE experiments and allows an easy identification of different power-laws dominating the correlation loss. Regarding α -relaxation and excess wing (or intermediate power-law⁴⁸), their power-law exponents β_{CD} and γ are expected to reappear as $F_p(t) \propto t^{-\alpha} = t^{-(1-\beta_{CD})}$ and $\propto t^{-(1-\gamma)}$, respectively. Indeed, in the case of salol, two power-laws are easily discernible: on one hand, the intermediate power-law at short times with an exponent $\alpha = 1 - \gamma = 0.8$, and on the other hand, a second one at longer times with exponent $1 - \beta_{CD} = 0.21$. The latter is the short-time or high-frequency contribution of the α -process and is called the von Schweidler law.⁴⁸ The part of the decay rising

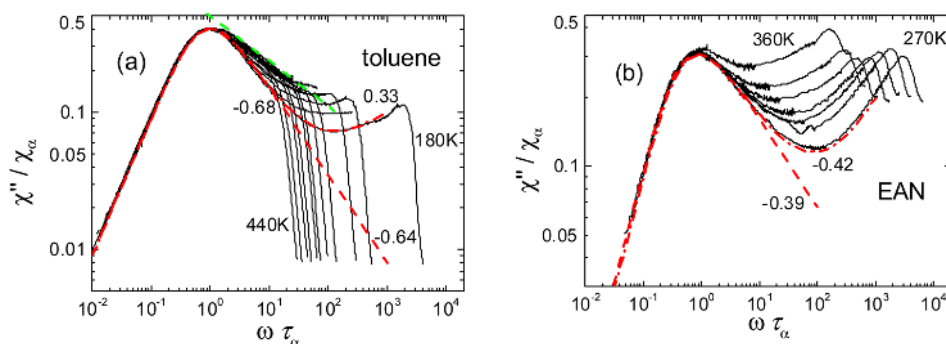


Figure 3. Spectra of (a) toluene (at temperature in K: 180, 200, 225, 250, 260, 280, 295, 320, 340, 360, 380, 400, 420, 440) and (b) EAN (at temperature in K: 270, 280, 290, 300, 320, 340, 360) shown in Figure 1 scaled on a common envelope of the α -process (α -scaling). Red dashed and dashed-dotted lines show fits by a CD or hybrid function (eq 2), respectively. In the case of toluene a hybrid function agrees with a MCT interpolation. Dashed green line in (a) represents high-temperature apparent envelope with an exponent of about -0.33 .

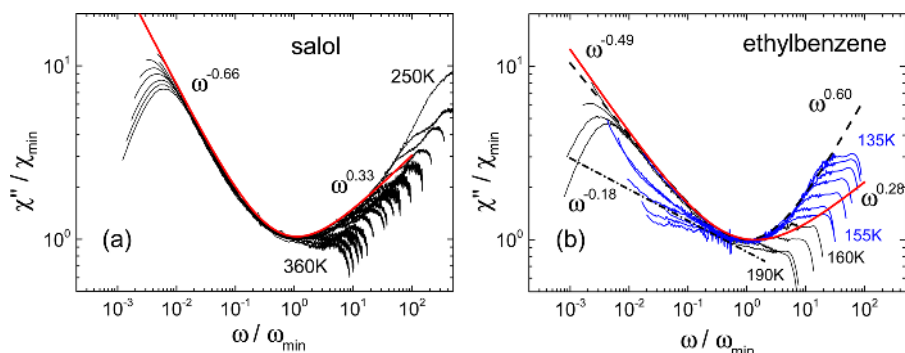


Figure 4. Spectra of (a) salol (at temperatures in K: 250, 260, 265, 270, 275, 280, 285, 290, 295, 300, 310, 320, 330, 340, 350, and 360) and (b) ethylbenzene (at temperatures in K: 133, 135, 137, 140, 145, 150, 155, 160, 170, 180, and 190) scaled on a common envelope of the minimum. For ethylbenzene a breakdown of the scaling is observed at temperatures below 155 K (blue vs black lines). Dashed line: fit by a sum of two power-laws without any restraints; red solid line: fit compatible with MCT; dash-dotted line: power-law with $\omega^{-0.18}$ reflecting the onset of the excess wing.

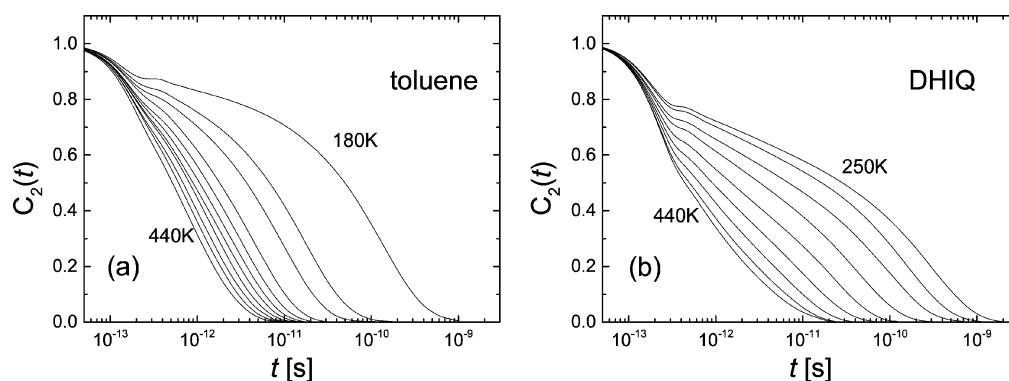


Figure 5. Reorientational correlation function $C_2(t)$ as obtained from the depolarized light scattering spectra in Figure 1 of (a) toluene and (b) DHIQ exhibiting rather different relaxation stretching and amplitude of fast dynamics.

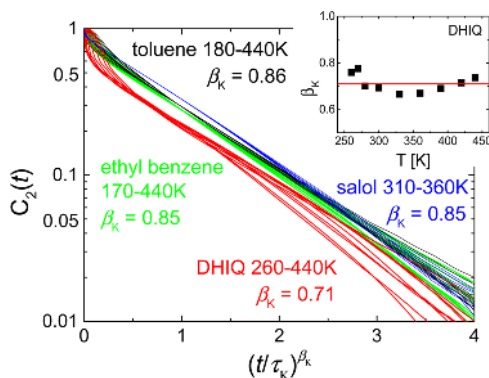


Figure 6. Logarithmic plot of $C_2(t)$ versus $(t/\tau_K)^{\beta_K}$ yielding linear long-time behavior. For each system, the stretching parameter β_K of the α -process is kept temperature independent. The inset shows variation of β_K around its mean value, if it was allowed to vary.

above the intermediate power-law is due to the fast dynamics. Actually, it is remarkable that the intermediate power-law can clearly be identified, although no traces of it are recognized in the frequency domain (cf. Figure 4a). Yet, identification in the pulse-response representation indicates that an interpolation of the susceptibility by superposition of two power-laws as done in Figure 3 is not strictly correct and contributions of the intermediate power-law are already observed at high temperatures (a finding which we were not aware in our previous publications^{15,30}). This may explain why the different interpolations of the susceptibility minimum provide somewhat

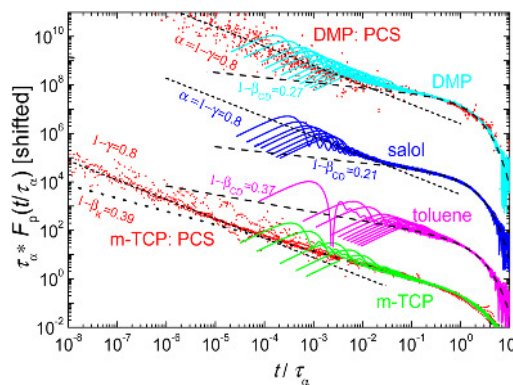


Figure 7. Pulse-response representation of the DLS data for the four liquids m-TCP,¹⁵ toluene, salol,³⁶ and DMP¹¹ obtained by PCS (points) and TFPI/DM (lines).

different exponents as discussed above in the context of α - and minimum scaling. We note that the intermediate power-law is not included in the asymptotic laws of MCT. As has been discussed by Brodin et al.,^{14,36,37} the intermediate power-law⁴⁸ is nothing else than the excess wing usually identified in dielectric spectroscopy. In the case of m-TCP the intermediate power-law is not discernible probably due to a strong contribution of the fast dynamics ($1-f$ is rather large, cf. Figure 2), yet it is well resolved by our PCS data which extend to much shorter rescaled times.¹⁵ Admittedly, the PCS data show a considerable amount of scatter, which is attributed mainly to the calculation of the pulse-response representation

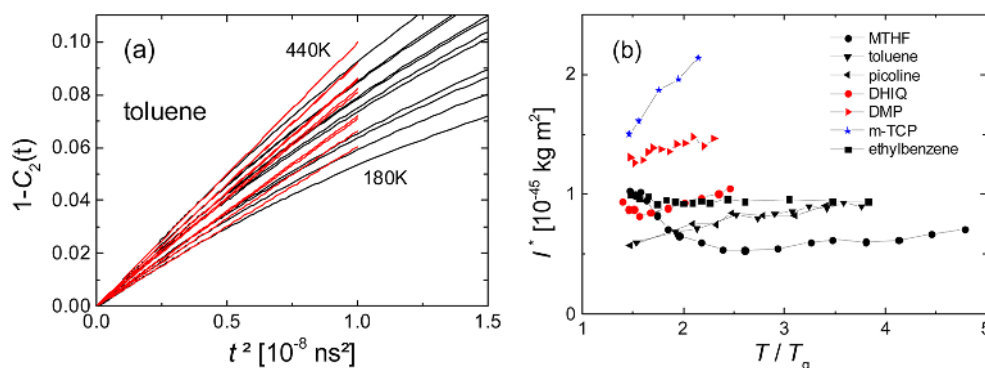


Figure 8. (a) Same data as shown in Figure 5a, but here $1 - C_2$ is plotted versus t^2 . The initial slope M_2 (red lines) is related to some effective moment of inertia I^* (cf. eq 7). (b) Temperature dependence of I^* for some selected liquids.

(e.g., making the derivative) from the PCS step-response approaching its resolution limit in the 10 ns regime. The original PCS decays of m-TCP are shown in ref 15, those of DMP in ref 11, and it is the first time that indications of the intermediate power-law are identified by PCS. In addition, the magnitude of the exponent of the second power-law, which in the case of m-TCP is interpolated better by the short-time expansion of a Kohlrausch decay (with $\beta_K \cong \beta_{CD} + 0.1$) is much higher compared to that of salol, making it further difficult to resolve the intermediate power-law. In the case of toluene, the intermediate power-law is not recognized, although the relaxation strength $1 - f$ is rather small (cf. Figure 3a). Here, the stretching parameter β_{CD} is the smallest among the four liquids discussed in Figure 7.

Still one difference among the correlation functions displayed in Figure 6 is of relevance and distinguishes the systems, namely, the time scale at shortest times. Classical correlation functions are an even function in time and they can be expanded in a power series. For short times, for the reorientational correlation function one has^{49,50}

$$C_2(t) = 1 - M_2 t^2 + M_4 t^4 - O(t^6) \quad (6)$$

In the case of linear molecules, the coefficient M_2 is related to the moment of inertia via

$$I = l(l + 1) \frac{k_B T}{2M_2} \quad (7)$$

with l being the rank of the correlation function probed. Ignoring that the present molecules are actually not linear, the important point is that the coefficient M_2 only reflects inertial features specific to the molecule and thus is independent of interaction effects in the liquid. This is also expected for nonlinear molecules. In Figure 8a, as an example, we plot $1 - C_2(t)$ versus t^2 for toluene. In this representation, the quadratic decay is represented by a straight line. One clearly sees the linear regime as indicated by the red lines. Figure 8b shows the temperature dependence of the apparent quantity I^* calculated along eq 6 for seven molecular liquids as a function of the reduced temperature T/T_g (cf. Table 1). While at high reduced temperatures, as expected, the quantity is virtually temperature independent, some decrease is observed at low temperatures (an exception is MTHF). In addition, a clear trend to higher values of I^* for higher masses is observed. MTHF, which is the lightest molecule ($M = 86 \text{ g mol}^{-1}$) investigated, has the lowest value of I^* , whereas m-TCP (386 g mol^{-1}) has the highest one. The quantity I^* is shown for some of the investigated liquids in

Figure 8b. Molecular moments of inertia are on the order of 10^{-45} kg m^2 in agreement with the scale in Figure 8b. Why a temperature trend (in most cases a decrease) sets in when approaching T_g is currently not clear. For further comparison, we used I^* at an isodynamic point of $\tau_\alpha \approx 10^{-11} \text{ s}$; these are the values given in Table 1 and displayed in Figure 9a. As note of caution, we are well aware that the short-time behavior of $C_2(t)$ may not only reflect reorientational dynamics but also collision induced contributions;¹⁸ yet, the temperature independency of the quantity I^* at high temperatures and the correlation with molecular mass may be taken as a hint that indeed reorientational contributions dominate in $C_2(t)$ even at short times.

Now that the DLS spectra of the liquids have been characterized by a set of parameters, namely, β_{CD} , $1 - f$, and I^* , we look for relations among them. First, Figure 9a displays the correlation between the effective momentum of inertia I^* and the molar mass M . As already mentioned, one finds a trend that molecules with higher values of M show a higher quantity I^* . Of course, different molecular geometries and sizes disturb a clear-cut relation between I^* and M . In Figure 9b the quantity $1 - f$ (relaxation strength of the fast dynamics) is plotted versus I^* . With a correlation coefficient of -0.64 we find a negative correlation: The higher $1 - f$, the lower is the inertial quantity I^* . Finally, in Figure 9c we consider the correlation among $1 - f$ and the stretching parameter β_{CD} . No correlation is observed. The width parameter lies in the range 0.32–0.80; no indication for a preferential value of $\beta_{CD} = 0.5$ is found as suggested by Nielsen et al.¹³

Next, we discuss the connection between the spectral parameters and those characterizing the temperature dependence of the time scale of the α -process $\tau_\alpha(T)$, namely, the high-temperature activation energy E_∞ , fragility index m , and the glass transition temperature T_g itself. As demonstrated in our previous works,^{10,11} well above the melting point and close to the boiling point the super-Arrhenius temperature dependence of $\tau_\alpha(T)$, which is observed close to T_g , crosses over to an Arrhenius law specified by the activation energy E_∞ . In Figure 10a we check for a correlation between β_{CD} and E_∞ ; no correlation is found. This also holds for $1 - f$ vs E_∞ (not shown). In Figure 10b the stretching parameter β_{CD} versus fragility index m is considered. Again, we do not find any correlation; relaxation stretching is independent of fragility. In Figure 10c, we check for a correlation between the stretching parameter β_{CD} and T_g . If at all, a weak increase of β_{CD} with T_g can be anticipated. Finally, in Figure 10d, the correlation between $1 - f$ and the fragility m is checked. A weak trend may

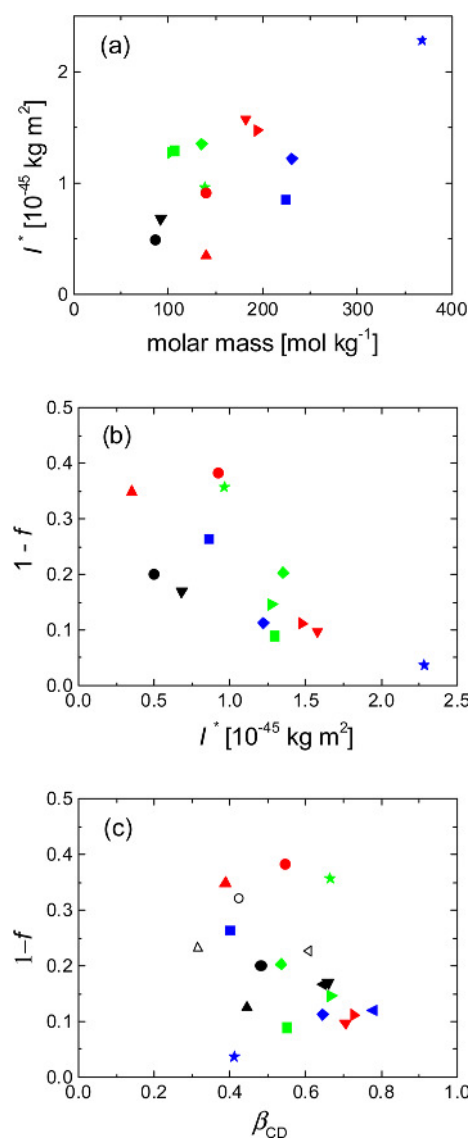


Figure 9. (a) Correlation between I^* and molar mass for molecular liquids. (b) Correlation between the strength of the microscopic dynamics $1-f$ and the effective moment of inertia I^* . (c) Intensity of the fast dynamics $1-f$ vs stretching parameter β_{CD} . All the numerical values are found in Table 1. RTIL: open symbols; Error bars are on the order of symbol size.

be observed: the more fragile, the higher $1-f$ is. In all cases, the ionic liquids do not display any particular behavior.

IV. DISCUSSION

Molecular glass formers and room temperature ionic liquids have been investigated by tandem-Fabry-Pérot interferometry and double monochromator over a large temperature range, in some cases up to the boiling point. With the analysis extended to longer times, PCS data have been included. The primary (α -) relaxation revealed in the spectra shows different relaxation broadening as well as different spectral weight with respect to the fast dynamics including boson peak and vibrational dynamics. Assuming that the spectra solely reflect reorientational dynamics, the corresponding reorientational rank-two correlation function is characterized by three parameters, namely, stretching parameter β_{CD} , strength of the fast dynamics $1-f$, and the time scale at shortest times in terms of an

effective moment of inertia I^* . In addition to the stretched long-time decay (α -process), an intermediate power-law regime (or excess wing in the frequency domain) with an exponent $\gamma \cong 0.2$ has to be taken into account in between α -process and fast dynamics. It has first been observed in optical Kerr effect decays⁴⁸ and is identified also in the TFPI/DM data provided that α -stretching is weak (as in salol). Yet, it is well resolved by PCS and dielectric spectroscopy; in the latter it shows up in the form of the excess wing.^{2,15,36,37,51}

For a given liquid all the three spectral parameters are virtually temperature independent up to the boiling point. Explicitly, the relaxation stretching does not change with temperature; thus, time-temperature superposition applies for the α -process up to highest temperature; there is no-crossover to an exponential long-time decay. Also, the amplitude $1-f$ is temperature independent, yet as for β_{CD} it may vary considerably among the different liquids. Thus, the usually found statement that in the high-temperature liquid the reorientational correlation function is essentially exponential is not tenable. All spectral features commonly characterized as “glassy dynamics” are already established well above the melting point, i.e., they determine the dynamics of most liquids in daily life.

Testing for correlations among the spectral parameters as well as with parameters specifying the temperature dependence of τ_α , we find no significant effects. In particular, the stretching parameter β_{CD} does not correlate with the fragility m . This is at variance with the conclusion of Böhmer et al.¹² which has been drawn when analyzing relaxation data close to T_g . As mentioned in the Introduction, we argue that at T_g the shape of the primary relaxation is obscured by the presence of secondary relaxation processes and determination of the stretching is not straightforward. A weak trend between $1-f$ and fragility m may be observed: the more fragile, the higher $1-f$ is. When inorganic network glasses are also included, an opposite trend was reported by Sokolov et al.⁵² The authors considered the susceptibility ratio of the boson peak maximum to the minimum instead of looking at the full integral over the fast dynamics spectrum $1-f$ as in the present case. The scale at shortest times reflects essentially inertial effects and it shows as expected some correlation with molecular mass.

Regarding ionic liquids (RTIL) with their quite different interaction potential compared to molecular liquids, no significantly different reorientational behavior was found; they behave just like molecular liquids. The present RTIL have also been investigated by OKE^{20–25} as well as dielectric spectroscopy.^{26–28} In the case of OKE experiments on molecular liquids collected by the Fayer²⁰ and Torre groups²¹ it has been shown^{36,37} that OKE and DLS essentially yield the same response: one the pulse-response function, the other the step-response of the rank-two reorientational correlation function. Most of the OKE experiments performed so far on RTIL are restricted to a rather short time interval, e.g., 1–10 ps, and the long-time decays are fitted to a sum of two exponentials.^{23,25} OKE experiments covering longer times of up to 4 ns by Turton et al.²² have described the response by two low-frequency relaxation modes and two to three Brownian oscillators (see also ref 24). Cang et al.,²⁰ again reaching the ns regime, have reported OKE experiments on EAN revealing an intermediate power-law at short times followed by a second power-law, the von Schweidler law. The authors concluded that “the orientational dynamics of ionic organic liquids are fundamentally the same as van der Waals liquids”. We draw

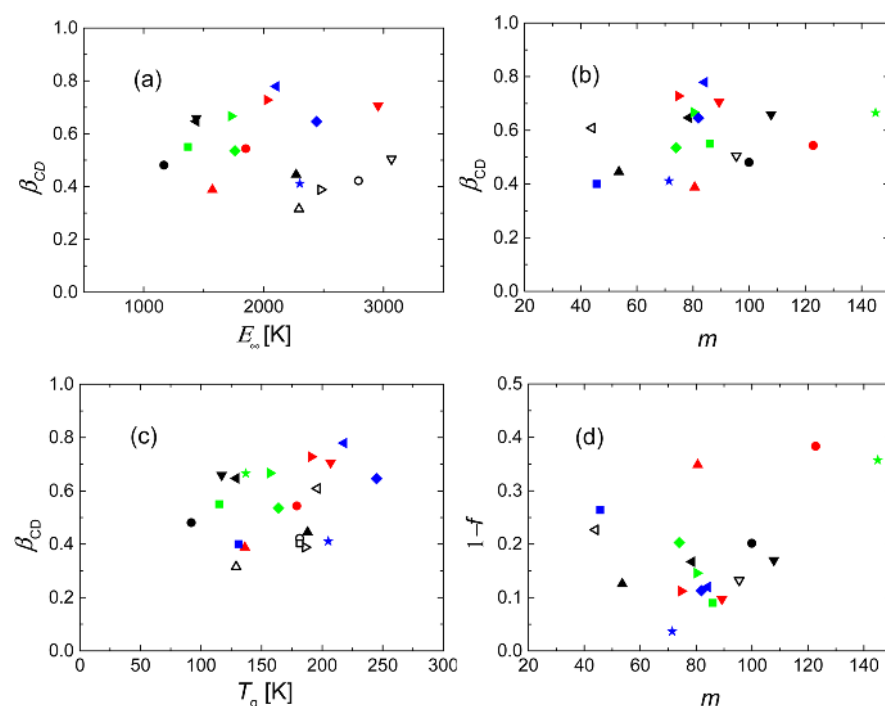


Figure 10. (a) Correlating fragility index m and stretching parameter β_{CD} . (b) Correlating glass transition temperature T_g and β_{CD} . (c) High-temperature activation energy E_∞ versus β_{CD} . (d) Correlating relaxation strength of the fast dynamics $1 - f$ and fragility index m . All the numerical values are found in Table 1. Error bars are on the order of symbol size; open symbols: RTIL.

exactly the same conclusion. In Figure 11 we display our results for the ionic liquids in the rescaled pulse-response representa-

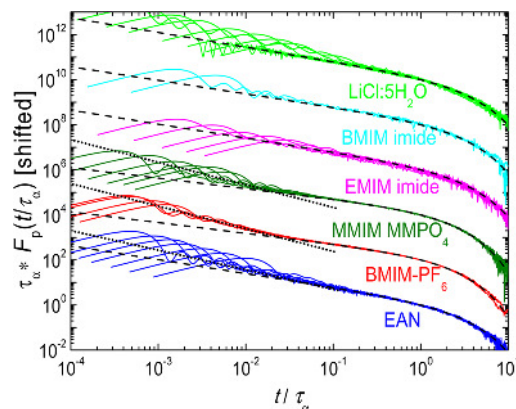


Figure 11. Pulse-response representation of the DLS data for the RTIL LiCl:5H₂O, BMIM imide, EMIM imide, MMIM MMPO₄, BMIM-PF₆, and EAN (top to bottom, cf. Table 1). Dashed lines: CD fits of the α -process, dotted lines: first traces of the intermediate power-law with $\gamma \cong 0.2$.

tion just as in Figure 7 for molecular liquids. Clearly the von Schweidler law is recognized followed by a more or less exponential cutoff at longest times. A CD fit interpolates the full α -decay (dashed line). At short times a crossover to the fast dynamics is recognized, and at lowest temperatures first traces of the intermediate power-law are found (dotted line) in the case of EAN, BMIM-PF₆, and MMIM MMPO₄. By comparing DS and DLS/OKE, similar results are observed; the stretching parameter β_{CD} deviates by no more than 0.07.^{26,27} In the case of the amplitude of the fast dynamics $1 - f$ strong differences are observed among the techniques.²⁸

As mentioned, the orientational correlation times of the molecular liquids have been presented in ref 10; for completeness the corresponding time constants $\tau_\alpha = \tau_{CD} \beta_{CD}$ of the RTIL studied in the present contribution are displayed in Figure 12, where we also included results from our dielectric²⁸

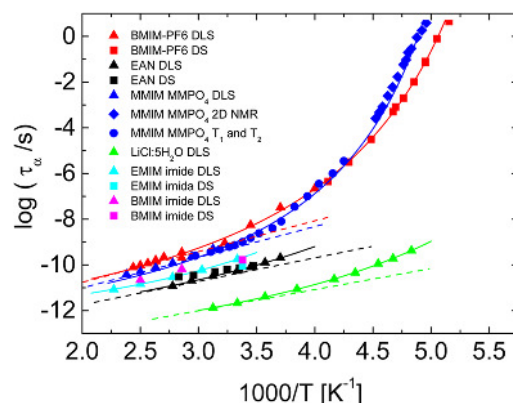


Figure 12. Reorientational time constants of the RTIL investigated (LiCl:5H₂O, BMIM imide,²⁷ EMIM imide,²⁷ MMIM MMPO₄, BMIM-PF₆,²⁸ and EAN;²⁶ see Table 1) by depolarized light scattering (DLS), dielectric spectroscopy (DS), 2D nuclear magnetic resonance spectroscopy (NMR), and spin–lattice relaxation (T_1) and spin–spin relaxation (T_2).⁵³ Lines are guides-to-the-eyes; dashed lines indicate Arrhenius behavior at high temperatures.

and NMR spectroscopy work.⁵³ The dashed lines indicate an Arrhenius behavior at high temperatures, as also reported for molecular liquids.¹⁰ We have to remark that the values of E_∞ might change a bit as soon as more high temperature time constants become available. No significant difference is observed among the results from the different techniques reporting collective as well as single-particle dynamics. Thus,

although in most of the RTIL light scattering as well as the dielectric response originate from both the cation and the anion dynamics, no indication of different time constants is found. Both species are part of a common cooperative process exhibiting features characteristic of what has been called glassy dynamics and is virtually the same as observed in molecular liquids. Finally, we note that all the spectra of the ionic liquids (as well as the molecular liquids) can be described well up to high temperatures by the schematic F_{12} model of MCT as will be shown in a follow-up study.

V. CONCLUSIONS

Molecular glass formers and room temperature ionic liquids have been studied by tandem-Fabry-Pérot interferometry and double monochromator over a large temperature range, in some cases up to the boiling point. The susceptibility spectra and the corresponding reorientational rank-two correlation functions are systematically compared. Time scales between 1 ps and 10 ns are accessed. The primary (α -) relaxation revealed in the spectra is described by a Cole-Davidson function showing among the systems different relaxation stretchings and different amplitudes f . The stretching parameter β_{CD} as well as strength of the fast dynamics $1 - f$ are virtually temperature independent up to highest temperatures. All spectral features commonly characterized as “glassy dynamics” are already established well above the melting point. In addition to a stretched long-time decay (α -process), an intermediate power-law regime (or excess wing in the frequency domain) is identified in between α -process and fast dynamics as also reported by OKE experiments. When testing for correlations among the spectral parameters, no correlation among $1 - f$ and β_{CD} is revealed. Also, no correlation between β_{CD} and fragility m is observed, which is at variance with the common assumption. Regarding molecular vs ionic liquids, no relevant difference in the evolution of their DLS spectra is observed. The orientational dynamics of ionic organic liquids are essentially the same as that of van der Waals liquids.

■ AUTHOR INFORMATION

Corresponding Author

*Phone: +49 921 55 3164. E-mail: ernst.roessler@uni-bayreuth.de.

Notes

The authors declare no competing financial interest.

■ ACKNOWLEDGMENTS

The authors thank T. Voigtmann for helpful discussions. Financial support of Deutsche Forschungsgemeinschaft (DFG) through project RO 907/11 and RO 907/15 is appreciated. H. Weingärtner thanks the Cluster of Excellence RESOLV (EXC 1069) at the Ruhr-University Bochum funded by the Deutsche Forschungsgemeinschaft for financial support.

■ REFERENCES

(1) Cummins, H. Z.; Li, G.; Hwang, Y. H.; Shen, G. Q.; Du, W. M.; Hernandez, J.; Tao, N. J. Dynamics of Supercooled Liquids and Glasses: Comparison of Experiments with Theoretical Predictions. *Z. Phys. B* **1997**, *103*, 501–519.
(2) Lunkenheimer, P.; Schneider, U.; Brand, R.; Loidl, A. Glassy Dynamics. *Contemp. Phys.* **2000**, *41*, 15–36.
(3) Tölle, A. Neutron Scattering Studies of the Model Glass Former Ortho-Terphenyl. *Rep. Prog. Phys.* **2001**, *64*, 1473–1532.

(4) Binder, K.; Kob, W. *Glassy Materials and Disordered Solids*; World Scientific: New Jersey, 2005.
(5) Blochowicz, T.; Brodin, A.; Rössler, E. A. Evolution of the Dynamic Susceptibility in Supercooled Molecular Liquids and Glasses. *Adv. Chem. Phys.* **2006**, *133*, 127–257.
(6) Dyre, J. C. The Glass Transition and Elastic Models of Glass-forming Liquids. *Rev. Mod. Phys.* **2006**, *78*, 953–972.
(7) Berthier, L.; Biroli, G. Theoretical Perspective on the Glass Transition and Amorphous Materials. *Rev. Mod. Phys.* **2011**, *83*, 587–645.
(8) Ediger, M. D.; Harrowell, P. Perspective: Supercooled Liquids and Glasses. *J. Chem. Phys.* **2012**, *137*, 080901.
(9) Richert, R. in *Structural Glasses and Supercooled Liquids*; Wolynes, P. G., Lubchenko, V., Eds.; Wiley: Hoboken, 2012; p 1.
(10) Schmidtke, B.; Petzold, N.; Kahlau, R.; Hofmann, M.; Rössler, E. A. From Boiling Point to Glass Transition Temperature: Transport Coefficients in Molecular Liquids Follow Three-Parameter Scaling. *Phys. Rev. E* **2012**, *86*, 041507.
(11) Schmidtke, B.; Petzold, N.; Kahlau, R.; Rössler, E. A. Reorientational Dynamics in Molecular Liquids as Revealed by Dynamic Light Scattering: From Boiling Point to Glass Transition Temperature. *J. Chem. Phys.* **2013**, *139*, 084504.
(12) Böhmer, R.; Ngai, K. L.; Angell, C. A.; Plazek, D. J. Non-exponential Relaxations in Strong and Fragile Glass-Formers. *J. Chem. Phys.* **1993**, *99*, 4201–4209.
(13) Nielsen, A. I.; Christensen, T.; Jakobsen, B.; Niss, K.; Olsen, N. B.; Richert, R.; Dyre, J. Prevalence of Approximate \sqrt{t} Relaxation for the Dielectric α -process in Viscous Organic liquids. *J. Chem. Phys.* **2009**, *130*, 154508.
(14) Brodin, A.; Gainaru, C.; Porokhonsky, V.; Rössler, E. A. Evolution of the Dynamic Susceptibility in Molecular Glass Formers - A Critical Assessment. *J. Phys.: Condens. Matter* **2007**, *19*, 205104.
(15) Petzold, N.; Schmidtke, B.; Kahlau, R.; Bock, D.; Meier, R.; Micko, B.; Kruk, D.; Rössler, E. A. Evolution of the Dynamic Susceptibility in Molecular Glass Formers: Results From Light Scattering, Dielectric Spectroscopy, and NMR. *J. Chem. Phys.* **2013**, *138*, 12A510.
(16) Comez, L.; Fioretto, D.; Palmieri, L.; Verdini, L.; Rolla, A. P.; Gapiński, J.; Pakula, T.; Patkowski, A.; Steffen, W.; Fischer, E. W. Light Scattering Study of a Supercooled Epoxy Resin. *Phys. Rev. E* **1999**, *60*, 3086–3096.
(17) Brodin, A.; Rössler, E. A.; Bergman, R.; Mattson, J. Light Scattering and Dielectric Manifestation of Secondary Relaxations in Molecular Glassformers. *Eur. Phys. J. B* **2003**, *36*, 349–357.
(18) Madden, P. A. in *Liquids, Freezing and Glass Transition*, Hansen, J. P., Ed.; Elsevier Science Publishers, 1991; course 7.
(19) Patkowski, A.; Steffen, W.; Nilgens, H.; Fischer, E. W.; Pecora, R. Depolarized Dynamic Light Scattering From Three Low Molecular Weight Glass Forming Liquids: A Test of the Scattering Mechanism. *J. Chem. Phys.* **1997**, *106*, 8401–8408.
(20) Cang, H.; Li, J.; Fayer, M. D. Orientational Dynamics of the Ionic Organic Liquid 1-ethyl-3-methylimidazolium Nitrate. *J. Chem. Phys.* **2003**, *119*, 13017–13023.
(21) Pratesi, G.; Bartolini, P.; Senatra, D.; Ricci, M.; Righini, R.; Barocchi, F.; Torre, R. Experimental Studies of the Ortho-toluidine Glass Transition. *Phys. Rev. E* **2003**, *67*, 021505.
(22) Turton, D. A.; Hunger, J.; Stoppa, A.; Hefter, G.; Thoman, A.; Walther, M.; Buchner, R.; Wynne, K. Dynamics of Imidazolium Ionic Liquids from a Combined Dielectric Relaxation and Optical Kerr Effect Study: Evidence for Mesoscopic Aggregation. *J. Am. Chem. Soc.* **2009**, *131*, 11140–11146.
(23) Xiao, D.; Hines, L. G.; Holtz, M. W.; Song, K.; Bartsch, R. A.; Quitevis, E. L. Effect of Cation Symmetry on the Low-frequency Spectra of Imidazolium ionic liquids: OKE and Raman Spectroscopic Measurements and DFT Calculations. *Chem. Phys. Lett.* **2010**, *497*, 37–42.
(24) Turton, D. A.; Sonnleitner, T.; Ortner, A.; Walther, M.; Hefter, G.; Seddon, K. R.; Stana, S.; Plechkova, N. V.; Buchner, R.; Wynne, K. Structure and Dynamics in Protic Ionic Liquids: A Combined Optical

Kerr-effect and Dielectric Relaxation Spectroscopy Study. *Faraday Discuss.* **2012**, *154*, 145–153.

(25) Jun, H.; Ouchi, Y.; Kim, D. Intermolecular Dynamics of Room Temperature Ionic Liquids Having Imidazolium Cations. *J. Mol. Liq.* **2013**, *179*, 54–59.

(26) Weingärtner, H.; Knocks, A.; Schrader, W.; Kaatze, U. Dielectric Spectroscopy of the Room Temperature Molten Salt Ethylammonium Nitrate. *J. Phys. Chem. A* **2001**, *105*, 8645–8650.

(27) Daguene, C.; Dyson, P. J.; Krossing, I.; Oleinikova, A.; Slattery, J.; Wakai, C.; Weingärtner, H. Dielectric Response of Imidazolium-Based Room-Temperature Ionic Liquids. *J. Phys. Chem. B* **2006**, *110*, 12682–12688.

(28) Rivera, A.; Brodin, A.; Pugachev, A.; Rössler, E. A. Orientational and Translational Dynamics in Room Temperature Ionic Liquids. *J. Chem. Phys.* **2007**, *126*, 114503.

(29) Wiedersich, J. A. H.; Surovtsev, N. V.; Novikov, V. N.; Rössler, E. Light Scattering Spectra of Fast Relaxation in Silica and CKN Glasses. *Phys. Rev. B* **2001**, *64*, 064207.

(30) Petzold, N.; Rössler, E. A. Light Scattering Study on the Glass Former o-Terphenyl. *J. Chem. Phys.* **2010**, *133*, 124512.

(31) Davidson, D. W.; Cole, R. H. Dielectric Relaxation in Glycerol, Propylene Glycol, and n-Propanol. *J. Chem. Phys.* **1951**, *19*, 1484–1490.

(32) Kohlrausch, R. Theorie des Elektrischen Rückstandes in der Leidner Flasche. *Ann. Phys. Chem.* **1854**, *91*, 56–82.

(33) Brodin, A.; Frank, M.; Wiebel, S.; Shen, G.; Wuttke, J.; Cummins, H. Z. Brillouin-Scattering Study of Propylene Carbonate: an Evaluation of Phenomenological and Mode Coupling Analyses. *Phys. Rev. E* **2002**, *65*, 051503.

(34) Brodin, A.; Rössler, E. A. Depolarized Light Scattering Study of Glycerol. *Eur. Phys. J. B* **2005**, *44*, 3–14.

(35) Adichtchev, S. V.; Benkhof, S.; Blochowicz, T.; Novikov, V. N.; Rössler, E.; Tschirwitz, C.; Wiedersich, J. A. H. Anomaly of the Non-ergodicity Parameter and Crossover to White Noise in the Fast Relaxation Spectrum of a Simple Glass Former. *Phys. Rev. Lett.* **2002**, *88*, 055703.

(36) Brodin, A.; Rössler, E. A. Depolarized Light Scattering versus Optical Kerr Effect Spectroscopy of Supercooled Liquids: Comparative Analysis. *J. Chem. Phys.* **2006**, *125*, 114502.

(37) Brodin, A.; Rössler, E. A. Depolarized Light Scattering versus Optical Kerr Effect Spectroscopy of Supercooled Liquids: Comparative Analysis, Part II. *J. Chem. Phys.* **2007**, *126*, 244508.

(38) Wiedersich, J.; Surovtsev, N.; Rössler, E. A. A Comprehensive Light Scattering Study of the Glass Former Toluene. *J. Chem. Phys.* **2000**, *113*, 1143–1153.

(39) Belieres, J.-P.; Angell, C. A. Protic Ionic Liquids: Preparation, Characterization, and Proton Free Energy Level Representation. *J. Phys. Chem. B* **2007**, *111*, 4926–4937.

(40) Duvvuri, K.; Richert, R. Dynamics of Glass-Forming Liquids. VI. Dielectric Relaxation Study of Neat Decahydro-Naphthalene. *J. Chem. Phys.* **2002**, *117*, 4414–4418.

(41) Tokuda, H.; Hayamizu, K.; Ishii, K.; Susan, M. A. B. H.; Watanabe, M. Physicochemical Properties and Structures of Room Temperature Ionic Liquids. 1. Variation of Anionic Species. *J. Phys. Chem. B* **2005**, *109*, 6103–6110.

(42) Blokhin, A. V.; Paulechka, Y. U.; Strechan, A. A.; Kabo, G. J. Physicochemical Properties, Structure, and Conformations of 1-Butyl-3-methylimidazolium Bis(trifluoro-methanesulfonyl)imide [$C_4\text{mim}$]-NTf₂ Ionic Liquid. *J. Phys. Chem. B* **2008**, *112*, 4357–4364.

(43) Li, G.; Du, W. M.; Sakai, A.; Cummins, H. Z. Light-scattering Investigation of and Relaxation Near the Liquid-glass Transition of the Molecular Glass Salol. *Phys. Rev. A* **1992**, *46*, 3343–3356.

(44) Wiedersich, J.; Surovtsev, N.; Rössler, E. A. Comprehensive Light Scattering Study of the Glass Former Toluene. *J. Chem. Phys.* **2000**, *113*, 1143–1153.

(45) Wiebel, S.; Wuttke, J. Structural Relaxation and Mode Coupling in a Non-glassforming Liquid: Depolarized Light Scattering in Benzene. *New J. Phys.* **2002**, *4*, 56.1–56.17.

(46) Götze, W. Recent Tests of The Mode-coupling Theory for Glassy Dynamics. *J. Phys.: Condens. Matter* **1999**, *11*, A1–A45.

(47) Lindsey, C. P.; Patterson, G. D. Detailed Comparison of the Williams–Watts and Cole-Davidson Functions. *J. Chem. Phys.* **1980**, *73*, 3348–3357.

(48) Cang, H.; Novikov, V. N.; Fayer, M. D. Experimental Observation of a Nearly Logarithmic Decay of the Orientational Correlation Function in Supercooled Liquids on the Picosecond-to-nanosecond Time Scales. *Phys. Rev. Lett.* **2003**, *90*, 197401.

(49) Lynden-Bell, R. M. in *Molecular Liquids*; Barnes, A. J., Orville-Thomas, W., Yarwood, J., Eds.; Reidel: Dordrecht, 1984.

(50) Hansen, J.-P.; McDonald, I. R. in *Theory of Simple Liquids*; Academic Press: London, 1976.

(51) Kudlik, A.; Benkhof, S.; Blochowicz, T.; Tschirwitz, C.; Rössler, E. The Dielectric Response of Simple Organic Glass Formers. *J. Mol. Struct.* **1999**, *479*, 201–218.

(52) Sokolov, A. P.; Rössler, E.; Kisluk, A.; Quitman, D. Dynamics of Strong and Fragile Glass Formers - Differences and Correlation with Low-temperature Properties. *Phys. Rev. Lett.* **1993**, *71*, 2062–2065.

(53) Pötzschnner, B.; Rössler, E. A. *Unpublished analysis*.

Publication 5

Depolarized light scattering spectra of molecular liquids: described in terms of mode coupling theory

B. Schmidtke, E. A. Rössler

The Journal of Chemical Physics **141**, 044511 (2014).

Copyright 2013 by The American Institute of Physics Publishing LLC

DOI: 10.1063/1.4890731

Depolarized light scattering spectra of molecular liquids: Described in terms of mode coupling theory

B. Schmidtke and E. A. Rössler

Citation: *The Journal of Chemical Physics* **141**, 044511 (2014); doi: 10.1063/1.4890731

View online: <http://dx.doi.org/10.1063/1.4890731>

View Table of Contents: <http://scitation.aip.org/content/aip/journal/jcp/141/4?ver=pdfcov>

Published by the [AIP Publishing](#)

Articles you may be interested in

[Study of the depolarized light scattering spectra of supercooled liquids by a simple mode-coupling model](#)

J. Chem. Phys. **107**, 3417 (1997); 10.1063/1.474484

[Experimental test of a recent theory of depolarized light scattering by molecular liquids](#)

J. Chem. Phys. **82**, 3934 (1985); 10.1063/1.448885

[Theory of depolarized light scattering](#)

J. Chem. Phys. **74**, 5929 (1981); 10.1063/1.441030

[Theory of depolarized Rayleigh–Brillouin spectra and rotation–translation coupling in molecular liquids and solids](#)

J. Chem. Phys. **70**, 3796 (1979); 10.1063/1.437930

[Theory of Depolarized Light Scattering from Molecular Liquids: Existence of the Central Diffuse Line and the Broad Background](#)

J. Chem. Phys. **56**, 2106 (1972); 10.1063/1.1677505



COMSOL
CONFERENCE
2014 BOSTON

The Multiphysics
Simulation
Event of the Year



LEARN MORE >>

COMSOL

Depolarized light scattering spectra of molecular liquids: Described in terms of mode coupling theory

B. Schmidtke and E. A. Rössler

Experimentalphysik II, Universität Bayreuth, D-95444 Bayreuth, Germany

(Received 23 May 2014; accepted 9 July 2014; published online 31 July 2014)

Depolarized light scattering spectra of eight molecular liquids as obtained from applying tandem-Fabry-Pérot interferometry and double monochromator are analyzed in the frame work of the mode coupling theory (MCT). The susceptibility spectra are fitted to the numerical solution of the schematic F_{12} model of MCT and the validity of the asymptotic laws is discussed. The model is able to quantitatively describe the spectra up to the boiling point, where the main (structural) relaxation and the contribution of the microscopic (vibrational) dynamics essentially merge, and down to the moderately super-cooled liquid where glassy dynamics establishes. The changes of the spectra with temperature are mapped to only two control parameters, which show a smooth variation with temperature. Strong correlation between experimental stretching parameters and extrapolated values from the model is found. The numerical solutions are extrapolated down to T_c , where the asymptotic scaling laws can be applied. Although the spectra apparently follow scaling relations, the application of the asymptotic laws usually overestimates T_c by up to 12 K. In all the cases, the experimental spectra are outside the applicability regime of the asymptotic laws. This is explained by more or less strong vibrational contributions. Within a phenomenological approach which extends the spectral analysis down to T_g and which allows for separating fast and slow dynamics, the strength of the fast dynamics $1 - f_{rel}$ is revealed. It shows the cusp-like anomaly predicted by MCT; yet, the corresponding critical temperature is significantly higher than that derived from the F_{12} model. In addition, we demonstrate that close to T_g , the susceptibility minimum is controlled by the interplay of the excess wing and the fast dynamics contribution. © 2014 AIP Publishing LLC. [<http://dx.doi.org/10.1063/1.4890731>]

I. INTRODUCTION

Recently, we have compiled depolarized light scattering (DLS) spectra of a large series of molecular as well as ionic liquids by applying double monochromator (DM), tandem-Fabry-Pérot interferometry (TFPI), and occasionally photon correlation spectroscopy (PCS).^{1,2} All these liquids can be easily super-cooled and temperatures up to well above the melting point, in some cases even reaching the boiling point have been covered. The spectra and likewise the corresponding reorientational correlation functions have been characterized by a stretching parameter β_{CD} for the long-time decay (α -process) and a strength of fast dynamics $1 - f$. Here f is the strength of the (α -process) or the non-ergodicity parameter. For a given system these spectral parameters are virtually temperature independent up to the boiling point. Thus, “glassy dynamics” thought to be characteristic of super-cooled liquids are actually observed well above T_m . Testing for correlations among these parameters, no correlation between $1 - f$ and β_{CD} has been revealed. Also, no correlation between β_{CD} and fragility m , describing the magnitude of the temperature dependence of the structural correlation time τ_α on a reduced temperature scale T/T_g , is found in contrast to correlations anticipated in previous works.^{3,4} Moreover, regarding molecular vs ionic liquids, no fundamental difference in the evolution of their DLS spectra is observed.

For the cases reaching the boiling point it has been demonstrated that at highest temperatures indeed an Arrhenius law emerges for the temperature dependence of the correlation time $\tau_\alpha(T)$ and a simple three-parameter description has been introduced based on the decomposition of the effective activation energy into a temperature independent high-temperature part and a contribution reflecting cooperative dynamics with an essentially exponential temperature dependence becoming relevant at low temperatures close to T_g .^{1,5}

In the past many studies have been devoted to analyze the evolution of the DLS spectra in the frame of the (idealized) mode coupling theory (MCT) of the glass transition that was originally developed by Götze and co-workers in the 1980s.⁶⁻⁹ The theory predicts a glass transition singularity at a temperature T_c that is now thought of as a crossover point from high temperature liquid-like dynamics to a low-temperature regime where different transport mechanisms dominate. Close to T_c , the theory provides asymptotic laws, which give a leading order description of the spectra around the susceptibility minimum separating α -relaxation from high-frequency contributions in terms of power-laws ($T > T_c$). These have been tested by various experimental techniques such as neutron and light scattering, optical Kerr effect (OKE), and dielectric spectroscopy, and thereby the crossover temperature $T_c > T_g$ is estimated.¹⁰⁻¹⁶ While in some cases a consistent description is possible, in other cases

inconsistencies across spectra obtained by different scattering methods occur, leading to some ambiguity in identifying T_c .

Less often the spectra have been analyzed by applying so-called schematic models of MCT, i.e., simplified models of the theory that allow to capture phenomena beyond the asymptotic description at the expense of introducing several fitting parameters. In addition, the models allow taking into account the microscopic dynamics, in particular spectral features like the boson peak which usually interfere in the frequency range considered. The most prominent example is the F_{12} model for the liquid-density fluctuations combined with a simple description of probe-density coupling through the so-called Sjögren model.^{17–24} In most cases, the spectral analysis is restricted to moderately low temperatures due to the fact that high temperature spectra were not available or not included. As we will demonstrate it turns out that the present DLS spectra can be quantitatively described up to the boiling point by the F_{12} model. At such high temperatures, the microscopic (vibrational) dynamics and structural relaxation have virtually merged and a single broadened relaxation peak characterizes the DLS spectra.^{1,2,25} Here, the asymptotic laws of MCT cannot be applied any longer. The capability of the F_{12} model to describe distinctly non-glassy dynamics at high temperatures was already demonstrated for the non-glass forming liquid benzene by Wiebel and Wuttke²¹ using DLS spectra and by Ricci *et al.*²² using OKE data. We extend a similar analysis to a series of molecular glass-forming liquids. Doing so, the numerical solutions of the model can be extrapolated to the vicinity of T_c , and the regime of validity of the asymptotic MCT scaling laws can be identified.¹⁹ We show that virtually all of the experimental data are collected at temperatures where the application of the asymptotic laws does not apply. At these temperatures, effects from the vibrational contributions to the spectra become important and distort the expected position of the susceptibility minimum. This may lead to an overestimation of T_c if solely the asymptotic laws are applied. Below T_c , the F_{12} model cannot be applied and we stick to a phenomenological approach allowing to determine $1 - f_{\text{rel}}$ as a function of temperature which leads to a crossover temperature still higher.

II. THEORETICAL BACKGROUND – THE F_{12} MODEL

MCT^{6–8} describes the evolution of the slow dynamics of dense liquids, i.e., the structural relaxation giving rise to the α -process, and the caging of particles at intermediate times that cause the dramatic slowing down of the final relaxation. Starting from an exact equation of motion for slow dynamical variables, which is derived using a projection-operator formalism, an integro-differential equation for the density correlation function $\Phi_q(t)$ can be written

$$0 = \Omega_q^{-2} \ddot{\Phi}_q(t) + \gamma_q \dot{\Phi}_q(t) + \Phi_q(t) + \int_0^t dt' m_q(t-t') \dot{\Phi}_q(t'). \quad (1)$$

Here, q is the wave vector of the density fluctuations, and the initial conditions $\Phi_q(0) = 1$ and $\dot{\Phi}_q(0) = 0$ hold. The memory

function $m_q(t)$,

$$m_q \{ \Phi(t) \} = \sum_{k+p=q} V_{qpk} \Phi_p(t) \Phi_k(t) \quad (2)$$

describes the slow relaxation as caused by slow fluctuating forces, and is in MCT approximated as a nonlinear form of the density correlation functions again. The coupling coefficients of the theory are fully determined through the equilibrium static structure of the system, such as the static structure factor $S(q)$ which varies only weakly with temperature. Depending on the coupling strength, the correlation function $\Phi_q(t)$ decays to zero at long times (liquid) or arrests at a finite value (glass). The bifurcation points in the coupling-coefficient parameter space, where this behavior changes from one case to the other, are identified as the idealized glass transitions of the theory. The full MCT equations have been solved for a number of model systems (such as the hard-sphere fluid).²⁶ For most molecular glass-forming liquids, the intra-particle complexity however renders this infeasible. In order to reduce mathematical complexity “schematic” models have been formulated which retain the generic behavior of the full equations, and replace the coupling coefficients of the full theory by a small set of *ad hoc* parameters. They also serve as convenient models to quantitatively fit experimental data. One of the simplest schematic models is the F_{12} model, for which one retains just a single wave-vector independent correlator, and the memory function reads^{6,8,17–24}

$$m(t) = v_1 \Phi(t) + v_2 \Phi(t)^2. \quad (3)$$

There are two (temperature dependent) coupling constants (or control parameters) v_1 and v_2 . For the analysis of DLS spectra, one extends this model by a second correlator $\Phi_s(t)$ that mimics the dynamical variables that are probed in a given experiment, which presumably capture the orientational degrees of freedom in the liquid coupling to the density fluctuations. The second correlator follows the same integro-differential equation as above (Eq. (1)) where $\Phi(t)$, Ω , γ , and $m(t)$ are replaced by $\Phi_s(t)$, Ω_s , γ_s , and $m_s(t)$. The second memory function is given by

$$m_s(t) = v_s \Phi(t) \Phi_s(t). \quad (4)$$

This kind of coupling of the equations guarantees that the dynamics of the probing variable $\Phi_s(t)$ is controlled by $\Phi(t)$ but not vice versa. In particular, the position of the transition at T_c is not changed by the introduction of the second correlator $\Phi_s(t)$.

The ideal glass transition takes place on a line in the v_1/v_2 parameter space which is parameterized by the exponent parameter λ that also fixes the asymptotic stretching of the α -relaxation via Eq. (8),¹⁹

$$\begin{aligned} v_1^c &= (2\lambda - 1) / \lambda^2 \\ v_2^c &= 1 / \lambda^2 \end{aligned} \quad (5)$$

As said the model has been successfully employed in several studies of glass-forming liquids.^{17–19} A detailed numeric study has confirmed the stability of such fits.²³

The equations were directly solved by a simple forward-stepping algorithm in the time domain exploiting the causality

TABLE I. Characteristic temperatures and temperature independent fit parameters of the description by the F_{12} model: glass transition temperature T_g , melting temperature T_m ,^{28,29} boiling temperature T_b ,^{28,29} critical temperature T_c obtained by the F_{12} model, T_c' extracted from applying asymptotic MCT laws, and T_c'' estimated from analyzing fast dynamics spectrum (see Fig. 9), high-frequency exponent of α -process b (stretching parameter; calculated via Eq. (8)); experimental stretching parameter β_{CD} , frequencies Ω and Ω_s and the damping parameters γ Ω^2 and γ_s Ω_s^2 .

	T_g (K)	T_m (K)	T_b (K)	T_c (K)	T_c' (K)	T_c'' (K)	b	β_{CD}	Ω (THz)	Ω_s (THz)	γ Ω^2 (THz)	γ_s Ω_s^2 (THz)
4-Tert-butyl pyridine (4TBP)	164	272	469	185	192	—	0.59	0.54	10	7.0	1.5	12
Benzophenone	207	322	578	245	248	—	0.70	0.71	6.5	3.8	2	11
Dimethyl phthalate (DMP)	191	233	565	238	248	267	0.72	0.73	8	4.6	1.2	22
2-Methyl tetrahydrofuran (MTHF)	92	137	352	102(?)	114	—	0.46	0.48	4.58	6.5	24	14
<i>o</i> -Terphenyl (OTP)	245	329	605	284	290 ¹⁴	316 ¹⁴	0.73	0.65	5	3.7	4	11
Ethyl benzene	115	179	409	133	145	166	0.56	0.55	6.8	4.0	0	1
Salol	218	314	445	250	261	—	0.70	0.78	3	1.5	0.1	0.5
Toluene	117	178	384	145	152	—	0.70	0.66	6.8	3.7	1.5	4

of Eq. (1), combined with a periodic doubling of step lengths to be able to cover the large dynamical windows typical for glassy dynamics. The procedure has been described and used previously.^{9,24} All in all, eight parameters have to be adjusted to match the model to the data at any given temperature. But five of them, which are the frequencies Ω_s and Ω , the damping γ_s and γ , and as will be shown, a linear combination of v_1 and v_2 could be kept constant for all temperatures; leaving these parameters free leads only to a weak change with temperature. So for every temperature an amplitude factor A , a linear combination of v_1 and v_2 , and the coupling v_s had to be varied in a smooth way.

III. EXPERIMENTAL DETAILS

The samples, listed in Table I, were commercially available (Sigma-Aldrich) and were investigated without further purification.^{1,2} A sample was vacuum-distilled right into glass tubes with an inner diameter of 8 mm. For measurements with TFPI and DM, the sample was either mounted in a self-built furnace or a CryoVac continuous-flow cryostat. As light source we used a vertically polarized Coherent Verdi-V2 laser at a wavelength of 532 nm and 200 mW optical power. Measurements with TFPI (JRS Scientific, triple-pass tandem Etalon) and DM (Jobin Yvon, U1000) were performed simultaneously and operated at horizontal polarization in almost backscattering geometry, whereas the DM was applied at orthogonal geometry. For details, the reader is referred to Ref. 27. The experimentally measured spectral density $S(\nu)$ was converted to the susceptibility representation via $\chi''(\nu) = (1 + n(\nu))^{-1}S(\nu)$, where $n(\nu)$ is the Bose factor. The spectra of each liquid were normalized by normalizing the corresponding correlation function after Fourier transforming the measured spectral density.

IV. RESULTS

A. Fits by the F_{12} model

Figure 1(a) shows the DLS susceptibility spectra of toluene ($T_g = 117$ K, $T_m = 178$ K, $T_b = 384$ K³⁰) as obtained by combing spectra from DM and TFPI measurements in the temperature range 148–440 K. The highest tempera-

ture is above the (ambient pressure) boiling point. At low temperatures and low frequencies the primary or α -relaxation is well recognized as a separate, asymmetrically broadened peak in addition to the boson peak around about 500 GHz and the microscopic peak around 1–2 THz; the latter reflect vibrational contributions. In between a minimum is observed. While heating, the α -process shifts to higher frequencies and approaches the microscopic excitations. At highest temperatures both contributions have virtually merged to become a broadened single peak. Analogous spectra have been collected for ethyl benzene ($T_g = 115$ K, $T_m = 179$ K, $T_b = 409$ K,³⁰ Figure 1(b); and for 2-methyl tetrahydrofuran (MTHF $T_g = 92$ K, $T_m = 137$ K, $T_b = 352$ K³⁰), Figure 1(c). In comparison with toluene and ethyl benzene the scattering power of the molecule MTHF is rather weak due to its low electronic polarizability and consequently the signal-to-noise ratio is relatively low. Figure 1(d) displays the spectra of dimethyl phthalate (DMP $T_g = 191$ K, $T_m = 233$ K, $T_b = 565$ K³¹). While the first three liquids are low- T_g systems this is not the case for DMP (cf. Table I). Its glass transition temperature is significantly higher, therefore α -relaxation and microscopic dynamics have not yet merged at the highest temperatures measured. We note that the spectra have been presented before.^{1,2,25}

The DLS spectra have been fitted by the F_{12} model described in Sec. II and the results are given as solid black lines in Figure 1. In most cases, a quite satisfying description is provided up to highest temperatures, in the case of toluene, ethyl benzene, and MTHF even up to the boiling for which contributions of α -process and fast dynamics have merged. Some deviations occur at low temperatures for which the fits not fully reproduce the susceptibility minimum. They become the larger the closer T_g is approached and we refrain to fit the spectra at the lowest temperatures. This is expected as the F_{12} model does not contain contributions from thermally activated hopping processes, which are expected to become important near and below T_c . Also at highest frequencies the fits are not always able to interpolate the spectral end of the microscopic peak. Yet, the overall quality of the fits is quite promising. In particular, the F_{12} model allows including the microscopic dynamics as well as the boson peak.

As already discussed in Sec. II, four of the eight parameters of the F_{12} model, which are the frequencies Ω_s and Ω , the damping parameters γ_s and γ , have been kept constant

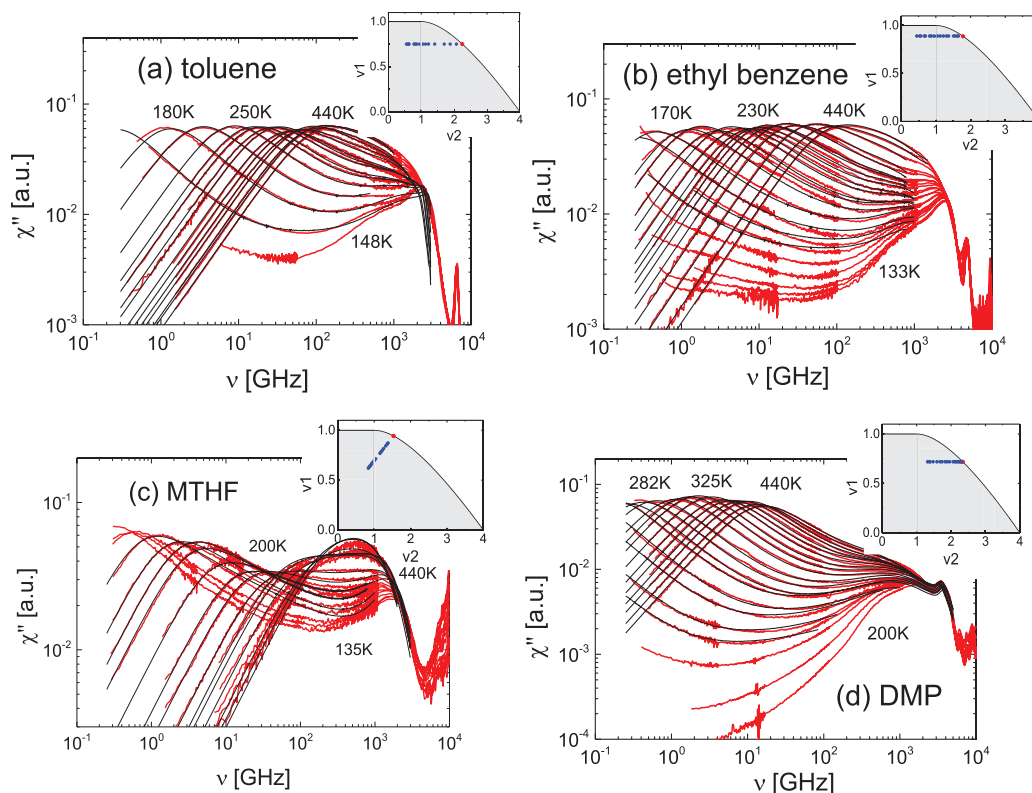


FIG. 1. DLS susceptibility spectra for (a) toluene, (b) ethyl benzene, (c) 2-methyl tetrahydrofuran (MTHF), and (d) dimethyl phthalate (DMP) fitted to the F_{12} model of MCT (black line). The v_1/v_2 parameter space is shown in the insets.

for a given liquid and their values are listed in Table I. These parameters reflect the vibrational frequencies and damping factors which are not expected to vary significantly with temperature. Then the temperature dependence of the spectra is represented by the variation of the parameters amplitude A , control parameters v_1 , v_2 , and the coupling v_s . As normalized DLS spectra are analyzed the amplitude A is essentially constant. Regarding the parameters v_1 and v_2 , their behavior is shown in parameter space representation in the insets of Figure 1 and in Figure 2, and in most cases v_1 could be kept constant for all temperatures. In all the cases a linear relationship among them is found. The data points come close to the line characterizing the transition from the liquid (shaded area) to the glass state. The actual intersection fixes the critical temperature T_c with a particular exponent parameter λ via $v_2^c = \lambda^{-2}$ and $v_1^c = (2\lambda - 1)\lambda^{-2}$.¹⁷ The parameter λ also fixes the exponents a and b of the asymptotic laws via Eq. (8) (see Table I). In the case of DMP, for example, the intersection with the glass line yields $\lambda = 0.65$ which corresponds to a stretching parameter $b = 0.72$. Concerning the temperature dependence of the parameters a smooth evolution is observed in Fig. 3. The data allow a linear extrapolation until the critical value v_2^c is reached (dashed line in Fig. 3(a)). Thereby the critical temperature T_c is extracted. In the case of MTHF, the linear extrapolation possibly yields uncertain results (T_c too close to T_g) as not enough low-temperature spectra close to T_c could be fitted. Also the coupling parameters v_s show a smooth evolution with temperature, as is displayed in Fig. 3(b). We note that the coupling parameters v_s show a trend to higher values for systems with higher β_{CD} parameters.

Fits by the F_{12} model have been done for other liquids (cf. Table I). In Figure 2, all the data for v_1 and v_2 are shown in the parameter space. They all exhibit a linear behavior. The red open circles mark the extrapolated critical parameters v_1^c and v_2^c which, as said, yield the exponents a and b as well as T_c . In Figure 4, the parameter b is compared to the experimentally determined width parameter β_{CD} as obtained by interpolating the α -relaxation by a Cole-Davidson (CD) susceptibility; these results have been reported previously¹ and are once again listed in Table I. The diagonal line represents perfect correlation; all the systems are near this line. Within the errors, the b values essentially match the experimental

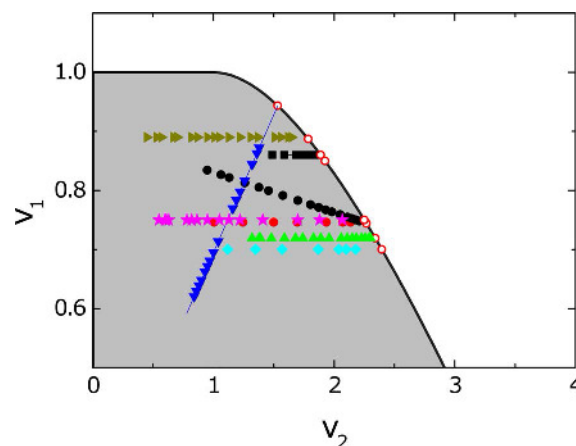


FIG. 2. Parameter space v_1/v_2 for all liquids investigated. Open red circles show extrapolated critical parameters.

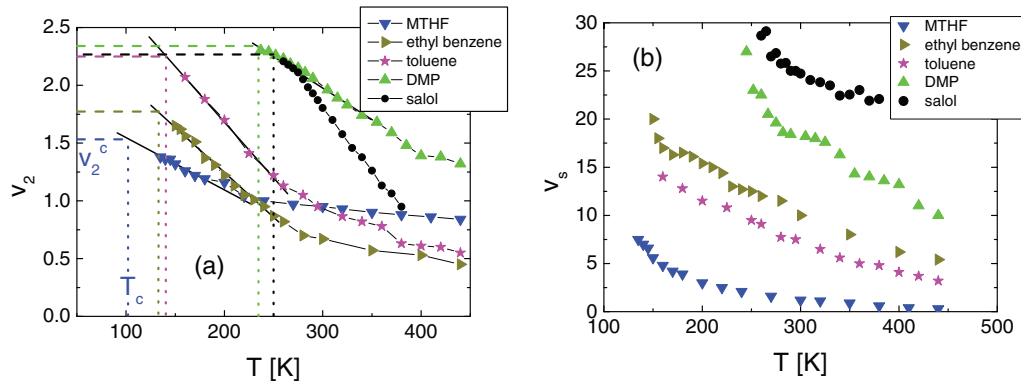


FIG. 3. (a) Temperature dependence of the control parameter v_2 approaching its critical value v_2^c (dashed lines) at T_c ; Solid line shows a linear extrapolation towards T_c (dotted lines). (b) Variation of v_s with temperature (cf. Eq. (4)).

ones. We note that this is not necessarily a consequence of MCT.³² The error of b does not only depend on the precision of the extrapolation in the v_1/v_2 parameter space, but also on the uniqueness of the fits by the F_{12} model. Slight changes in the parameters v_1 and v_2 may lead to similarly good MCT interpolation of the data by the F_{12} model. We estimate the error in the MCT b value to be about the same as the experimental β_{CD} values have.

B. Testing the validity of the asymptotic laws

By applying the asymptotic laws of MCT the analysis of the DLS spectra concerns frequency ν_{\min} and amplitude χ''_{\min} of the susceptibility minimum between α -peak and the fast dynamics contribution. The minimum is interpolated by a sum of two power-laws with the exponents a and b ; explicitly

$$\chi''(\nu) = \chi''_{\min} \left(b \left(\nu/\nu_{\min} \right)^a + a \left(\nu/\nu_{\min} \right)^{-b} \right) / (a + b). \quad (6)$$

Thus, by scaling the DLS spectra with ν_{\min} and χ''_{\min} , a master curve results (“minimum scaling”) with an envelope described by Eq. (6). The temperature dependence of ν_{\min} , χ''_{\min}

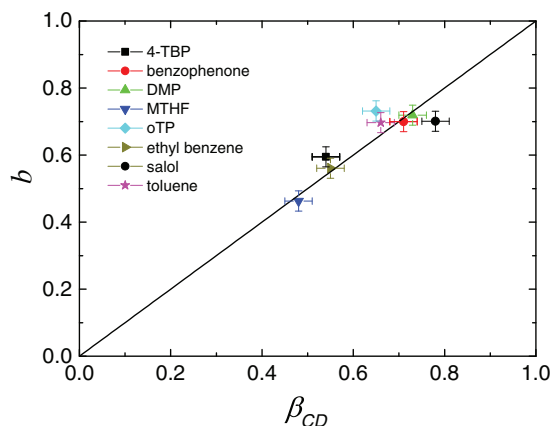


FIG. 4. Comparison of the experimental stretching parameters β_{CD} with the b values of the F_{12} model.

and of the time scale τ_α are expected to follow:⁶

$$\begin{aligned} \chi''_{\min} &\propto (T - T_c)^{1/2} \\ \nu_{\min} &\propto (T - T_c)^{1/2a} \quad T > T_c \\ \tau_\alpha &\propto (T - T_c)^{-\gamma_{MCT}} \end{aligned} \quad (7)$$

The exponents in Eq. (6) are not independent; they are related to the exponent parameter λ via

$$\lambda = \frac{\Gamma^2(1-a)}{\Gamma(1-2a)} = \frac{\Gamma^2(1+b)}{\Gamma(1+2b)}, \quad (8)$$

while the exponent γ_{MCT} in Eq. (7) is related to the exponents a and b via $\gamma_{MCT} = 1/(2a) + 1/(2b)$.

Figure 5(a) shows the susceptibility minimum for DMP with the interpolation along Eq. (6) with the exponents $a = 0.33$ and $b = 0.66$ fixed by $\lambda = 0.69$. The minimum is well reproduced, yet, at low temperatures and high frequencies deviations occur which are the larger the lower the temperature is. Figure 5(b) shows the same plot for the spectra of salol. Here, the deviations on the high-frequency side of the susceptibility minimum are even smaller.

The rectified temperature dependence of ν_{\min} and χ''_{\min} is shown in Figure 6 together with that of the time constant $\tau_\alpha(T)$. Extracting $\tau_\alpha(T)$ has been carried out by interpolating the α -relaxation peak with a CD function as has been demonstrated in our previous publication.¹ For both liquids, the values follow a linear temperature dependence, and a critical temperature $T_c = 248 \pm 7$ K is extracted for DMP, and $T_c = 261 \pm 7$ K for salol, being very close to a previous MCT analysis, where $T_c = 262$ K was found.¹⁰ The T_c values are systematically higher than the corresponding value (238 K and 250 K, respectively) obtained by applying the F_{12} model (cf. Table I). The results for the other liquids are listed in Table I. Indeed, in all the cases the asymptotic laws overestimate T_c . Below we will give a possible explanation. In any case, occurrence of linear dependencies in the rectifying plot does not necessarily give a hint whether the correct temperature interval is considered. Here it suffices to note that the high-frequency side of the minimum deviates the stronger from the MCT asymptotic laws the lower the temperature is. Moreover, the deviations are the stronger the more pronounced the boson peak (and/or the microscopic peak) is. Actually, in all the experimental spectra the fast dynamics

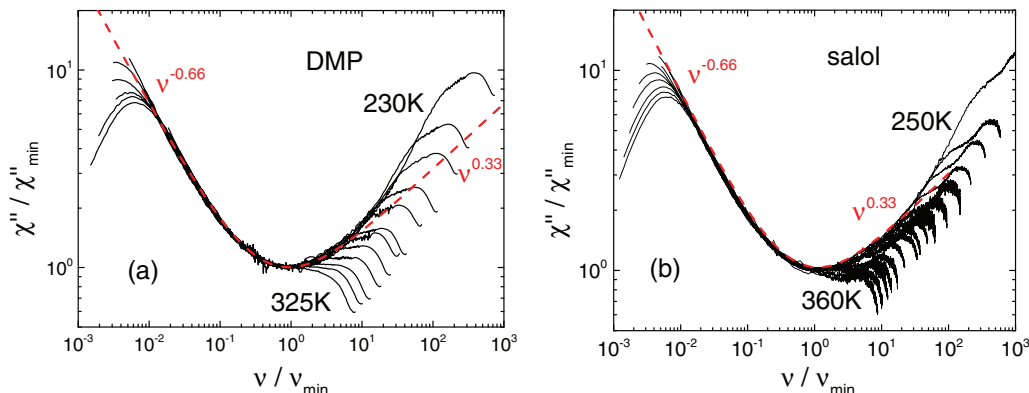


FIG. 5. Master curve (“minimum scaling”) for the susceptibility minimum for (a) dimethyl phthalate (DMP; 230–325 K) and (b) salol (250–360 K) with interpolation according to the asymptotic laws of MCT (dashed red line).

exponent a cannot be extracted reliably due to the interference of the vibrational contributions. In contrast the high-frequency flank of the α -process is always well identified.

Regarding the F_{12} model, the smooth temperature dependence of the control parameters (cf. Figure 3) allows us to extrapolate the calculations to lower temperatures. This will enable us to test whether the experimental spectra lie in the regime for which the asymptotic laws actually apply. For the parameters ν_2 and ν_s , we used a linear extrapolation as Figure 3 suggests. The temperatures below the lowest fitted experimental temperature are chosen as a geometric series approaching T_c . The results of this calculation are shown for DMP in Figure 7(a). Full lines represent the interpolation of the experimental spectra, while dashed lines show the extrapolated spectra. The red dots mark the position of the minima, i.e., ν_{\min} and χ''_{\min} . From the asymptotic laws (Eq. (7)) a relation $\chi''_{\min} \propto \nu_{\min}^a$ follows, which in the case of DMP leads to a power-law with exponent $a = 0.35$. This power-law relation is only observed at temperatures where the susceptibility minimum is separated far enough from the vibrational contributions. Inspecting Figure 7(a), this is only the case for the extrapolated spectra, and only here, the exponent a determines the high-frequency flank of the susceptibility minimum. For the measured spectra, however, the minimum position follows an apparent behavior $\chi''_{\min} \propto \nu_{\min}^{0.51}$ with an effective exponent

significantly higher than $a = 0.35$. Similar values of the effective exponent are found for most liquids; see Figure 10(a) and discussion below. The deviation of the relation forecast between ν_{\min} and χ''_{\min} may be a strong indicator that the asymptotic laws do not apply although the rectification plot (Fig. 6) may yield straight lines. On the other hand, as mentioned when discussing Figure 1 the calculated spectra do not interpolate the experimental spectra at low temperatures as T_c is surpassed. Thus, there is no experimental chance to confirm the asymptotic laws. Down to T_c all measured spectra are spoiled by a more or less strong boson peak contribution which makes application of the asymptotic laws obsolete.

We have evaluated the calculated spectra in Figure 7(a) as we have done with the experimental spectra, and Figure 7(b) shows the corresponding minimum scaling. The spectra at low temperatures very close to T_c yield a common envelope which can be described by the sum of two power-laws with exponents forecast by MCT (Eqs. (6) and (8)). Thus, the asymptotic laws apply only very close to T_c , i.e., for temperature for which the experimental spectra cannot be described by the F_{12} model any longer. Figure 8 shows the rectification plot of ν_{\min} , χ''_{\min} , and ν_{\max} versus temperature with the data taken from the calculated spectra close to T_c . A critical temperature $T_c = 248 \pm 7$ K (as before in Figure 6) is found for DMP. Inspecting Figure 8(a) in detail one

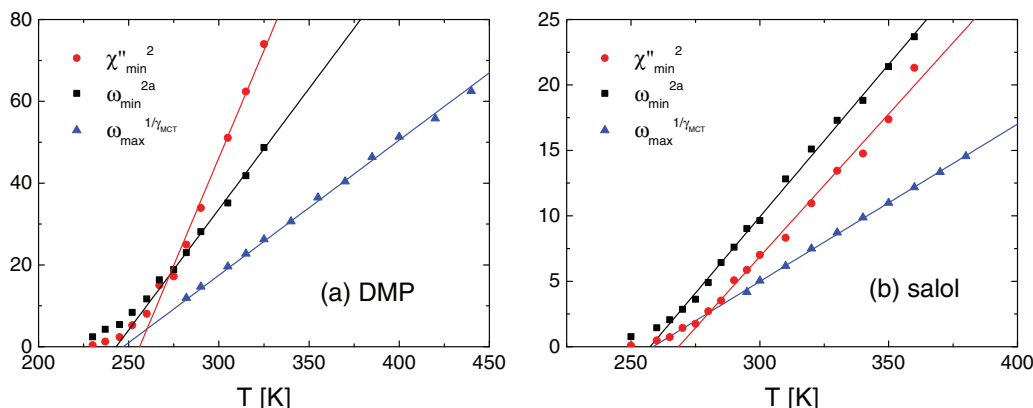


FIG. 6. ν_{\min} , χ''_{\min} , and ν_{\max} plotted versus temperature in a rectifying plot for (a) DMP and (b) salol. Lines extrapolate to an average $T_c \approx 248 \pm 7$ K and $T_c \approx 261 \pm 7$ K, respectively.

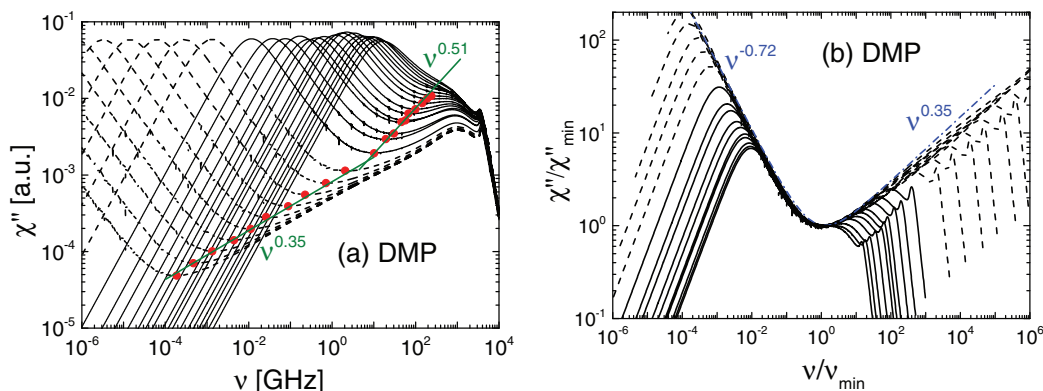


FIG. 7. (a) Extrapolation of the F_{12} model fits to temperatures very close to T_c for DMP. Dashed lines represent spectra for extrapolated, full ones for experimental temperatures. Red dots mark the position of each minimum. The minima positions follow power laws indicated as green lines. (b) Master curve for the susceptibility minimum with interpolation by the asymptotic power-law (dashed-dotted blue line), corresponding exponents a and b are determined by the extrapolated λ parameter in Figure 2.

recognizes that below, say 260 K, the linear extrapolation does not hit the data. In Figure 8(b), the data in Figure 8(a) are shown very close to T_c and a consistent $T_c = 238$ K is found. Thus, the extrapolation from the experimental spectra at high temperature overestimates T_c as given by the F_{12} model up to 12 K. We note, as the maximum position is least influenced by vibrational contributions, the extrapolation of the maximum position ν_{\max} should give the most robust value for T_c .

C. Phenomenological analyses

One may also analyze the DLS spectra compiled without taking explicitly recourse to quantitative MCT analyses but still looking for MCT signatures. Regarding the validity of frequency-temperature superposition at high temperatures, this has been done in a previous publication.¹ Here, this is carried out for extracting the relaxation strength of the fast dynamics $1 - f$ and for discussing the susceptibility minimum position with respect to τ_α down to low temperatures which allows to identify the emergence of another spectral feature not included in the F_{12} model, namely, the excess wing contribution.

1. Determining the strength of the fast dynamics $1 - f$

An alternative method of estimating T_c is the evaluation of the temperature dependence of the relaxation strength f ,^{7,12,33} or in the case of analyzing DLS spectra, of the fast dynamics $1 - f$, for which MCT forecasts a cusp-like anomaly at T_c .⁶⁻⁸ Here, the precondition is that spectra above as well as below T_c have been measured and that fast and slow dynamics can be disentangled. Yet, so far this is not so easily possible in a model independent way due to the narrow spectral range covered by the DM/TFPI setup; moreover, theoretical predictions concerning the evolution of the spectra below T_c are missing. At low temperatures, as mentioned, all spectra show deviations from the minimum scaling in the sense that the susceptibility minimum becomes broader, best recognized in the case of ethyl benzene (cf. Fig. 1(b)). The broadening has been attributed to the emergence of the excess wing usually observed in the dielectric spectra as an additional power-law regime with a rather small exponent $\gamma_{\text{ex}} \cong 0.2 < \beta_{\text{CD}}$.^{25,34-36} The OKE experiments revealed a so-called intermediate power-law³⁷ which has been interpreted as the excess wing in the time domain.^{25,34,35,38} Recently, the excess wing has also been identified by photon correlation

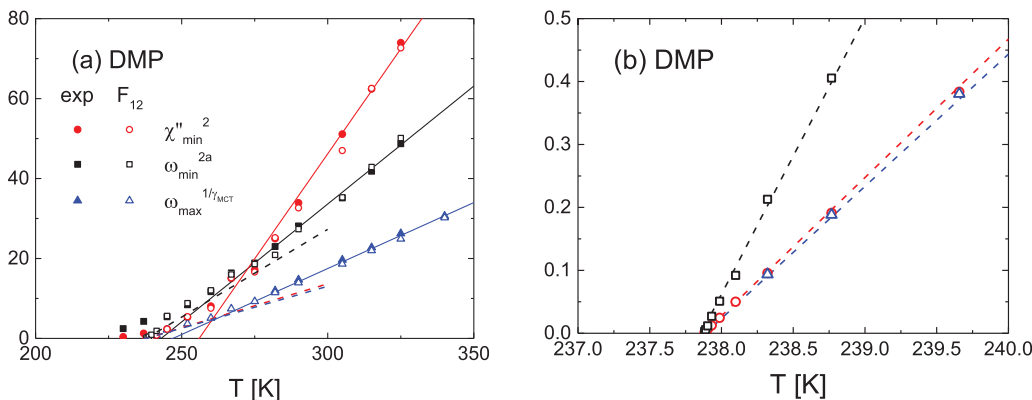


FIG. 8. Rectification plot for $\nu_{\min}(T)$, $\chi''_{\min}(T)$, and $\nu_{\max}(T)$, corresponding to Fig. 7(b), as a function of temperature. Open symbols represent data obtained from spectra calculated by the F_{12} model, while full symbols represent data from experimental spectra. (a) and (b) show different temperature scales. The lines show linear extrapolations estimating T_c as Eq. (7) predicts: Dashed lines take only temperatures close to T_c into account, while solid lines extrapolate high temperature data.

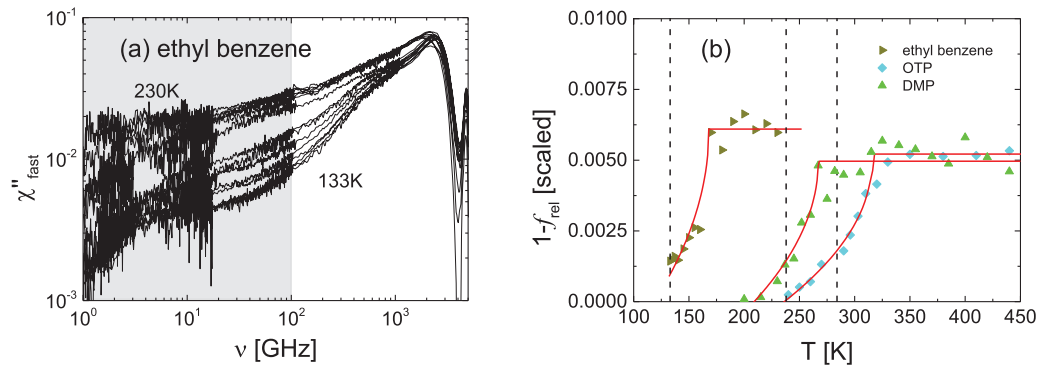


FIG. 9. (a) Fast dynamics spectrum of ethyl benzene after subtraction of the α -process contribution. (b) Square root singularity observed for the temperature dependence of the amplitude of the fast dynamics $1 - f_{rel}$ in the case of ethyl benzene and DMP as well as o-terphenyl (OTP).¹⁴ Red lines are guide-for-the-eyes. Straight dashed lines represent the T_c values obtained by the F_{12} model.

spectroscopy.^{2,25} As an example, we analyze the spectra of ethyl benzene for which the asymmetric broadening of the susceptibility minimum is best documented (cf. Fig. 1).

The relaxation strength of the fast dynamics $1 - f_{rel}$ is obtained by subtracting the slow dynamics (α -process and excess wing) from the overall susceptibility spectrum and then integrating up to a cutoff frequency ν_{cut} ,

$$1 - f_{rel} = \int_{-\infty}^{\ln \nu_{cut}} \chi''_{fast}(\nu) d \ln \nu. \quad (9)$$

The cut-off is introduced in order to become more sensitive solely to the relaxational contribution to $1 - f$. The major part of $1 - f$ is given by the vibrational spectrum which actually does not change much with temperature. For the calculation, the susceptibility minimum of the spectra of ethyl benzene is fitted to a sum of three power-laws with exponents fixed: $\beta_{CD} = 0.55$, $\gamma_{ex} = 0.20$ for the excess wing, and $a = 0.30$ for the fast dynamics power-law; so only the relative amplitudes are varied. Then, the contribution of the slow dynamics is subtracted and the resulting fast dynamics spectrum is shown in Figure 9(a) and the temperature dependence of $1 - f_{rel}$ in Figure 9(b). The integral was taken up to an upper cutoff frequency $\nu_{cut} = 100$ GHz (shaded area in Figure 9(a)). As expected by MCT, $1 - f_{rel}$ shows a crossover to a plateau at about 166 K. However, the crossover temper-

ature estimated this way is significantly higher than the one from applying the F_{12} model ($T_c = 133$ K). Re-inspecting the spectra of ethyl benzene in Fig. 1(b), indeed, the fit quality by the F_{12} model becomes less good, say, below 170 K, and the contribution of the fast dynamics is overestimated. The same trend is revealed when analyzing the present DMP data (cf. Fig. 9(b)). A systematically higher T_c has also been reported for glycerol¹³ and o-terphenyl¹⁴ (data of the latter system is included in Figure 8(b) and see Table I). We note that the results in Figure 9(b) are essentially independent of the strategy applied to disentangle fast and slow dynamics.

2. Analysis of the position of the susceptibility minimum

As already briefly discussed in Sec. B the minimum position, i.e., the relation between χ''_{min} and ν_{min} as predicted by MCT, is not revealed for the experimental spectra (cf. Figure 7(a)). We interpret this as a consequence of the influence of vibrational contributions, in particular, the boson peak leading to an effective exponent a_{eff} significantly larger than a . In Figure 10(a), we have collected the spectral data for a selection of liquids investigated by DLS.^{2,14} In most cases, a_{eff} is significantly higher than a being always close to $a = 0.3$. In particular, for the non-fragile glass former

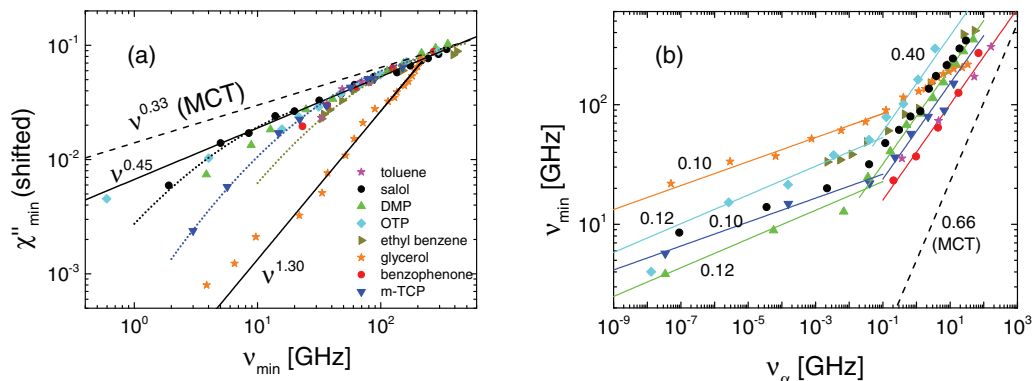


FIG. 10. (a) Amplitude χ''_{min} vs frequency ν_{min} of the susceptibility minimum for several liquids. Solid lines indicate apparent power-laws, dashed line corresponding prediction by MCT, dotted curved lines are guides-for-the-eye (b) ν_{min} plotted vs characteristic frequency of the α -process ν_{α} , solids lines reflect high- and low-temperature power-laws with slopes s indicated; dashed line: MCT prediction.

glycerol with a comparatively strong boson peak the deviation from MCT predictions is largest.³⁷ Yet, the majority of liquids show a similar behavior which can be interpolated by a power-law with a mean exponent $a_{\text{eff}} = 0.45$. At low frequencies/temperatures a trend to a larger exponent is recognized.

In Figure 10(b), ν_{min} is plotted vs $\nu_{\alpha} = 1/2\pi\tau_{\alpha}$, the characteristic frequency of the α -relaxation, which better allows to understand the evolution of the susceptibility when approaching T_g . Again, the data do not follow the power-law behavior expected by MCT. At high temperatures an apparent power-law is found with an exponent which is smaller than that predicted by MCT ($\nu_{\text{min}} \propto \nu_{\alpha}^s$ with $s = b/(a+b) \approx 0.66$). Yet, at low temperatures a crossover to a much smaller exponent is revealed. This means the susceptibility minimum close to T_g shifts more weakly towards lower frequencies. Again, we attribute this to the occurrence of the excess wing which broadens the minimum. In other words, the presentation of the data in Figure 10(b) gives a clear hint at what time constant (and thus temperature), the excess wing enters the DLS frequency window and controls the position of the susceptibility minimum. In all cases, the excess wing appears around $\tau_{\alpha} \cong 10^{-9}$ s which is consistent with values previously reported.^{34,35} Transforming DLS spectra into the time domain we have recently identified the excess wing as an intermediate power-law already at rather elevated temperatures, indicating that it is a spectral feature which may appear already above T_c .^{2,37} We note that the failure of describing consistently the position of the susceptibility minimum was recognized very early³⁹ and discussed recently again in the case of dielectric spectra.^{40,41} For glycerol, the latter authors reported $s = 0.28$, while the DLS spectra reveal $s \cong 0.10$. As noted the F_{12} model does not include the excess wing phenomenon, although some special MCT scenarios may produce spectral features like an excess wing.⁴²

V. DISCUSSION AND CONCLUSION

DLS spectra of several molecular liquids have been analyzed in the frame work of MCT. The susceptibility spectra are fitted to the numerical solution of the schematic F_{12} model and the validity of the MCT asymptotic laws has been tested. The model offers an analysis beyond applying the asymptotic laws including also vibrational excitations, such as the boson peak and the microscopic peak at highest frequencies. It is able to fully describe the spectra up to the boiling point, where main relaxation and vibrational contributions have essentially merged, and down to the super-cooled liquid which displays glassy dynamics. The latter actually are found well above the melting point. As mentioned, it has been shown that the F_{12} model is able to describe high-temperature dynamics of the liquid benzene yet investigating temperatures below the melting point is not possible for the non-glass-forming liquid benzene.^{21,22} Also in the case of water, the F_{12} model has been recently applied successfully.⁴³ The changes of the spectra with temperature are mapped to two relevant control parameters which show a smooth variation with temperature which allows to determine the critical temperature T_c .

Applying instead the asymptotic laws of MCT, the rectification plot testing the forecast power-law behavior of the

parameters of the susceptibility minimum appears to work satisfactorily as well as does the construction of a minimum master curve, yet, usually T_c is overestimated up to 12 K with respect to T_c derived from the F_{12} model. All the experimentally obtained spectra are beyond the applicable regime of the asymptotic laws. This failure is explained by the more or less strong vibrational contributions, in particular the boson peak, which spoils the high-frequency flank of the susceptibility minimum, and not necessarily by a too large distance from T_c where corrections to the leading order asymptotic laws may become relevant. A consistent MCT analysis is facilitated by a high stretching parameter β_{CD} and weak boson peak which yields pronounced susceptibility minima up to high temperatures and which then can be analyzed accordingly. The power-law relation between ν_{min} and χ''_{min} , always showing deviations from MCT forecast, rather than their temperature dependence, may be taken as an indicator whether the asymptotic laws do apply or not. We confirm conclusions drawn quite a while ago.³⁷

The schematic model has been applied before in several publications for various liquids, yet except for benzene²¹ only for low temperatures with well established glassy dynamics.^{9,17–20,23,24} In contrast to our findings, Krakoviack *et al.*¹⁸ reported control parameters (ν_1 and ν_2) for salol and the ionic liquid CKN which followed the transition line without crossing it, while Franosch *et al.*¹⁹ as well as Singh *et al.*²⁰ found smooth temperature dependence of the control parameters in the case of glycerol and o-terphenyl, respectively. Götze and Voigtmann⁹ concluded that the non-universal corrections of the asymptotic laws have important impact when analyzing experimental spectra. Independent of the specific results, the papers all agree in emphasizing that the asymptotic laws fail in most cases. All in all, we can state that most results from earlier MCT analyses, regarding the applicability and the quantitative aspects of the theory have been confirmed. For the first time, a variety of systems is considered in this work, which allows drawing qualitative statements on the typical deviations and limitations of the asymptotic laws and the F_{12} model as well.

The schematic models, of course, fail to describe spectra at temperatures close and below T_c , i.e., approaching T_g , as they do not include further relaxation processes like those from hopping dynamics. In particular, in the case of ethyl benzene the susceptibility minimum broadens at low temperatures what is explained by the emergence of the excess wing, the latter assumed to be the frequency domain equivalent of the intermediate power-law identified in the time domain OKE experiments.³⁷ The excess wing is a well documented phenomenon in the dielectric spectra of glass-forming liquids, however, difficult to quantitatively assess in the DLS spectra with their limited frequency window but clear evidence has been reported for several liquids.^{34,35} Recently, the excess wing has also been identified in PCS decays.¹⁴ Separating fast and slow dynamics by applying a phenomenological model reveals the strengths of the fast dynamics $1 - f_{\text{rel}}$, which shows the cusp-like anomaly predicted by MCT shown here for ethyl benzene, DMP and OTP and previously for other liquids, including also analyses of dielectric spectra.^{13,14,44} Yet, the corresponding critical temperature is significantly

higher than that derived from the F_{12} model. Plotting v_{\min} vs v_a reveals two power-laws; the crossover of which signals the appearance of the excess wing and thus indicates the breakdown of the high-temperature scenario for the evolution of the DLS spectra. In other words, at low temperatures the susceptibility minimum is controlled by the interplay of excess wing and fast dynamics contribution.

Given the quite satisfying interpolations of the susceptibility spectra up to the boiling point with only a few temperature dependent control parameters, MCT can be regarded as an approach that describes simple liquid dynamics from highest temperatures down to temperatures close to the moderately super-cooled liquid. In comparison with phenomenological analyses comprising several relaxation modes and damped harmonic oscillator functions, the results are more convincing. For temperatures close to T_g , the approach fails due to the emergence of further relaxation processes. In particular, the excess wing contribution shows up and its role is not understood so far. Moreover, the discrepancy between T_c from the F_{12} model and from the phenomenological approach revealing clearly the cusp-like behavior of $1 - f_{\text{rel}}$ deserves an explanation. Spectra covering the whole frequency range of glassy dynamics, which possibly can be supplied by dielectric spectroscopy, would be helpful in this context.

ACKNOWLEDGMENTS

The authors thank T. Voigtmann for very helpful discussions and providing the C++ program for applying the F_{12} model. Financial support of Deutsche Forschungsgemeinschaft (DFG) through Project Nos. RO 907/11 and RO 907/15 is appreciated.

- ¹B. Schmidtke, N. Petzold, R. Kahlau, and E. A. Rössler, *J. Chem. Phys.* **139**, 84504 (2013).
- ²B. Schmidtke, N. Petzold, B. Pötzschner, H. Weingärtner, and E. A. Rössler, *J. Phys. Chem. B* **118**, 7108 (2014).
- ³A. P. Sokolov, E. A. Rössler, A. Kisliuk, and D. Quitman, *Phys. Rev. Lett.* **71**, 2062 (1993).
- ⁴R. Böhmer, K. L. Ngai, C. A. Angell, and D. J. Plazek, *J. Chem. Phys.* **99**, 4201 (1993).
- ⁵B. Schmidtke, N. Petzold, R. Kahlau, M. Hofmann, and E. A. Rössler, *Phys. Rev. E* **86**, 041507 (2012).
- ⁶W. Götze and L. Sjögren, *Rep. Prog. Phys.* **55**, 241 (1992).
- ⁷W. Götze, *Phys. Cond. Matt.* **11**, A1 (1999).
- ⁸W. Götze, *Complex Dynamics of Glass Forming Liquids. A Mode-Coupling Theory* (Oxford University Press, Oxford, 2009).
- ⁹W. Götze and T. Voigtmann, *Phys. Rev. E* **61**, 4133 (2000).
- ¹⁰H. Z. Cummins, G. Li, Y. H. Hwang, G. Q. Shen, W. M. Du, J. Hernandez, and N. J. Tao, *Z. Phys. B* **103**, 501 (1997).
- ¹¹P. Lunkenheimer, U. Schneider, R. Brand, and A. Loidl, *Contemp. Phys.* **41**(1), 15–36 (2000).
- ¹²A. Tölle, *Rep. Prog. Phys.* **64**, 1473 (2001).
- ¹³S. V. Adichtchev, S. Benkhof, T. Blochowicz, V. N. Novikov, E. A. Rössler, C. Tschirwitz, and J. A. H. Wiedersich, *Phys. Rev. Lett.* **88**, 055703 (2002).
- ¹⁴N. Petzold and E. A. Rössler, *J. Chem. Phys.* **133**, 124512 (2010).
- ¹⁵R. Torre, P. Bartolini, M. Ricci, and R. M. Pick, *Europhys. Lett.* **52**(3), 324 (2000).
- ¹⁶G. Hinze, D. Brace, S. D. Gottke, and M. D. Fayer, *J. Chem. Phys.* **113**, 3723 (2000).
- ¹⁷C. Alba-Simionesco and M. Krauzman, *J. Chem. Phys.* **102**, 6574 (1995).
- ¹⁸V. Krakoviack, C. Alba-Simionesco, and M. Krauzman, *J. Chem. Phys.* **107**, 3417 (1997).
- ¹⁹T. Franosch, W. Götze, M. Mayr, and A. P. Singh, *Phys. Rev. E* **55**, 3183 (1997).
- ²⁰A. P. Singh, G. Li, W. Götze, M. Fuchs, T. Franosch, and H. Z. Cummins, *J. Non-Cryst. Solids* **235–237**, 66–70 (1998).
- ²¹S. Wiebel and J. Wuttke, *New J. Phys.* **4**, 56.1–56.17 (2002).
- ²²M. Ricci, S. Wiebel, P. Bartolini, A. Taschin, and R. Torre, *Philos. Mag.* **84**, 1491 (2004).
- ²³V. Krakoviack and C. Alba-Simionesco, *J. Chem. Phys.* **117**, 2161 (2002).
- ²⁴M. Domschke, M. Marsilius, T. Blochowicz, and T. Voigtmann, *Phys. Rev. E* **84**, 031506 (2011).
- ²⁵N. Petzold, B. Schmidtke, R. Kahlau, D. Bock, R. Meier, B. Micko, D. Kruk, and E. A. Rössler, *J. Chem. Phys.* **138**, 12A510 (2013).
- ²⁶U. Bengtzelius, W. Götze, and A. Sjolander, *J. Phys. C: Solid State Phys.* **17**, 5915 (1984).
- ²⁷J. A. H. Wiedersich, N. V. Surovtsev, V. N. Novikov, and E. A. Rössler, *Phys. Rev. B* **64**, 064207 (2001).
- ²⁸Data from www.dguv.de/ifa/stoffdatenbank Deutsche Gesetzliche Unfallversicherung e.V.
- ²⁹Data from www.sigmaaldrich.com Copyright © 2014 Sigma-Aldrich Co.
- ³⁰K. A. Kobe, A. E. Ravicz, and S. P. Vohra, "Critical properties and vapor pressures of some ethers and heterocyclic compounds," *J. Chem. Eng. Data* **1**, 50–56 (1956).
- ³¹W. M. Haynes, *CRC Handbook of Chemistry and Physics*, 93rd ed. (Taylor and Francis, New York, 2012).
- ³²M. Fuchs, *J. Non-Cryst. Solids* **172–174**, 241 (1994).
- ³³W. Petry and J. Wuttke, *Trans. Theory. Stat. Phys.* **24**, 1075 (1995).
- ³⁴A. Brodin and E. A. Rössler, *J. Chem. Phys.* **125**, 114502 (2006).
- ³⁵A. Brodin and E. A. Rössler, *J. Chem. Phys.* **126**, 244508 (2007).
- ³⁶C. Gainaru, R. Kahlau, E. A. Rössler, and R. Böhmer, *J. Chem. Phys.* **131**, 184510 (2009).
- ³⁷H. Cang, V. N. Novikov, and M. D. Fayer, *Phys. Rev. Lett.* **90**, 197401 (2003).
- ³⁸A. Brodin, C. Gainaru, V. Porokhonsky, and E. A. Rössler, *J. Phys. Condens. Matter* **19**, 205104 (2007).
- ³⁹A. P. Sokolov, W. Steffen, and E. A. Rössler, *Phys. Rev. E* **52**, 5105 (1995).
- ⁴⁰M. Köhler, P. Lunkenheimer, Y. Goncharov, R. Wehn, and A. Loidl, *J. Non-Cryst. Solids* **356**, 529 (2010).
- ⁴¹M. Köhler, P. Lunkenheimer, Y. Goncharov, and A. Loidl, *Phys. Rev. E* **87**, 062320 (2013).
- ⁴²W. Götze and M. Sperl, *Phys. Rev. Lett.* **92**, 105701 (2004).
- ⁴³A. Taschin, P. Bartolini, R. Eramo, R. Righini, and R. Torre, *Nat. Commun.* **4**, 2401 (2013).
- ⁴⁴S. Adichtchev, T. Blochowicz, C. Tschirwitz, V. N. Novikov, and E. A. Rössler, *Phys. Rev. E* **68**(1), 011504 (2003).

Bibliography

- [1] J. Zarzycki, *Glasses and the vitreous state*, Cambridge University Press (1991).
- [2] P. Lunkenheimer, U. Schneider, R. Brand, A. Loidl, *Contemporary Physics* 41, 15 (2000).
- [3] W. Götze, *Complex Dynamics of Glass-Forming Liquids - A Mode-Coupling Theory*, Oxford University Press, New York (2009).
- [4] J. L. Yarnell, M. J. Katz, R. G. Wenzel, S. H. Koenig, *Phys. Rev. A* 7, 2130 (1973).
- [5] E. Donth, *The Glass Transition - Relaxation Dynamics in Liquids and Disordered Materials*, Springer, Berlin, Heidelberg (2001).
- [6] C. A. Angell, K. L. Ngai, G. B. McKenna, P. F. McMillan, and S. W. Martin, *Journal of Applied Physics* 88, 3113 (2000).
- [7] Bible, Book of Judges, Ch. 5, Verse 5 (the translation of the Hebrew text is somewhat equivocal here: the English translation reads 'the mountains melted' while the Latin translation reads 'montes fluxerunt').
- [8] D. Bingemann, N. Wirth, J. Gmeiner, and E. A. Rössler, *Macromolecules* 40, 5379 (2007).
- [9] I. Gutzow and J. Schmelzer, *The Vitreous State*, Springer, Berlin (1995).
- [10] D. Richter, M. Monkenbusch, A. Arbe, J. Colmenero, *Advances in Polymer Science* 174, 1 (2005).
- [11] E. Bartsch, F. Fujara, B. Geil, M. Kiebel, W. Petry, W. Schnauss, H. Sillescu, J. Wuttke, *Physica A* 201, 223 (1993).
- [12] W. Petry, J. Wuttke, *Transport Theory and Statistical Physics* 24, 1075 (1995).
- [13] A. Tölle, *Reports on Progress in Physics* 64, 1473 (2001).
- [14] R. Torre, P. Bartolini, R. M. Pick, *Physical Review E* 57,1912 (1998).
- [15] G. Hinze, D. D. Brace, S. D. Gottke, M. D. Fayer, *Journal of Chemical Physics* 113, 3723 (2000).
- [16] H. Cang, V. N. Novikov, M. D. Fayer, *Journal of Chemical Physics* 118, 2800 (2003).
- [17] D. Kruk, A. Herrmann, E. A. Rössler, *Progress in Nuclear Magnetic Resonance Spectroscopy* 63, 33 (2012).
- [18] N. Petzold, *diploma thesis* (2008).

- [19] http://www.rp-photonics.com/neodymium_doped_gain_media.html, RP Photonics Consulting GmbH.
- [20] <http://www.repairfaq.org/sam/laserfil.htm>, Sci. Electronics Repair FAQ, Filip M. Gieszczykiewicz and Samuel M. Goldwasser.
- [21] *operator's manual - Verdi V2*, Coherent Laser Group (1999).
- [22] *TANDEM FABRY-PEROT INTERFEROMETER TFP-1 Operator Manual*, Dr. J.R. Sandercock, JRS Scientific Instruments (2011).
- [23] E. Hecht, *optics*, 3rd Edition, Addison Wesley Longman (1998).
- [24] Bedienungsanleitung zum Jobin-Yvon Monochromator U1000.
- [25] M. Young, *Optics and Lasers*, Springer, Berlin (1993).
- [26] J. D. Jackson, *Classical Electrodynamics*, John Wiley & Sons, New York (1962).
- [27] W. Greiner, *Theoretische Physik, Band 3: Klassische Elektrodynamik*, Verlag Harri Deutsch, Frankfurt am Main (1990).
- [28] L. D. Landau, E. M. Lifschitz, *Lehrbuch der theoretischen Physik*, Band II und VIII, Akademie-Verlag, Berlin (1985).
- [29] B. J. Berne and R. Pecora, *dynamic light scattering*, Wiley Interscience, New York (1976).
- [30] A: Einstein, Ann. Phys. 33, 1275 (1910).
- [31] N. V. Surovtsev, V. N. Novikov, E. Duval, J. Phys.: Condens. Matter 10, L113 (1998).
- [32] R. Zwanzig, Ann. Rev. Phys. Chem. 16, 67 (1965).
- [33] N. Wax, *Selected Papers on Noise and Stochastic Processes*, Dover, New York (1954).
- [34] W. Kob, H. C. Andersen, Phys. Rev. E 48, 4364 (1993).
- [35] A. Khintchine, Mathematische Annalen 109, (1934).
- [36] H. Nyquist, Phys. Rev., 32, 110 (1928).
- [37] H. B. Callen and T. A. Welton, Phys Rev. 83, 34 (1954).
- [38] D. Forster, *Hydrodynamic fluctuations, broken symmetry, and correlation functions*, Addison-Wesley, New York (1975).
- [39] H. Cang, J. Li, M. D. Fayer, J. Chem. Phys. 119, 13017 (2003).

- [40] G. Pratesi, P. Bartolini, D. Senatra, M. Ricci, R. Righini, F. Barocchi, R. Torre, *Phys. Rev. E*, 67, 021505 (2003).
- [41] A. Brodin, E. A. Rössler, *J. Chem. Phys.* 125, 114502 (2006).
- [42] S. Kastner, M. Köhler, Y. Goncharov, P. Lunkenheimer, A. Loidl, *J. Non-Cryst. Solids* 357, 510 (2011).
- [43] G. Li, W. M. Du, X. K. Chen, H. Z. Cummins, *Phys. Rev. A* 45, 3867 (1997).
- [44] S. Wiebel, J. Wuttke, *New Journal of Physics* 4, 56.1 (2002).
- [45] A. Brodin, E. A. Rössler, *Eur. Phys. J. B* 44, 3 (2005).
- [46] R. Meier, A. Herrmann, M. Hofmann, B. Schmidtke, B. Kresse, A. F. Privalov, D. Kruk, F. Fujara, E. A. Rössler, *Macromolecules* 46, 5538 (2013).
- [47] C. Gainaru, O. Lips, A. Troshagina, R. Kahlau, A. Brodin, F. Fujara, E.A. Rössler, *J. Chem. Phys.* 128, 174505 (2008).
- [48] M.J. Lebon, C. Dreyfus, Y. Guissani, R.M. Pick, and H.Z. Cummins, *Z. Phys. B* 103, 433 (1997).
- [49] T. Blochowicz A. Kudlik, S. Benkhof, J. Senker, E. Rössler, G. Hinze, *J. Chem. Phys.* 110, 12011 (1999).
- [50] N. Petzold, B. Schmidtke, R. Kahlau, D. Bock, R. Meier, B. Micko, D. Kruk, E. A. Rössler, *J. Chem. Phys.* 138, 12A510 (2013).
- [51] A. Brodin, C. Gainaru, V. Porokhonsky, E. A. Rössler, *J. Phys. Cond. Matt.* 19, 205104 (2007).
- [52] A. Brodin, E. A. Rössler, *J. Chem. Phys.* 125, 114502 (2006).
- [53] A. Brodin, E. A. Rössler, *J. Chem. Phys.* 126, 244508 (2007).
- [54] C. Daguenet, P. J. Dyson, I. Krossing, A. Oleinikova, J. Slattery, C. Wakai, H. Weingärtner, *J. Phys. Chem. B*. 110, 12682 (2006).
- [55] A. I. Nielsen, T. Christensen, B. Jakobsen, K. Niss, N. B. Olsen, R. Richert, J. Dyre, *J. Chem. Phys.* 130, 154508 (2009).
- [56] R. Böhmer, K. L. Ngai, C. A. Angell, D. J. Plazek, *J. Chem. Phys.* 99, 4201 (1993).
- [57] A. P. Sokolov, E. A. Rössler, A. Kisliuk, D. Quitman, *Phys. Rev. Lett.* 71, 2062 (1993).
- [58] N. Petzold, E.A. Rössler, *J. Chem. Phys.* 133, 124512 (2010).
- [59] C. J. F. Böttcher, P. Bordewijk: *Theory of electronic Polarization, Part II*, Elsevier Scientific Polarization, Amsterdam 1978.

- [60] R. Kahlau, D. Kruk, Th. Blochowicz, V.N. Novokov, E.A. Rössler, *J. Phys. Condens. Matter* 22, 365101 (2010).
- [61] K. Binder, W. Kob, *Glassy Materials and Disordered Solids*, World Scientific, New Jersey (2005).
- [62] W. Götze, *J. Phys. Condensed Matter* 11, A1 (1999).
- [63] R. M. Lynden-Bell, in *Molecular Liquids*, Editors: A. J. Barnes; W. Orville-Thomas; J. Yarwood; Reidel, Dorecht, 1984.
- [64] J.-P. Hansen; I. R. McDonald, in *Theory of Simple Liquids*, Academic Press, London 1976.
- [65] H. Vogel, *Phys. Z.* 22, 645 (1921); G. S. Fulcher, *J. Am. Ceram. Soc.* 8, 339 (1925); G. Tammann and W. Hesse, *Z. Anorg. Allg. Chem.* 156, 245 (1926).
- [66] F. Stickel, E. W. Fischer, and R. Richert, *J. Chem. Phys.* 104, 2043 (1996).
- [67] T. Heckscher, A. I. Nielsen, N. B. Olsen, and J. C. Dyre, *Nat. Phys.* 4, 737 (2008).
- [68] J. C. Mauro, Y. Yue, A. J. Ellison, P. K. Gupta, D. C. Allen, *Proc. Natl. Acad. Sci. USA* 103, 19780 (2009).
- [69] P. Lunkenheimer, S. Kastner, M. Köhler, A. Loidl, *Phys. Rev. E* 81, 051504 (2010).
- [70] T. R. Kirkpatrick, D. Thirumalai, and P. G. Wolynes, *Phys. Rev. A* 40, 1045 (1989).
- [71] G. Tarjus, D. Kivelson, P. Viot, *J. Phys.: Condens. Matter* 12, 6497 (2000).
- [72] G. Tarjus, S. A. Kivelson, Z. Nussinov, P. Viot, *J. Phys.: Condens. Matter* 17, R1143 (2005).
- [73] L. Berthier and G. Biroli, *Rev. Mod. Phys.* 83, 587 (2011).
- [74] Ch. Alba-Simionesco, D. Kivelson, G. Trajus, *J. Chem. Phys.* 116, 5033 (2002).
- [75] S. Sastry, *PhysChemComm* 3, 79 (2000).
- [76] W. Götze and L. Sjörger, *Rep. Prog. Phys.* 55, 241 (1992).
- [77] Y. Elmatad, J. P. Garrahan, D. Chandler, *J. Phys. Chem. B* 113, 5563 (2009).
- [78] E. A. Moelwyn-Hughes, *Physikalische Chemie* (Thieme, Stuttgart, 1970).
- [79] F. Stickel, E. W. Fischer, and R. Richert, *J. Chem. Phys.* 104, 2043 (1996).
- [80] Ch. Alba-Simionesco, D. Kivelson, and G. Trajus, *J. Chem. Phys.* 116, 5033 (2002).
- [81] D. Kivelson, S. A. Kivelson, X. L. Zhao, Z. Nussinov, G. Tarjus, *Physica A* 219, 27 (1995).

- [82] S. Mirigan and K. S. Schweizer, *J. Chem. Phys.* 140, 194507 (2014).
- [83] K. Kawasaki and J. Gunton, *Phys. Rev. B* 13, 11 (1976).
- [84] U. Bengtzelius, W. Götze and A. Sjölander, *J. Phys. C: Solid State Phys.* b17, 5915 (1984).
- [85] E. Leutheuser, *Phys. Rev. A* 29, 2765 (1984).
- [86] T. Franosch, M. Fuchs, W. Götze, M. R. Mayr and A. P. Singh, *Phys. Rev. E* 56, 5659 (1997).
- [87] R. Schilling and T. Scheidsteger, *Phys. Rev. E* 56, 2935 (1997).
- [88] R. Schilling and T. Scheidsteger, *Phil. Mag. B* 77, 305 (1998).
- [89] S.-H. Chong and M. Fuchs, *Phys. Rev. Lett.* 88, 185702 (2002).
- [90] R. Schilling in *disorder Effects in Supercooled liquids-Mode Coupling Theory and Its Experimental Tests*, edited by R. Richert and A. Blumen, Springer, 193, (1994).
- [91] R. Schilling in *Collective Dynamics of Nonlinear and Disordered Systems*, edited by G. Radons, W. Just, and P. Haeussler, Springer, 171 (2003); arXiv:cond- mat/0305565.
- [92] W. Götze, *J. Phys.: Condensed Matter* 11, A1 (1999).
- [93] H. Z. Cummins, *J. Phys.: Condens. Matter* 11, A95 (1999).
- [94] S. P. Das, *Phase Transitions: A Multinational Journal*, 50:1-3, 7 (1994).
- [95] J.-L. Barrat, M. L. Klein, *Annu. Rev. Phys. Chem.* 42, 23-53 (1991)
- [96] F. Sciortino, P. Tartaglia, *Physica A* 236, 140-148, (1997).
- [97] F. Sciortino, L. Fabbian, S. H. Chen, P. Tartaglia, *Phys. Rev. E* 56, 5397-5404, (1997).
- [98] E. Bartsch in *Relaxation Kinetics in Supercooled Liquids - Mode Coupling Theory and Its Experimental Tests*, edited by S. Yip, *Transp. Theory and Statist. Phys.* 24, 1125 (1995).
- [99] W. van Meegen, *Transport Theory and Statistical Physics*, 24, 1017-1051(1995).
- [100] M. Mézard, G. Parisi, *J. Phys. A.: Math. Gen.* 29, 6515 (1996).
- [101] M. Mézard, G. Parisi, *Phys. Rev. Lett.* 82, 747 (1999).
- [102] T. R. Kirkpatrick, D. Thirumalai, *Transp. Theory and Stat. Mech.* 24, 927- 945 (1995).
- [103] D. Kivelson, G. Tarjus, S. A. Kivelson, *Prog. Theor. Phys. Suppl* 126, 289 (1997).
- [104] C. A. Angell, *J. Non-Cryst. Solids* 131/133, 13 (1991).

- [105] C. A. Angell, *Science*, 267, 1924 (1995).
- [106] F. H. Stillinger, *Science*, 267, 1935 (1995).
- [107] P. G. Debenedetti, F. H. Stillinger, *Nature* 410, 259 (2001).
- [108] F. H. Stillinger and P. G. Debenedetti, *J. Chem. Phys.* 116, 3353 (2002).
- [109] S. P. Das and G. F. Mazenko, *Phys Rev. A* 34, 3 (1986).
- [110] W. Götze and L. Sjögren, *Z. Phys. B: Condens. Matter* 65, 415 (1987).
- [111] G. Wahnström und L. Sjölander, *J. Phys. C* 17, 5915 (1984)
- [112] C. Morkel und W. Gläser, *Phys. Rev. A* 33, 3383 (1986)
- [113] U. Balucani und M. Zoppi, *Dynamics of the Liquid State*, Clarendon: Oxford (1994).
- [114] W. Götze, *Z. Phys. B* 56, 139 (1984).
- [115] L. Sjörgen, *Phys. Rev. A* 33, 1254 (1986).
- [116] C. Alba-Simionesco und M. Krauzmann, *J. Chem. Phys.* 102, 6574 (1995).
- [117] T. Franosch, M. Fuchs, W. Götze, M. R. Mayr and A. P. Singh, *Phys. Rev. E* 56, 5659 (1997).
- [118] V. Krakoviack, C. Alba-Simionesco und M. Krauzmann, *J. Chem. Phys.* 107, 3417 (1997).
- [119] A. P. Singh, G. Li, W. Götze, M. Fuchs, T. Franosch, H. Z. Cummins, *J Non-Cryst. Solids* 235-237, 66 (1998).
- [120] M. Ricci, S. Wiebel, P. Bartolini, A. Taschin, R. Torre, *Philosophical Magazine* 84, 1491 (2004).
- [121] A. Taschin, P. Bartolini, R. Eramo, R. Righini, R. Torre, *Nature Communications* 4, 2401 (2013).
- [122] W. Götze und T. Voigtmann, *Phys. Rev. E* 61, 4133 (2000).
- [123] V. Krakoviack and C. Alba-Simionesco, *J. Chem. Phys.* 117, 2161 (2002).
- [124] A. P. Sokolov, W. Steffen, E. A. Rössler, *Phys. Rev. E* 82, 5105 (1995).
- [125] Th. Bauer, P. Lunkenheimer, S. Kastner, A. Loidl, *Phys. Rev. Lett.* 110, 107603 (2013).
- [126] R. Böhmer, K. L. Ngai, C. A. Angell, D. J. Plazek, *J. Chem. Phys.* 99, 4201 (1993).
- [127] H. Weingärtner, A. Knocks, W. Schrader, U. Kaatz, *J. Phys. Chem. A.* 105, 8645 (2001).